

Supporting Information  
Experimental and Theoretical Data

**Table of Contents**

Table of Contents.....	2
1. Method Evaluation for Selectivity Determination in Kinetic Resolution Reactions.....	3
1.1. Definition of Enantioselectivity.....	3
1.2. Absolute Rate Measurements.....	3
1.3. Derivation of Kagan's formulas.....	4
1.4. Kinetic Resolution Experiments.....	6
1.5. Error Estimation of Single Point Kinetic Resolution Experiments.....	7
1.6. Linear Regression.....	9
1.7. Simulation of Effective Rate Constants.....	12
1.8. Chemoselectivity.....	14
1.9. Methodological Conclusion.....	16
2. Determination of Relative Rates.....	17
2.1. Experimental Protocol for Competitive Linear Regression Experiments.....	17
2.2. Determination of Absolute Configurations.....	17
2.3. Analysis of Experiments.....	18
2.4. Results with Chiral Catalysts.....	20
2.5. From Experimental Data to Relative Rates.....	38
2.6. Reliability Estimation of Relative Rates.....	43
2.7. Results with Achiral Catalysts.....	45
2.8. Correlation of Relative Rates and Size Parameter.....	53
2.9. Background Measurements.....	55
3. Experimental Procedures.....	58
3.1. General Procedures.....	58
3.2. Synthesis of Catalysts.....	59
3.3. Synthesis of Alcohols.....	65
3.4. Synthesis of Esters.....	67
3.5. X-Ray Crystal Structure Data.....	70
4. Computational Study.....	74
4.1. Computational Methods.....	74
4.2. Energy Profile of the Reaction.....	75
4.3. Correlation of Enantioselectivity and Computational Results.....	77
4.4. Comparison of Optimization Methods.....	78
4.5. Benchmarking of Single Point Calculations.....	79
4.6. Geometrical Analysis of Conformational Space for TS2.....	80
4.7. Energetical Analysis of Selectivity-Determining Transition State Structures.....	86
4.8. Quantification of Intramolecular Non-Covalent Interactions.....	90
4.8.1. H-Capping Strategy.....	91
4.8.2. Local Energy Decomposition (LED) analysis.....	93
4.9. Qualitative Investigation of Non-Covalent Interactions.....	94
4.9.1. AIM Analysis.....	94
4.9.2. NCI Plots.....	98
4.10. Analysis of Thermodynamics and Substrate Properties.....	101
5. Supplementary References.....	104
6. NMR spectra.....	105
7. HPLC traces.....	121
8. Tables of Energies, Free Energies and Enthalpies.....	149
8.1. Conformers of TS2.....	149
8.2. Reactants, products, intermediates, TS1 of energy profile.....	157
8.3. Analysis of reactants and products.....	162

## 1. Method Evaluation for Selectivity Determination in Kinetic Resolution Reactions

In order to answer the research question in this project properly, quite accurate measurements of relative rates for highly selective kinetic resolution reactions are needed. Therefore, in this chapter different approaches to determine the selectivity of kinetic resolution reactions are discussed and evaluated.

### 1.1. Definition of Enantioselectivity

The central descriptor for enantiomeric purity of a sample is the enantiomeric excess (*ee*) defined by Eq. S1.

$$ee = \frac{[major\ enantiomer] - [minor\ enantiomer]}{[major\ enantiomer] + [minor\ enantiomer]} \quad \text{Eq. S1}$$

*Ee* values are conversion-dependent and therefore at least two values have to be reported (e.g. *ee* of substrate and *ee* of product or *ee* of product/substrate and conversion) which makes it inconvenient to compare different *ee* values. Thus, it is established to report the selectivity value *s* which is defined as the relative rate constant of the faster enantiomer to the slower one (Eq. S2).

$$s = \frac{k_{fast}}{k_{slow}} \quad \text{Eq. S2}$$

### 1.2. Absolute Rate Measurements

Selectivity values *s* can be measured directly through determination of absolute rates of each of the two enantiomers. However, in practice this approach is chosen very rarely due to the following experimental problems:

1. Usually the enantiopure substrates are not easily accessible.
2. For the reliable determination of absolute rate constants the reaction should be followed to almost full conversion. In highly selective reactions the minor enantiomer reacts very slowly. Reaction times of several weeks especially at very low temperatures lead to inaccuracies due to factors like evaporation of solvent, precipitation of substrates or products or hydrolysis. To avoid those problems, in this study no data of kinetic resolution experiments running longer than approx. four days are used to ensure experimental reliability.
3. The reliability of direct kinetic measurements is limited due to differences in the experimental environment of two independent reactions. However, even minor differences in temperature, catalyst or reagent concentration impacts absolute rates significantly. This is especially true in kinetic resolution reactions, where mostly very low absolute quantities are used and thus the impact of relatively small experimental errors (e.g. weighing in of the catalyst) becomes crucial. In general, it is recommendable to work with stock solutions which allows to weigh

in larger quantities. However, availability and solubility of chiral catalysts often limits possibilities for stock solutions.

Thus, comparison of independently measured rate constants bears very often internal errors. In this project direct kinetic measurements were only used to measure background reaction with 4-dimethylaminopyridine (DMAP, **5**) (see Chapter 2.8).

### 1.3. Derivation of Kagan's formulas

To avoid the mentioned problems of absolute rate measurements most commonly competition experiments with the racemic substrate are performed. This guarantees exactly comparable reaction conditions and allows analysis with chiral high performance liquid chromatography (HPLC) or chiral gas chromatography (GC). Moreover, reactions ideally run only to 50% total conversion  $c$  resulting in much shorter reaction times, as they are mainly dominated by the absolute rate of the fast reacting enantiomer. As mentioned above  $ee$  values are conversion dependent and thus reporting the selectivity value  $s$  is preferable as  $s$  values can be directly compared. Kagan and Fiaud<sup>[1]</sup> developed fundamental equations to experimentally determine  $s$  values. In the following the derivation of these central equations is described. Therefore, we assume a racemic mixture of two enantiomers R and S with a total starting concentration of 1 (unit). Furthermore, we assume that R and S react with B in an irreversible (pseudo-)first order reaction to products P and Q.



The first-order rate law (Eq. S5) can be integrated by separation of the variable and gives Eq. S9. Similar operations can be performed for the reaction of S.

$$\frac{d[R]}{dt} = -k_R[R] \quad \text{Eq. S5}$$

$$\frac{d[R]}{[R]} = -k_R dt \quad \text{Eq. S6}$$

$$\int_{[R]_0}^{[R]} \frac{1}{[R]} d[R] = \int_0^t -k_R dt \quad \text{Eq. S7}$$

$$\ln[R] - \ln[R]_0 = -k_R t \quad (\text{for } t \neq 0) \quad \text{Eq. S8}$$

$$k_R = \ln\left(\frac{[R]}{[R]_0}\right) \left(-\frac{1}{t}\right) \quad (\text{for } t \neq 0) \quad \text{Eq. S9}$$

If we assume that  $k_R > k_S$  (as herein), selectivity  $s$  is defined by Eq. S10. Together with Eq. S9 and the assumed starting concentrations of 0.5 (units) for both enantiomers,  $s$  can be expressed by Eq. S13.

$$s = \frac{k_R}{k_S} \quad \text{Eq. S10}$$

$$s = \frac{\ln\left(\frac{[R]}{[R]_0}\right)}{\ln\left(\frac{[S]}{[S]_0}\right)} \quad \text{Eq. S11}$$

$$[R]_0 = [S]_0 = 0.5 \quad \text{Eq. S12}$$

$$s = \frac{\ln(2[R])}{\ln(2[S])} \quad \text{Eq. S13}$$

The conversion  $c$  (Eq. S14) can be described relative to the substrate concentrations by Eq. S16. Combining the conversion with the definition of  $ee$  in Eq. S19 gives Eq. S23 and similarly Eq. S24 for  $[S]$ .

$$c = \frac{[P] + [Q]}{[R]_0 + [S]_0} \quad \text{Eq. S14}$$

$$[P] = [R]_0 - [R] \quad \text{and} \quad [Q] = [S]_0 - [S] \quad \text{Eq. S15}$$

$$1 - c = \frac{[R] + [S]}{[R]_0 + [S]_0} \quad (\text{with } [R]_0 + [S]_0 = 1) \quad \text{Eq. S16}$$

$$1 - c = [R] + [S] \quad \text{Eq. S17}$$

$$[S] = 1 - c - [R] \quad \text{Eq. S18}$$

$$ee_{\text{substrate}} = \frac{[S] - [R]}{[S] + [R]} \quad \text{Eq. S19}$$

$$ee_{\text{substrate}} = \frac{[S] - [R]}{1 - c} \quad \text{Eq. S20}$$

$$ee_{\text{substrate}} = \frac{(1 - c - [R]) - [R]}{1 - c} \quad \text{Eq. S21}$$

$$2[R] = -ee_{\text{substrate}}(1 - c) + (1 - c) \quad \text{Eq. S22}$$

$$2[R] = (1 - c)(1 - ee_{\text{substrate}}) \quad \text{Eq. S23}$$

$$2[S] = (1 - c)(1 + ee_{\text{substrate}}) \quad \text{Eq. S24}$$

Inserting Eq. S23 and Eq. S24 into Eq. S13 yields Kagan's central formula Eq. S25.

$$s = \frac{\ln((1 - c)(1 - ee_{\text{substrate}}))}{\ln((1 - c)(1 + ee_{\text{substrate}}))} \quad \text{Eq. S25}$$

Similar mathematical operations on  $ee_{\text{product}}$  (Eq. S26) with Eq. S17 and Eq. S15 for irreversible reactions yields the second formulation of Kagan's formulas Eq. S28.

$$ee_{\text{product}} = \frac{[Q] - [P]}{[Q] + [P]} \quad \text{Eq. S26}$$

$$ee_{\text{product}} = \frac{[S] - [R]}{c} \quad \text{Eq. S27}$$

$$s = \frac{\ln(1 - c(1 + ee_{\text{product}}))}{\ln(1 - c(1 - ee_{\text{product}}))} \quad \text{Eq. S28}$$

The conversion  $c$  can be determined by directly measured concentrations (e.g. by NMR, GC, HPLC) using Eq. S29. If the conversion is known exactly, only the  $ee$  of either the substrates or the products are needed. However,  $ee$  values can be determined experimentally more exactly than conversion

values.<sup>[2]</sup> The division of Eq. S27 by Eq. S20 gives Eq. S32 and makes it thus possible to calculate conversion and *s* directly from the *ee* values of substrate and product.

$$c_{direct} = \frac{[P] + [Q]}{[P] + [Q] + [R] + [S]} \quad \text{Eq. S29}$$

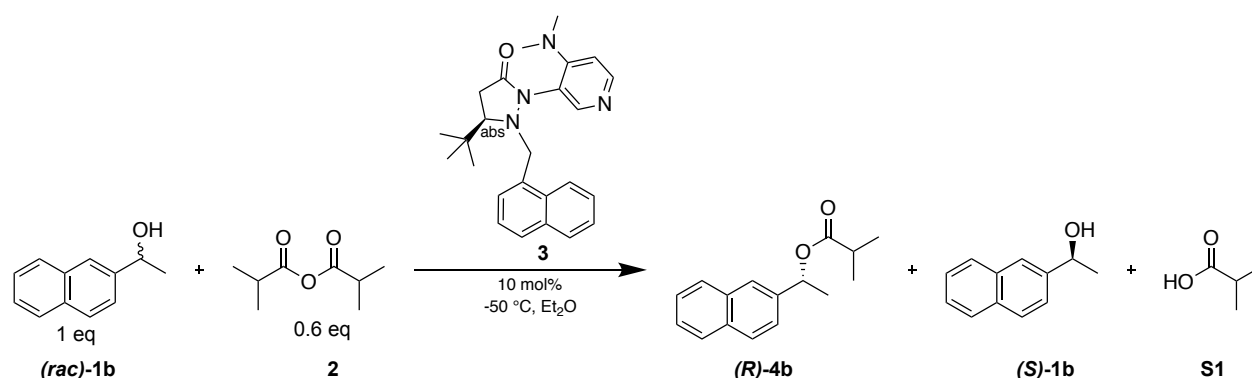
$$\frac{ee_{product}}{ee_{substrate}} = \frac{\frac{[S] - [R]}{c}}{1 - c} \quad \text{Eq. S30}$$

$$\frac{ee_{product}}{ee_{substrate}} = \frac{1 - c}{c} \quad \text{Eq. S31}$$

$$c_{ee} = \frac{ee_{substrate}}{ee_{substrate} + ee_{product}} \quad \text{Eq. S32}$$

### 1.4. Kinetic Resolution Experiments

As a benchmark experiment the kinetic resolution of 1-(2-naphthyl)ethanol (**1b**) with catalyst **3** as presented in **Scheme S1** is used. Sibi *et al.*<sup>[3]</sup> reported an enantioselectivity of *s* = 37 for this reaction under the stated conditions.



**Scheme S1.** Kinetic resolution of 1-(2-naphthyl)ethanol (**1b**) with catalyst **3**.

#### *Experimental procedure for kinetic resolution experiments:*

1 eq of alcohol **1b** and 10 mol% of catalyst **3** are weighed into a Schlenk flask, dissolved under N<sub>2</sub> in 1.8 mL of dry diethyl ether and cooled to -50 °C. 0.2 mL of a stock solution of freshly distilled isobutyric anhydride (**2**, 0.6 eq) in dry diethyl ether is added. After 48 hours the reaction is quenched through addition of 1 mL of methanol. Substrates and products are separated by column chromatography (hexanes/EtOAc = 9/1). Enantiomeric excess is determined by chiral HPLC chromatography (Chiracel IB-N5, flow 0.5 mL/min, T = 10 °C, λ = 289 nm, *n*Hex/*i*Prop = 90/10 (substrate), *n*Hex/*i*Prop = 98/2 (product)). HPLC traces are presented in **Figure S1**, calculation of *s* value in Table S1.

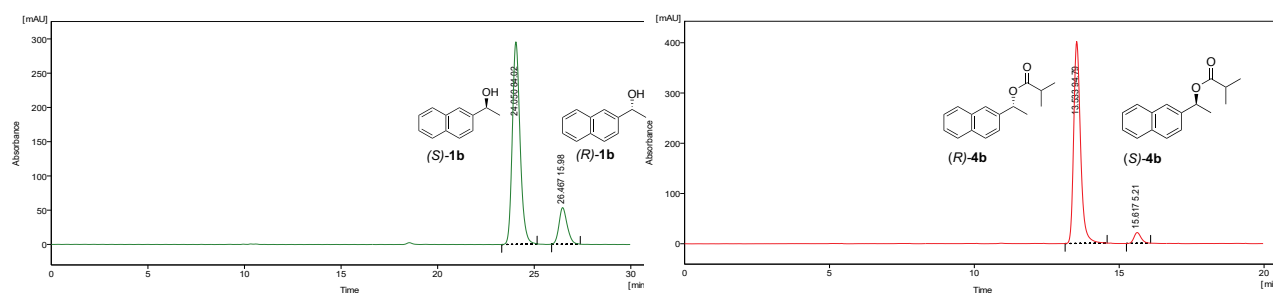


**Figure S1.** HPLC traces of substrates (left) and products (right) for the kinetic resolution experiment shown in **Scheme S1**.

**Table S1.** Calculation of conversion, *ee* values and enantioselectivity value *s* for the reaction shown in **Scheme S1**.

	UV-Absorbance HPLC ( $\lambda = 285$ nm), raw data [mAU]		Enantiomeric excess (Eq. S1)	Conversion (Eq. S32)	Selectivity (Eq. S25)
	(S)-enantiomer	(R)-enantiomer			
1-(2-naphthyl)ethanol ( <b>1b</b> )	8247	1569	0.680	43.2%	37.0
1-(2-naphthyl)ethyl isobutyrate ( <b>4b</b> )	363	6600	0.896		

Due to the high suitability and practicability kinetic resolution experiments are almost exclusively analysed in this manner. However, the reliability of single point kinetic resolution experiments is questionable especially for *s* values larger than 50.<sup>[2, 4]</sup> This is mainly caused by the logarithmic nature of the equations magnifying experimental inaccuracies in determining *ee* and conversion values, which will be investigated in the next chapter.

### 1.5. Error Estimation of Single Point Kinetic Resolution Experiments

In order to gain a better understanding of error influences on selectivity values we simulated kinetic resolution (KR) experiments with a hypothetical selectivity value of *s* = 80 and *s* = 200 using CoPaSi<sup>[5]</sup>. These exactly calculated intermediate concentrations were altered by a randomized error of -0.5% to +0.5%, which is in the range of typical errors in kinetic resolution experiments analysed by chiral HPLC<sup>[4b]</sup>. From 1 000 randomly distorted intermediate concentrations selectivity values were calculate by:

- (1) Kagan's equation for products Eq. S28 with conversion calculated from Eq. S29
- (2) Kagan's equation for substrates Eq. S25 with conversion calculated from Eq. S29 and
- (3) Kagan's equation Eq. S28 with conversion calculated from Eq. S32 (which is equivalent to use Eq. S25 and conversions from Eq. S32).

**Table S2.** Error estimates for the evaluation of single point kinetic resolution experiments with implemented randomized relative errors. Data was gained from 1000 runs.

	Reaction with $s = 80$ Randomized relative error of $\pm 0.5\%$			Reaction with $s = 200$ Randomized relative error of $\pm 0.5\%$		
	Eq. S28 with Eq. S29 (ee product, direct conversion)	Eq. S28 with Eq. S25 (ee substrate, direct conversion)	Eq. S28 with Eq. S32 (conversion from both ee values)	Eq. S28 with Eq. S29 (ee product, direct conversion)	Eq. S28 with Eq. S25 (ee substrate, direct conversion)	Eq. S28 with Eq. S32 (conversion from both ee values)
Average	80.1	81.0	80.0	201.4	209.0	200.0
Standard Deviation	2.8	8.5	0.7	11.3	48.4	1.7
Mean absolute error	2.3	6.9	0.6	9.1	37.3	1.4

**Table S2** demonstrates that calculating  $s$  values from direct conversions results in high standard deviations. However, it seems that using the conversion calculated by Eq. S32 gives very reliable results even for high selectivity values. Nonetheless, relative errors do not properly describe experimental realities as especially small numbers are less accurate to measure and several disruptive factors (e.g. baseline inaccuracies) add rather absolute than relative errors to measured data. Therefore, in another experiment a randomized absolute error in the range of  $\pm 0.25\%$  of absolute starting concentrations was added to each compound and evaluated in the same ways as described above.

**Table S3.** Error estimation for the evaluation of single point kinetic resolution experiments with implemented randomized absolute errors. Data was gained from 1000 runs.

	Reaction with $s = 80$ Randomized absolute error of $\pm 0.25\%$ of start concentration			Reaction with $s = 200$ Randomized absolute error of $\pm 0.25\%$ of start concentration		
	Eq. S28 with Eq. S29 (ee product, direct conversion)	Eq. S28 with Eq. S25 (ee substrate, direct conversion)	Eq. S28 with Eq. S32 (conversion from both ee values)	Eq. S28 with Eq. S29 (ee product, direct conversion)	Eq. S28 with Eq. S25 (ee substrate, direct conversion)	Eq. S28 with Eq. S32 (conversion from both ee values)
Average	80.2	80.2	80.2	201.1	201.1	200.9
Standard Deviation	3.4	3.4	3.0	17.3	17.7	15.5
Mean absolute error	2.9	2.8	2.6	14.9	14.1	13.3
Smallest obtained $s$	73.4	71.5	74.4	170.0	159.0	172.9
Biggest obtained $s$	87.8	91.8	87.0	241.9	265.6	235.4

First of all, deviation and mean absolute errors in **Table S3** show, in agreement with **Table S2**, that it is most convenient to calculate conversion by Eq. S32, even if differences between the methods are much smaller than above. Only in cases with extremely high enantioselectivity values it may be necessary to use directly calculated conversion as analysis of ee of the products is out of experimental possibilities.<sup>[4a]</sup> Moreover, the obtained standard deviations in **Table S3** demonstrate that selectivity values around 80 can still be reported with acceptable reliability, while selectivity values of around 200 cannot be properly determined using single point kinetic resolution experiments. In those cases, maximal and minimal selectivity values from the simulation differ by 70 or more. Thus, several authors propose to rely on *s* values higher than 50 only to the closest ten and to not report higher *s* values than 200.<sup>[2, 4b]</sup> To illustrate the problem of measuring high *s* values, in **Figure S2** the ee values of the products for simulated reactions with defined enantioselectivity values are plotted against conversion values. It becomes obvious, that while ee differences are prominent for *s* values smaller than around 30, for higher *s* values the curves are lying together closely. However, most prominent differences can be found in the region of 40 – 52% conversion, so that most kinetic resolution reactions aim to target into that region. For *s* > 200 the differences become too small to be measured accurately in experiments.

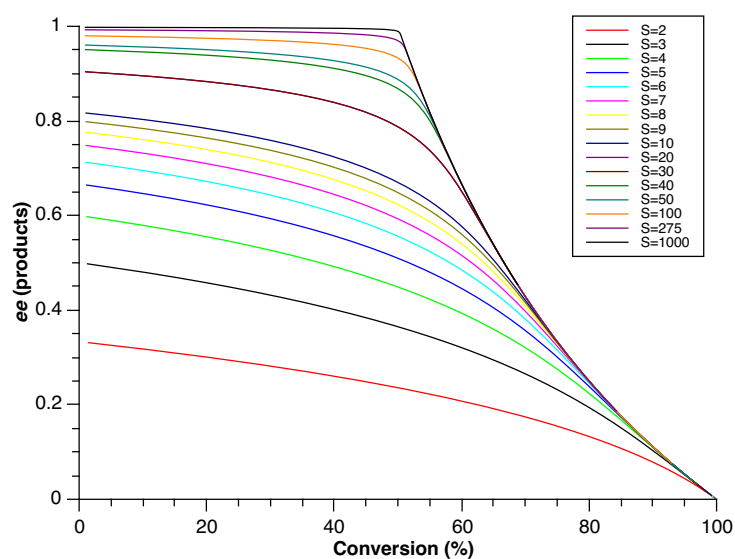


**Figure S2.** Plot of ee values of products against conversion values for reactions with different selectivity values. Intermediate concentrations of substrates and products were determined by simulation with CoPaSi<sup>[5]</sup> and plotted with QTPlot<sup>[6]</sup>.

## 1.6. Linear Regression

Additional to the evaluated inaccuracies of single point kinetic resolution measurements there are two conceptual problems related to the use of Kagan's formulas at a single concentration:

- 1) Relying on a single measured point is in most cases inappropriate as internal consistency cannot be controlled if only one value is obtained as the result.

- 2) As outlined above the KR formulas only apply to (pseudo) first order reaction that are not reversible and without any further reaction or decomposition of products.<sup>[1, 4b]</sup> However, using a single point measurement does not allow to control these conditions.

A more elaborate way to measure enantioselectivity values is therefore the use of a linear regression analysis. Intermediate concentrations of product and substrate are measured at different conversion points. Thus,  $ee_{products}$  and  $ee_{substrates}$  can be calculated. Eq. S32 allows to determine the intermediate conversion. As outlined in Chapter 1.3  $s$  can be expressed by Eq. S25. Plotting the numerator  $\ln(1 - c)(1 - ee_{substrate})$  against the denominator  $\ln(1 - c)(1 + ee_{substrate})$  for different conversion points should thus give a straight line through the origin with its slope being the selectivity value.<sup>[4, 7]</sup> Statistical analysis of the correlation allows to control internal consistency of the measurements. The  $R^2$  value describes the goodness of fit and displays if the conditions for the use of Kagan's formula are fulfilled.<sup>[4b]</sup> The deviation of intercept from zero mainly reflects experimental and analytical inaccuracies of measurements.

*Experimental procedure for kinetic resolution experiments analysed by linear regression:*

10 mol% of catalyst are weighed into a Schlenk flask, evacuated and filled with  $N_2$ . 1.8 mL of a stock solution of racemic alcohol (1 eq) in dry diethyl ether are added and cooled to  $-50^\circ C$ . 0.2 mL of a stock solution of freshly distilled isobutyric anhydride (0.6 eq) in dry diethyl ether is added. After defined periods of time probes of 0.05 mL of the reaction mixture are taken by syringe and quenched in 0.1 mL of methanol in a HPLC vial. 1 mL of *n*-hexane is added and a chiral HPLC spectrum is recorded (Chiracel IB-N5, flow 0.5 mL/min,  $T = 10^\circ C$ ,  $\lambda = 285$  nm,  $nHex/iPr = 90/10$ ).

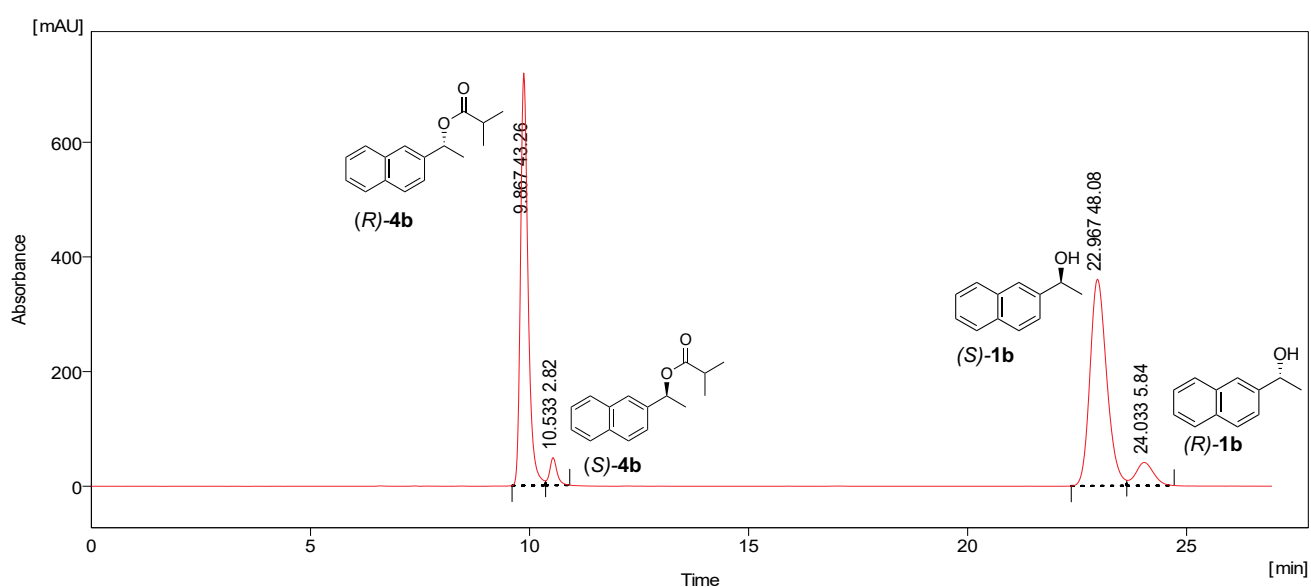


**Figure S3.** HPLC traces of reaction mixture for one point (47%) of the linear regression experiment shown in **Scheme S1**.

As an example, for a linear regression analysis experimental data for the experiment shown in **Scheme S1** are outlined. Choosing an appropriate HPLC methods as shown in **Figure S3** allows to quantify substrate and product concentrations at the same time and makes a manual separation by column chromatography redundant. This allows to investigate numerous experiments in this manner. In both independent runs of the experiment the points fit the line in **Figure S4** excellent with negligible intercept. The slope of this line reflects the selectivity value of  $s = 38.5 \pm 1.25$  in good agreement with the previous obtained value. Every measured point is the equivalent of a kinetic resolution as reported above. Major deviations of the selectivity values can be observed, however, if they are calculated from a single conversion point as shown in column 9 of **Table S4**. Thus, even for medium enantioselectivity values results of linear regression are more reliable than single point kinetic resolution measurements. This trend gets even more important as selectivity values increase.

**Table S4.** Raw data for two independent runs of linear regression shown in **Scheme S1**.

run	time [min]	UV-Absorbance HPLC ( $\lambda = 285$ nm), raw data [mAU]				Enantiomeric excess ee (Eq. S1)		conversion c (Eq. S32)	s (Eq. S25)	$\ln((1-c)/(1+ee_{alc}))$	$\ln((1-c)/(1-ee_{alc}))$
		R-NpEtOiPr (R)- <b>4b</b>	S-NpEtOiPr (S)- <b>4b</b>	S-NpEtOH (R)- <b>1b</b>	R-NpEtOH (S)- <b>1b</b>	Ester <b>4b</b>	Alcohol <b>1b</b>				
1	91	819.1	26.6	7099.8	6561.5	0.9370	0.0394	4.035%	32.0	-0.00254	-0.08139
1	424	1556.4	56.9	4073.3	2677.7	0.9294	0.2067	18.20%	33.5	-0.01293	-0.43241
1	1314	5187.3	251.6	7332.4	2481.0	0.9075	0.4944	35.27%	33.7	-0.03317	-1.11680
1	1982	4534.7	230.3	5420.5	1145.9	0.9033	0.6510	41.88%	38.6	-0.04132	-1.59534
1	2696	6954.8	433.0	7663.3	1110.2	0.8828	0.7469	45.83%	36.0	-0.05522	-1.98713
1	3138	8919.7	575.9	9585.4	1174.3	0.8787	0.7817	47.08%	36.7	-0.05880	-2.15833
2	31	153.9	6.0	3954.8	3809.2	0.9245	0.0187	1.988%	26.0	-0.001503	-0.039006
2	94	333.1	11.4	3464.1	3123.6	0.9336	0.0517	5.247%	30.6	-0.003492	-0.106971
2	180	631.4	22.0	3878.4	3257.1	0.9326	0.0871	8.539%	31.2	-0.005774	-0.180361
2	976	5175.1	192.4	10376.0	5096.5	0.9283	0.3412	26.88%	37.5	-0.019453	-0.730403
2	1272	6422.9	262.3	11431.7	4700.1	0.9215	0.4173	31.17%	36.9	-0.024762	-0.913567
2	1525	6690.6	287.2	11004.7	4014.8	0.9177	0.4654	33.65%	36.9	-0.028085	-1.036429
2	2945	6309.7	324.8	7914.9	1516.0	0.9021	0.6785	42.93%	39.5	-0.042946	-1.695612

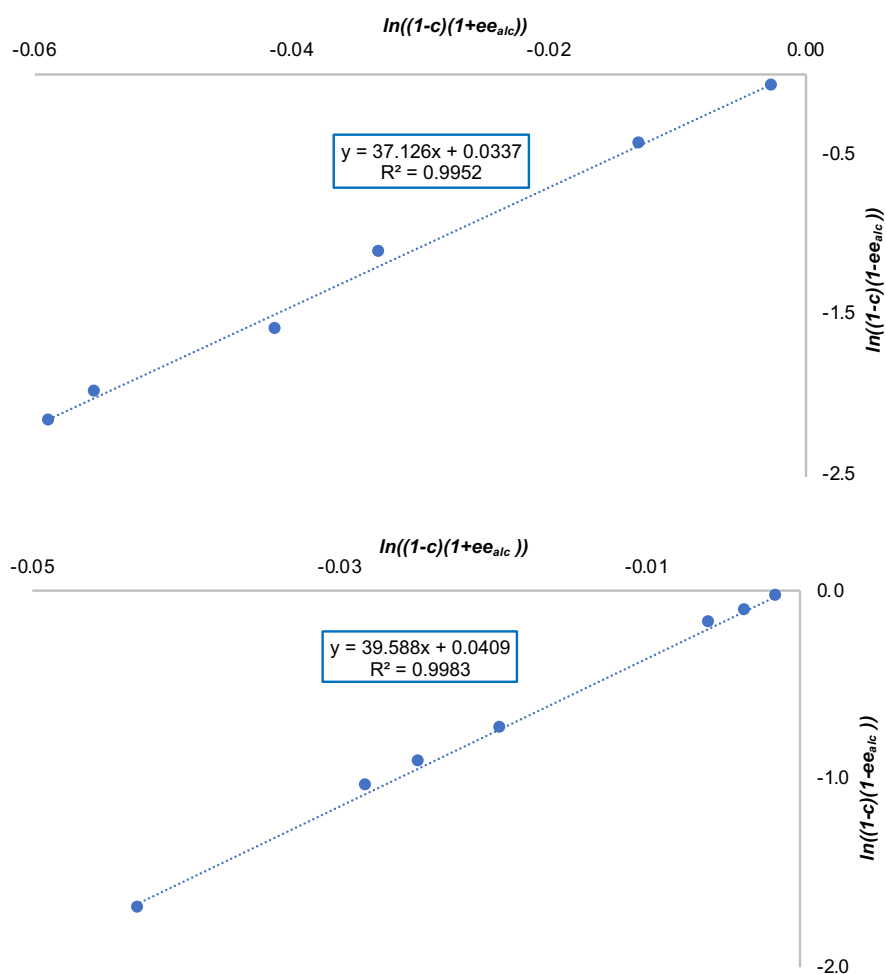


**Figure S4.** Linear regression analysis of data shown in **Table S4** (upper graph: run 1, lower graph: run 2).

### 1.7. Simulation of Effective Rate Constants

Another possibility especially for cases that do not follow pseudo-first order kinetics is the simulation of reaction curves. In linear regression experiments several intermediate concentrations of a reaction are measured. Those values together with the reaction times as reported in **Table S4** allow to plot time-turnover curves and to calculate effective rate constants (for technical details see Chapter 2.3).

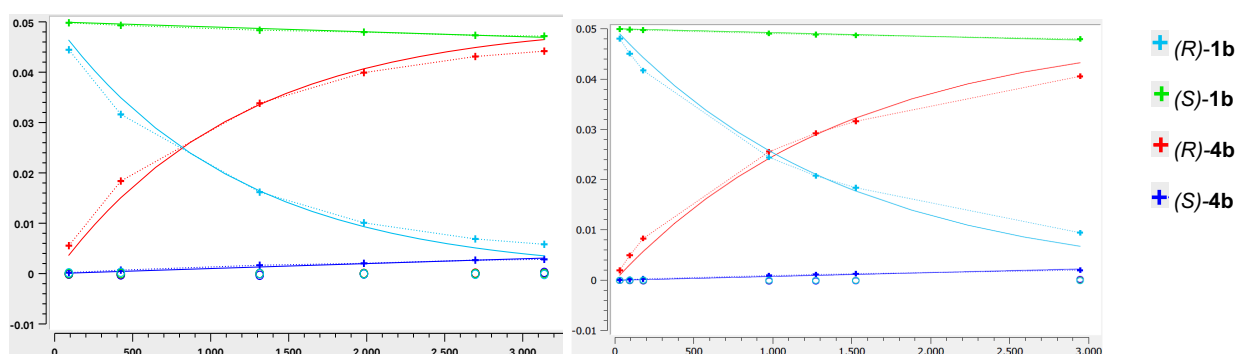


**Figure S5.** Fitted time [min] (x-axis) vs. intermediate concentration [ $\text{mol L}^{-1}$ ] (y-axis) curve of data shown in **Table S4** (left: run 1, right: run 2). Hollow circles show weighted errors.

**Table S5.** Results of Copasi parameter estimation for linear regression shown in **Scheme S1**.

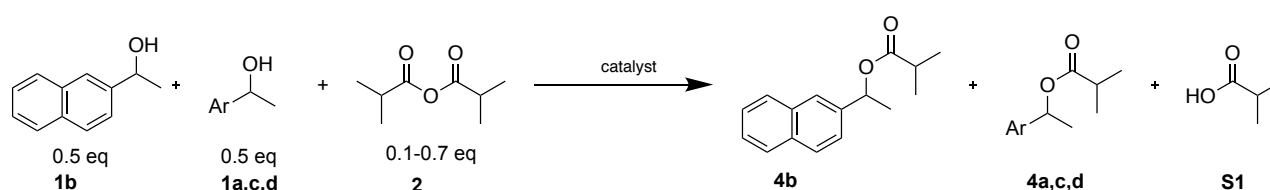
	Run 1			Run 2		
	Estimated effective rate constant	Standard Deviation of Parameter Estimation	$s = \frac{k_{(R)}}{k_{(S)}}$	Estimated effective rate constant	Standard Deviation of Parameter Estimation	$s = \frac{k_{(R)}}{k_{(S)}}$
$k_{(S)-1b}$	0.002045	3.09E-04	41.8	0.001562	3.77E-05	43.5
$k_{(R)-1b}$	0.085408	0.0126		0.067928	0.0027	

As **Figure S5** shows the fitting of the concentration of the faster alcohol (red line) is satisfying. For the slower alcohol (dark-blue line) conversion is very low and therefore the fitted relative rate value is rather unreliable. As discussed in Chapter 1.2 absolute rate constants carry a major deviation. Despite those limitations the enantioselectivity value of  $42.6 \pm 0.84$  is still quite close to the expected value of 39.

Regarding reliable simulations, the conversion of each substrate should be higher (ideally close to 100%) and more points should be measured. In kinetic resolution experiments with high enantioselectivities this poses again the problem that the reaction of the slower enantiomer exceeds in general well-controllable reaction times. Hence, the same problems as described for absolute rate measurements occur.

## 1.8. Chemoselectivity

Additional to relative rates of two enantiomers also relative rates of two different aromatic alcohols have to be investigated as shown in **Scheme S2**. This chemoselectivity can be defined in perfect analogy to enantioselectivity. In this report (*R*)-1-(2-naphthyl)ethanol (**1b**) is always used as the reference for relative rates if not stated otherwise (Eq. S33). Instead of starting the reaction with a racemic mixture a 1 : 1 mixture of two competing substrates is reacted and relative concentrations of substrates and products at different conversion values are analysed. In practice, either several independent reactions with a varying under-stoichiometric concentration of substrate can be run or one reaction can be quenched at different times. The chemoselectivity *C* for the products (Eq. S34) is calculated (equivalent to *ee* values) and the selectivity can be obtained via formula Eq. S35 with conversion values *c* calculated by Eq. S36.



**Scheme S2.** Competition experiment of 1-(2-naphthylethanol) (**1b**) and an aromatic alcohol.

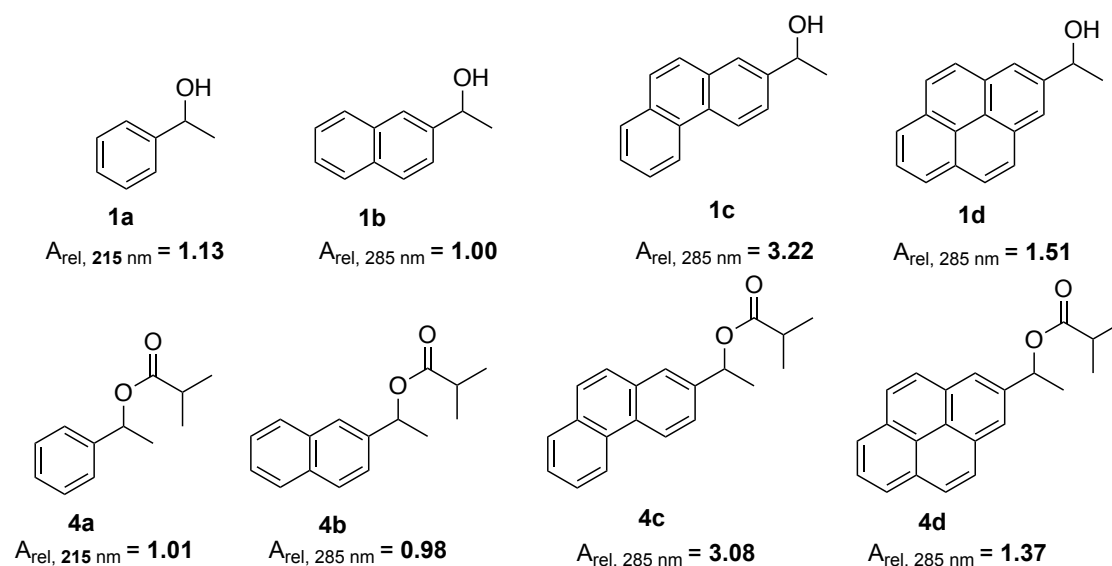
$$s = \frac{k(\mathbf{1a, c, d})}{k(\mathbf{1b})} \quad \text{Eq. S33}$$

$$C = \frac{[\mathbf{4a, c, d}] - [\mathbf{4b}]}{[\mathbf{4a, c, d}] + [\mathbf{4b}]} \quad \text{Eq. S34}$$

$$s = \frac{\ln(1 - c(1 + C))}{\ln(1 - c(1 - C))} \quad \text{Eq. S35}$$

$$c = \frac{[\mathbf{4a, c, d}] + [\mathbf{4b}]}{[\mathbf{4a, c, d}] + [\mathbf{4b}] + [\mathbf{1a, c, d}] + [\mathbf{1b}]} \quad \text{Eq. S36}$$

Intermediate concentrations of substrates and products as needed in Eq. S34 can be obtained for example via NMR, GC or HPLC. While NMR integrals of appropriate protons can be directly used to determine the intermediate concentrations, GC or HPLC signal intensities have to be normalized using a calibration curve. In HPLC analysis with a UV detector the absorbance mainly depends on the size of the chromophore system. The alcohols in this project bear by design very differently sized aromatic moieties. While UV absorbance of alcohol substrates and ester products are very similar as the chromophore system does not grow significantly, differences magnify for the different aromatic systems (see **Scheme S3**). For 1-phenylethanol (**1a**) a smaller wavelength must be used than for the big aromatic systems. For the other alcohols too high UV absorbance values at low wavelengths have to be avoided, as the linear dependence on the concentration is only true for UV absorbances up to 1.5 AU.



**Scheme S3.** UV absorbance values  $A_{\text{rel}}$  relative to 1-(2-naphthyl)ethanol (**1b**) determined by calibration curves.

To avoid major deviations of results through calibration errors only similarly absorbing species should be compared. Therefore, conversion values  $c$  are calculated for each substrate separately (Eq. S37 and Eq. S38). Thus, Eq. S39 is used instead of Eq. S34 for the calculation of chemoselectivity values  $C$  as in reaction mixtures starting from a 1 : 1 ratio of two substrates Eq. S40 becomes valid. Moreover, a correction factor from minor deviations of the 1 : 1 starting conditions<sup>[8]</sup> becomes redundant.

$$c_{Np} = \frac{[\mathbf{4b}]}{[\mathbf{4b}] + [\mathbf{1b}]} \quad \text{Eq. S37}$$

$$c_{Ar} = \frac{[\mathbf{4a, c, d}]}{[\mathbf{4a, c, d}] + [\mathbf{1a, c, d}]} \quad \text{Eq. S38}$$

$$C = \frac{c_{Ar} - c_{Np}}{c_{Ar} + c_{Np}} \quad \text{Eq. S39}$$

$$[\mathbf{4b}] + [\mathbf{1b}] = [\mathbf{4a, c, d}] + [\mathbf{1a, c, d}] \quad \text{Eq. S40}$$

### 1.9. Methodological Conclusion

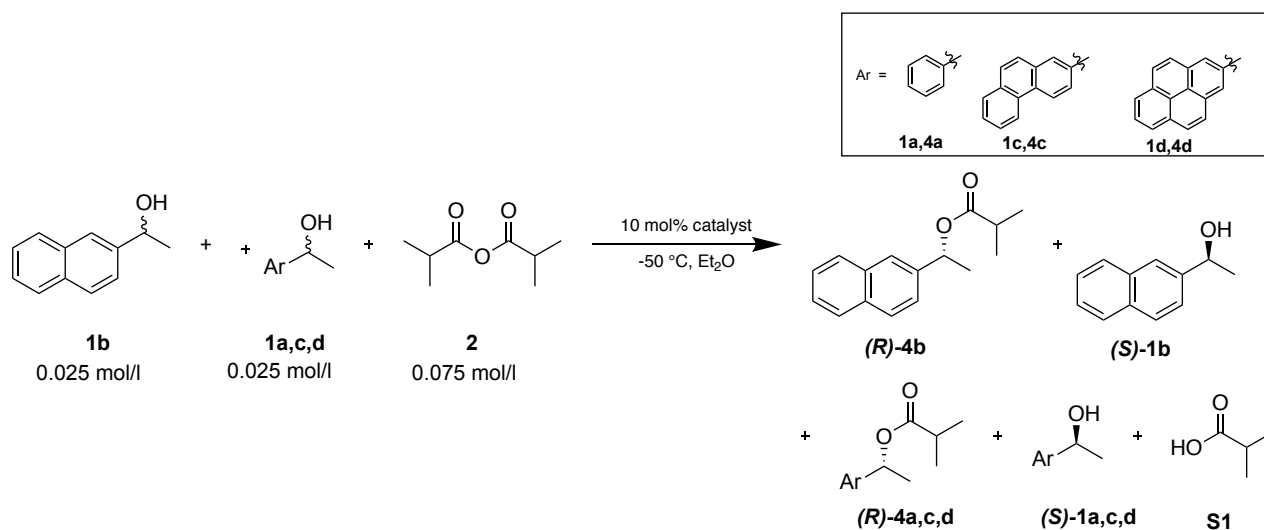
Answering the research question of this projects needs reliable measurements of relative rates for different alcohols in kinetic resolution experiments. Regarding the outlined methods above it should be guaranteed, that:

- 1) Rather than single point kinetic resolution experiments linear regression experiments are performed.
- 2) Conversion values are not directly measured but calculated from ee of product and ee of substrate by Eq. S32.
- 3) While those methods seem robust for selectivity values up to 80, selectivity values greater than 200 should be investigated carefully.
- 4) Instead of absolute rates relative rates should be measured to guarantee similar reaction conditions and to avoid reaction times that are out of experimental accuracy.

Thus, a protocol for “competitive linear regression for kinetic resolution” was developed. Racemic 1-(2-naphthyl)ethanol (**1b**) was chosen as the reference system allowing the determination of relative rates for (*R*) and (*S*) enantiomers of more selective reagents. To guarantee faster reactions and higher conversion rates of the slower enantiomer 1.5 eq of anhydride **2** were used.

## 2. Determination of Relative Rates

### 2.1. Experimental Protocol for Competitive Linear Regression Experiments



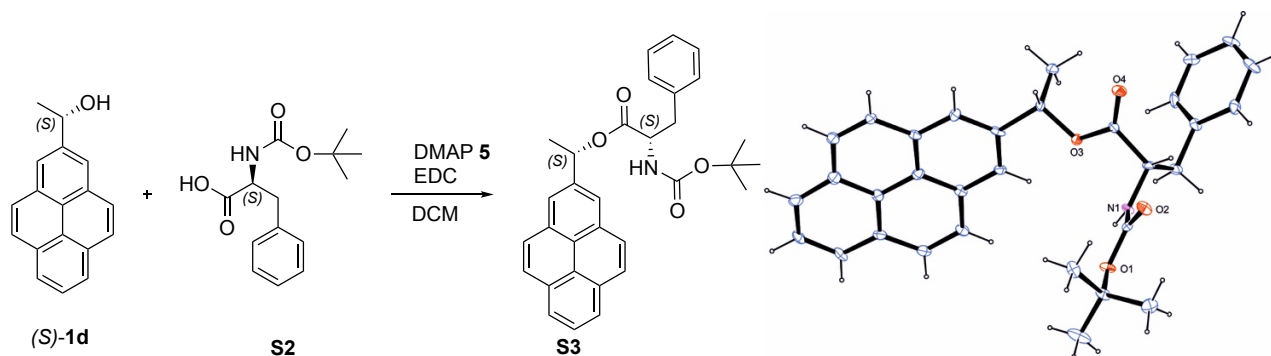
**Scheme S4.** Competitive linear regression for the kinetic resolution of 1-(2-naphthyl)ethanol (**1b**) and alcohols **1a-4a**.

0.01 mmol (10%) of catalyst are weighed into an oven dried Schlenk flask with magnetic stir bar, evacuated and filled with N<sub>2</sub>. 1.8 mL of a 1 : 1 molar stock solution of the two racemic alcohols (0.05 mmol of each) in dry diethyl ether are added. After cooling the solution to -50 °C 0.2 mL of a stock solution of freshly distilled isobutyric anhydride (0.15 mmol, 1.5 eq) in dry diethyl ether is added and stirred at -50 °C under N<sub>2</sub>. After defined periods of time probes of 0.05 mL of the reaction mixture are gathered by syringe and quenched in 0.1 mL of methanol in an HPLC vial. 1 mL of *n*-hexanes is added and a chiral HPLC spectrum of the reaction mixture is recorded (Chiracel IB-N5, flow 0.5 mL/min, T = 10 °C, λ = 285 nm or λ = 215 nm, gradients of *n*-hexanes and *iso*-propanol). All measurements were repeated independently and analysed in three different ways as discussed below.

### 2.2. Determination of Absolute Configurations

Absolute configurations for *(R)*- and *(S)*-1-(2-naphthyl)ethanol (**1b**) and *(R)*- and *(S)*-1-phenylethanol (**1a**) were determined through comparison of HPLC retention times with original samples of commercial available enantiopure alcohols. For 1-(2-phenanthryl)ethanol (**1c**) and 1-(2-pyrenyl)ethanol (**1d**) remaining alcohol after a kinetic resolution experiment with catalyst **3** and isobutyric anhydride (**2**, 0.6 eq) was isolated by column chromatography. The slow-reacting enantiomer of 1-(2-phenanthryl)ethanol **1c** could be identified as (-)-*(S)*-enantiomer through comparison of its optical rotation ( $[\alpha]_{25}^D = -48.4^\circ$ , 0.41 g/L, CHCl<sub>3</sub>) with literature values<sup>[9]</sup>. The slow-reacting enantiomer of 1-(2-pyrenyl)ethanol (**1d**) was esterified by a Steglich reaction with *N*-(*tert*-butoxycarbonyl)-L-phenylalanine (**S2**) (**Scheme S5**). The configuration of diastereomeric **S3** was

determined by X-ray crystal structure analysis. Absolute configuration of (*S*)-**1d** could then be determined relative to the known absolute configuration of **S2**.



**Scheme S5.** Esterification of (*S*)-1-(2-pyrenyl)ethanol (**1d**) with *N*-(*tert*-butoxycarbonyl)-*L*-phenylalanine **S2**. Right side: Single crystal X-ray crystal structure of **S3** with stereochemistry resolved relative to (*S*)-BOC-phenylalanine **S2**. For full details see Chapter 3.5.

The absolute configuration of ester products **4a** - **4d** was determined through deprotection and comparison of retention times with known alcohols.

### 2.3. Analysis of Experiments

The UV absorbance of all species in the HPLC spectra from competitive linear regression experiments as described in Chapter 2.1 were integrated. If intermediate concentrations in the UV-Vis spectrum were too small to be integrated reliably, intermediate concentrations were not determined (n.d.). Integrals were calibrated and corrected by the ratio of the enantiomers from the stock solution. All calculations were performed with Microsoft Excel if not stated differently.

Enantiomeric excess was calculated by Eq. S1, conversion (*c*) from *ee* of substrates and products by Eq. S32 and selectivity values by Eq. S25. Linear regression was performed with Microsoft Excel, graphs with linear fit and mean square error are given below.

Chemoselectivity values were calculated for the two fast reacting enantiomers and respectively for the two slow reacting enantiomers as discussed in Chapter 1.8. Only data points with a minimal conversion of 4% and a maximal conversion of 96% for both substrates are considered to avoid errors from too small absolute intermediate concentrations. On the one hand this is due to the higher relative analytical error in integrating very small values, on the other hand this can be rationalized when considering the conversion-chemoselectivity-relation as shown in **Figure S2**. As (chemo)selectivity values are always below 10 in this project, error estimation as discussed in Chapter 1.5 becomes not significant and numbers from Kagan's formulas are reliable.

Intermediate concentrations for each enantiomer  $[x]$  at a time  $t$  were calculated from the calibrated UV absorption of each compound in the HPLC spectra by Eq. S41.

$$[x]_t = \frac{[product]}{[product] + [substrate]} \cdot [x]_0 \quad \text{Eq. S41}$$

Reactions were simulated with CoPaSi<sup>[6]</sup> using the kinetic model shown in **Table S6**. Parameter estimation for those reactions was done by “Differential Evolution” algorithm (Number of generations: 2000, population size: 10).

**Table S6.** Kinetic model for the simulation of reaction course with CoPaSi.

Name	Reaction	Rate Law
cat loading	cat + anhydride -> cat-complex	Mass action (irreversible)
R-Alc1	R-Alc1 + cat-complex -> R-Est1 + cat + acid	Mass action (irreversible)
S-Alc1	S-Alc1 + cat-complex -> S-Est1 + cat + acid	Mass action (irreversible)
R-Alc2	R-Alc2 + cat-complex -> R-Est2 + cat + acid	Mass action (irreversible)
S-Alc2	S-Alc2 + cat-complex -> S-Est2 + cat + acid	Mass action (irreversible)



Run	time [min]	UV-Absorbance HPLC ( $\lambda = 285$ nm (naphthyl), ( $\lambda = 215$ nm (phenyl)), raw data [mAU])								Enantioselectivity PhEtOH 1a				Enantioselectivity NpEtOH 1b			
		R-PhEtOiPr (R)-4a	S-PhEtOiPr (S)-4a	R-NpEtOiPr (R)-4b	S-NpEtOiPr (S)-4b	R-PhEtOH (R)-1a	S-PhEtOH (S)-1a	S-NpEtOH (S)-1b	R-NpEtOH (R)-1b	$ee_{\text{product}}$	$ee_{\text{substrate}}$	c	s	$ee_{\text{product}}$	$ee_{\text{substrate}}$	c	s
2	182	1173.8	185.9	6028.3	283.8	10189.7	11018.2	11816.7	6215.0	0.731	0.030	4.0%	6.6	0.910	0.313	25.6%	28.7
2	564	2310.1	287.1	7089.9	446.9	7103.7	8633.1	8504.2	1163.7	0.782	0.089	10.2%	8.9	0.881	0.760	46.3%	36.1
2	842	3021.4	414.3	7108.9	652.9	6111.4	8097.1	7711.2	391.9	0.762	0.131	14.7%	8.4	0.831	0.904	52.1%	33.4
2	1176	3657.5	554.6	7156.1	840.5	5188.0	7652.9	6850.6	69.1	0.741	0.184	19.9%	8.0	0.789	0.980	55.4%	38.0
2	1794	5843.4	890.8	8000.4	1533.6	5025.7	8926.9	7774.5	n.d.	0.739	0.272	26.9%	8.7	0.677	n.d.	n.d.	n.d.
2	3197	4760.0	1076.8	4998.7	1497.3	1628.0	5196.8	3951.2	n.d.	0.636	0.517	44.8%	7.4	0.537	n.d.	n.d.	n.d.

**Table S8.** Chemoselectivity values for the two fast reacting and the two slow reacting enantiomers for the competition experiment shown in **Scheme S6**. To minimize influence of analytical errors, only data points with at minimum 4% and maximal 96% conversion (c) for both substrates are analysed. Selectivity was derived as described in Chapter 1.8.

Run	time [min]	c (R)-1b	c (R)-1d	total c	Chemosel	Select	StDev	Run	time [min]	c (S)-1b	c (S)-1d	total c	Chemosel	Select	StDev
1	321	69.8%	15.9%	42.8%	-0.629	0.145	0.007	1	1259	13.7%	8.2%	11.0%	-0.247	0.586	0.031
1	421	81.3%	20.4%	50.8%	-0.599	0.136		1	1806	18.2%	11.7%	15.0%	-0.220	0.616	
1	566	89.4%	26.7%	58.0%	-0.541	0.138		1	3282	28.9%	19.2%	24.0%	-0.202	0.624	
2	564	86.3%	26.6%	56.4%	-0.529	0.156		2	842	8.0%	5.4%	6.7%	-0.197	0.661	
2	842	94.9%	35.5%	65.2%	-0.456	0.147		2	1176	11.2%	7.5%	9.3%	-0.202	0.651	
-								2	1794	16.9%	10.0%	13.4%	-0.257	0.569	
-								2	3197	28.1%	18.7%	23.4%	-0.200	0.629	
					<b>average</b>	<b>0.144</b>								<b>average</b>	

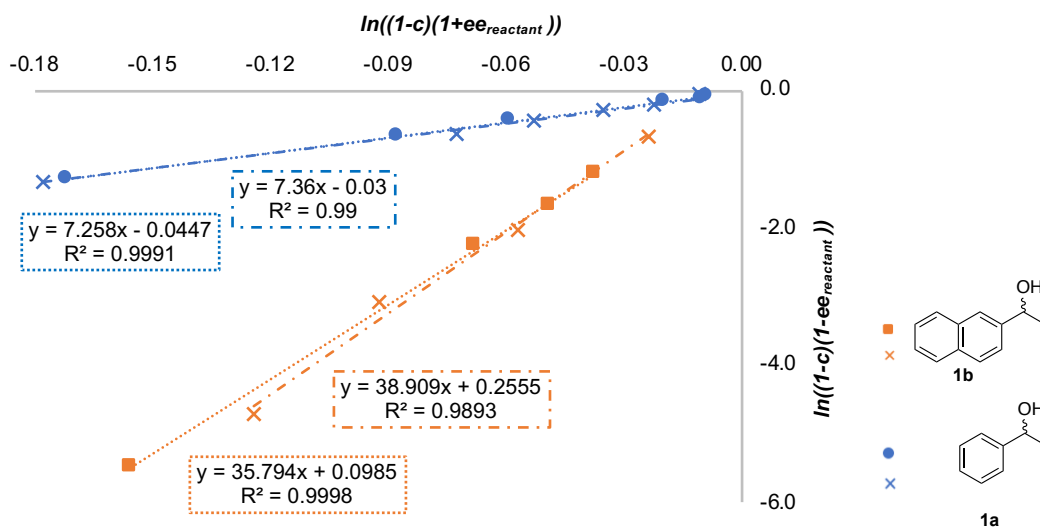


Figure S6. Linear regression analysis of two independent runs of competition experiment shown in Scheme S6.

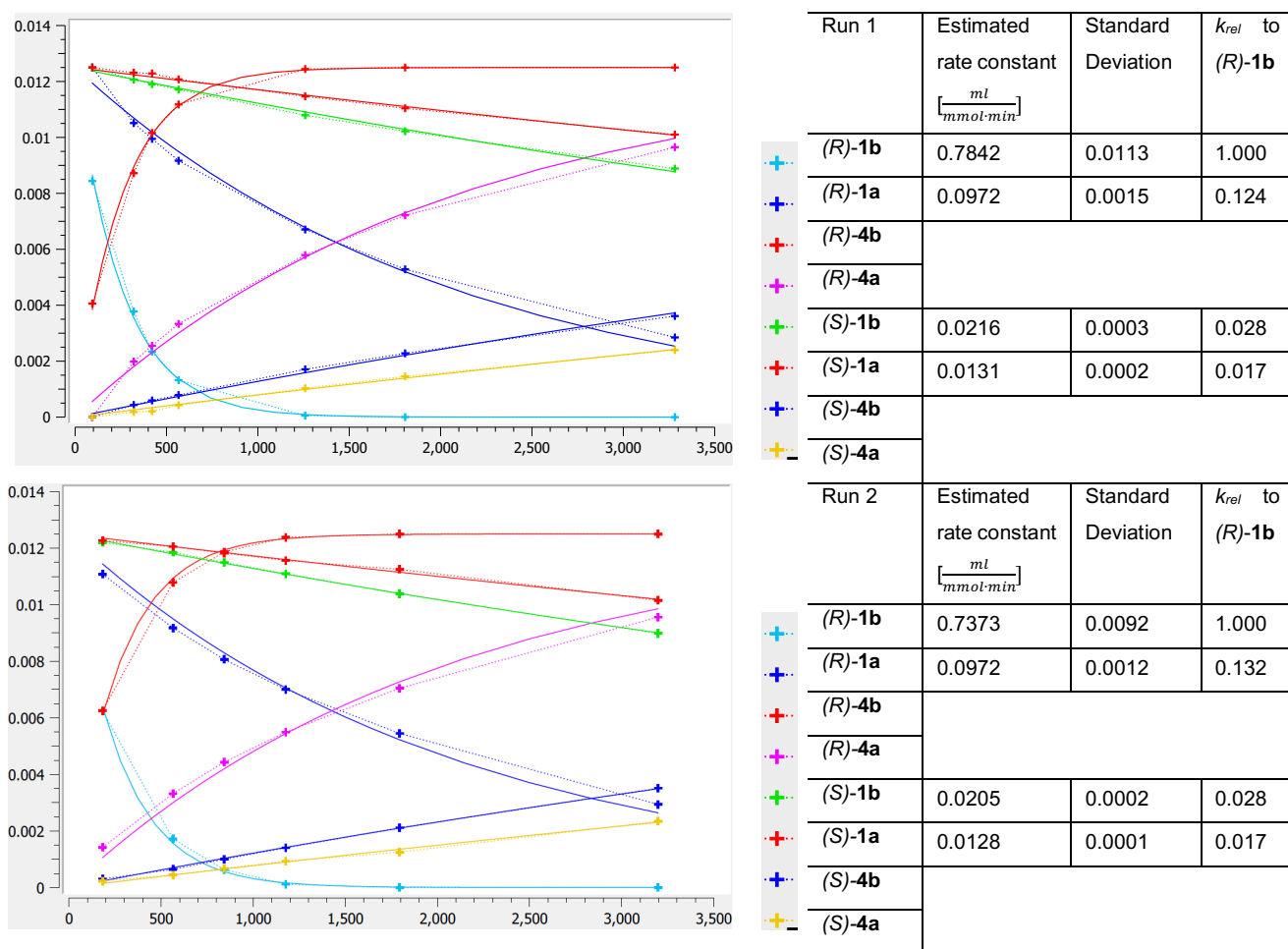
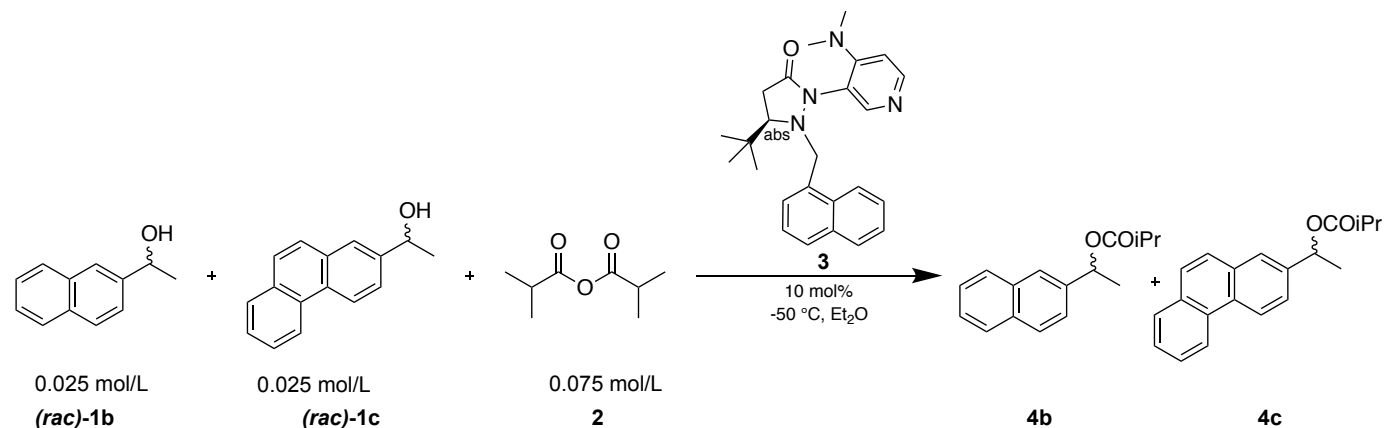


Figure S7. Parameter estimation for competition experiment shown in Scheme S6. Estimation was performed with CoPaSi<sup>[5]</sup>, x-axis shows time in min, y-axis intermediate concentration in mol/L of each species. Estimated rate constants with standard deviation for each alcohol are shown right hand.



**Scheme S7.** Competitive linear regression of *(rac)*-1-(2-naphthyl)ethanol (**1b**) (NpEtOH) and *(rac)*-1-(2-phenanthryl)ethanol (**1c**) (PhantEtOH) yielding **4b** (NpEtOiPr) and **4c** (PhantEtOiPr) with catalyst **3**.

**Table S9.** Raw HPLC absorbance data for competitive linear regression shown in **Scheme S7**. Data were calibrated and normalized from the stock solution before analysis. Concentrations too small to be integrated reliably were not determined (n.d.). Enantiomeric excess was calculated by Eq. S1, conversion (*c*) by Eq. S32 and Selectivity by Eq. S25.

Run	time [min]	UV-Absorbance HPLC ( $\lambda = 285 \text{ nm}$ ), raw data [mAU]								Enantioselectivity NpEtOH <b>1b</b>				Enantioselectivity PhantEtOH <b>1c</b>			
		R-NpEtOiPr (R)- <b>4b</b>	S-NpEtOiPr (S)- <b>4b</b>	R-Phant-EtOiPr (R)- <b>4c</b>	S-Phant-EtOiPr (S)- <b>4c</b>	S-NpEtOH (S)- <b>1b</b>	R-NpEtOH (R)- <b>1b</b>	S-Phant-EtOH (S)- <b>1c</b>	R-Phant-EtOH (R)- <b>1c</b>	$ee_{\text{product}}$	$ee_{\text{substrate}}$	<i>c</i>	<i>s</i>	$ee_{\text{product}}$	$ee_{\text{substrate}}$	<i>c</i>	<i>s</i>
1	0	-	-	-	-	2845.0	2842.9	8719.0	8705.4	-	-	-	-	-	-	-	-
1	28	252.3	n.d.	1556.9	n.d.	3589.1	3360.7	11078.5	9564.4	n.d.	0.032	n.d.	n.d.	n.d.	0.073	n.d.	n.d.
1	66	389.6	n.d.	2311.1	48.8	2689.3	2322.2	8299.8	6005.7	n.d.	0.073	n.d.	n.d.	0.959	0.160	14.3%	55.5
1	182	1063.5	37.7	5523.4	137.5	3190.4	2133.9	9977.0	4274.6	0.932	0.198	17.5%	34.3	0.951	0.399	29.6%	59.6
1	362	1235.4	54.3	5471.1	255.5	2207.2	1005.3	6744.7	1211.0	0.916	0.374	29.0%	32.8	0.911	0.695	43.3%	44.6
1	558	1252.6	60.5	4811.3	277.2	1704.1	487.3	5153.1	339.6	0.908	0.555	37.9%	36.2	0.891	0.876	49.6%	50.0
1	859	2185.0	150.6	7342.7	631.9	2375.9	298.9	7015.7	75.8	0.871	0.776	47.1%	34.1	0.842	0.979	53.8%	51.9
1	1166	1275.2	108.6	3904.7	500.6	1249.9	56.0	3713.0	n.d.	0.843	0.914	52.0%	37.5	0.773	n.d.	n.d.	n.d.
1	1791	2369.0	323.0	6832.0	1299.7	2089.4	n.d.	6027.3	n.d.	0.760	n.d.	n.d.	n.d.	0.681	n.d.	n.d.	n.d.
1	3199	2719.1	644.4	7519.4	2256.7	2162.3	n.d.	5922.5	n.d.	0.617	n.d.	n.d.	n.d.	0.539	n.d.	n.d.	n.d.

Run	time [min]	UV-Absorbance HPLC ( $\lambda = 285$ nm), raw data [mAU]								Enantioselectivity NpEtOH 1b				Enantioselectivity PhantEtOH 1c			
		R-NpEtOiPr (R)-4b	S-NpEtOiPr (S)-4b	R-Phant-EtOiPr (R)-4c	S-Phant-EtOiPr (S)-4c	S-NpEtOH (S)-1b	R-NpEtOH (R)-1b	S-Phant-EtOH (S)-1c	R-Phant-EtOH (R)-1c	$ee_{\text{product}}$	$ee_{\text{substrate}}$	c	s	$ee_{\text{product}}$	$ee_{\text{substrate}}$	c	s
2	0	-	-	-	-	4674.7	4808.4	14867.1	14587.7	-	-	-	-	-	-	-	-
2	35	277.0	n.d.	1681.9	n.d.	3163.4	3314.4	10577.0	8796.4	n.d.	n.d.	n.d.	n.d.	n.d.	0.082	n.d.	n.d.
2	75	437.1	10.3	2559.8	66.4	2694.0	2365.0	8597.2	5963.9	0.953	0.079	7.7%	44.8	0.950	0.172	15.3%	46.5
2	199	1096.5	31.5	5832.5	168.5	3202.7	2232.4	10167.9	4255.6	0.943	0.192	16.9%	40.8	0.945	0.402	29.8%	52.3
2	359	2357.3	82.6	10813.6	416.1	4434.0	2209.2	13860.8	2860.5	0.930	0.347	27.2%	38.9	0.927	0.652	41.3%	52.1
2	511	1958.6	74.3	7937.6	375.1	2843.4	1029.7	8882.9	885.4	0.925	0.479	34.1%	41.2	0.911	0.816	47.2%	54.5
2	1237	3254.9	229.3	10350.6	1066.6	3305.8	182.6	9986.2	n.d.	0.865	0.898	50.9%	42.0	0.816	n.d.	n.d.	n.d.
2	2980	3030.3	448.2	9273.0	2020.8	2680.6	n.d.	7840.4	n.d.	0.736	n.d.	n.d.	n.d.	0.648	n.d.	n.d.	n.d.

**Table S10.** Chemoselectivity values for the two fast reacting and the two slow reacting enantiomers for the competition experiment shown in **Scheme S7**. To minimize influence of analytical errors, only data points with at minimum 4% and maximal 96% conversion (c) for both substrates are analysed. Selectivity was derived as described in Chapter 1.8.

Run	time [min]	c (R)-1b	c (R)-1c	total c	Chemosel	Select	StDev	Run	time [min]	c (S)-1b	c (S)-1c	total c	Chemosel	Select	StDev
1	28	7.2%	14.5%	10.9%	0.339	2.1	0.039	1	859	6.1%	8.6%	7.4%	0.168	1.4	0.111
1	66	14.7%	28.7%	21.7%	0.321	2.1		1	1166	8.2%	12.3%	10.3%	0.201	1.5	
1	182	33.9%	57.4%	45.7%	0.257	2.1		1	1791	13.7%	18.4%	16.1%	0.145	1.4	
1	362	55.9%	82.5%	69.2%	0.193	2.1		1	3199	23.5%	28.5%	26.0%	0.096	1.3	
1	558	72.6%	93.7%	83.1%	0.127	2.1		2	1237	6.7%	10.0%	8.4%	0.202	1.5	
2	35	7.9%	16.6%	12.3%	0.355	2.2		2	2980	14.7%	21.2%	17.9%	0.181	1.5	
2	75	16.0%	30.9%	23.5%	0.319	2.1		-							
2	199	33.6%	58.9%	46.2%	0.273	2.2		-							
2	359	52.4%	79.8%	66.1%	0.208	2.2		-							
2	511	66.2%	90.3%	78.3%	0.154	2.2		-							
					<b>average</b>	<b>2.1</b>	<b>0.039</b>						<b>average</b>	<b>1.4</b>	<b>0.111</b>

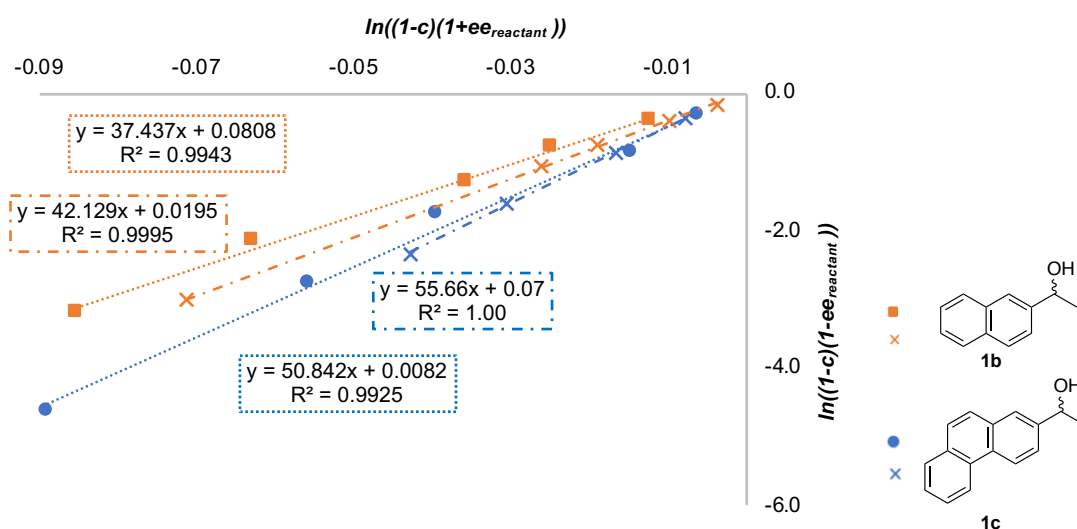


Figure S8. Linear regression analysis of two independent runs of competition experiment shown in Scheme S7.

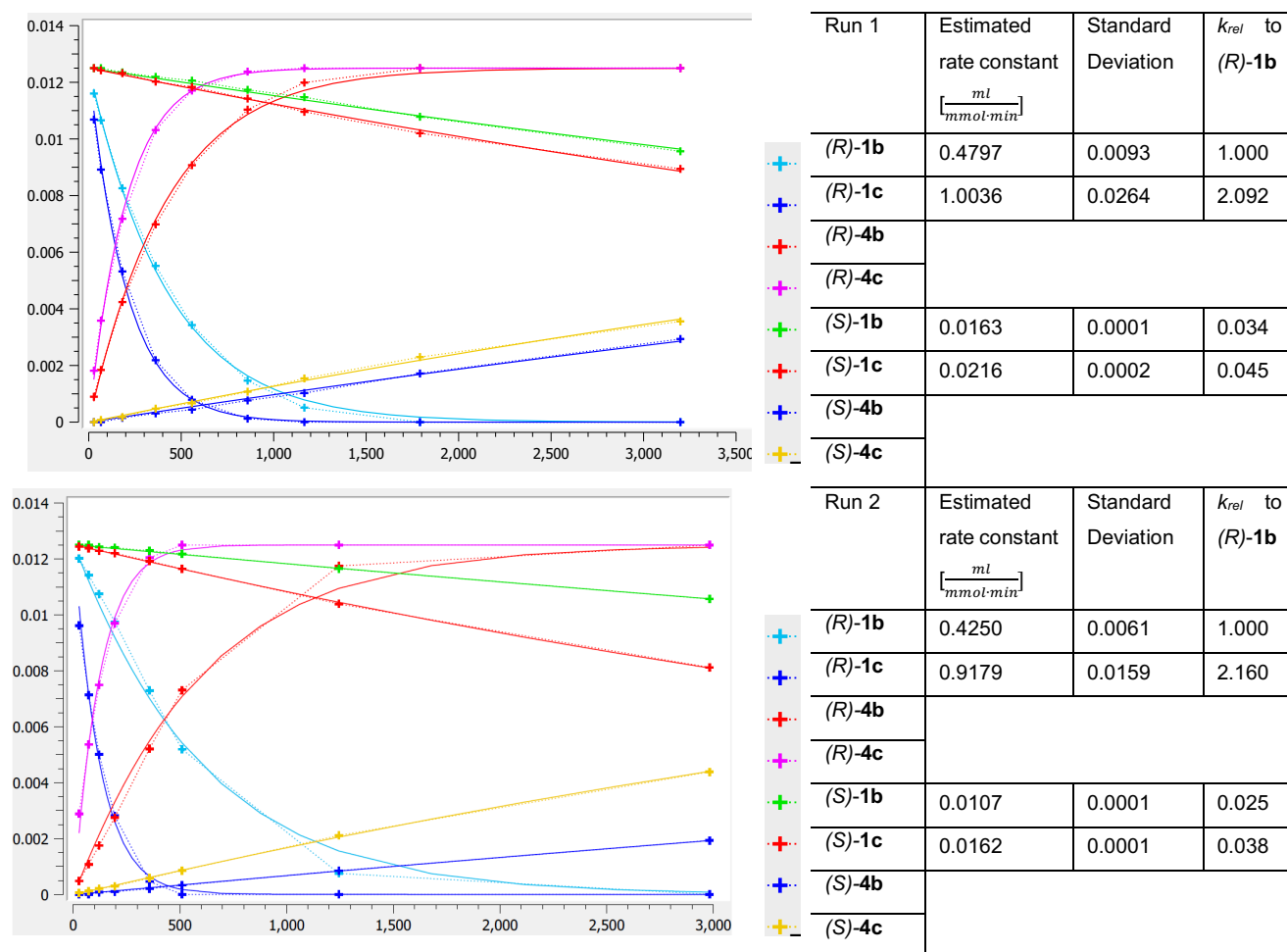
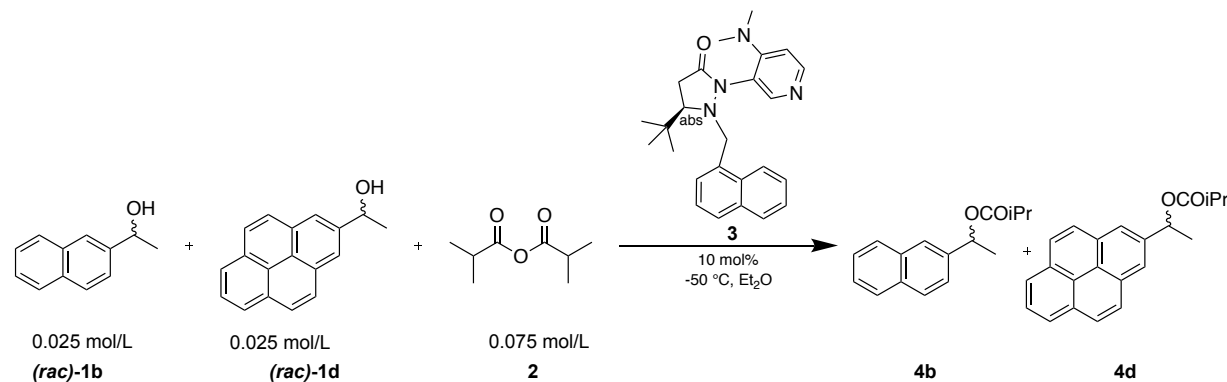


Figure S9. Parameter estimation for competition experiment shown in Scheme S7 (run 1). Estimation was performed with CoPaSi<sup>[5]</sup>, x-axis shows time in min, y-axis intermediate concentration in mol/L of each species. Estimated rate constants with standard deviation for each alcohol are shown right hand.



**Scheme S8.** Competitive linear regression of *(rac)*-1-(2-naphthyl)ethanol (**1b**) (NpEtOH) and *(rac)*-1-(2-pyrenyl)ethanol (**1d**) (PyrEtOH) yielding **4b** (NpEtOiPr) and **4a** (PyrEtOiPr) with catalyst **3**.

**Table S11.** Raw HPLC absorbance data for competitive linear regression shown in **Scheme S8**. Data were calibrated and normalized from the stock solution before analysis. Concentrations too small to be integrated reliably were not determined (n.d.). Enantiomeric excess was calculated by Eq. S1, conversion (c) by Eq. S32 and Selectivity by Eq. S25.

Run	time [min]	UV-Absorbance HPLC ( $\lambda = 285\text{ nm}$ ), raw data [mAU]								Enantioselectivity NpEtOH <b>1b</b>				Enantioselectivity PyrEtOH <b>1d</b>			
		R-NpEtOiPr (R)- <b>4b</b>	S-NpEtOiPr (S)- <b>4b</b>	R-PyrEtOiPr (R)- <b>4d</b>	S-PyrEtOiPr (S)- <b>4d</b>	S-NpEtOH (S)- <b>1b</b>	R-NpEtOH (R)- <b>1b</b>	S-PyrEtOH (S)- <b>1d</b>	R-PyrEtOH (R)- <b>1d</b>	$ee_{\text{product}}$	$ee_{\text{substrate}}$	c	s	$ee_{\text{product}}$	$ee_{\text{substrate}}$	c	s
1	0	-	-	-	-	5978.9	5985.5	7365.4	7703.8	-	-	-	-	-	-	-	-
1	25	132.2	n.d.	887.3	n.d.	3245.5	3122.6	4156.5	3451.3	n.d.	0.020	n.d.	n.d.	n.d.	0.115	10.3%	n.d.
1	62	258.6	n.d.	1579.6	25.6	3065.5	2813.9	3979.0	2500.4	n.d.	0.043	n.d.	n.d.	0.967	0.249	20.5%	75.4
1	117	450.0	16.2	2249.1	38.6	2967.4	2533.2	3833.9	1566.2	0.931	0.079	7.9%	30.1	0.965	0.438	31.2%	85.8
1	176	704.2	24.5	2864.4	85.6	3079.3	2346.9	3882.3	926.3	0.933	0.136	12.7%	32.7	0.939	0.629	40.1%	61.0
1	360	1541.3	62.4	3725.6	203.5	3319.8	1814.9	4116.3	99.5	0.922	0.294	24.2%	32.8	0.892	0.955	51.7%	66.5
1	563	1806.3	81.3	3134.5	281.2	2668.4	903.9	3326.3	n.d.	0.914	0.494	35.1%	36.3	0.828	n.d.	n.d.	n.d.
1	854	2586.0	164.2	3546.2	522.7	2983.2	479.7	3572.4	n.d.	0.880	0.723	45.1%	34.0	0.733	n.d.	n.d.	n.d.
1	1174	4188.7	344.0	5072.2	1037.5	4309.0	299.3	4828.2	n.d.	0.848	0.870	50.6%	34.3	0.648	n.d.	n.d.	n.d.
1	1789	3354.4	389.5	3937.3	1192.7	3109.6	31.9	3412.7	n.d.	0.792	0.980	55.3%	38.4	0.519	n.d.	n.d.	n.d.
1	4688	2514.6	668.7	2981.2	1747.6	1921.7	n.d.	1581.7	n.d.	0.579	n.d.	n.d.	n.d.	0.240	n.d.	n.d.	n.d.

Run	time [min]	UV-Absorbance HPLC ( $\lambda = 285$ nm), raw data [mAU]								Enantioselectivity NpEtOH 1b				Enantioselectivity PyrEtOH 1d			
		R-NpEtOiPr (R)-4b	S-NpEtOiPr (S)-4b	R-PyrEtOiPr (R)-4d	S-PyrEtOiPr (S)-4d	S-NpEtOH (S)-1b	R-NpEtOH (R)-1b	S-PyrEtOH (S)-1d	R-PyrEtOH (R)-1d	$ee_{\text{product}}$	$ee_{\text{substrate}}$	c	s	$ee_{\text{product}}$	$ee_{\text{substrate}}$	c	s
2	0	-	-	-	-	3622.7	3810.1	5121.0	5283.3	-	-	-	-	-	-	-	-
2	28	132.7	n.d.	1025.2	19.4	3308.1	3415.0	4735.6	3792.2	n.d.	0.009	n.d.	n.d.	0.962	0.126	11.6%	58.0
2	73	220.2	n.d.	1469.7	30.9	2458.8	2397.3	3622.4	2164.8	n.d.	0.038	n.d.	n.d.	0.957	0.266	21.8%	59.7
2	122	569.9	22.8	3125.3	83.6	3924.1	3586.6	5494.5	2312.3	0.919	0.070	7.1%	25.5	0.946	0.421	30.8%	54.8
2	195	717.9	23.7	3234.9	96.8	3125.9	2610.6	4486.4	1037.4	0.933	0.115	11.0%	32.2	0.940	0.634	40.3%	62.2
2	358	1850.4	70.1	5168.2	258.7	4319.4	2653.7	5898.1	218.5	0.923	0.263	22.1%	32.4	0.902	0.931	50.8%	66.0
2	510	2233.8	96.4	4627.6	333.9	3693.6	1626.1	5047.0	n.d.	0.913	0.410	31.0%	32.9	0.861	n.d.	n.d.	n.d.
2	1245	3421.5	245.5	4583.0	811.1	3466.6	224.2	4430.3	n.d.	0.860	0.884	50.7%	38.8	0.691	n.d.	n.d.	n.d.
2	2982	2160.9	333.6	2818.5	1058.4	1872.5	n.d.	2170.1	n.d.	0.721	n.d.	n.d.	n.d.	0.442	n.d.	n.d.	n.d.

**Table S12.** Chemoselectivity values for the two fast reacting and the two slow reacting enantiomers for the competition experiment shown in **Scheme S8**. To minimize influence of analytical errors, only data points with at minimum 4% and maximal 96% conversion (c) for both substrates are analysed. Selectivity was derived as described in Chapter 1.8.

Run	time [min]	c (R)-1b	c (R)-1d	total c	Chemosel	Select	StDev	Run	time [min]	c (S)-1b	c (S)-1d	total c	Chemosel	Select	StDev
1	62	8.6%	41.2%	24.9%	0.654	5.9		1	1174	7.6%	19.2%	13.4%	0.435	2.7	
1	117	15.4%	61.4%	38.4%	0.599	5.7		1	1789	11.4%	27.9%	19.6%	0.421	2.7	
1	176	23.5%	77.4%	50.5%	0.534	5.5		1	4688	26.3%	55.0%	40.7%	0.353	2.6	
2	73	8.6%	42.9%	25.8%	0.666	6.2		2	1245	6.8%	16.9%	11.8%	0.427	2.6	
2	122	14.0%	59.9%	37.0%	0.621	6.1		2	2982	15.4%	35.1%	25.3%	0.389	2.6	
2	195	22.0%	77.5%	49.8%	0.558	6.0		-							
					<b>average</b>	<b>5.9</b>		<b>0.231</b>						<b>average</b>	

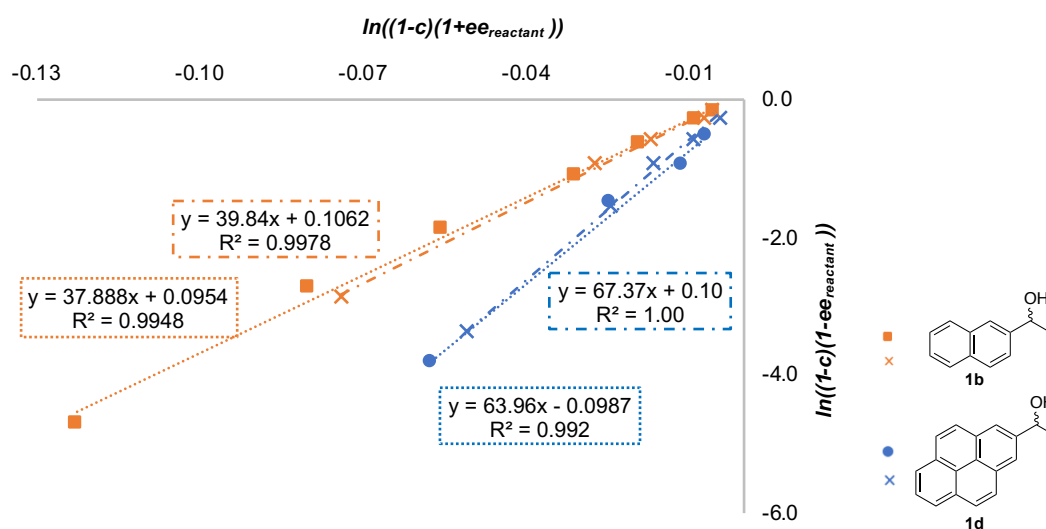


Figure S10. Linear regression analysis of two independent runs of competition experiment shown in **Scheme S8**.

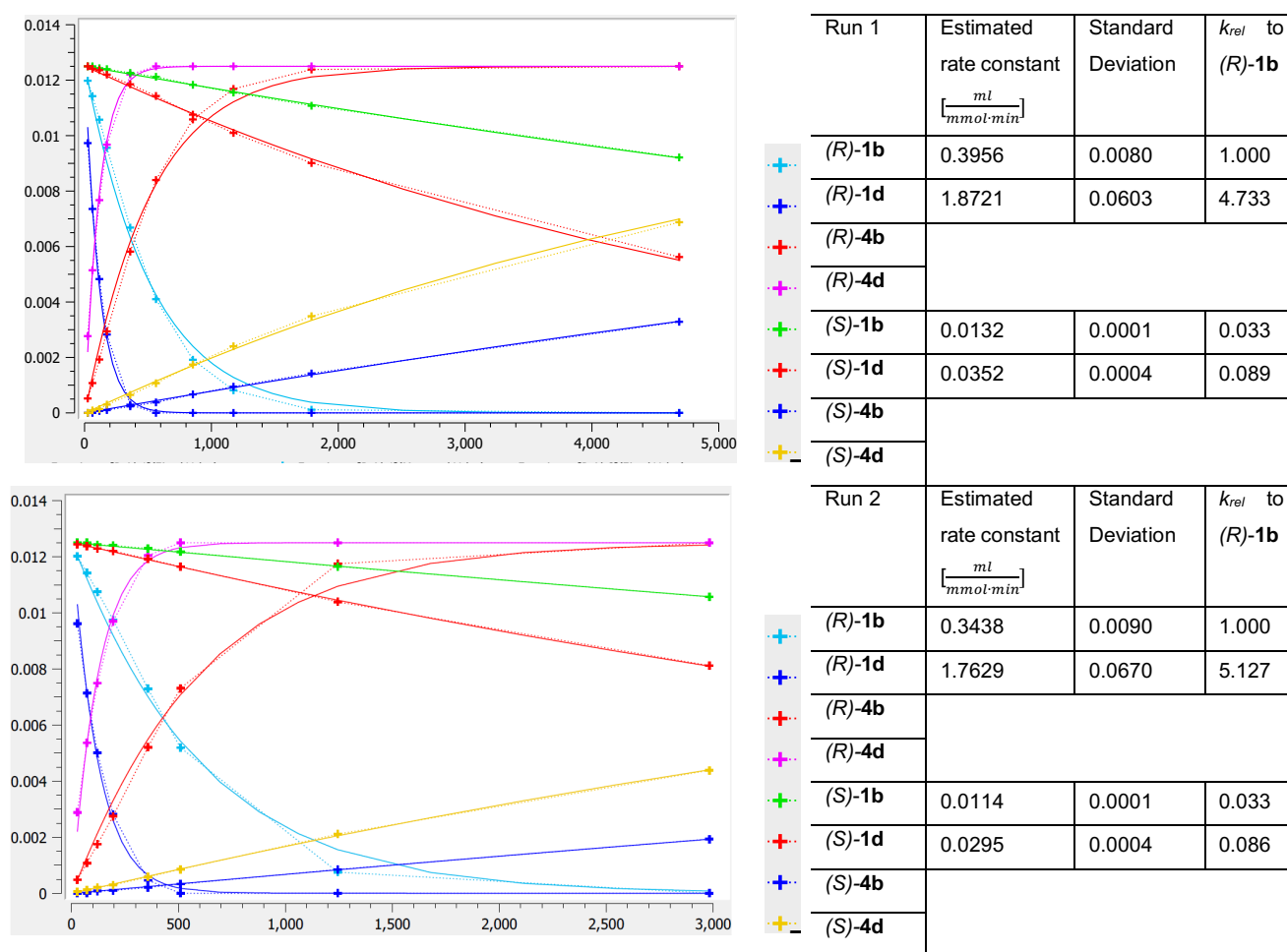
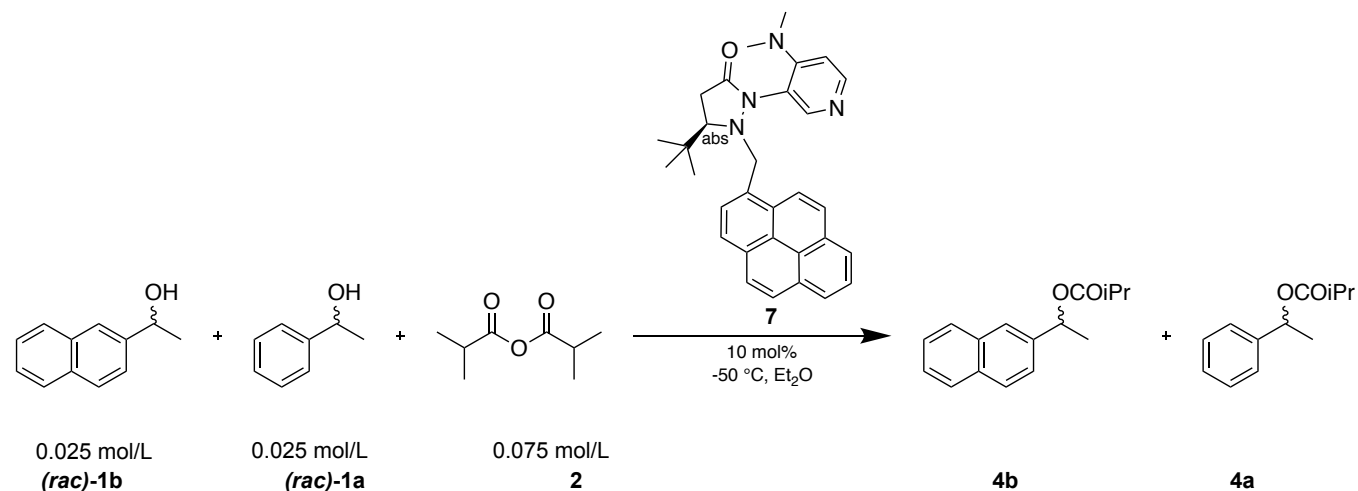


Figure S11. Parameter estimation for competition experiment shown in **Scheme S8**. Estimation was performed with CoPaSi<sup>[5]</sup>, x-axis shows time in min, y-axis intermediate concentration in mol/L of each species. Estimated rate constants with standard deviation for each alcohol are shown right hand.



**Scheme S9.** Competitive linear regression of (*rac*)-1-(2-naphthyl)ethanol (**1b**) (NpEtOH) and (*rac*)-1-phenylethanol (**1a**) (PhEtOH) yielding **4b** (NpEtOiPr) and **4a** (PhEtOiPr) with catalyst **7**.

**Table S13.** Raw HPLC absorbance data for competitive linear regression shown in **Scheme S9**. Data were calibrated and normalized from the stock solution before analysis. Concentrations too small to be integrated reliably were not determined (n.d.). Enantiomeric excess was calculated by Eq. S1, conversion (c) by Eq. S32 and Selectivity by Eq. S25.

Run	time [min]	UV-Absorbance HPLC ( $\lambda = 285 \text{ nm}$ (naphthyl), ( $\lambda = 215 \text{ nm}$ (phenyl)), raw data [mAU]								Enantioselectivity PhEtOH <b>1a</b>				Enantioselectivity NpEtOH <b>1b</b>			
		R-PhEtOiPr (R)- <b>4a</b>	S-PhEtOiPr (S)- <b>4a</b>	R-NpEtOiPr (R)- <b>4b</b>	S-NpEtOiPr (S)- <b>4b</b>	R-PhEtOH (R)- <b>1a</b>	S-PhEtOH (S)- <b>1a</b>	S-NpEtOH (S)- <b>1b</b>	R-NpEtOH (R)- <b>1b</b>	$ee_{\text{product}}$	$ee_{\text{substrate}}$	c	s	$ee_{\text{product}}$	$ee_{\text{substrate}}$	c	s
1	0	-	-	-	-	7327.0	7508.6	7359.2	7427.4	-	-	-	-	-	-	-	-
1	92	144.0	n.d.	920.4	25.4	7935.7	8171.6	8226.8	7376.6	n.d.	n.d.	n.d.	n.d.	0.946	0.059	5.9%	38.0
1	201	220.1	n.d.	1246.4	38.2	5917.8	6138.4	5740.1	4510.9	n.d.	0.006	n.d.	n.d.	0.940	0.124	11.7%	36.5
1	321	403.9	n.d.	2271.7	75.3	6558.8	6905.7	6657.4	4433.6	n.d.	0.014	n.d.	n.d.	0.935	0.205	18.0%	36.5
1	421	534.4	n.d.	2720.1	98.0	6295.3	6746.5	6249.6	3598.1	n.d.	0.022	n.d.	n.d.	0.930	0.274	22.7%	35.9
1	566	903.4	129.7	4366.2	170.4	7296.5	7990.1	7688.8	3413.6	0.754	0.033	4.2%	7.4	0.924	0.389	29.6%	37.2
1	1259	2157.5	220.5	6588.3	362.8	6349.4	7734.7	7483.8	821.4	0.819	0.086	9.5%	10.9	0.895	0.804	47.3%	44.4
1	1806	3030.9	359.0	6730.7	496.8	5406.9	7363.5	6993.6	179.9	0.793	0.141	15.1%	9.9	0.861	0.950	52.5%	49.6
1	3282	5138.3	799.4	6757.6	986.6	3348.3	6978.1	6299.0	n.d.	0.736	0.341	31.6%	9.2	0.743			

Run	time [min]	UV-Absorbance HPLC ( $\lambda = 285$ nm (naphthyl), ( $\lambda = 215$ nm (phenyl)), raw data [mAU])								Enantioselectivity PhEtOH 1a				Enantioselectivity NpEtOH 1b			
		R-PhEtOiPr (R)-4a	S-PhEtOiPr (S)-4a	R-NpEtOiPr (R)-4b	S-NpEtOiPr (S)-4b	R-PhEtOH (R)-1a	S-PhEtOH (S)-1a	S-NpEtOH (S)-1b	R-NpEtOH (R)-1b	$ee_{\text{product}}$	$ee_{\text{substrate}}$	c	s	$ee_{\text{product}}$	$ee_{\text{substrate}}$	c	s
2	0	-	-	-	-	4652.7	4733.3	4102.3	4123.1	-	-	-	-	-	-	-	-
2	74	260.6	n.d.	1327.9	52.7	10433.5	10854.9	11743.9	10507.2	n.d.	0.011	n.d.	n.d.	0.923	0.058	5.9%	26.6
2	188	444.6	n.d.	2890.1	84.8	8264.7	8761.5	8807.7	6174.6	n.d.	0.021	n.d.	n.d.	0.943	0.178	15.9%	40.4
2	571	968.1	n.d.	4092.2	164.8	5799.3	6586.7	6096.1	1914.6	n.d.	0.055	n.d.	n.d.	0.922	0.524	36.2%	41.7
2	846	1632.6	201.3	5294.4	263.7	5860.8	7037.3	6482.9	1042.9	0.784	0.083	9.5%	9.0	0.905	0.724	44.5%	43.3
2	1180	3316.7	371.2	8206.8	530.1	7239.3	9263.3	9151.0	481.0	0.802	0.114	12.5%	10.2	0.878	0.901	50.6%	47.3
2	1798	4876.3	569.7	9436.3	871.1	6224.9	9187.3	8969.2	61.6	0.794	0.184	18.8%	10.4	0.830	0.986	54.3%	52.5
2	3201	4874.9	762.8	6198.9	971.1	2657.9	6191.7	5329.3	n.d.	0.733	0.392	34.8%	9.5	0.728	n.d.	n.d.	n.d.

**Table S14.** Chemoselectivity values for the two fast reacting and the two slow reacting enantiomers for the competition experiment shown in **Scheme S9**. To minimize influence of analytical errors, only data points with at minimum 4% and maximal 96% conversion (c) for both substrates are analysed. Selectivity was derived as described in Chapter 1.8.

Run	time [min]	c (R)-1b	c (R)-1d	total c	Chemosel	Select	StDev	Run	time [min]	c (S)-1b	c (S)-1d	total c	Chemosel	Select	StDev
1	201	22.2%	4.0%	13.1%	-0.696	0.162	0.005	1	1259	4.8%	3.1%	3.9%	-0.215	0.640	0.036
1	321	34.6%	6.4%	20.5%	-0.687	0.156		1	1806	6.8%	5.1%	6.0%	-0.140	0.747	
1	421	43.8%	8.6%	26.2%	-0.671	0.157		1	3282	13.9%	11.3%	12.6%	-0.103	0.801	
1	566	56.9%	12.1%	34.5%	-0.649	0.153		2	1798	9.1%	6.5%	7.8%	-0.170	0.699	
1	1259	89.2%	27.4%	58.3%	-0.530	0.144		2	3201	15.8%	12.1%	13.9%	-0.135	0.746	
2	188	32.5%	5.6%	19.1%	-0.704	0.148		-							
2	571	68.8%	15.7%	42.2%	-0.629	0.146		-							
2	846	84.0%	23.7%	53.8%	-0.560	0.147		-							
2	1180	94.6%	33.8%	64.2%	-0.474	0.141		-							
					<b>average</b>	<b>0.149</b>								<b>average</b>	

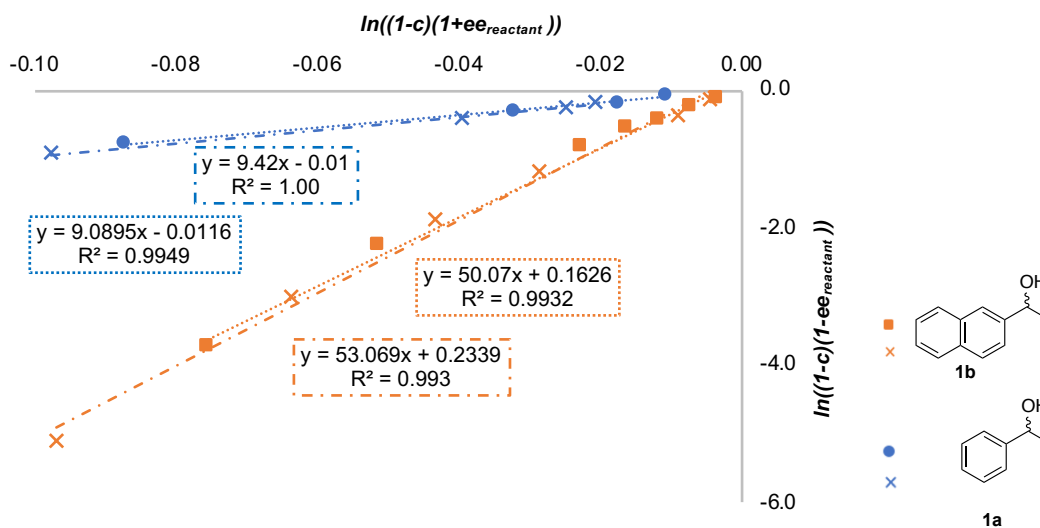


**Figure S12.** Linear regression analysis of two independent runs of competition experiment shown in **Scheme S9**.

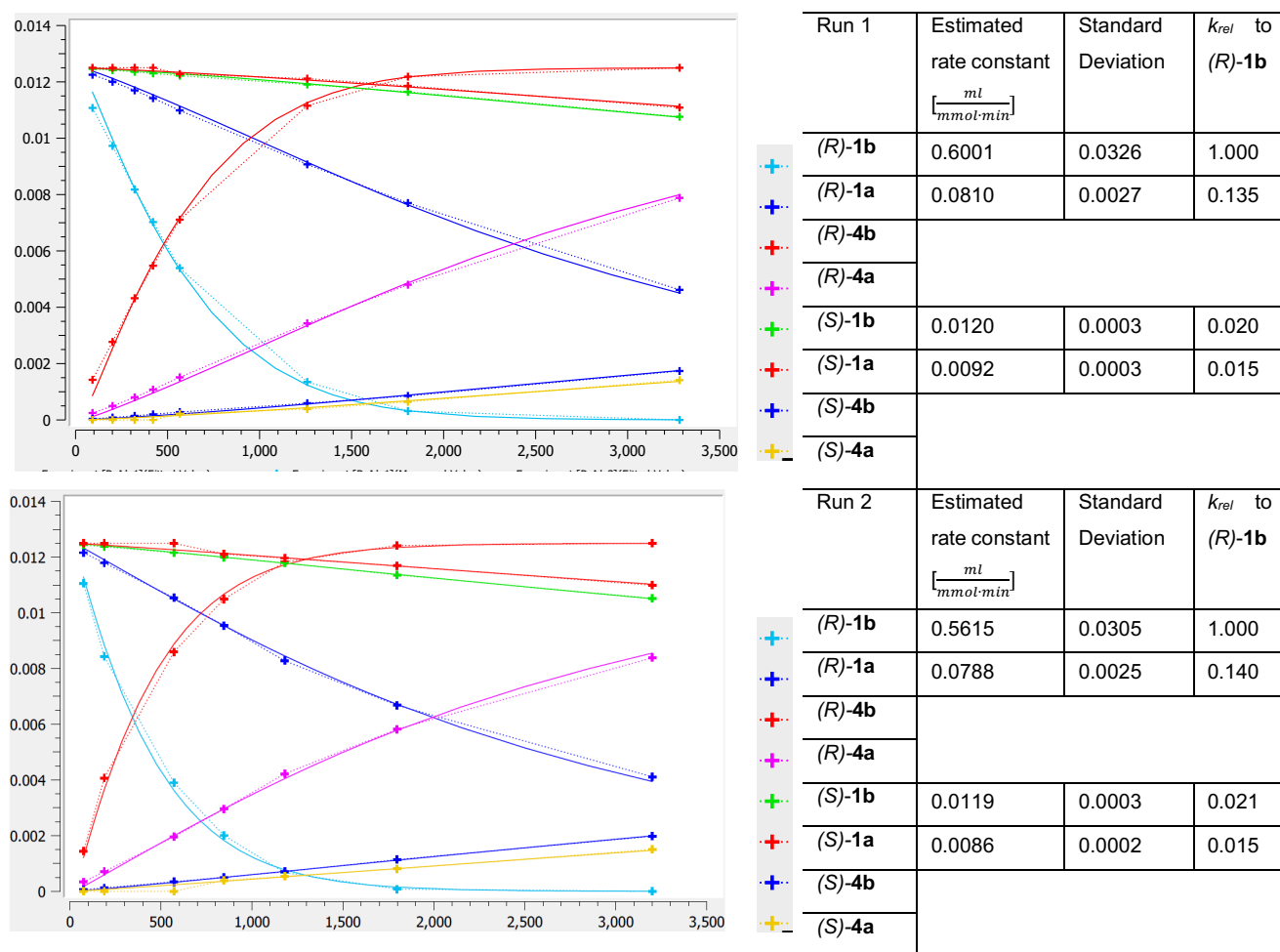
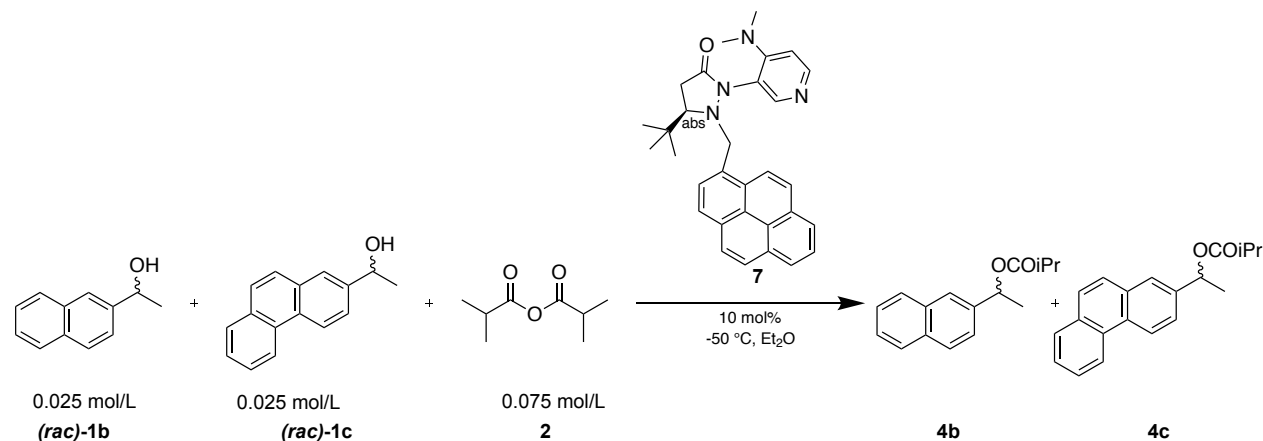


**Figure S13.** Parameter estimation for competition experiment shown in **Scheme S9**. Estimation was performed with CoPaSi<sup>[5]</sup>, x-axis shows time in min, y-axis intermediate concentration in mol/L of each species. Estimated rate constants with standard deviation for each alcohol are shown right hand.



**Scheme S10.** Competitive linear regression of (*rac*)-1-(2-naphthyl)ethanol (**1b**) (NpEtOH) and (*rac*)-1-(2-phenanthryl)ethanol (**1c**) (PhantEtOH) yielding **4b** (NpEtOiPr) and **4c** (PhantEtOiPr) with catalyst **7**.

**Table S15.** Raw HPLC absorbance data for competitive linear regression shown in **Scheme S10**. Data were calibrated and normalized from the stock solution before analysis. Concentrations too small to be integrated reliably were not determined (n.d.). Enantiomeric excess was calculated by Eq. S1, conversion (*c*) by Eq. S32 and Selectivity by Eq. S25.

Run	time [min]	UV-Absorbance HPLC ( $\lambda = 285$ nm), raw data [mAU]								Enantioselectivity NpEtOH <b>1b</b>				Enantioselectivity PhantEtOH <b>1c</b>			
		R-NpEtOiPr ( <i>R</i> )- <b>4b</b>	S-NpEtOiPr ( <i>S</i> )- <b>4b</b>	R-Phant-EtOiPr ( <i>R</i> )- <b>4c</b>	S-Phant-EtOiPr ( <i>S</i> )- <b>4c</b>	S-NpEtOH ( <i>S</i> )- <b>1b</b>	R-NpEtOH ( <i>R</i> )- <b>1b</b>	S-Phant-EtOH ( <i>S</i> )- <b>1c</b>	R-Phant-EtOH ( <i>R</i> )- <b>1c</b>	<i>ee</i> <sub>product</sub>	<i>ee</i> <sub>substrate</sub>	<i>c</i>	<i>s</i>	<i>ee</i> <sub>product</sub>	<i>ee</i> <sub>substrate</sub>	<i>c</i>	<i>s</i>
1	0	-	-	-	-	2845.0	2842.9	8719.0	8705.4	-	-	-	-	-	-	-	-
1	28	146.1	n.d.	997.7	n.d.	4112.9	4037.7	12545.1	11757.1	n.d.	0.009	n.d.	n.d.	n.d.	0.032	n.d.	n.d.
1	66	279.6	10.4	1913.5	64.2	4803.1	4586.6	14785.1	12938.7	0.928	0.023	2.4%	27.4	0.935	0.066	6.6%	31.9
1	182	634.6	21.3	3904.8	97.8	4144.8	3554.1	13085.0	9342.6	0.935	0.076	7.5%	32.1	0.951	0.166	14.9%	47.0
1	362	561.9	14.9	3283.4	64.4	2197.6	1655.9	6806.8	3468.3	0.948	0.140	12.9%	43.3	0.962	0.324	25.2%	70.1
1	558	1336.8	36.2	6884.4	177.1	3435.6	2156.5	10566.0	3556.0	0.947	0.228	19.4%	46.1	0.950	0.496	34.3%	63.8
1	859	1600.1	43.8	7176.4	213.9	2862.1	1299.1	8759.1	1431.6	0.947	0.375	28.4%	52.9	0.942	0.719	43.3%	72.4
1	1166	2061.8	73.4	8211.9	332.1	2944.2	881.3	8968.0	602.1	0.931	0.539	36.7%	48.3	0.922	0.874	48.7%	71.1
1	1791	2635.9	128.2	8786.0	541.6	2939.5	341.2	8915.5	66.5	0.907	0.792	46.6%	49.8	0.884	0.985	52.7%	78.6
1	3199	2273.9	187.7	6784.2	783.8	2179.6	n.d.	6525.6	n.d.	0.848	n.d.	n.d.	n.d.	0.793	n.d.	n.d.	n.d.

Run	time [min]	UV-Absorbance HPLC ( $\lambda = 285$ nm), raw data [mAU]								Enantioselectivity NpEtOH 1b				Enantioselectivity PhantEtOH 1c			
		R-NpEtOiPr (R)-4b	S-NpEtOiPr (S)-4b	R-Phant-EtOiPr (R)-4c	S-Phant-EtOiPr (S)-4c	S-NpEtOH (S)-1b	R-NpEtOH (R)-1b	S-Phant-EtOH (S)-1c	R-Phant-EtOH (R)-1c	$ee_{\text{product}}$	$ee_{\text{substrate}}$	c	s	$ee_{\text{product}}$	$ee_{\text{substrate}}$	c	s
2	0	-	-	-	-	4674.7	4808.4	14867.1	14587.7	-	-	-	-	-	-	-	-
2	35	125.7	n.d.	828.7	n.d.	2642.8	2594.4	8359.4	7487.4	n.d.	0.023	n.d.	n.d.	n.d.	0.046	n.d.	n.d.
2	74	206.8	n.d.	1343.0	n.d.	2261.1	2114.0	7072.3	5777.0	n.d.	0.048	n.d.	n.d.	n.d.	0.091	n.d.	n.d.
2	198	711.6	14.1	4295.3	66.2	3521.4	2903.1	11103.3	6698.0	0.960	0.110	10.3%	54.7	0.970	0.239	19.7%	83.5
2	360	1090.2	22.2	5983.2	100.1	3331.1	2318.6	10405.0	4306.3	0.959	0.193	16.7%	57.5	0.968	0.407	29.6%	90.9
2	510	1529.6	38.0	7750.4	170.6	3518.1	2078.5	11073.9	3073.0	0.950	0.270	22.1%	51.0	0.958	0.559	36.9%	81.4
2	2982	2828.8	207.8	8661.2	831.6	2738.0	n.d.	8402.6	n.d.	0.859	n.d.	n.d.	n.d.	0.828	n.d.	n.d.	n.d.

**Table S16.** Chemoselectivity values for the two fast reacting and the two slow reacting enantiomers for the competition experiment shown in **Scheme S10**. To minimize influence of analytical errors, only data points with at minimum 4% and maximal 96% conversion (c) for both substrates are analysed. Selectivity was derived as described in Chapter 1.8.

Run	time [min]	c (R)-1b	c (R)-1c	total c	Chemosel	Select	StDev	Run	time [min]	c (S)-1b	c (S)-1c	total c	Chemosel	Select	StDev
1	66	5.9%	13.4%	9.6%	0.387	2.4	0.043	1	1791	4.3%	6.0%	5.1%	0.162	1.4	0.042
1	182	15.5%	30.4%	23.0%	0.323	2.1		1	3199	8.1%	11.1%	9.6%	0.155	1.4	
1	362	25.9%	49.7%	37.8%	0.315	2.3		2	2982	7.3%	9.4%	8.3%	0.127	1.3	
1	558	39.0%	66.9%	52.9%	0.264	2.2		-							
1	859	55.9%	84.0%	69.9%	0.200	2.2		-							
1	1166	70.7%	93.4%	82.1%	0.139	2.2		-							
2	74	9.2%	19.5%	14.3%	0.362	2.3		-							
2	198	20.2%	40.1%	30.1%	0.331	2.3		-							
2	360	32.6%	59.2%	45.9%	0.289	2.3		-							
					<b>average</b>	<b>2.2</b>								<b>average</b>	

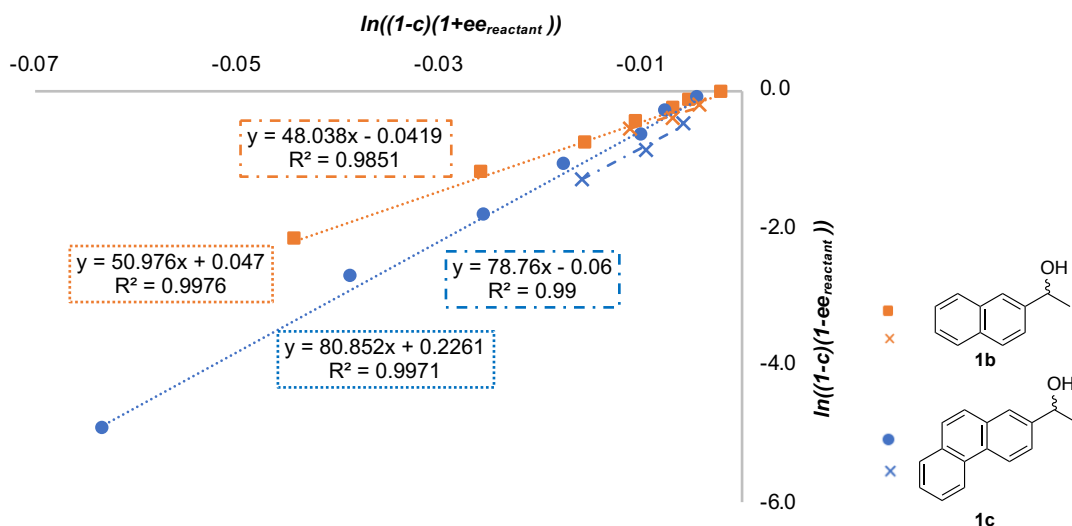


**Figure S14.** Linear regression analysis of two independent runs of competition experiment shown in **Scheme S10**.

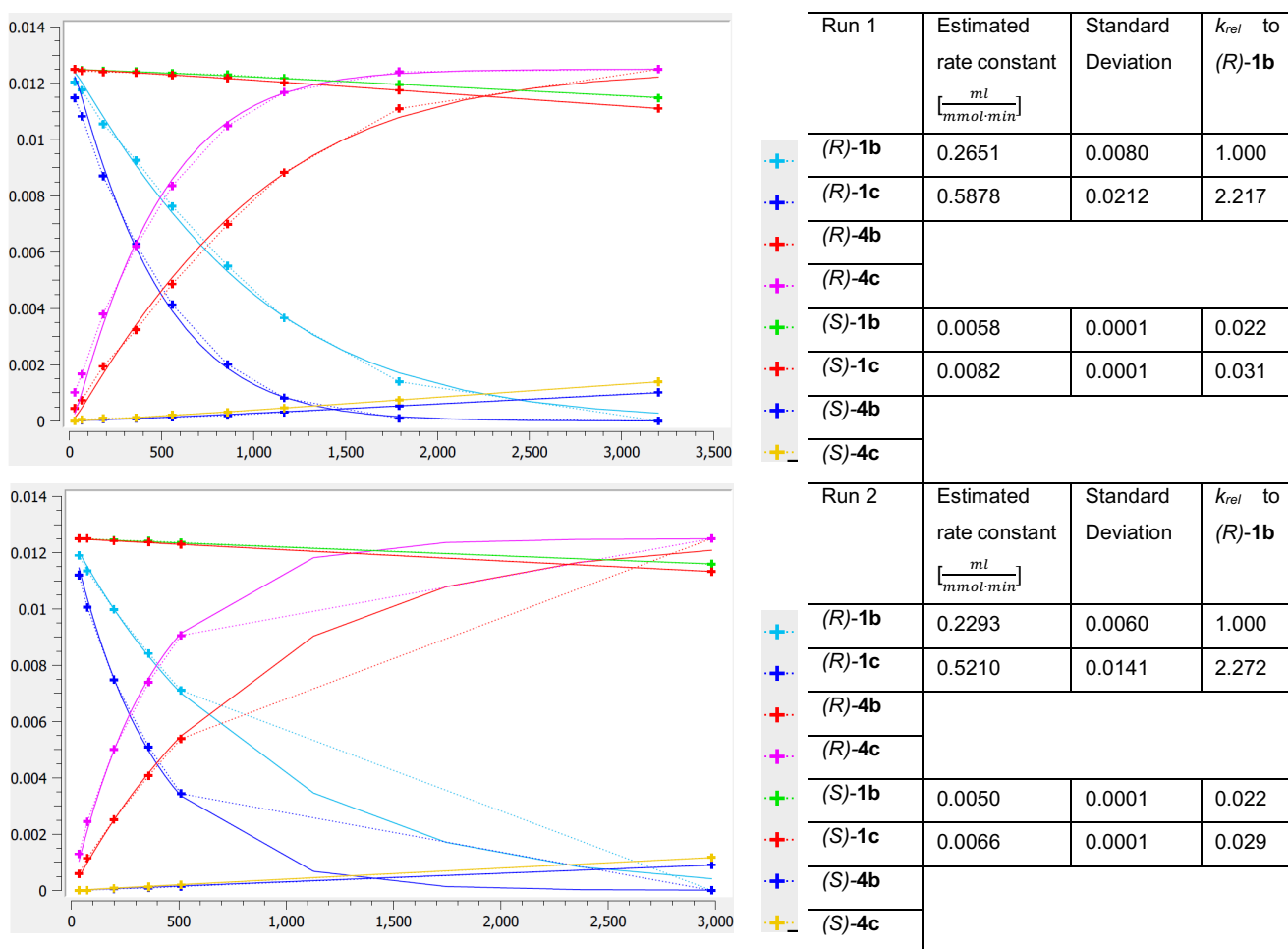
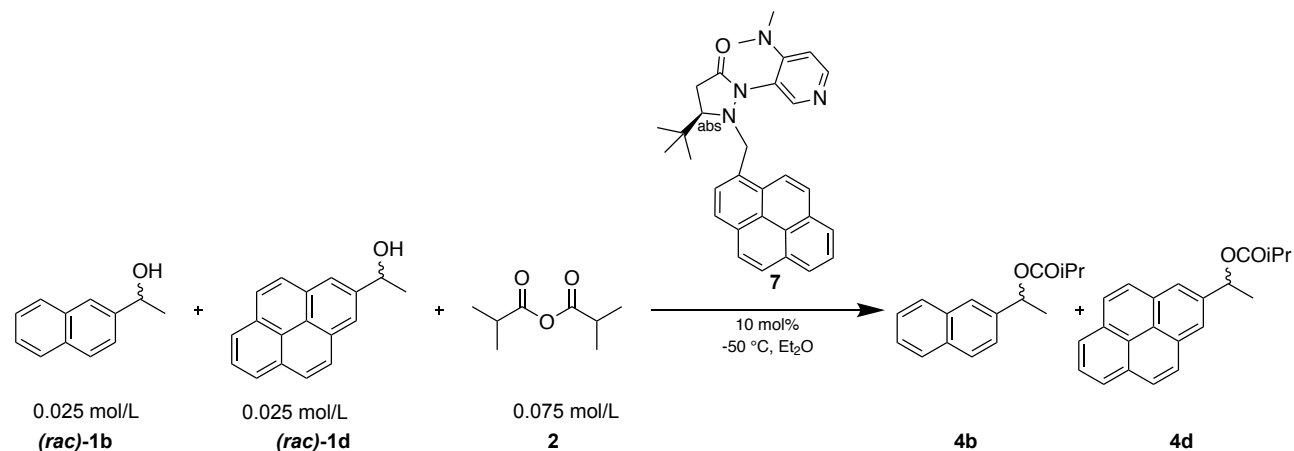


**Figure S15.** Parameter estimation for competition experiment shown in **Scheme S10**. Estimation was performed with CoPaSi<sup>[5]</sup>, x-axis shows time in min, y-axis intermediate concentration in mol/L of each species. Estimated rate constants with standard deviation for each alcohol are shown right hand.



**Scheme S11.** Competitive linear regression of *(rac)*-1-(2-naphthyl)ethanol (**1b**) (NpEtOH) and *(rac)*-1-(2-pyrenyl)ethanol (**1d**) (PyrEtOH) yielding **4b** (NpEtOiPr) and **4a** (PyrEtOiPr) with catalyst **7**.

**Table S17.** Raw HPLC absorbance data for competitive linear regression shown in **Scheme S11**. Data were calibrated and normalized from the stock solution before analysis. Concentrations too small to be integrated reliably were not determined (n.d.). Enantiomeric excess was calculated by Eq. S1, conversion (c) by Eq. S32 and Selectivity by Eq. S25.

Run	time [min]	UV-Absorbance HPLC ( $\lambda = 285\text{ nm}$ ), raw data [mAU]								Enantioselectivity NpEtOH <b>1b</b>				Enantioselectivity PyrEtOH <b>1d</b>			
		R-NpEtOiPr ( <i>R</i> )- <b>4b</b>	S-NpEtOiPr ( <i>S</i> )- <b>4b</b>	R-PyrEtOiPr ( <i>R</i> )- <b>4d</b>	S-PyrEtOiPr ( <i>S</i> )- <b>4d</b>	S-NpEtOH ( <i>S</i> )- <b>1b</b>	R-NpEtOH ( <i>R</i> )- <b>1b</b>	S-PyrEtOH ( <i>S</i> )- <b>1d</b>	R-PyrEtOH ( <i>R</i> )- <b>1d</b>	$ee_{\text{product}}$	$ee_{\text{substrate}}$	c	S	$ee_{\text{product}}$	$ee_{\text{substrate}}$	c	S
1	0	-	-	-	-	5978.9	5985.5	7365.4	7703.8	-	-	-	-	-	-	-	-
1	25	69.6	n.d.	536.5	n.d.	3555.5	3485.0	4569.7	4229.6	n.d.	0.011	n.d.	n.d.	n.d.	0.061	n.d.	n.d.
1	64	79.7	n.d.	575.2	n.d.	2183.1	2109.0	2933.4	2432.3	n.d.	0.018	n.d.	n.d.	n.d.	0.116	n.d.	n.d.
1	119	219.7	7.4	1576.7	16.8	3679.0	3458.1	4713.4	3321.3	0.935	0.032	3.3%	30.5	0.978	0.195	16.6%	108.6
1	178	242.4	7.3	1535.1	18.0	2664.1	2428.9	3511.7	1993.8	0.942	0.047	4.7%	34.9	0.976	0.296	23.3%	109.2
1	366	614.3	19.2	2841.8	30.8	3089.6	2516.0	3995.4	962.7	0.939	0.103	9.9%	35.3	0.978	0.626	39.0%	168.1
1	566	1118.2	26.2	3529.8	55.1	3217.2	2135.1	4154.8	239.8	0.954	0.203	17.5%	51.9	0.968	0.895	48.1%	187.2
1	854	1692.6	47.3	3454.6	82.1	3001.9	1317.3	3877.5	13.5	0.946	0.390	29.2%	52.4	0.951	0.993	51.1%	228.5
1	1174	2357.8	73.0	3657.2	145.4	3170.2	810.2	4046.2	n.d.	0.940	0.593	38.7%	59.0	0.920	n.d.	n.d.	n.d.

Run	time [min]	UV-Absorbance HPLC ( $\lambda = 285$ nm), raw data [mAU]								Enantioselectivity NpEtOH 1b				Enantioselectivity PyrEtOH 1d			
		R-NpEtOiPr (R)-4b	S-NpEtOiPr (S)-4b	R-PyrEtOiPr (R)-4d	S-PyrEtOiPr (S)-4d	S-NpEtOH (S)-1b	R-NpEtOH (R)-1b	S-PyrEtOH (S)-1d	R-PyrEtOH (R)-1d	$ee_{\text{product}}$	$ee_{\text{substrate}}$	c	S	$ee_{\text{product}}$	$ee_{\text{substrate}}$	c	S
1	1789	3451.3	151.2	4256.9	313.4	3655.0	258.4	4573.6	n.d.	0.916	0.868	48.7%	64.5	0.857	n.d.	n.d.	n.d.
1	4688	3178.5	401.8	3700.9	774.0	2907.0		3511.1	n.d.	0.775	n.d.	n.d.	n.d.	0.641	n.d.	n.d.	n.d.
2	0	-	-	-	-	3622.7	3810.1	5121.0	5283.3	-	-	-	-	-	-	-	-
2	28	64.5	n.d.	522.0	n.d.	2500.2	2570.4	3645.3	3184.9	n.d.	0.011	n.d.	n.d.	n.d.	0.083	n.d.	n.d.
2	72	113.4	n.d.	880.9	n.d.	1988.6	2006.6	2970.1	2132.3	n.d.	0.021	n.d.	n.d.	n.d.	0.179	n.d.	n.d.
2	124	178.1	4.9	1270.6	16.8	1860.5	1788.9	2771.1	1525.8	0.944	0.045	4.5%	36.1	0.973	0.304	23.8%	98.5
2	197	262.1	5.2	1641.8	18.4	1952.0	1803.6	2911.1	1211.2	0.959	0.065	6.3%	51.0	0.977	0.425	30.3%	131.5
2	358	382.0	7.3	1765.1	25.4	1524.9	1204.6	2302.9	342.5	0.961	0.142	12.9%	57.5	0.971	0.748	43.5%	152.4
2	509	1253.9	29.2	4148.7	64.1	3385.2	2318.2	4781.9	224.0	0.952	0.211	18.2%	50.2	0.969	0.913	48.5%	202.5
2	1247	2890.6	86.2	4439.2	201.3	3570.8	756.1	4871.5	n.d.	0.939	0.665	41.4%	63.8	0.911	n.d.	n.d.	n.d.
2	2980	2743.6	181.4	3569.0	390.3	2649.9	n.d.	3647.1	n.d.	0.870	n.d.	n.d.	n.d.	0.797	n.d.	n.d.	n.d.

**Table S18.** Chemoselectivity values for the two fast reacting and the two slow reacting enantiomers for the competition experiment shown in **Scheme S11**. To minimize influence of analytical errors, only data points with at minimum 4% and maximal 96% conversion (c) for both substrates are analysed. Selectivity was derived as described in Chapter 1.8.

Run	time [min]	c (R)-1b	c (R)-1d	total c	Chemosel	Select	StDev	Run	time [min]	c (S)-1b	c (S)-1d	total c	Chemosel	Select	StDev
1	119	6.1%	34.5%	20.3%	0.699	6.7	0.133	1	1789	4.1%	7.1%	5.6%	0.268	1.8	0.053
1	178	9.3%	46.0%	27.6%	0.664	6.3		1	4688	12.4%	19.6%	16.0%	0.225	1.6	
1	366	20.0%	76.6%	48.3%	0.586	6.5		2	2980	6.6%	10.6%	8.6%	0.235	1.7	
1	566	34.9%	94.2%	64.6%	0.459	6.6		-							
2	72	5.5%	31.4%	18.4%	0.703	6.7		-							
2	124	9.3%	48.0%	28.6%	0.676	6.7		-							
2	197	13.0%	60.0%	36.5%	0.645	6.6		-							
2	358	24.5%	85.1%	54.8%	0.552	6.8		-							
					<b>average</b>	<b>6.6</b>							<b>average</b>	<b>1.7</b>	

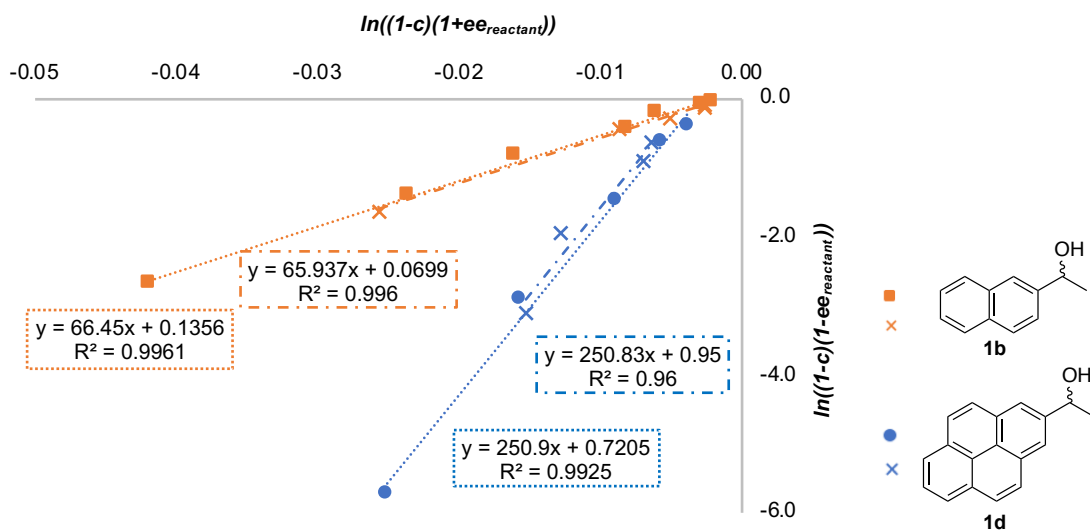


**Figure S16.** Linear regression analysis of two independent runs of competition experiment shown in **Scheme S11**.

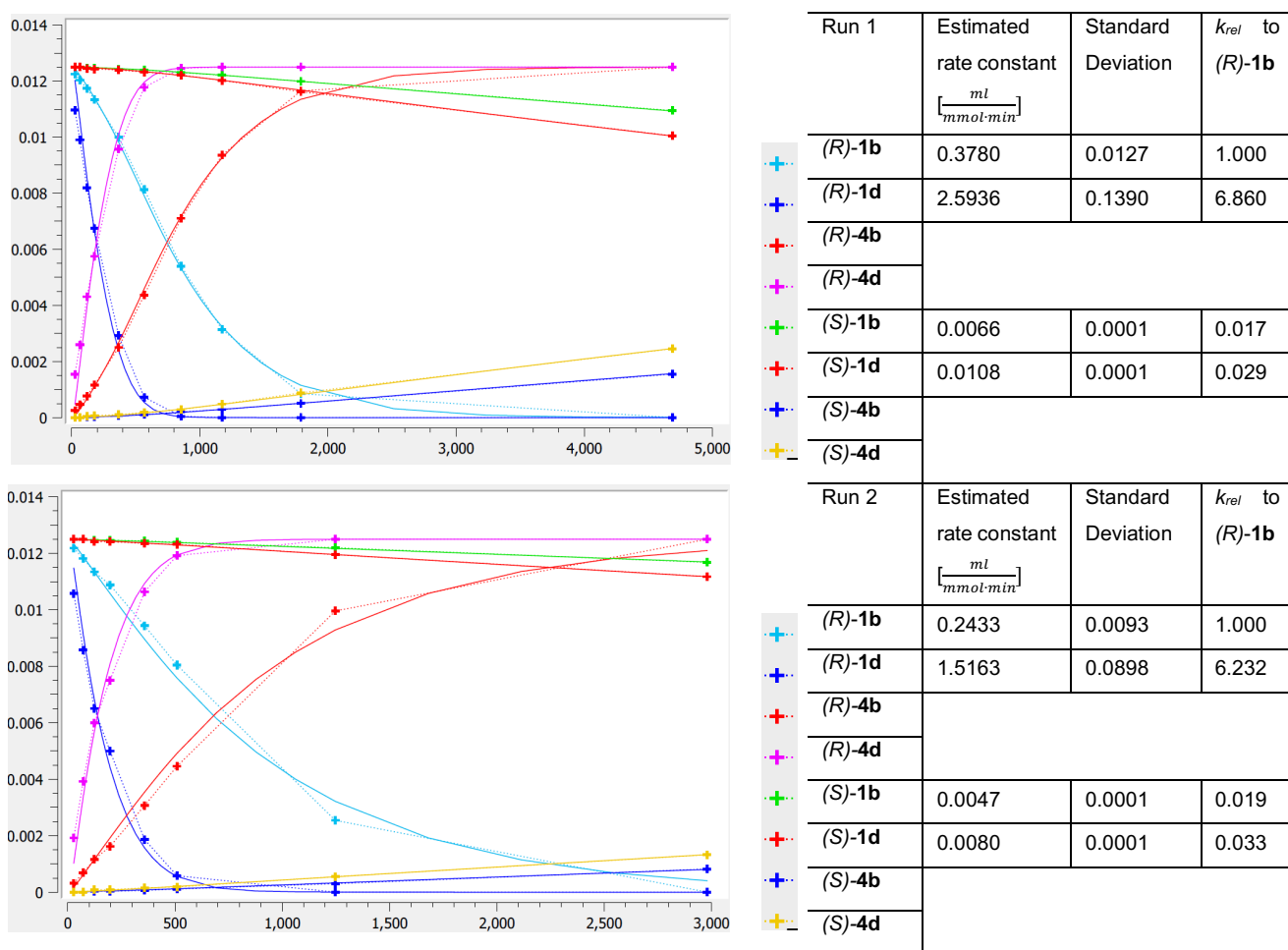
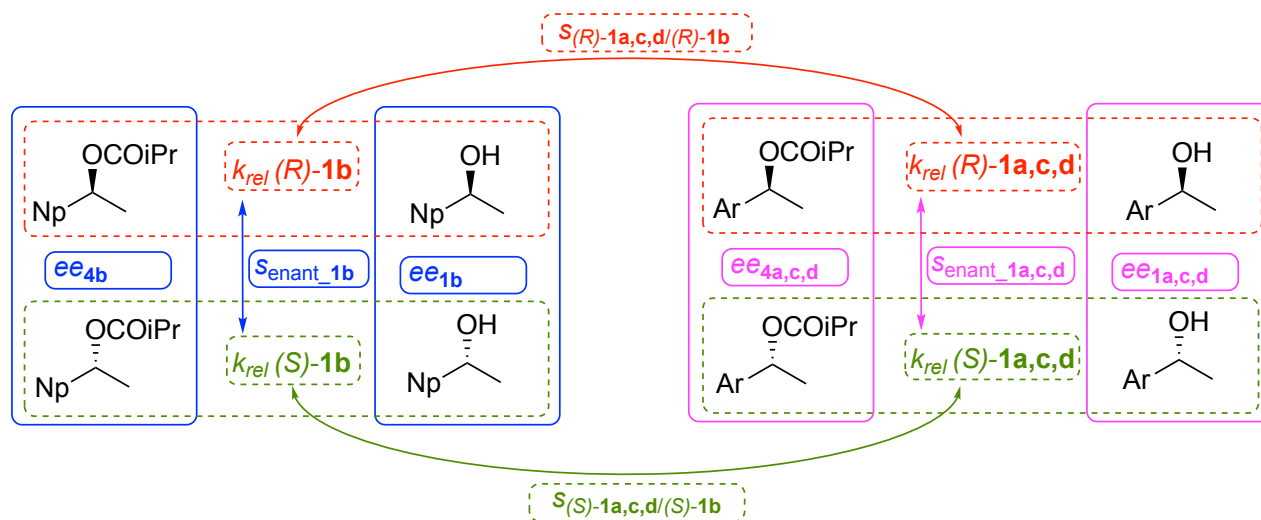


**Figure S17.** Parameter estimation for competition experiment shown in **Scheme S11**. Estimation was performed with CoPaSi<sup>[6]</sup>, x-axis shows time in min, y-axis intermediate concentration in mol/L of each species. Estimated rate constants with standard deviation for each alcohol are shown right hand.

## 2.5. From Experimental Data to Relative Rates

Through experiments and chiral HPLC analysis described in Chapter 2.1 intermediate concentrations of eight species can be followed over the course of a reaction. **Scheme S12** gives an overview of those species and the possible selectivity values that can be gathered.



**Scheme S12.** Overview of different approaches to analyse reaction mixtures gained by competitive linear regression experiments as described in Chapter 2.1.

- Enantioselectivity:** (blue and pink boxes in **Scheme S12**): Enantioselectivity values for each alcohol can be calculated by linear regression (see Chapter 1.6) from ee values of substrates and products. This gives the enantioselectivity of 1-(2-naphthyl)ethanol **1b** ( $s_{\text{enant\_1b}}$ , blue lines in **Scheme S12**) and for the competing alcohol ( $s_{\text{enant\_1a,c,d}}$ , pink lines in **Scheme S12**). As several conversion points are used in linear regression, gained enantioselectivity values are more reliable than those of single point kinetic resolution measurements.
- Chemoselectivity:** Chemoselectivity of two different alcohols can be gained as outlined in Chapter 1.8 from individual conversion values of enantiopure alcohols. This value is gathered at different total conversions and averaged. In principle chemoselectivity could be obtained for each pair of enantiopure alcohols in the system. However, relative rates are most reliable for reactions that occur with comparable rates (the same error considerations as outlined for kinetic resolution in Chapter 1.5 become significant for cases if reaction rates differ too much). Thus, reliable chemoselectivity values can be gained for the two fast reacting enantiomers in relation to each other ( $s_{(R)-1a,c,d}/(R)-1b}$ , red lines in **Scheme S12**) and for the two slow reacting enantiomers vice versa ( $s_{(S)-1a,c,d}/(S)-1b}$ , green lines in **Scheme S12**). However, for the slow enantiomers experimental data are less reliable as reactions cannot be followed to full conversion without significant experimental errors due to the slow absolute reaction rates (as outlined in Chapter 1.2).

Combining the different selectivity values as shown in Eq. S42 - Eq. S46 leads to comparable relative rate values for all species:

$$k_{rel}((R)\text{-}\mathbf{1b}) = 1 \quad \text{Eq. S42}$$

$$k_{rel}((S)\text{-}\mathbf{1b}) = \frac{1}{S_{enant\_1b}} \quad \text{Eq. S43}$$

$$k_{rel}((R)\text{-}\mathbf{1a,c,d}) = S_{(R)\text{-}\mathbf{1a,c,d}/(R)\text{-}\mathbf{1b}} \quad \text{Eq. S44}$$

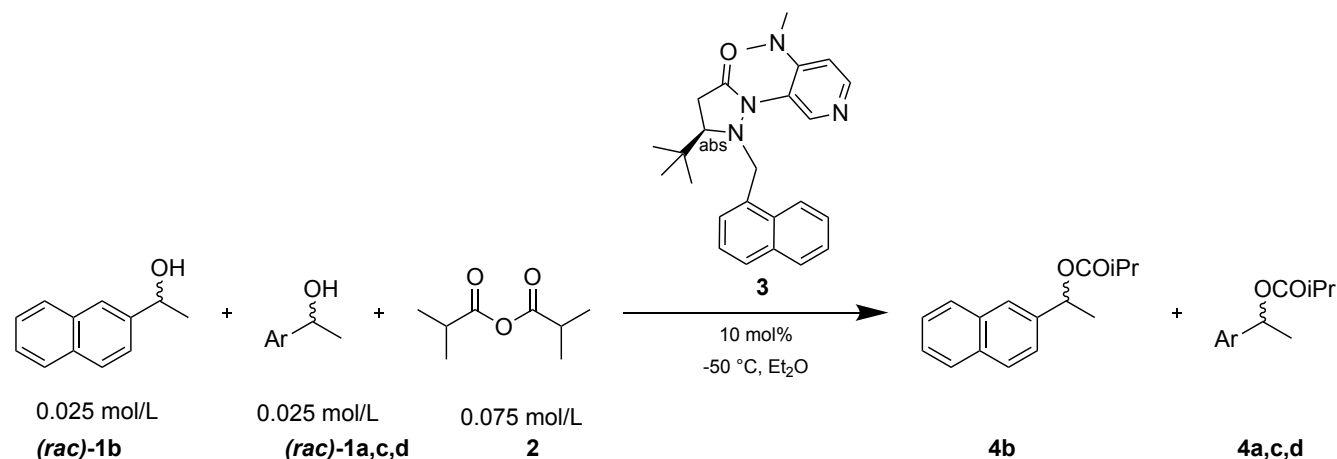
$$k_{rel}((S)\text{-}\mathbf{1a,c,d}) = \frac{k_{rel}((R)\text{-}\mathbf{1a,c,d})}{S_{enant\_1a,c,d}} \quad \text{Eq. S45}$$

$$k_{rel}((S)\text{-}\mathbf{1a,c,d}) = k_{rel}((S)\text{-}\mathbf{1b}) \cdot S_{(S)\text{-}\mathbf{1a,c,d}/(S)\text{-}\mathbf{1b}} \quad \text{Eq. S46}$$

As a reference the rate for  $(R)\text{-}\mathbf{1b}$  is set to 1. The relative rate for  $(S)\text{-}\mathbf{1b}$  can be directly calculated by the enantioselectivity value by Eq. S43 (blue line in **Scheme S12**). As this enantioselectivity value was obtained by repeated independent methods (see Chapter 1) it is reliable. The chemoselectivity for the two fast reacting enantiomers (red line in **Scheme S12**) can also be measured reliably and the relative rate of the fast reacting enantiomer of the second alcohol can thus be calculated by Eq. S44. This gives two possibilities to calculate relative rates for the slow enantiomer of the competing alcohol: It can either be calculated by the enantioselectivity with Eq. S45 from the relative rate of the corresponding fast enantiomer (red line and then pink line in **Scheme S12**) or by the chemoselectivity relative to  $(S)\text{-}\mathbf{1b}$  by Eq. S46 (blue line and then green line in **Scheme S12**). Those two pathways are largely independent as enantioselectivity values by linear regression are mainly calculated from conversion values smaller than 52 %, while for the chemoselectivity of the slower enantiomers measuring points with more than 50% conversion are needed.

A third method of analysis is a simulation of the reaction course giving directly all relative rates as described in Chapter 1.7.

All three analysis methods were performed with all experiments as shown in Chapter 2.4. All results and the resulting selectivity values are compiled on the following pages and discussed below.

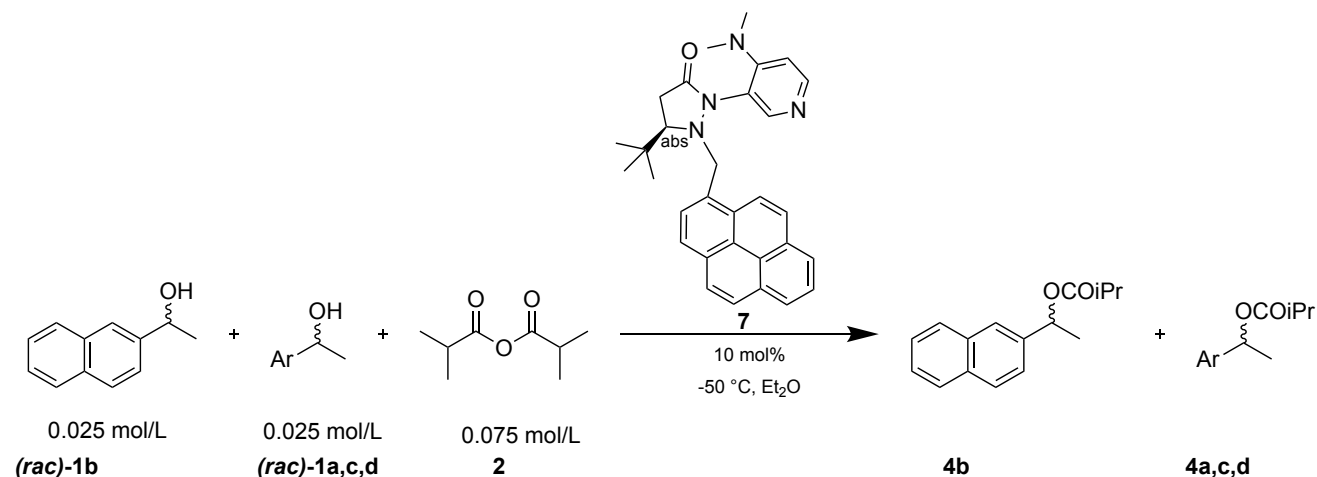


**Scheme S13.** Competitive linear regression of (*rac*)-1-(2-naphthyl)ethanol (**1b**) with aromatic alcohol **1a** - **1d** with catalyst **3**.

**Table S19.** Rates for the reaction shown in **Scheme S13** relative to (*R*)-1-(2-naphthyl)ethanol (**1b**) calculated by different pathways with colour code as defined in **Scheme S12**. Standard deviations are derived from two independent runs.

Pathway	Rates relative to ( <i>R</i> )-NpEtOH ( <i>R</i> )- <b>1b</b>								Enantioselectivity			
	( <i>S</i> )-PhEtOH ( <i>S</i> )- <b>1a</b>	( <i>S</i> )-NpEtOH ( <i>S</i> )- <b>1b</b>	( <i>S</i> )-Phant EtOH ( <i>S</i> )- <b>1c</b>	( <i>S</i> )-Pyr EtOH ( <i>S</i> )- <b>1d</b>	( <i>R</i> )-PhEtOH ( <i>R</i> )- <b>1a</b>	( <i>R</i> )-Np EtOH ( <i>R</i> )- <b>1b</b>	( <i>R</i> )-Phant EtOH ( <i>R</i> )- <b>1c</b>	( <i>R</i> )-Pyr EtOH ( <i>R</i> )- <b>1d</b>	Ph EtOH <b>1a</b>	Np EtOH <b>1b</b>	PhantEtOH <b>1c</b>	PyrEtOH <b>1d</b>
<b>1</b> via <i>S</i> <sub>enant-1b</sub> (blue <sup>a</sup> ), <i>S</i> <sub>R-1a,c,d/R-1b</sub> (red <sup>a</sup> ), <i>S</i> <sub>S-1a,c,d/S-1b</sub> (green <sup>a</sup> )	0.0166 ±0.0004 (Eq. S46)	0.0259 ±0.0007 (Eq. S43)	0.0356 ±0.0006 (Eq. S46)	0.0682 ±0.0027 (Eq. S46)	0.1443 ±0.0069 (Eq. S44)	1	2.1421 ±0.0387 (Eq. S44)	5.9068 ±0.2308 (Eq. S44)	8.8 ±0.58	38.6 ±1.00	58.3 ±1.73	87.0 ±6.33
<b>2</b> via <i>S</i> <sub>enant-1b</sub> (blue <sup>a</sup> ), <i>S</i> <sub>R-1a,c,d/R-1b</sub> (red <sup>a</sup> ), <i>S</i> <sub>enant_1a,c,d</sub> (pink <sup>a</sup> )	<b>0.0197</b> ±0.0007 (Eq. S45)	<b>0.0259</b> ±0.0007 (Eq. S43)	<b>0.0402</b> ±0.0013 (Eq. S45)	<b>0.0900</b> ±0.0007 (Eq. S45)	<b>0.1443</b> ±0.0069 (Eq. S44)	1	<b>2.1421</b> ±0.0387 (Eq. S44)	<b>5.9068</b> ±0.2308 (Eq. S44)	<b>7.3</b> ±0.05	<b>38.6</b> ±1.00	<b>53.3</b> ±2.40	<b>65.7</b> ±1.70
<b>S</b> CoPaSi simulation	0.0170 ±0.0003	0.0302 ±0.0034	0.0416 ±0.0034	0.0874 ±0.0016	0.1279 ±0.0040	1	2.1261 ±0.0338	4.9300 ±0.1971	7.5 ±0.10	33.6 ±3.89	51.1 ±5.03	56.4 ±3.28

<sup>a</sup>colours refer to the pathways depicted in **Scheme S12**.



**Scheme S14.** Competitive linear regression of *(rac)*-1-(2-naphthyl)ethanol (**1b**) with aromatic alcohol **1a** - **1d** with catalyst **7**.

**Table S20.** Rates for the reaction shown in **Scheme S14** relative to *(R)*-1-(2-naphthyl)ethanol (**1b**) calculated by different pathways as shown in **Scheme S12**. Standard deviations are derived from two independent runs.

Pathway	Rates relative to <i>(R)</i> -NpEtOH ( <i>R</i> )- <b>1b</b>								Enantioselectivity			
	<i>(S)</i> -PhEtOH <i>(S)</i> - <b>1a</b>	<i>(S)</i> -NpEtOH <i>(S)</i> - <b>1b</b>	<i>(S)</i> -PhantEtOH <i>(S)</i> - <b>1c</b>	<i>(S)</i> -PyrEtOH <i>(S)</i> - <b>1d</b>	<i>(R)</i> -PhEtOH <i>(R)</i> - <b>1a</b>	<i>(R)</i> -NpEtOH <i>(R)</i> - <b>1b</b>	<i>(R)</i> -PhantEtOH <i>(R)</i> - <b>1c</b>	<i>(R)</i> -PyrEtOH <i>(R)</i> - <b>1d</b>	PhEtOH <b>1a</b>	NpEtOH <b>1b</b>	PhantEtOH <b>1c</b>	PyrEtOH <b>1d</b>
<b>1</b> via $S_{\text{enant-1b}}$ (blue <sup>a</sup> ), $S_{\text{R-1a,c,d/R-1b}}$ (red <sup>a</sup> ), $S_{\text{S-1a,c,d/S-1b}}$ (green <sup>a</sup> )	0.0145 ±0.0005 (Eq. S46)	0.0198 <sup>b</sup> ±0.0004 (Eq. S43)	0.0272 ±0.0001 (Eq. S46)	0.0255 ±0.0003 (Eq. S46)	0.1491 ±0.0054 (Eq. S44)	1	2.2430 ±0.0433 (Eq. S44)	6.6180 ±0.1325 (Eq. S44)	10.6 ±0.04	50.5 <sup>b</sup> ±1.03	82.8 ±0.66	261.1 ±6.20
<b>2</b> via $S_{\text{enant-1b}}$ (blue <sup>a</sup> ), $S_{\text{R-1a,c,d/R-1b}}$ (red <sup>a</sup> ), $S_{\text{enant-1a,c,d}}$ (pink <sup>a</sup> )	<b>0.0161</b> <b>±0.0008</b> (Eq. S45)	<b>0.0198<sup>b</sup></b> <b>±0.0022</b> (Eq. S43)	<b>0.0281</b> <b>±0.0005</b> (Eq. S45)	<b>0.0264</b> <b>±0.0003</b> (Eq. S45)	<b>0.1491</b> <b>±0.0054</b> (Eq. S44)	1	<b>2.2430</b> <b>±0.0433</b> (Eq. S44)	<b>6.6180</b> <b>±0.1325</b> (Eq. S44)	<b>9.3</b> <b>±0.17</b>	<b>50.5<sup>b</sup></b> <b>±1.03</b>	<b>79.8</b> <b>±1.05</b>	<b>250.9</b> <b>±0.04</b>
<b>S</b> CoPaSi simulation	0.0153 ±0.0000	0.0203 ±0.0016	0.0299 ±0.0011	0.0306 ±0.0021	0.1377 ±0.0027	1	2.2447 ±0.0275	6.5464 ±0.3141	9.0 ±0.20	49.6 ±4.09	75.3 ±3.77	215.4 ±24.8

<sup>a</sup>colours refer to the pathways depicted in **Scheme S12**. <sup>b</sup>without value (*s* = 66) from competition experiment with PyrEtOH **1d** (Table S17) as discussed below.

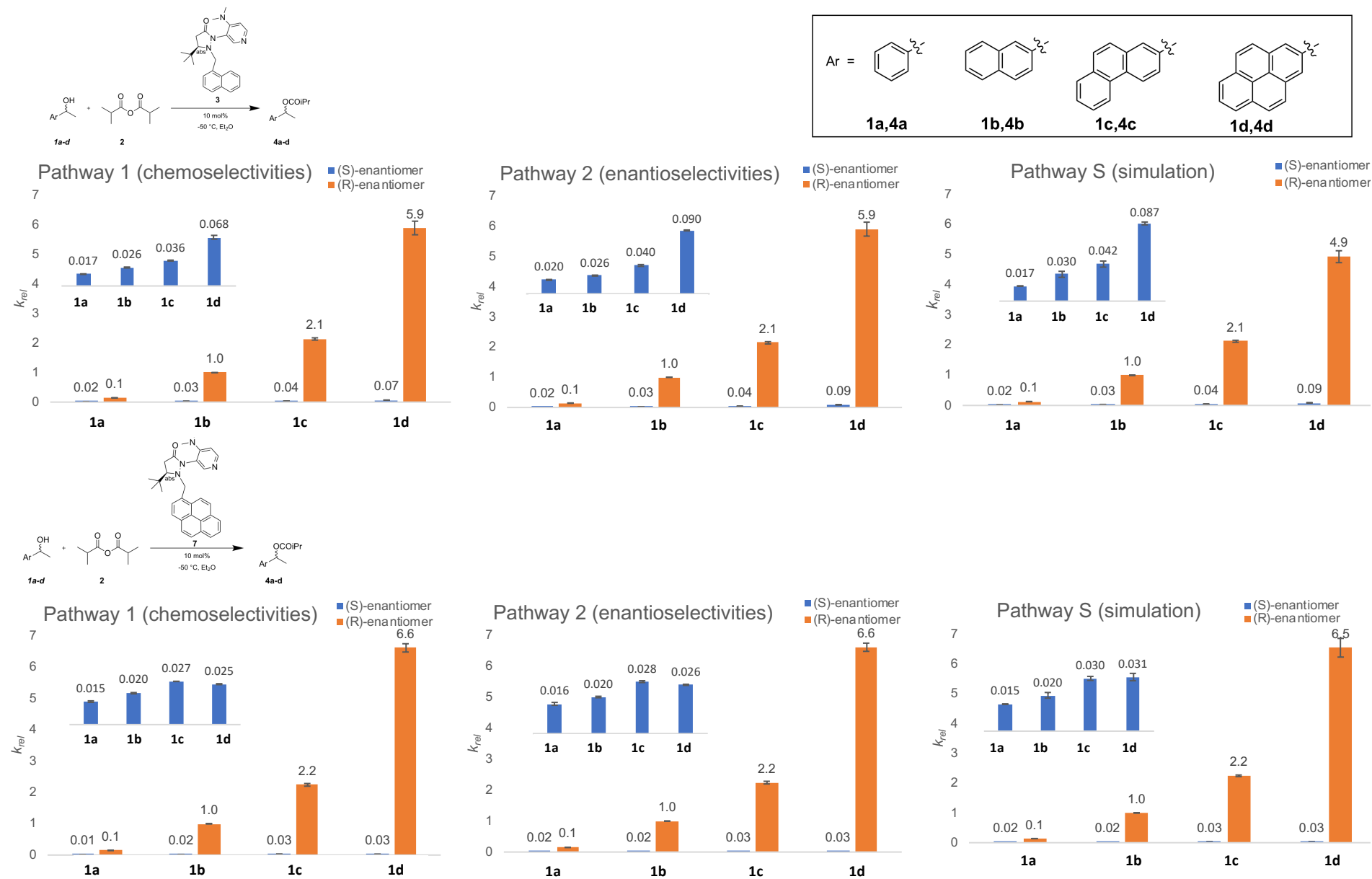


Figure S18. Overview of resulting relative rate constants for the different alcohols via different pathways of analysis as described in Table S19 and Table S20.

## 2.6. Reliability Estimation of Relative Rates

The gathered data allow now to validate the different methods to determine relative rates and enantioselectivity values:

- Single point kinetic resolution: Enantioselectivity values obtained by the Kagan formulas for a single point (reported in **Table S7** to **Table S18**) are – as expected – very dependent on the conversion especially for high selectivity values. As an example, in **Table S17** enantioselectivity values vary from  $s = 109$  (conversion 16.6%) to  $s = 229$  (conversion 51.5%). However, values obtained close to 50% conversion are at least comparable with values obtained from linear regression experiments.
- Linear regression: Root mean square values (0.985 – 0.999) as well as small intercepts from 0 indicate in all experiments with a selectivity value  $< 100$  a very good linear fit. Even for selectivity values  $> 200$  (see **Figure S16**) good root mean square values (0.960 - 0.993) and acceptable intercepts were found. Reproducibility of slopes (=selectivity values) in independent experiments is good. Relative standard deviations for the two independent runs are in the range of 0.1% to 3.0% except for the experiment shown in **Figure S8** (relative standard deviation of 5.9%). As all discussed differences in this project are far above those deviations linear regression values can be used as valid descriptors.
- Competitive linear regression: It must be excluded, that the changed experimental environment through the addition of a second alcohol to the reaction mixture in linear regression experiments impacts the selectivity of the reaction. As a measure of quality the selectivity values for the acylation of 1-(2-naphthyl)ethanol **1b** with catalyst **3** can be used. The literature value for kinetic resolution ( $s = 37$ )<sup>[3]</sup>, standard kinetic resolution experiments ( $s = 37.0$ , see Chapter 1.3), the result of independent single-alcohol linear regression ( $s = 38.5 \pm 1.25$ , see Chapter 1.6) and values reported for the different competitive linear regression experiments above ( $s = 38.9 \pm 0.98$  in competition with PyrEtOH **1d**,  $s = 39.8 \pm 2.41$  in competition with PhantEtOH **1c**,  $s = 37.4 \pm 1.56$  in competition with PhEtOH **1a**) are in good agreement. Similarly, selectivity values for 1-(2-naphthyl)ethanol (**1b**) with catalyst **7** are in good agreement for the competition experiments with PhEtOH (**1a**) ( $s = 51.6 \pm 1.50$ ) and PhantEtOH (**1c**) ( $s = 49.5 \pm 1.47$ ). However, in the highly selective competitive linear regression experiment with PyrEtOH (**1d**) a slightly higher selectivity value of  $s = 66.2 \pm 0.26$  was measured. As those values were reproducible in independent experiments, it is likely that the changed reaction environment influences the selectivity for **1b** slightly, which could be explained by the changed polarity of the solvent-substrate mixture (see Chapter 4.7). Thus, that value was dismissed for the enantioselectivity of **1b** with catalyst **7** to guarantee comparable reaction conditions in all cases.
- There are two pathways to determine relative rates for the slower (S)-enantiomer as shown in **Scheme S12**. For all experiments calculation of relative rates by the chemoselectivity of

the slower enantiomer relative to (*S*)-NpEtOH (**1b**) (first row in **Table S19** and **Table S20**) gives comparable, but slightly higher enantioselectivities than by direct linear regression (second row in **Table S19** and **Table S20**). Most chemoselectivity values for the slower enantiomer could only be measured for conversion values smaller than 30%. Thus, the relative standard deviation of chemoselectivities for the slow reacting enantiomer is up to 7.9% and the use of linear regression analysis is more reliable. However, general trends are well confirmed by those independent chemoselectivity values.

- Simulation of relative rates with CoPaSi<sup>[5]</sup>: As outlined above the determination of absolute rates especially at -50 °C and with low concentrations has a significant error margin. Hence, the absolute rates of two independent measurements have relative standard deviations of up to 26.2% even for the fast reacting enantiomer and are therefore not reliable. In contrast, relative standard deviation of relative rates is smaller than 4.8% for the fast reacting enantiomer and for the slow reacting enantiomer smaller than 8.4%. Thus, the enantioselectivity values obtained by simulations have higher standard deviations compared to linear regression methods and differ also from reported values. Despite some deviations, trends for relative rates and enantioselectivity values obtained from simulations are in general also in agreement with the other methods.

In conclusion, data analysis by three different and partially independent methods and independent repetition of experiments proves the reliability of the reported data. Values determined by linear regression (for conversion values smaller than 52%) are in satisfactory agreement with those depicted by chemoselectivity of fast and slow reacting enantiomer with the reference system. Also, simulation of reactions leads to comparable results. The compilation of different data above also indicates that enantioselectivity values of up to 80 can be measured reliably by linear regression in the range of  $\pm 5\%$ . For  $s > 200$  reliability estimation is not possible in this project as only one system is in that range. However, the values obtained from different analytical methods and two independent runs allow to report values to the nearest 50.

For all cases, standard deviations for independent experiments are by far the lowest by using linear regression analysis. Thus, all numbers discussed in the main text are gathered from those experiments, if not stated differently.

## 2.7. Results with Achiral Catalysts

As benchmark experiments for the reactivity of the alcohols, relative rates for the acylation were also measured with achiral catalysts DMAP (**5**) and tri(*n*-butyl)phosphane PBU<sub>3</sub> (**6**). The reaction setup, data collection (by chiral HPLC analysis) and – as far as meaningful – data analysis was performed as described in the chapters above for chiral catalysts in order to ensure full comparability. **Figure S19** gives an overview of results, the tables below report full data of measurements. Reactions catalysed by achiral amine Lewis bases diazabicycloundecene (DBU, **S4**) and diazabicyclooctane (DABCO, **S5**) did not give any conversion. As also reactions with PBU<sub>3</sub> (**6**) were found to be very slow, catalyst concentration was increased to 40%. Control measurements at low conversion values with 10% PBU<sub>3</sub> (**6**) confirmed that increased catalyst loading does not affect relative rates.

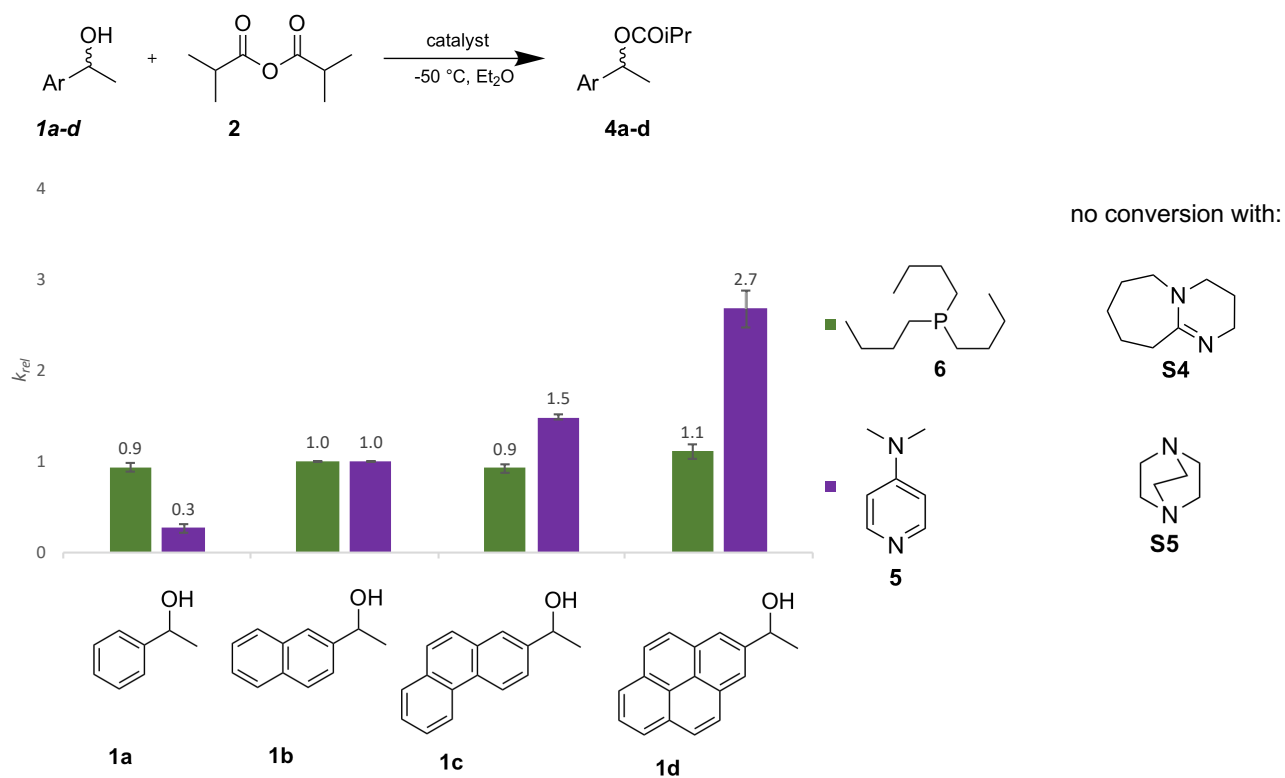
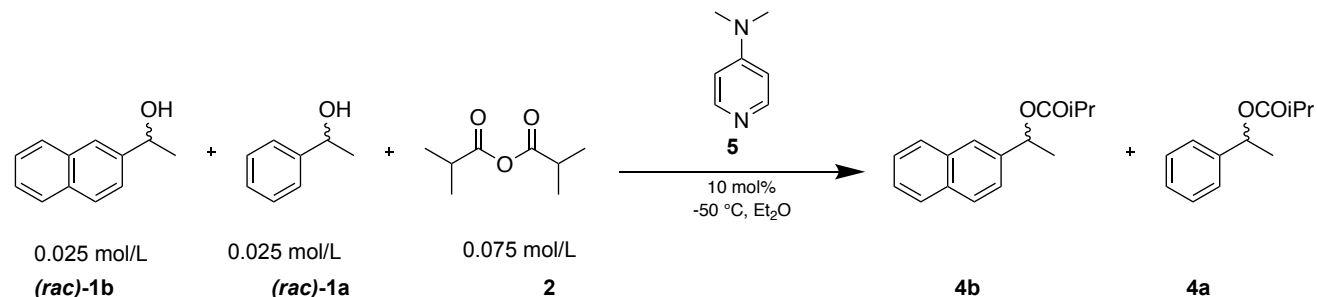


**Figure S19.** Overview of relative rate constants for the acylation of different alcohols with achiral catalysts as described in the tables below.

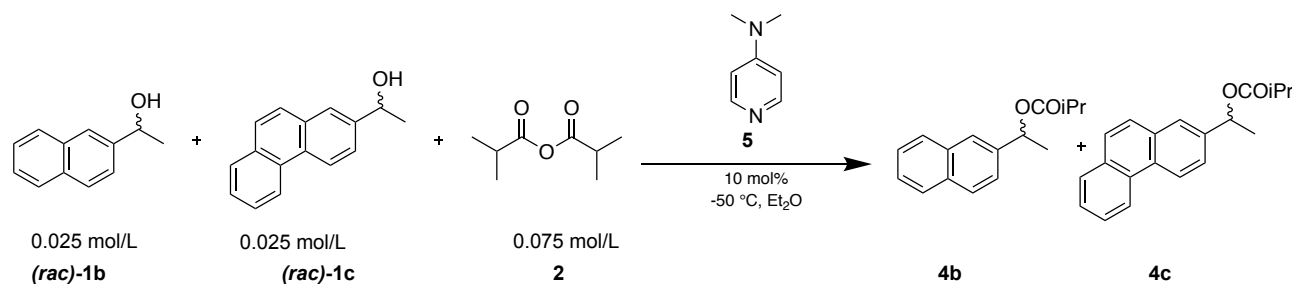


**Scheme S15.** Competition experiment of *(rac)*-1-(2-naphthyl)ethanol (**1b**) and *(rac)*-1-phenylethanol (**1a**) with DMAP (**5**).

**Table S21.** Raw HPLC absorbance data for competitive linear regression shown in **Scheme S15**. Data were calibrated and normalized from the stock solution before analysis. To minimize influence of analytical errors selectivities were not determined (n.d.) for points with a conversion lower than 4% or higher than 96% for one substrate. Selectivity was derived as described in Chapter 1.8.

		UV-Absorbance HPLC ( $\lambda = 285$ nm (naphthyl), $\lambda = 215$ nm (phenyl)), raw data [mAU]								Chemoselectivity					
Run	time [min]	R-PhEtOiPr (R)-4a	S-PhEtOiPr (S)-4a	R-NpEtOiPr (R)-4b	S-NpEtOiPr (S)-4b	R-PhEtOH (R)-1a	S-PhEtOH (S)-1a	S-NpEtOH (S)-1b	R-NpEtOH (R)-1b	c 1a	c 1b	total c	Chemo-selectivity	s	StDev
1	17	635.1	546.6	2048.8	2021.1	6701.5	6804.8	4803.7	4808.6	8.9%	30.4%	19.6%	-0.548	0.26	
1	28	1087.5	1044.6	3384.0	3339.7	7375.9	7508.0	4948.8	4952.6	13.7%	41.2%	27.5%	-0.499	0.28	
1	49	1573.1	1521.9	4427.7	4428.0	7181.5	7279.4	3773.3	3774.6	19.2%	54.7%	37.0%	-0.480	0.27	
1	83	2130.8	2041.5	5238.8	5264.4	6485.9	6591.3	2621.4	2624.6	26.2%	67.4%	46.8%	-0.440	0.27	
1	180	2757.4	2803.0	5458.0	5495.9	4826.7	4859.2	971.6	949.5	39.0%	85.5%	62.2%	-0.374	0.26	
1	304	4127.2	4170.9	7313.5	7289.1	4881.8	4941.6	532.3	525.8	48.4%	93.4%	70.9%	-0.317	0.24	
1	549	3610.0	3672.6	5122.3	5217.5	2601.6	2601.9	97.3	92.1	n.d.	n.d.	n.d.	n.d.	n.d.	
2	0	-	-	-	-	7327.0	7508.6	7359.2	7427.4	-	-	-	-	-	
2	9	588.6	584.7	1995.6	1975.0	7816.2	7974.9	6498.5	6575.2	7.6%	23.8%	15.7%	-0.515	0.29	
2	20	688.6	661.2	2276.6	2220.7	5751.2	5829.1	3770.6	3798.4	11.5%	38.0%	24.7%	-0.536	0.26	
2	31	1274.2	1200.2	3756.4	3769.3	7044.9	7178.9	4276.2	4307.9	16.2%	47.5%	31.8%	-0.491	0.27	
2	66	1748.8	1702.0	4605.6	4651.1	6088.8	6163.8	2632.5	2653.2	23.9%	64.4%	44.1%	-0.459	0.26	
2	127	2210.2	2263.3	5008.6	5042.4	5107.0	5141.4	1420.8	1419.3	32.7%	78.5%	55.6%	-0.412	0.26	

		UV-Absorbance HPLC ( $\lambda = 285$ nm (naphthyl), ( $\lambda = 215$ nm (phenyl)), raw data [mAU])								Chemoselectivity					
Run	time [min]	R-PhEtOiPr (R)-4a	S-PhEtOiPr (S)-4a	R-NpEtOiPr (R)-4b	S-NpEtOiPr (S)-4b	R-PhEtOH (R)-1a	S-PhEtOH (S)-1a	S-NpEtOH (S)-1b	R-NpEtOH (R)-1b	c 1a	c 1b	total c	Chemo-selectivity	s	StDev
2	240	3335.1	3366.2	6279.7	6311.0	4792.5	4827.8	730.8	734.5	43.7%	89.9%	66.8%	-0.346	0.25	
2	467	4014.8	3979.6	5876.3	5996.1	3276.2	3286.3	169.3	163.8	n.d.	n.d.	n.d.	n.d.	n.d.	
													average	0.26	0.013

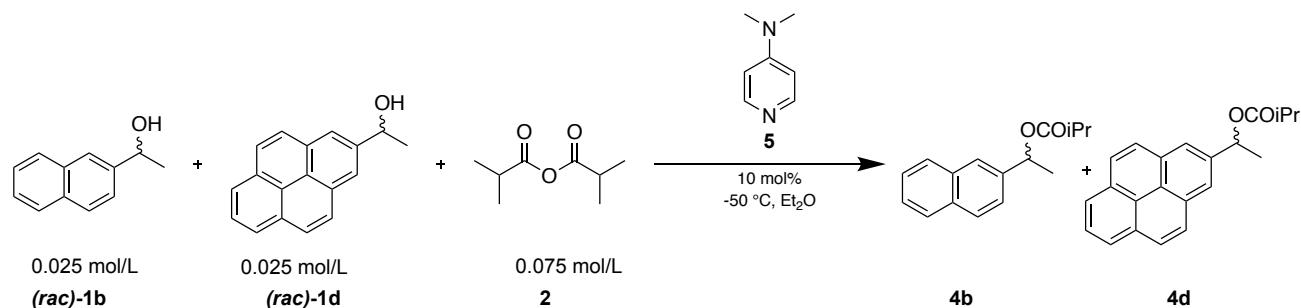


**Scheme S16.** Competition experiment of *(rac)*-1-(2-naphthyl)ethanol (**1b**) and *(rac)*-1-(2-phenanthryl)ethanol (**1c**) with DMAP (**5**).

**Table S22.** Raw HPLC absorbance data for competitive linear regression shown in **Scheme S16**. Data were calibrated and normalized from the stock solution before analysis. To minimize influence of analytical errors selectivities were not determined (n.d.) for points with a conversion lower than 4% or higher than 96% for one substrate. Selectivity was derived as described in Chapter 1.8.

		UV-Absorbance HPLC ( $\lambda = 285$ nm), raw data [mAU])								Chemoselectivity					
Run	time [min]	R-NpEtOiPr (R)-4b	S-NpEtOiPr (S)-4b	R-Phant-EtOiPr (R)-4c	S-Phant-EtOiPr (S)-4c	S-NpEtOH (S)-1b	R-NpEtOH (R)-1b	S-Phant-EtOH (S)-1c	R-Phant-EtOH (R)-1c	c 1b	c 1c	total c	Chemo-selectivity	s	StDev
1	0	-	-	-	-	2845.0	2842.9	8719.0	8705.4	-	-	-	-	-	
1	6	506.3	501.9	2265.9	2240.4	3913.9	3915.1	11432.3	11405.5	11.7%	17.1%	14.4%	0.187	1.50	
1	11	964.1	954.5	4117.8	4154.8	4839.6	4860.3	13753.2	13724.8	16.9%	23.9%	20.4%	0.171	1.47	
1	30	980.4	971.6	4156.1	4149.7	2089.4	2093.8	5487.8	5493.4	32.5%	44.1%	38.3%	0.152	1.48	
1	65	2269.4	2255.3	9177.2	9244.2	3247.1	3257.4	7798.6	7779.7	41.7%	55.3%	48.5%	0.139	1.49	
1	223	1395.3	1397.2	5173.4	5136.1	618.2	622.8	1091.2	1096.0	69.9%	83.1%	76.5%	0.087	1.48	

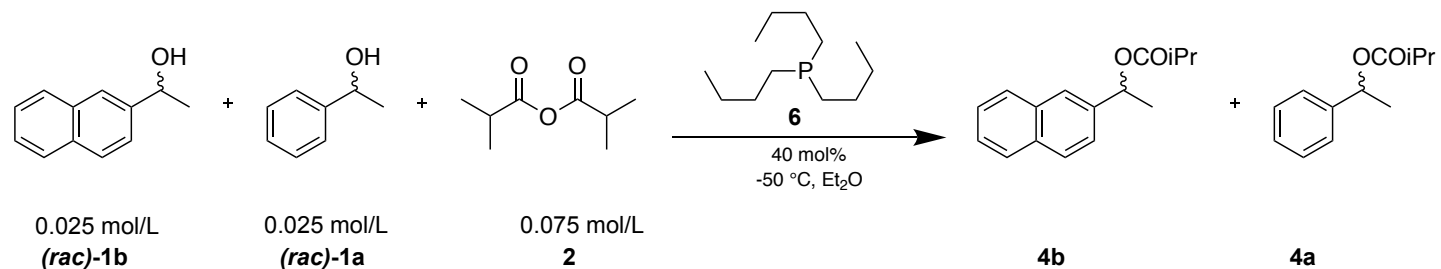
		UV-Absorbance HPLC ( $\lambda = 285$ nm), raw data [mAU]								Chemoselectivity					
Run	time [min]	R-NpEtOiPr (R)- <b>4b</b>	S-NpEtOiPr (S)- <b>4b</b>	R-Phant-EtOiPr (R)- <b>4c</b>	S-Phant-EtOiPr (S)- <b>4c</b>	S-NpEtOH (S)- <b>1b</b>	R-NpEtOH (R)- <b>1b</b>	S-Phant-EtOH (S)- <b>1c</b>	R-Phant-EtOH (R)- <b>1c</b>	c <b>1b</b>	c <b>1c</b>	total c	Chemo-selectivity	s	StDev
1	1195	1615.5	1639.6	4958.8	4868.6	18.9	22.9	16.7	15.4	n.d.	n.d.	n.d.	n.d.	n.d.	
2	0	-	-	-	-	2542.1	2545.5	8037.2	8022.9	-	-	-	-	-	
2	6	298.4	297.3	1457.6	1427.1	2135.6	2123.2	6741.1	6733.0	12.6%	18.3%	15.4%	0.184	1.50	
2	13	532.4	531.7	2560.3	2515.6	2595.6	2586.5	8005.2	7991.7	17.5%	24.9%	21.2%	0.175	1.49	
2	24	616.6	616.6	2892.9	2839.5	1978.6	1968.7	5840.5	5833.1	24.3%	33.9%	29.1%	0.164	1.48	
2	45	1015.5	1017.0	4606.4	4627.6	1991.8	1983.1	5481.7	5458.7	34.5%	46.8%	40.7%	0.152	1.49	
2	80	1495.5	1498.0	6482.9	6539.0	1842.5	1836.1	4639.2	4641.7	45.6%	59.4%	52.5%	0.132	1.48	
2	180	1414.9	1407.4	5758.1	5804.3	836.3	839.8	1741.9	1734.5	63.4%	77.6%	70.5%	0.101	1.49	
2	304	2151.0	2137.0	8287.9	8429.7	749.0	745.8	1291.2	1294.3	74.7%	87.1%	80.9%	0.077	1.49	
2	549	2463.4	2438.9	8884.4	8956.4	382.2	381.6	475.5	477.8	86.9%	95.1%	91.0%	0.045	1.49	
													<b>average</b>	<b>1.49</b>	<b>0.007</b>



**Scheme S17.** Competition experiment of *(rac)*-1-(2-naphthyl)ethanol (**1b**) and *(rac)*-1-(2-pyrenyl)ethanol (**1d**) with DMAP (**5**).

**Table S23.** Raw HPLC absorbance data for competitive linear regression shown in **Scheme S17**. Data were calibrated and normalized from the stock solution before analysis. To minimize influence of analytical errors selectivities were not determined (n.d.) for points with a conversion lower than 4% or higher than 96% for one substrate. Selectivity was derived as described in Chapter 1.8.

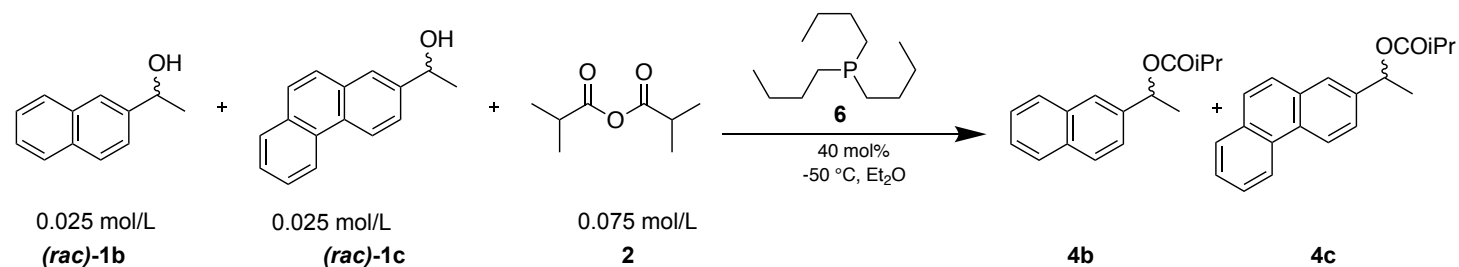
Run	time [min]	UV-Absorbance HPLC ( $\lambda = 285 \text{ nm}$ ), raw data [mAU]								Chemoselectivity					
		R-NpEtOiPr (R)-4b	S-NpEtOiPr (S)-4b	R-PyrEtOiPr (R)-4d	S-PyrEtOiPr (S)-4d	S-NpEtOH (S)-1b	R-NpEtOH (R)-1b	S-PyrEtOH (S)-1d	R-PyrEtOH (R)-1d	c 1d	c 1b	total c	Chemo-selectivity	s	StDev
1	0	-	-	-	-	5978.9	5985.5	7365.4	7703.8	-	-	-	-	-	
1	7	292.7	299.7	912.7	927.4	3007.5	3016.0	3322.0	3453.1	9.2%	23.1%	16.1%	0.433	2.74	
1	12	531.1	528.2	1574.9	1593.3	3614.3	3631.0	3667.6	3813.2	13.0%	31.9%	22.5%	0.420	2.76	
1	31	914.5	913.0	2450.5	2448.9	3235.7	3248.4	2750.3	2847.5	22.4%	49.2%	35.8%	0.374	2.67	
1	66	1628.0	1670.1	3775.8	3892.6	3192.8	3588.7	2259.5	2313.6	33.3%	65.0%	49.1%	0.323	2.60	
1	225	1549.5	1562.1	2878.9	2971.9	1169.2	1176.5	368.4	375.2	57.6%	89.7%	73.7%	0.218	2.65	
1	1194	2916.6	2913.4	3450.5	3541.0	55.1	57.7	11.1	10.7	n.d.	n.d.	n.d.	n.d.	n.d.	
2	0	-	-	-	-	2889.2	2899.9	2347.0	2405.6	-	-	-	-	-	
2	9	255.0	250.8	797.7	805.8	2358.8	2352.2	2626.4	2726.0	9.9%	24.9%	17.4%	0.431	2.75	
2	15	397.8	392.6	1179.2	1192.8	2492.1	2489.8	2574.6	2669.8	14.0%	33.4%	23.7%	0.409	2.69	
2	26	647.9	646.9	1820.0	1816.0	2623.5	2621.9	2400.5	2486.2	20.2%	45.2%	32.7%	0.382	2.66	
2	47	897.8	902.9	2271.3	2276.8	2194.8	2190.6	1657.2	1708.3	29.6%	59.9%	44.8%	0.338	2.60	
2	81	1236.7	1248.5	2770.5	2852.4	1888.1	1881.0	1083.1	1109.1	40.4%	74.0%	57.2%	0.294	2.60	
2	180	1826.4	1824.3	3318.7	3409.7	1286.9	1287.3	378.8	382.0	59.3%	90.7%	75.0%	0.210	2.65	
2	304	2369.1	2372.7	3688.9	3808.3	916.2	912.5	128.8	129.2	72.7%	97.0%	84.8%	0.143	2.70	
2	549	2810.8	2828.0	3776.8	3866.2	436.8	439.4	18.0	18.8	n.d.	n.d.	n.d.	n.d.	n.d.	
													<b>average</b>	<b>2.67</b>	<b>0.054</b>



**Scheme S18.** Competition experiment of *(rac)*-1-(2-naphthyl)ethanol (**1b**) and *(rac)*-1-phenylethanol (**1a**) with tri-*n*-butyl phosphane (**5**).

**Table S24.** Raw HPLC absorbance data for competitive linear regression shown in **Scheme S18**. Data were calibrated and normalized from the stock solution before analysis. To minimize influence of analytical errors selectivities were not determined (n.d.) for points with a conversion lower than 4% or higher than 96% for one substrate. Selectivity was derived as described in Chapter 1.8.

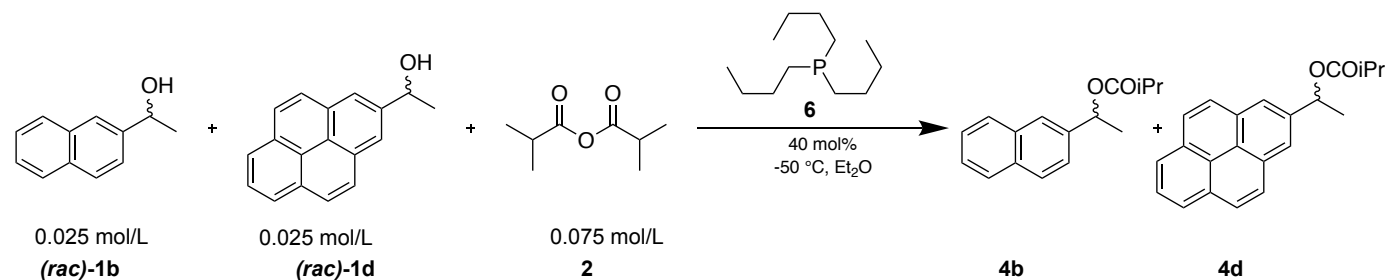
		UV-Absorbance HPLC ( $\lambda = 285$ nm (naphthyl), $\lambda = 215$ nm (phenyl)), raw data [mAU]								Chemoselectivity					
Run	time [min]	R-PhEtOiPr (R)-4a	S-PhEtOiPr (S)-4a	R-NpEtOiPr (R)-4b	S-NpEtOiPr (S)-4b	R-PhEtOH (R)-1a	S-PhEtOH (S)-1a	S-NpEtOH (S)-1b	R-NpEtOH (R)-1b	c 1a	c 1b	total c	Chemo-selectivity	s	StDev
1	1754	833.5	831.8	871.8	825.6	5245.2	5224.5	4633.4	4656.7	15.0%	15.8%	15.4%	-0.026	0.94	
1	7090	1931.2	1967.8	1899.4	1914.0	5073.8	5082.2	4335.6	4347.2	29.9%	31.2%	30.5%	-0.020	0.95	
1	10130	3303.0	3345.3	3278.5	3235.4	4774.8	4871.0	3952.4	3974.1	43.4%	45.9%	44.6%	-0.028	0.93	
1	12914	4015.2	4092.2	3839.7	3833.2	3845.2	3928.7	3019.9	3023.7	53.7%	56.7%	55.2%	-0.027	0.92	
													average	0.94	0.013



**Scheme S19.** Competition experiment of *(rac)*-1-(2-naphthyl)ethanol (**1b**) and *(rac)*-1-(2-phenanthryl)ethanol (**1c**) with tri-*n*-butyl phosphane (**5**).

**Table S25.** Raw HPLC absorbance data for competitive linear regression shown in **Scheme S19**. Data were calibrated and normalized from the stock solution before analysis. To minimize influence of analytical errors selectivities were not determined (n.d.) for points with a conversion lower than 4% or higher than 96% for one substrate. Selectivity was derived as described in Chapter 1.8.

Run	time [min]	UV-Absorbance HPLC ( $\lambda = 285$ nm), raw data [mAU]								Chemoselectivity					
		R-NpEtOiPr (R)-4b	S-NpEtOiPr (S)-4b	R-Phant-EtOiPr (R)-4c	S-Phant-EtOiPr (S)-4c	S-NpEtOH (S)-1b	R-NpEtOH (R)-1b	S-Phant-EtOH (S)-1c	R-Phant-EtOH (R)-1c	c 1b	c 1c	total c	Chemo-selectivity	s	StDev
1	1754	243.1	243.2	653.8	600.9	1497.5	1506.3	4219.2	4217.2	14.3%	13.4%	13.9%	-0.031	0.94	
1	7090	897.9	892.1	2215.2	2216.0	2374.8	2391.5	6716.7	6700.0	27.9%	25.6%	26.8%	-0.042	0.91	
1	10130	886.6	877.9	2253.3	2212.6	1376.4	1371.3	3952.8	3955.8	39.8%	37.1%	38.5%	-0.035	0.91	
1	12914	1801.5	1792.0	4603.5	4618.8	1873.7	1890.2	5398.1	5401.2	49.6%	47.1%	48.4%	-0.025	0.93	
													<b>average</b>	<b>0.92</b>	<b>0.012</b>



**Scheme S20.** Competition experiment of *(rac)*-1-(2-naphthyl)ethanol (**1b**) and *(rac)*-1-(2-pyrenyl)ethanol (**1d**) with tri-*n*-butyl phosphane (**5**).

**Table S26.** Raw HPLC absorbance data for competitive linear regression shown in **Scheme S20**. Data were calibrated and normalized from the stock solution before analysis. To minimize influence of analytical errors selectivities were not determined (n.d.) for points with a conversion lower than 4% or higher than 96% for one substrate. Selectivity was derived as described in Chapter 1.8.

		UV-Absorbance HPLC ( $\lambda = 285 \text{ nm}$ ), raw data [mAU <sub>s</sub> ]								Chemoselectivity					
Run	time [min]	R-NpEtOiPr ( <i>R</i> )- <b>4b</b>	S-NpEtOiPr ( <i>S</i> )- <b>4b</b>	R-PyrEtOiPr ( <i>R</i> )- <b>4d</b>	S-PyrEtOiPr ( <i>S</i> )- <b>4d</b>	S-NpEtOH ( <i>S</i> )- <b>1b</b>	R-NpEtOH ( <i>R</i> )- <b>1b</b>	S-PyrEtOH ( <i>S</i> )- <b>1d</b>	R-PyrEtOH ( <i>R</i> )- <b>1d</b>	<i>c</i> <b>1d</b>	<i>c</i> <b>1b</b>	total <i>c</i>	Chemo-selectivity	<i>s</i>	StDev
1	1754	234.5	228.0	340.5	348.0	1385.2	1389.6	1917.3	1980.9	14.6%	16.4%	15.5%	0.057	1.13	
1	7090	1152.7	1185.6	1606.2	1639.0	2760.5	2765.3	3527.2	3676.6	30.2%	33.3%	31.8%	0.048	1.12	
1	10130	1301.3	1303.5	1771.7	1814.8	1600.8	1606.1	2080.8	2155.6	45.4%	48.4%	46.9%	0.032	1.09	
1	12914	2077.4	2064.3	2746.6	2759.6	1607.3	1612.2	2034.2	2101.8	56.7%	59.6%	58.1%	0.025	1.08	
													<b>average</b>	<b>1.11</b>	<b>0.021</b>

## 2.8. Correlation of Relative Rates and Size Parameter

For a quantitative analysis of size-effects on relative rates the polarizability and the volume of the alcohol reagent were obtained from frequency calculation of the optimized reagents at the B3LYP-D3/6-31+G(d) level of theory (as described in Chapter 4.10). The cavity volume as used by the SMD solvation model based on the van der Waals surface and the “Exact polarizability” of the alcohol reagent were taken and Boltzman-averaged based on their DLPNO-CCSD(T) free energies (see **Table S53**). The correlations with the  $\ln$  of the experimental relative rates and selectivity values are depicted below.

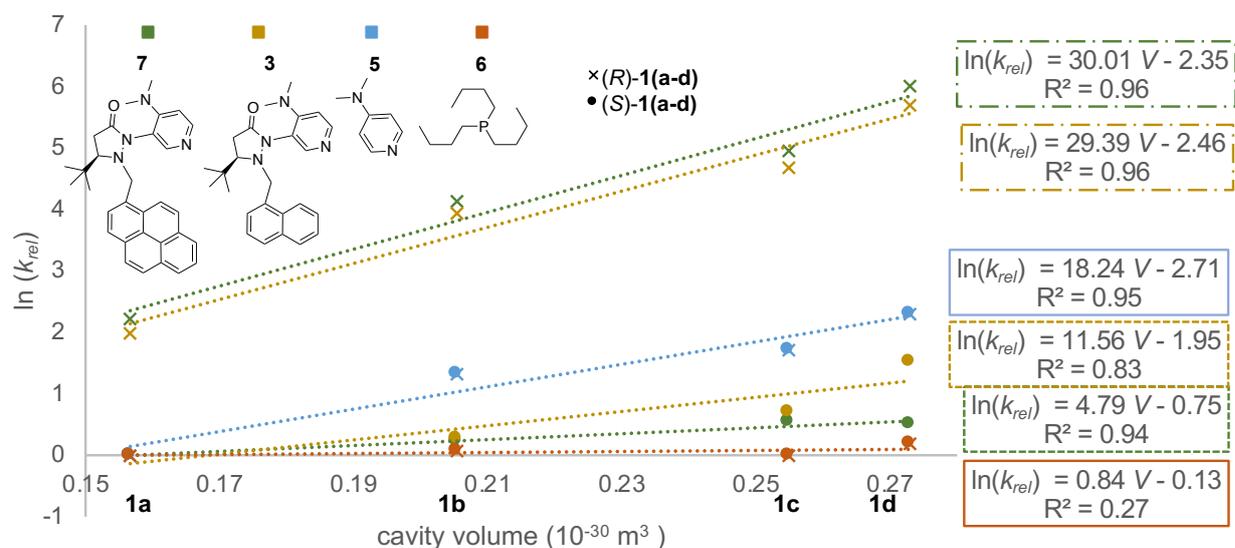


**Figure S20.** Correlation of  $\ln(k_{rel})$  for the different catalysts and alcohols with the reagent cavity volume calculated at the B3LYP-D3/6-31+G(d) level of theory.

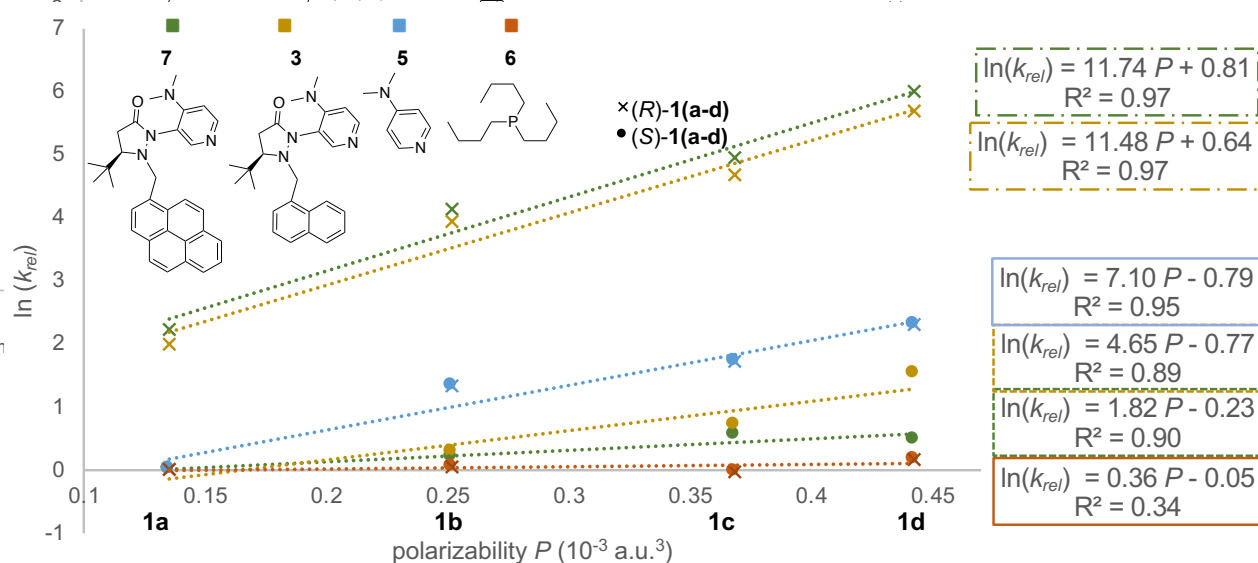


**Figure S21.** Correlation of  $\ln(k_{rel})$  for the different catalysts and alcohols with the reagent polarizability calculated at the B3LYP-D3/6-31+G(d) level of theory.

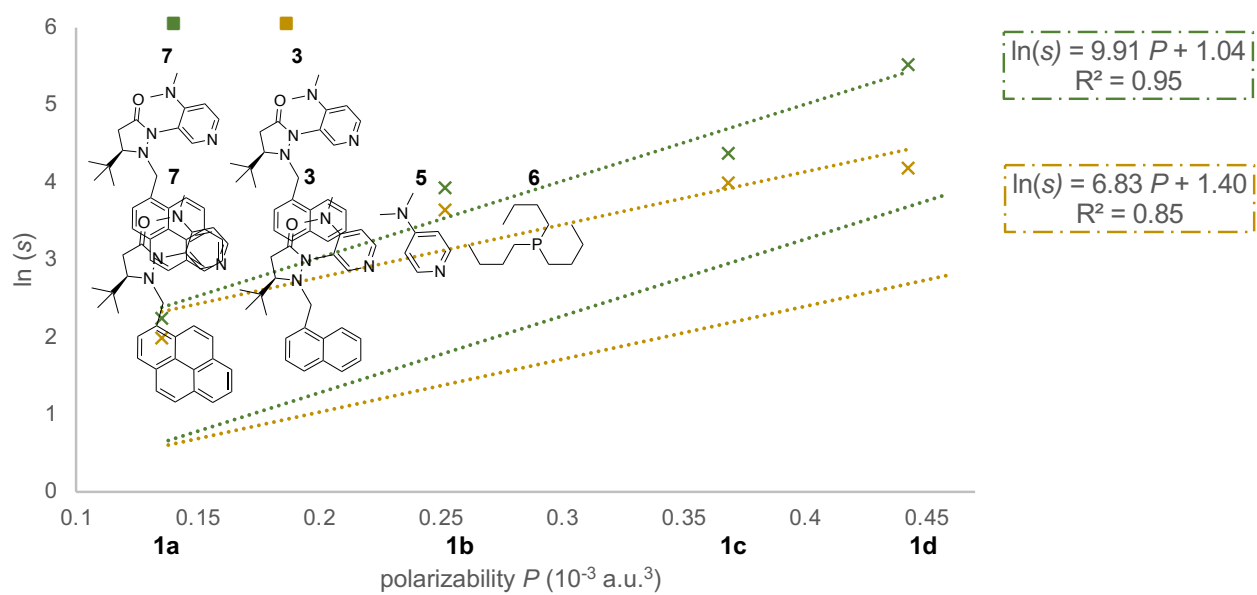


**Figure S22.** Correlation of enantioselectivity for the different catalysts and alcohols with the reagent polarizability calculated at the B3LYP-D3/6-31+G(d) level of theory.

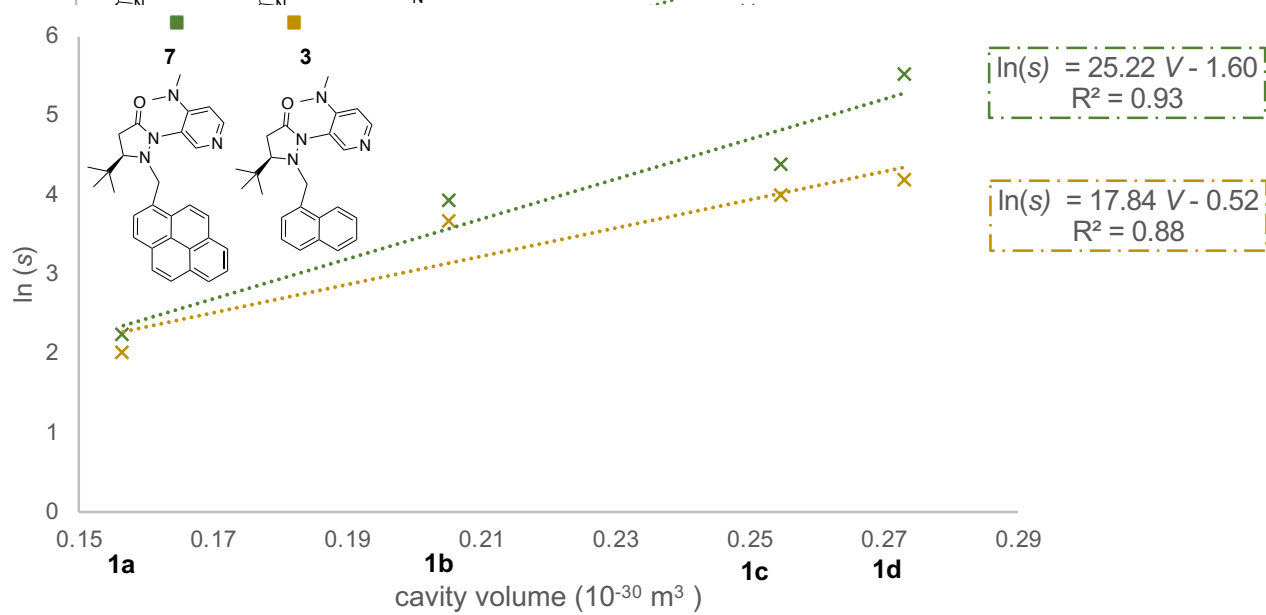


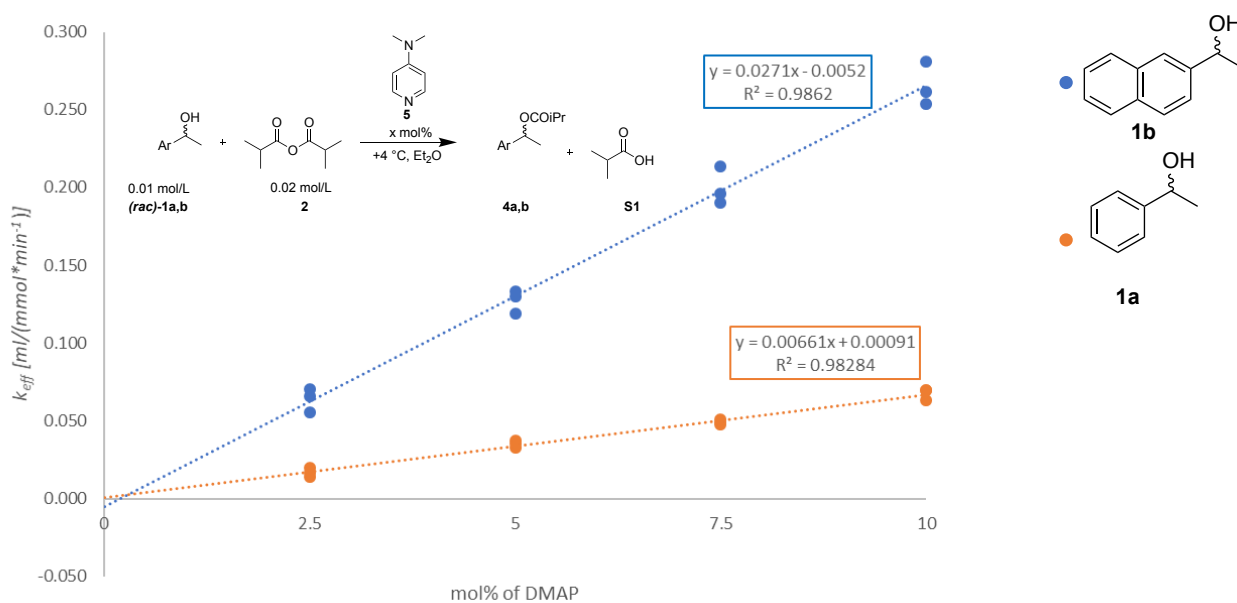
**Figure S23.** Correlation of enantioselectivity for the different catalysts and alcohols with the reagent cavity volume calculated at the B3LYP-D3/6-31+G(d) level of theory.

## 2.9. Background Measurements

In order to estimate the rates of the uncatalysed background reaction for the acylation of alcohols **1a** and **1b** with isobutyric anhydride (**2**) in this project, absolute rate measurements with different concentrations of DMAP (**5**) were performed. For practical reasons these measurements were performed at +4 °C.

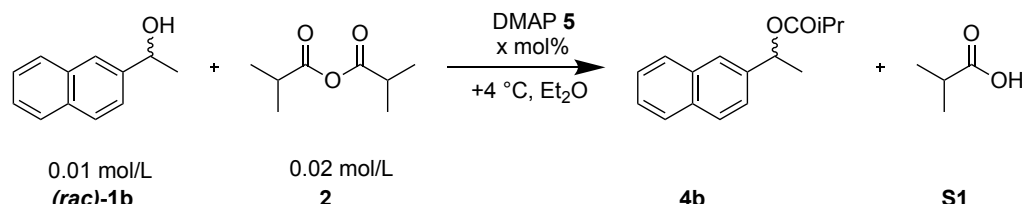
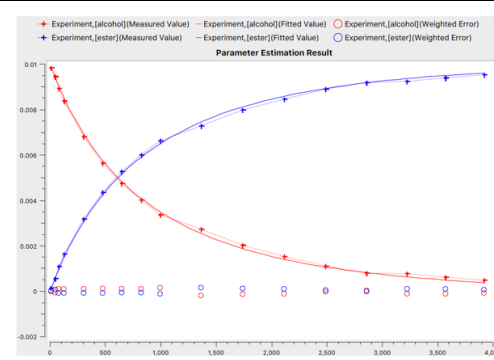
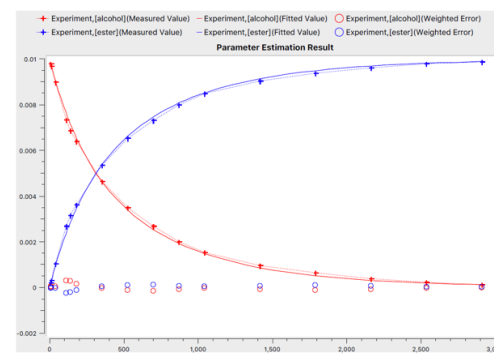
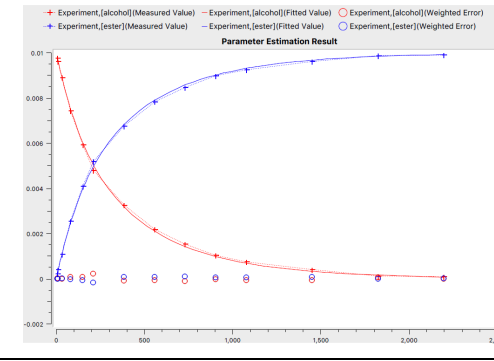
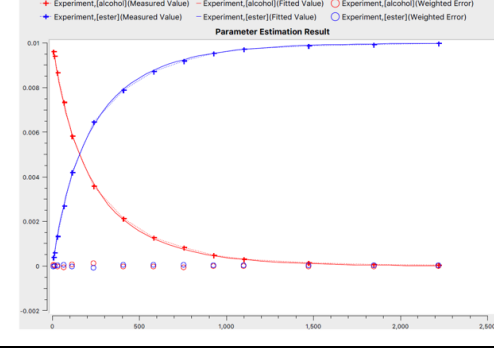
### General procedure

Stock solutions for alcohol ( $c = 0.03 \text{ mol/L}$ ), catalyst ( $c = 0.003 \text{ mol/L}$ ) and freshly distilled isobutyric anhydride ( $c = 0.06 \text{ mol/L}$ ) in dry diethyl ether are prepared. After cooling 0.8 mL stock solution alcohol and 0.8 mL stock solution catalyst in a 20 mL flask to 4 °C ( $\text{N}_2$ , stirring), 0.8 mL of pre-cooled stock solution anhydride is added. A 0.5 mL sample of the reaction mixture is then transferred into a nitrogen-flushed HPLC flask (4 vials in total), closed with a screw septum cap and kept at +4 °C. A sample of 1  $\mu\text{L}$  (4  $\mu\text{L}$  in the case of 1-phenylethanol) of the reaction mixture is taken by the HPLC autosampler after a defined time and a HPLC spectrum (Vertex Eurospher II, 1.5 mL/min,  $n\text{Hexan}/i\text{Propanol} = 100/0 \rightarrow 93/7$ ,  $T = 10 \text{ }^\circ\text{C}$ ,  $t = 3 \text{ min}$ ,  $\lambda = 275 \text{ nm}$  [ $\text{NpEtOH}$ ]/  $\lambda = 210 \text{ nm}$  [ $\text{PhEtOH}$ ]) is measured (max. 4 times per vial). The substrate/product ratio is calculated using calibration curves of optical absorbance and concentration. Simulation of the reaction with CoPaSi leads to the effective rate constants  $k$ . **Figure S24** demonstrates that for both alcohols no significant background reaction occurs at +4 °C. Raw data can be found below.

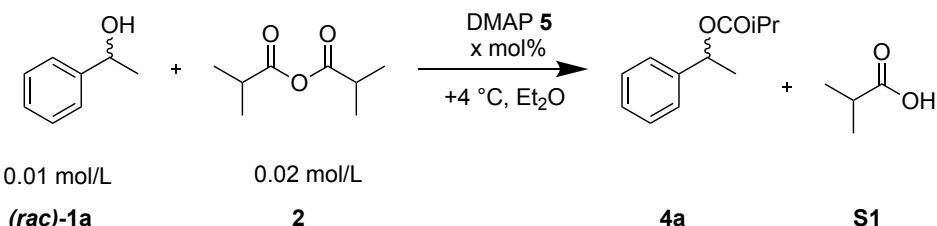
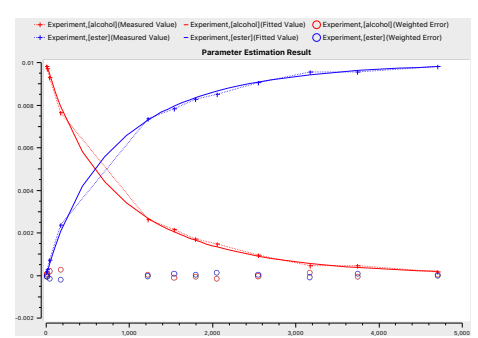
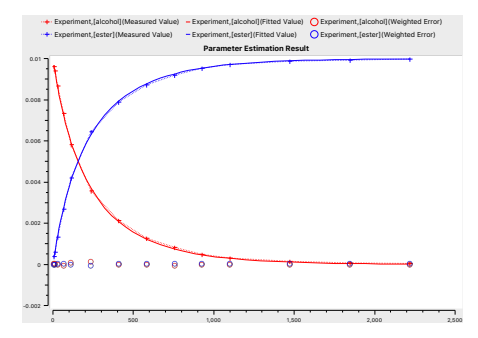
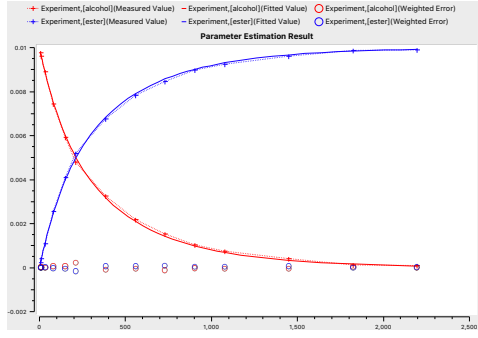
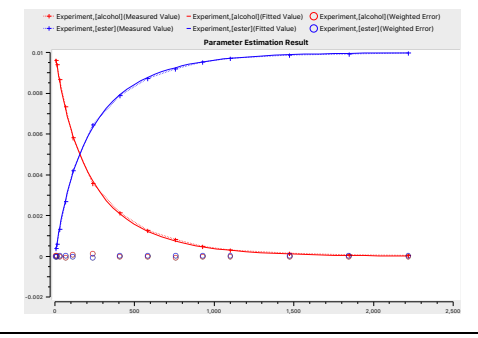


**Figure S24.** Plots of effective rate constants shown in **Table S27** and **Table S28** to determine rate constant and background reaction.

**Table S27.** Effective rate constants for the acetylation of 1-(2-naphthyl)ethanol (**1b**) with isobutyric anhydride (**2**, 2 eq) catalysed by DMAP (**5**). The results of three independent runs of each experiment are presented. A representative CoPaSi simulation for one run is shown, x-axis gives time [min], y-axis intermediate concentration [mol/L] for substrate (red) and product (blue).

				
Catalyst [mol%]	Representative CoPaSi simulation	$k_{eff}$ [ml/(mmol*min <sup>-1</sup> )]	Averaged $k_{eff}$	St.Dev.
2.5		0.066	0.064	0.008
		0.055		
		0.070		
5.0		0.130	0.127	0.008
		0.119		
		0.134		
7.5		0.190	0.200	0.012
		0.213		
		0.196		
10.0		0.262	0.266	0.014
		0.254		
		0.281		

**Table S28.** Effective rate constants for the acetylation of 1-phenylethanol (**1a**) with isobutyric anhydride (**2**, 2 eq) catalysed by DMAP (**5**). The results of three independent runs of each experiment are presented. A representative CoPaSi simulation for one run is shown, x-axis gives time [min], y-axis intermediate concentration [mol/L] for substrate (red) and product (blue).

				
Catalyst [mol%]	Representative CoPaSi simulation	$k_{eff}$ [ml/(mmol*min <sup>-1</sup> )]	Averaged $k_{eff}$	St.Dev.
2.5		0.017	0.017	0.003
		0.020		
		0.014		
5.0		0.033	0.035	0.002
		0.036		
		0.037		
7.5		0.049	0.049	0.002
		0.047		
		0.051		
10.0		0.063	0.067	0.004
		0.070		
		0.069		

### 3. Experimental Procedures

#### 3.1. General Procedures

**General methods:** All reactions sensitive to air and moisture were proceeded under a nitrogen atmosphere and the glassware as well as magnetic stir bars were dried overnight in a dry oven at 110 °C.

**Solvents, reagents, and catalysts:** All reagents and solvents were purchased from the companies TCI, Sigma Aldrich or Fisher Scientific. Diethyl ether was purchased “extra-dry over molecular sieves” from Sigma-Aldrich.  $\text{CDCl}_3$  was freshly distilled from calcium hydride ( $\text{CaH}_2$ ) under nitrogen atmosphere. 1-Phenylethanol (**1a**) was purified by flash chromatography prior to use. Isobutyric anhydride (**2**) and  $\text{PBU}_3$  (**6**) were freshly purified by Kugelrohr-distillation under  $\text{N}_2$  before every use. All other reagents were used without further purification, if not mentioned otherwise. All air- or water-sensitive reagents were stored under nitrogen.

**HPLC analysis:** All HPLC spectra were measured on a Knauer Azura machine with normal-phase optimized pump P6.1L, autosampler AS6.1, column thermostat CT2.1 and diode array detector DAD2.1L. Chiralpak IB-N5 250 x 4.6 mm 5 mic and Vertex Eurospher II 50 x 4.6 mm columns were utilized. Data analysis was performed with ClarityChrom 7.4.1.

**Cryostat:** For reactions at +4 °C the thermostat of the HPLC autosampler AS6.1 was used. For reactions at -50 °C an isopropanol bath cooled by the immersion cooler of a Huber TC100E cryostat was used.

**Chromatography:** Silica gel for column chromatography was purchased from Acros Organics (mesh 35-70). Thin-layer chromatography was performed by using TLC plates purchased by Merck (silica gel 60 F254, thickness 0.2 mm).

**NMR spectroscopy:** All  $^1\text{H}$ -NMR spectra were recorded by Varian INOVA 400 or a Bruker BioSpin NanoBay 400 machine in  $\text{CDCl}_3$  at 400 MHz at 23 °C. All  $^{13}\text{C}$ -NMR spectra were recorded respectively at 101 MHz. The chemical shifts for  $^1\text{H}$  and  $^{13}\text{C}$ -NMR spectra are reported in ppm ( $\delta$ ), relative to the chemical shift of tetramethylsilane (TMS) and the resonance of  $\text{CHCl}_3$  at  $\delta = 7.26$  ppm resp.  $\delta = 77.16$  ppm was used as an internal reference. Spectra were imported and processed in the MestreNova 12.0.4 program. For  $^1\text{H}$ -NMR spectra multiplicity (d = doublet, t = triplet, q = quartet, hept = heptet, dd = doublet of doublets, m = multiplet), coupling constants  $J$ , number of protons and assignment to the structure are reported. In  $^{13}\text{C}$ -NMR spectra singular carbons are marked with (s).

**Mass spectrometry:** Electron ionization (EI) HRMS spectra were recorded on a Thermo Finnigan LTQ FT machine of the MAT 95 type with a direct exposure probe (DEP) and electron impact ionization (EI, 70 eV). For electrospray ionization (ESI) spectra a Thermo Finnigan LTQ FT Ultra Fourier Transform Ion Cyclotron Resonance Mass Spectrometer was utilized.

**X-ray crystallography:** Crystallographic measurements were done using an Oxford Diffraction XCalibur with Saphir CCD-detector and a molybdenum-K $\alpha$ -source ( $\lambda = 0.71073 \text{ \AA}$ ) with concentric circle kappa-device. Structures were resolved using SHELXS or SIR97 and refined with SHELXS.

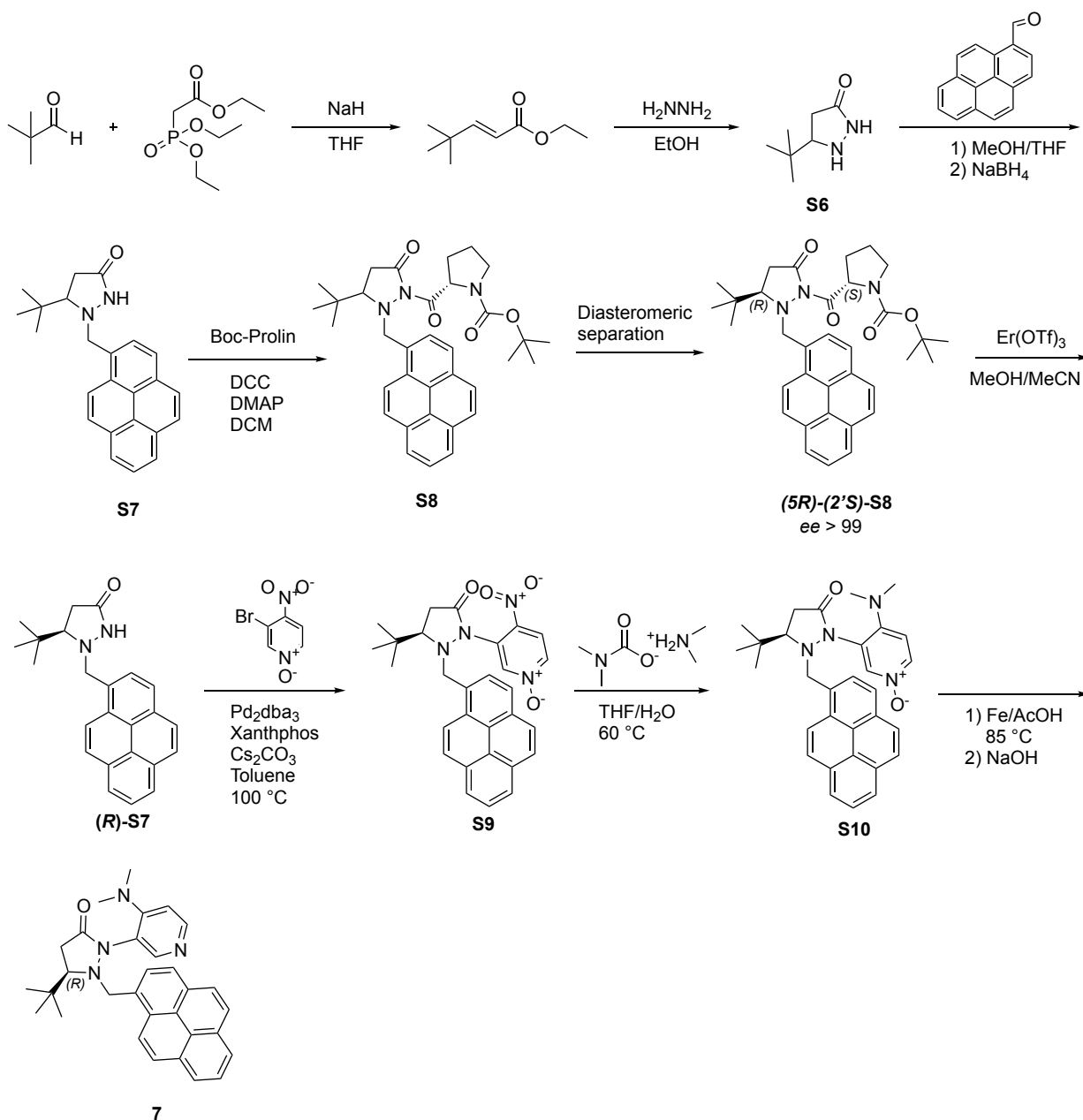
**Optical rotation:** Optical rotation were measured at a Krüss P8000 machine.

**Infrared spectroscopy:** Infrared (IR) spectra were measured at FT-IR Perkin Elmer Spectrum BXII/1000 with Smiths ATR.

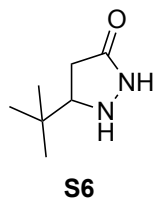
**Melting points:** Melting point were measure at a Büchi M560 and are stated uncorrected.

### 3.2. Synthesis of Catalysts

Catalyst **7** was synthesized following an adapted protocol reported by Sibi *et al.*<sup>[3, 10]</sup> as shown in **Scheme S21**.

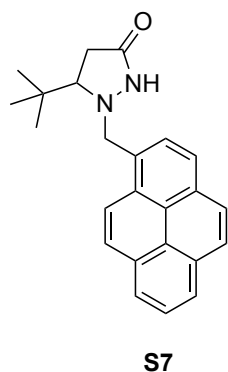


**Scheme S21.** Synthesis of catalyst **7**.<sup>[3, 10]</sup>

**5-(*Tert*-butyl)pyrazolidin-3-one (S6)**

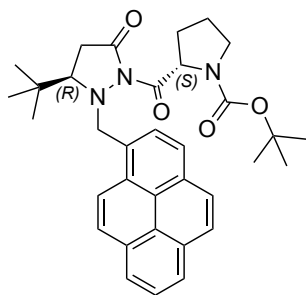
Pivaldehyd (2.15 g, 25.0 mmol, 1.00 eq) is suspended in 30 mL dry THF under N<sub>2</sub> atmosphere, cooled to 0 °C and triethyl phosphonoacetate (6.16 g, 27.5 mmol, 1.10 eq) is added dropwise. After stirring for 15 min sodium hydride (660 mg, 27.5 mmol, 1.10 eq) is carefully added. The mixture is stirred overnight, quenched through addition of 30 mL water, stirred for another 15 min and extracted with diethyl ether (3 x 20 mL), dried over magnesium sulphate, filtered and the solvent was removed under reduced pressure. The solution is used without further purification in the next step.

To the crude solution 50 mL of Ethanol and 2.02 mL of hydrazine monohydrate (1.25 g, 25 mmol, 1.00 eq of hydrazine) is added and heated to reflux for 20 hours. Excess of reagents and solvent is removed under reduced pressure and the residue is used directly without further purification in the next step.

**5-(*Tert*-butyl)-1-(1-pyrenylmethyl)pyrazolidin-3-one (S7)**

Crude **S6** (3.55 g, 25.0 mmol, 1.00 eq) is dissolved in 120 mL of MeOH/THF (1 : 1) and cooled to 0 °C. Pyren-1-carbaldehyde (5.47 g, 23.8 mmol, 0.95 eq) is added and stirred overnight at rt. The solution is cooled to 0 °C and NaBH<sub>4</sub> (898 mg, 23.8 mmol, 0.95 eq) is slowly added. After stirring for 10 min at 0 °C and 30 min at rt a saturated solution of NaHCO<sub>3</sub> and water is added. The dispersion is filtered, the filtrate extracted with DCM (3 x 20 mL), washed with brine, dried over MgSO<sub>4</sub> and the solvent is removed under reduced pressure. After column chromatography (silica gel, *i*Hex/EtOAc = 1/1 – 0/1) 3.78 g of **S7** (10.6 mmol, 45% over three steps) is obtained as a yellow powder.

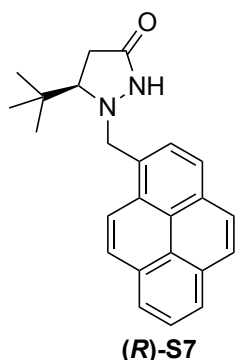
**mp** +178.2 °C. **R<sub>f</sub>** 0.21 (*i*Hex:EtOAc = 1:1). **<sup>1</sup>H NMR** (400 MHz, CDCl<sub>3</sub>) δ 8.48 (d, *J* = 9.3 Hz, 1H, Ar-*H*), 8.22 (dd, *J* = 7.6, 2.6 Hz, 2H, Ar-*H*), 8.19 – 8.12 (m, 2H, Ar-*H*), 8.12 – 8.00 (m, 3H, Ar-*H*), 7.95 (d, *J* = 7.8 Hz, 1H, Ar-*H*), 6.65 (s, 1H, NH), 4.63 (d, *J* = 12.1 Hz, 1H, NCH<sub>2</sub>), 4.52 (d, *J* = 12.1 Hz, 1H, NCH<sub>2</sub>), 3.23 (dd, *J* = 9.6, 2.1 Hz, 1H, COCH<sub>2</sub>), 3.03 (dd, *J* = 17.4, 9.6 Hz, 1H, CH*t*Bu), 2.32 (dd, *J* = 17.4, 2.1 Hz, 1H, COCH<sub>2</sub>), 0.88 (s, 9H, *t*BuH) ppm. **<sup>13</sup>C NMR** (101 MHz, CDCl<sub>3</sub>) δ = 174.6 (C=O), 131.6 (s), 131.4 (s), 130.9 (s), 130.1 (s), 129.6, 129.2, 128.0, 127.8, 127.5, 126.2, 125.6, 125.5, 125.1 (s), 124.8 (s), 124.7, 123.8, 71.8, 63.9, 35.1, 30.2, 25.8 ppm. **ESI-HRMS** *m/z* calc. for C<sub>24</sub>H<sub>24</sub>N<sub>2</sub>O [M+H]<sup>+</sup> 357.1967; found 357.19658; [M-H]<sup>-</sup> 355.1816; found 355.18167. **IR** ν = 3033 (w, =C-H), 2948 (w, -C-H), 1694 (vs, C=O), 1348 (m), 839 (s), 711 (m) cm<sup>-1</sup>.

**2-(*L*-Boc-prolyl)-5-(*R*)-(tert-butyl)-1-(1-pyrenylmethyl)pyrazolidin-3-one (**S8**)****(5*R*)-(2'*S*)-S8**  
ee > 99

A flask with **S7** (3.78 g, 10.6 mmol, 1.00 eq), *N,N'*-dicyclohexyl carbodiimide (2.28 g, 10.6 mmol, 1.00 eq), and DMAP (258 mg, 2.12 mmol, 0.20 eq) is evacuated, purged with N<sub>2</sub> and 110 mL dry DCM is added. After addition of 3.78 g *L*-Boc-prolin (10.6 mmol, 1.00 eq) the mixture is stirred for 48 h. The mixture is filtered and the solvent is evaporated under reduced pressure. After column chromatography (silica, *i*Hex/Acetone = 4/1) 4.85 g (8.76 mmol, 83%) of diastereomeric **S8** is obtained. (*5R*)-(2'*S*)-**S8** (1.87 g, 3.38 mmol, 63% of (*R*)-substrate)

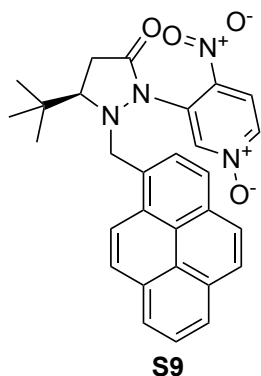
was isolated by repeated column chromatography (silica gel, *i*Hex/Acetone = 9/1, later diastereomer) followed by repeated recrystallization from *i*Hex/Acetone = 9/1 with diastereomeric excess > 99.5 analysed by NMR and HPLC as a white powder.

**mp** +212.2°C. **R<sub>f</sub>** 0.23 (*i*Hex/Acetone = 9/1).  $[\alpha]_{25}^D = -81.7^\circ$  (c 0.50, CHCl<sub>3</sub>). **<sup>1</sup>H NMR** (400 MHz, CDCl<sub>3</sub>)  $\delta$  9.24 (dd, *J* = 9.2, 5.4 Hz, 1H, Ar-*H*), 8.33 – 8.17 (m, 3H, Ar-*H*), 8.16 – 7.98 (m, 4H, Ar-*H*), 7.93 – 7.85 (m, 1H, Ar-*H*), 5.38 (dd, *J* = 9.0, 2.3 Hz, 1H, NCHCO), 5.08 (dd, *J* = 11.4, 8.3 Hz, 1H, NCH<sub>2</sub>Pyr), 4.18 (dd, *J* = 16.4, 11.5 Hz, 1H, NCH<sub>2</sub>Pyr), 3.71 (tt, *J* = 13.4, 5.8 Hz, 1H), 3.63 – 3.42 (m, 1H), 3.31 – 2.99 (m, 2H), 2.58 (d, *J* = 18.1 Hz, 1H), 2.52 – 2.29 (m, 1H), 2.04 – 1.75 (m, 3H), 1.48 (d, *J* = 32.7 Hz, 9H, *t*Bu*H*), 0.43 (d, *J* = 13.3 Hz, 9H, *t*Bu*H*) ppm. **<sup>13</sup>C NMR** (101 MHz, CDCl<sub>3</sub>)  $\delta$  = 174.6 (d, C=O), 169.4 (d, C=O), 154.3 (C=O), 131.8 (d), 131.5, 131.3, 131.2, 129.5, 129.0, 128.2 (d), 128.0 (d), 127.3, 126.2 (d), 125.8 (d), 125.6 (d), 125.2 (d), 125.0, 124.6, 124.2, 79.8 (d), 64.0 (d), 60.6, 59.8, 47.0 (d), 34.5 (d), 32.0, 31.6, 28.6 (d, 3C, *t*Bu), 25.6 (3C, *t*Bu), 22.6 ppm. **ESI-HRMS** *m/z* calc. for C<sub>34</sub>H<sub>39</sub>N<sub>3</sub>O<sub>4</sub> [M+H]<sup>+</sup> 554.30133; found 554.30239; [M-H]<sup>-</sup> 552.28678; found 552.28726. **IR**  $\nu$  = 2928 (w, -C-H), 1734 (s, C=O ester), 1713 (vs, C=O), 1685 (vs, C=O), 1415 (s), 1249 (s), 1199 (s), 1154 (s), 853 (vs) cm<sup>-1</sup>.

**(*R*)-5-(Tert-butyl)-1-(1-pyrenylmethyl)pyrazolidin-3-one (**S7**)****(*R*)-S7**

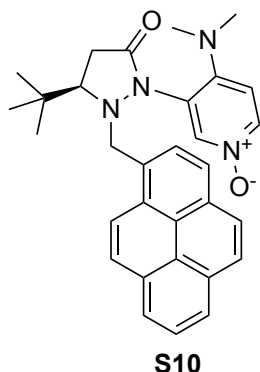
**S8** (1.75 g, 3.16 mmol, 1.00 eq) and Er(OTf)<sub>3</sub> (388 mg, 0.64 mmol, 0.20 eq) is dissolved in 45 mL of MeOH/MeCN (3 : 2) and stirred at rt for two weeks. Solvent is removed under reduced pressure and purification by column chromatography (silica gel, *i*Hex/EtOAc = 1:1) gives 490 mg enantiopure (*R*)-**S7** (1.38 mmol, 44%) as a yellow powder.

$[\alpha]_{25}^D = +99.0^\circ$  (c 0.51, CHCl<sub>3</sub>). Other analytical data are in accordance with (*rac*)-**S7**.

**(R)-3-(3-(tert-butyl)-5-oxo-2-(1-pyrenylmethyl)pyrazolidin-1-yl)-4-nitropyridine N-oxide (S9)**

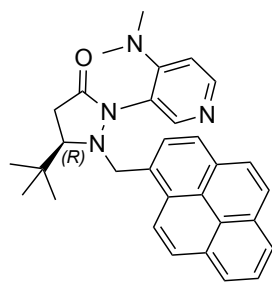
A flask with (*R*)-**S7** (151 mg, 0.42 mmol, 1.0 eq), 3-bromo-4-nitropyridine N-oxide (93 mg, 0.42 mmol, 1.0 eq), Pd<sub>2</sub>dba<sub>3</sub> (19 mg, 0.021 mmol, 0.050 eq), Xantphos (12 mg, 0.021 mmol, 0.050 eq), and Cs<sub>2</sub>CO<sub>3</sub> (239 mg, 0.51 mmol, 1.20 eq) is evacuated, purged with N<sub>2</sub> (3x) and 30 mL dry toluene is added. The mixture is degassed and stirred for 19 h at 100 °C. After cooling and filtration, the solvent is evaporated under reduced pressure. Column chromatography (silica gel, *i*Hex/EtOAc = 1/1) gives 130 mg (0.263 mmol, 62%) of **S9** as a white solid.

**mp** +153°C. **R<sub>f</sub>** 0.23 (*i*Hex/EtOAc = 1/1). [ $\alpha$ ]<sub>25</sub><sup>D</sup> = -309.7 ° (c 0.51, CHCl<sub>3</sub>). **<sup>1</sup>H NMR** (400 MHz, CDCl<sub>3</sub>)  $\delta$  8.50 (s, 1H, Ar-*H*), 8.40 (d, *J* = 9.2 Hz, 1H, Ar-*H*), 8.33 – 8.16 (m, 3H, Ar-*H*), 8.12 – 7.90 (m, 5H, Ar-*H*), 7.54 (s, 2H, Ar-*H*), 4.86 (s, 2H, NCH<sub>2</sub>), 3.39 – 3.25 (m, 2H, COCH<sub>2</sub>), 2.61 – 2.46 (m, 1H, *CHt*Bu), 0.76 (s, 9H, *t*BuH) ppm. **<sup>13</sup>C NMR** (101 MHz, CDCl<sub>3</sub>)  $\delta$  171.1 (C=O), 136.7 (s), 135.7, 134.5, 131.9 (s), 131.2 (s), 130.7 (s), 130.2 (s), 130.0, 129.4 (s), 129.2, 128.3, 127.6 (s), 127.2, 126.5, 126.0 (2C), 124.7 (s), 124.7 (s), 124.3, 122.5, 121.6, 68.9, 62.1, 35.0, 31.0, 25.8 (3C) ppm. **ESI-HRMS** *m/z* calc. for C<sub>29</sub>H<sub>26</sub>N<sub>4</sub>O<sub>4</sub> [M+H]<sup>+</sup> 495.20268; found 495.20215; [M-H]<sup>-</sup> 493.18813; found 493.18817. **IR**  $\nu$  = 2960 (w, -C-H), 1722 (vs, C=O), 1465 (s), 1268 (s), 847 (s), 748 (s) cm<sup>-1</sup>.

**(R)-3-(3-(tert-butyl)-5-oxo-2-(1-pyrenylmethyl)pyrazolidin-1-yl)-DMAP N-oxide (S10)**

**S9** (202 mg, 0.408 mmol, 1.00 eq) and dimethylammonium dimethylcarbamate (Dimcarb, 1.44 mL, 1.52 g, 20.0 eq) are stirred in 10 mL THF/H<sub>2</sub>O (9/1) at 85 °C for 10 days. The solvent is evaporated under reduced pressure. Column chromatography (silica gel, EtOAc/MeOH = 9/1 → EtOAc/MeOH/NEt<sub>3</sub> = 85/10/5) yields 163 mg (0.33 mmol, 81%) of **S10** as orange powder. The product still contained hardly removable traces of a triethylammonium salt and was used without further purification in the next step.

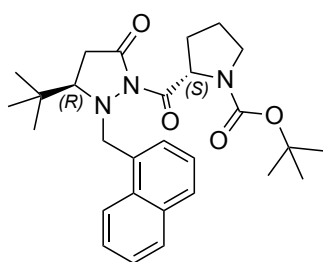
**mp** +177°C. **R<sub>f</sub>** 0.16 (EtOAc/MeOH = 9/1). [ $\alpha$ ]<sub>25</sub><sup>D</sup> = -110.2 ° (c 0.51, CHCl<sub>3</sub>). **<sup>1</sup>H NMR** (400 MHz, CDCl<sub>3</sub>)  $\delta$  8.82 (d, *J* = 2.1 Hz, 1H, Ar-*H*), 8.29 (d, *J* = 9.3 Hz, 1H, Ar-*H*), 8.25 – 8.18 (m, 3H, Ar-*H*), 8.17 – 7.99 (m, 5H, Ar-*H*), 7.95 (d, *J* = 7.8 Hz, 1H, Ar-*H*), 6.73 (d, *J* = 7.4 Hz, 1H, Ar-*H*), 5.07 (d, *J* = 11.6 Hz, 1H, NCH<sub>2</sub>), 4.54 (d, *J* = 11.7 Hz, 1H, NCH<sub>2</sub>), 3.50 – 3.40 (m, impurities of HNEt<sub>3</sub><sup>+</sup>), 3.33 – 3.19 (m, 2H, COCH<sub>2</sub>, *CHt*Bu), 3.04 (s, 6H, NEt<sub>2</sub>), 2.54 (d, *J* = 17.1 Hz, 1H, COCH<sub>2</sub>), 1.97 (s, impurities of HNEt<sub>3</sub><sup>+</sup>), 1.41 – 1.13 (t, impurities of HNEt<sub>3</sub><sup>+</sup>), 0.41 (s, 9H, *t*BuH) ppm. **<sup>13</sup>C NMR** (101 MHz, CDCl<sub>3</sub>)  $\delta$  169.5 (C=O), 145.9 (s), 137.7, 137.0, 131.8 (s), 131.3 (s), 130.8 (s), 130.5 (s), 129.4, 129.0, 128.2, 128.1, 127.4, 126.4, 125.9, 125.8, 124.9 (s), 124.7 (s), 124.4, 123.1 (s), 122.8, 113.9, 66.2, 59.6, 41.3 (2C), 34.5, 31.1, 25.6 (3C) ppm. **ESI-HRMS** *m/z* calc. for C<sub>31</sub>H<sub>32</sub>N<sub>4</sub>O<sub>2</sub> [M+H]<sup>+</sup> 493.25980; found 493.25906. **IR**  $\nu$  = 2956 (w, -C-H), 1698 (vs, C=O), 1424 (s), 1241 (s), 844 (s), 716 (vs) cm<sup>-1</sup>.

**(R)-3-(3-(tert-butyl)-5-oxo-2-(1-pyrenylmethyl)pyrazolidin-1-yl)-DMAP (7)****7**

**S10** (164 mg, 0.333 mmol, 1.00 eq) and iron powder (93 mg, 1.66 mmol, 5.00 eq) are suspended in 8 mL of glacial acetic acid and heated to 85 °C for 21 h. Crushed ice is added and the mixture is basified through addition of 32% NaOH. 10 mL of EtOAc are added and stirred heavily for 1 hour. After filtration the aqueous phase is extracted with EtOAc (3 x 15 mL). The combined organic layers are dried over MgSO<sub>4</sub> and the solvent is evaporated under reduced pressure. Column chromatography (silica gel, EtOAc/MeOH = 98/2) yields 65 mg (0.14 mmol, 41%) of **7** as brown needles.

**mp** +234 °C (decomposition). **R<sub>f</sub>** 0.29 (EtOAc/MeOH = 98/2). [ $\alpha$ ]<sub>25</sub><sup>D</sup> = +38.9 ° (c 0.48, CHCl<sub>3</sub>). **<sup>1</sup>H NMR** (400 MHz, CDCl<sub>3</sub>)  $\delta$  8.99 (s, 1H, Ar-H), 8.28 (d, *J* = 5.9 Hz, 1H, Ar-H), 8.19 (d, *J* = 7.6 Hz, 2H, Ar-H), 8.16 – 7.98 (m, 6H, Ar-H), 7.91 (d, *J* = 7.7 Hz, 1H, Ar-H), 6.74 (d, *J* = 5.9 Hz, 1H, Ar-H), 5.16 (d, *J* = 11.8 Hz, 1H, NCH<sub>2</sub>), 4.46 (d, *J* = 11.7 Hz, 1H, NCH<sub>2</sub>), 3.44 (dd, *J* = 16.9, 9.7 Hz, 1H, CHtBu), 3.24 (d, *J* = 9.6 Hz, 1H, COCH<sub>2</sub>), 3.08 (s, 6H, NEt<sub>2</sub>), 2.56 (d, *J* = 16.9 Hz, 1H, COCH<sub>2</sub>), 0.42 (s, 9H, tBuH) ppm. **<sup>13</sup>C NMR** (101 MHz, CDCl<sub>3</sub>)  $\delta$  = 169.7 (C=O), 152.7 (s), 149.4 (s), 148.7 (s), 131.6 (s), 131.3 (s), 130.9 (s), 130.6 (s), 129.2, 129.1, 128.2, 127.9, 127.4, 126.2, 125.7, 125.5, 124.9 (s), 124.7 (s), 124.3, 123.5, 121.4, 111.6, 66.3, 59.5, 41.2 (2C), 34.6, 31.5, 25.6 (3C) ppm. **ESI-HRMS** *m/z* calc. for C<sub>31</sub>H<sub>32</sub>N<sub>4</sub>O [M+H]<sup>+</sup> 477.26489; found 477.26468. **EA** calc. for C<sub>31</sub>H<sub>32</sub>N<sub>4</sub>O N 11.76, C 78.12, H 6.77, O 3.36; found N 11.62, C 77.34, H 7.01. **IR**  $\nu$  = 2947 (w, -C-H), 1700 (vs, C=O), 1592 (s), 1382 (m), 854 (vs) cm<sup>-1</sup>. **Crystal structure** see Chapter 3.5.

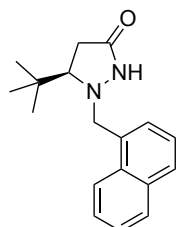
Catalyst **3** was freshly synthesized following the protocol described by Sibi *et al.*<sup>[3, 10]</sup> described above.

**2-L-Boc-prolin-5-(R)-(tert-butyl)-1-(1-naphthylmethyl)pyrazolidin-3-one (S12)****(R)-S12**  
ee > 99

Following literature procedure<sup>[3]</sup> with 2.51 g (8.9 mmol) racemic 5-(tert-butyl)-1-(1-naphthylmethyl)pyrazolidin-3-one **S11** yields 1.05 g of **(R)-S12** (2.18 mmol, 49%) as colourless crystals. Diastereomeric separation was performed by repeated column chromatography (silica gel, *i*Hex/Acetone = 9/1, later diastereomer) followed by repeated recrystallization from *i*Hex/Acetone = 9/1 yielding a diastereomeric excess > 99.5 analysed by NMR and HPLC. Absolute configuration was confirmed by single crystal X-ray analysis. Analytical data are in accordance with literature values.<sup>[3]</sup> [ $\alpha$ ]<sub>25</sub><sup>D</sup> = -32.8 ° (c 0.50, CHCl<sub>3</sub>). **<sup>1</sup>H NMR** (400 MHz, CDCl<sub>3</sub>)  $\delta$  9.03 (t, *J* = 7.6, 7.6 Hz, 1H), 7.83 (t, *J* = 7.0 Hz, 2H), 7.65 (q, *J* = 6.8, 6.8, 5.5 Hz, 1H), 7.51 (t, *J* = 7.0 Hz, 1H), 7.37 (dt, *J* = 14.4, 6.9 Hz, 2H), 5.34 (d, *J* = 8.9 Hz, 1H), 4.82 (t, *J* = 10.3 Hz, 1H), 3.97 – 3.82 (m, 1H), 3.76 – 3.62 (m, 1H), 3.62 – 3.42 (m, 1H), 3.23 – 2.94 (m, 2H), 2.54 (d, *J* = 18.1 Hz, 1H), 2.50 – 2.34 (m, 1H), 1.99 – 1.72 (m, 3H), 1.45 (d, *J* = 32.1 Hz, 9H), 0.47 (d, *J* = 10.9 Hz, 9H) ppm. **<sup>13</sup>C NMR** (101 MHz, CDCl<sub>3</sub>)  $\delta$

174.6 (d), 169.3 (d), 154.3 (d), 133.8, 133.3, 132.2 (d), 129.6, 129.4 (d), 128.0 (d), 126.8 (d), 126.8 (d), 126.3 (d), 124.7 (d), 79.7 (d), 63.9 (d), 60.5, 59.8 (d), 47.0 (d), 34.4 (d), 31.9, 31.0 (d), 28.6 (d), 25.7, 23.3 (d) ppm. **ESI-HRMS**  $m/z$  calc. for  $C_{28}H_{37}N_3O_4$   $[M+H]^+$  480.28568; found 480.28627;  $[M-H]^-$  478.27113; found 478.27142. **Crystal structure** see Chapter 3.5.

**(R)-5-(Tert-butyl)-1-(1-naphthylmethyl)pyrazolidin-3-one ((R)-S11)**

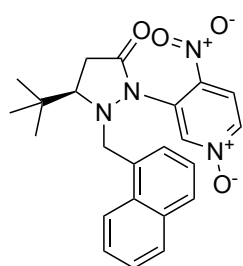


**(R)-S11**

Following literature procedure<sup>[3]</sup> with 1.04 g (2.2 mmol) **(R)-S12** yields 850 mg (1.77 mmol, 84%) of **(R)-S11** as yellow solid. Analytical data are in accordance with literature values.<sup>[3]</sup>

$[\alpha]_{25}^D = -158.5^\circ$  (c 0.42,  $CHCl_3$ ). **<sup>1</sup>H NMR** (400 MHz,  $CDCl_3$ )  $\delta$  8.26 (d,  $J = 8.3$  Hz, 1H), 7.93 – 7.77 (m, 2H), 7.60 – 7.47 (m, 2H), 7.47 – 7.37 (m, 2H), 6.78 (s, br, 1H), 4.39 (d,  $J = 12.1$  Hz, 1H), 4.23 (d,  $J = 12.1$  Hz, 1H), 3.14 (dd,  $J = 9.6, 2.0$  Hz, 1H), 2.99 (dd,  $J = 17.4, 9.6$  Hz, 1H), 2.30 (d,  $J = 19.4$  Hz, 1H), 0.88 (s, 9H) ppm. **<sup>13</sup>C NMR** (101 MHz,  $CDCl_3$ ) 174.5, 134.0, 132.2, 132.2, 129.2, 129.0, 128.8, 126.4, 126.0, 125.3, 124.6, 71.8, 64.0, 35.1, 30.1, 25.8 ppm. **ESI-HRMS**  $m/z$  calc. for  $C_{18}H_{22}N_2O$   $[M+H]^+$  283.1810; found 283.1808;  $[M-H]^-$  281.1659; found 281.1658.

**(R)-3-(3-(tert-butyl)-5-oxo-2-(1-naphthylmethyl)pyrazolidin-1-yl)-4-nitropyridine N-oxide (S13)**



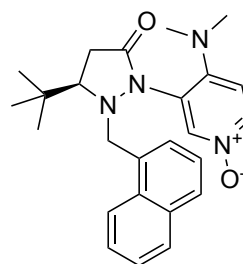
**S13**

**(S13)**

Following literature procedure<sup>[3]</sup> with 419 mg (1.49 mmol) **(R)-S12** yields 474 mg (1.13 mmol, 76%) of **(R)-S11** as reddish solid. Analytical data are in accordance with literature values.<sup>[3]</sup>

$[\alpha]_{25}^D = -559.4^\circ$  (c 0.51,  $CHCl_3$ ). **<sup>1</sup>H NMR** (400 MHz,  $CDCl_3$ )  $\delta$  8.22 (d,  $J = 8.5$  Hz, 1H), 8.09 (s, 1H), 7.83 (dd,  $J = 8.3, 1.2$  Hz, 1H), 7.75 – 7.63 (m, 2H), 7.63 – 7.48 (m, 4H), 7.24 – 7.13 (m, 1H), 4.67 (d,  $J = 12.1$  Hz, 1H), 4.55 (d,  $J = 12.1$  Hz, 1H), 3.42 – 3.27 (m, 2H), 2.53 (d,  $J = 16.0$  Hz, 1H), 0.89 (s, 9H) ppm. **<sup>13</sup>C NMR** (101 MHz,  $CDCl_3$ )  $\delta$  171.0, 136.1, 135.5, 134.3, 133.4, 132.0, 130.4, 130.3, 129.9, 129.5, 129.1, 127.5, 126.5, 124.8, 123.3, 121.4, 70.1, 63.1, 35.2, 31.0, 25.9 ppm. **ESI-HRMS**  $m/z$  calc. for  $C_{23}H_{24}N_4O_4$   $[M+H]^+$  421.1876; found 421.1877;  $[M-H]^-$  419.1725; found 419.1728.

**(R)-3-(3-(tert-butyl)-5-oxo-2-(1-naphthylmethyl)pyrazolidin-1-yl)-DMAP N-oxide (S14)**



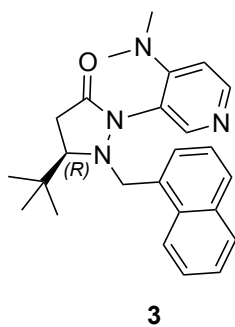
**S14**

Following literature procedure<sup>[3]</sup> with 463 mg (1.10 mmol) **S13** yields 323 mg (0.84 mmol, 77%) of **S14** as yellow solid. Analytical data are in accordance with literature values.<sup>[3]</sup>

$[\alpha]_{25}^D = -166^\circ$  (c 0.49,  $CHCl_3$ ). **<sup>1</sup>H NMR** (400 MHz,  $CDCl_3$ )  $\delta$  8.66 (d,  $J = 2.2$  Hz, 1H), 8.07 – 7.91 (m, 2H), 7.91 – 7.78 (m, 2H), 7.71 – 7.60 (m, 1H), 7.50 (t,  $J = 7.5, 7.5$  Hz, 1H), 7.46 – 7.34 (m, 2H), 6.71 (d,  $J = 7.4$  Hz, 1H), 4.84 (d,  $J = 11.6$  Hz, 1H), 4.23 (d,  $J = 11.6$  Hz, 1H), 3.35 (dd,  $J = 17.1, 9.8$  Hz, 1H),

3.16 (d,  $J = 10.9$  Hz, 1H), 3.01 (s, 6H), 2.49 (d,  $J = 18.3$  Hz, 1H), 0.47 (s, 9H) ppm.  $^{13}\text{C}$  NMR (101 MHz,  $\text{CDCl}_3$ )  $\delta$  169.6, 146.0, 137.7, 137.1, 133.7, 132.5, 131.1, 129.6, 129.4, 128.8, 127.4, 126.4, 124.8, 123.6, 123.1, 113.7, 66.3, 59.8, 41.3, 34.5, 31.0, 25.6 ppm. **ESI-HRMS**  $m/z$  calc. for  $\text{C}_{25}\text{H}_{30}\text{N}_4\text{O}_2$   $[\text{M}+\text{H}]^+$  419.2447; found 419.2452;  $[\text{M}-\text{H}]^-$  417.2296; found 417.2303.

### (*R*)-3-(3-(*tert*-butyl)-5-oxo-2-(1-naphthylmethyl)pyrazolidin-1-yl)-DMAP (3)

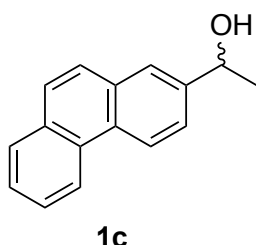


Following literature procedure<sup>[3]</sup> with 200 mg (0.48 mmol) **S14** yields 102 mg (0.25 mmol, 53%) of **S14** as colourless crystals. Analytical data are in accordance with literature values.<sup>[3]</sup>

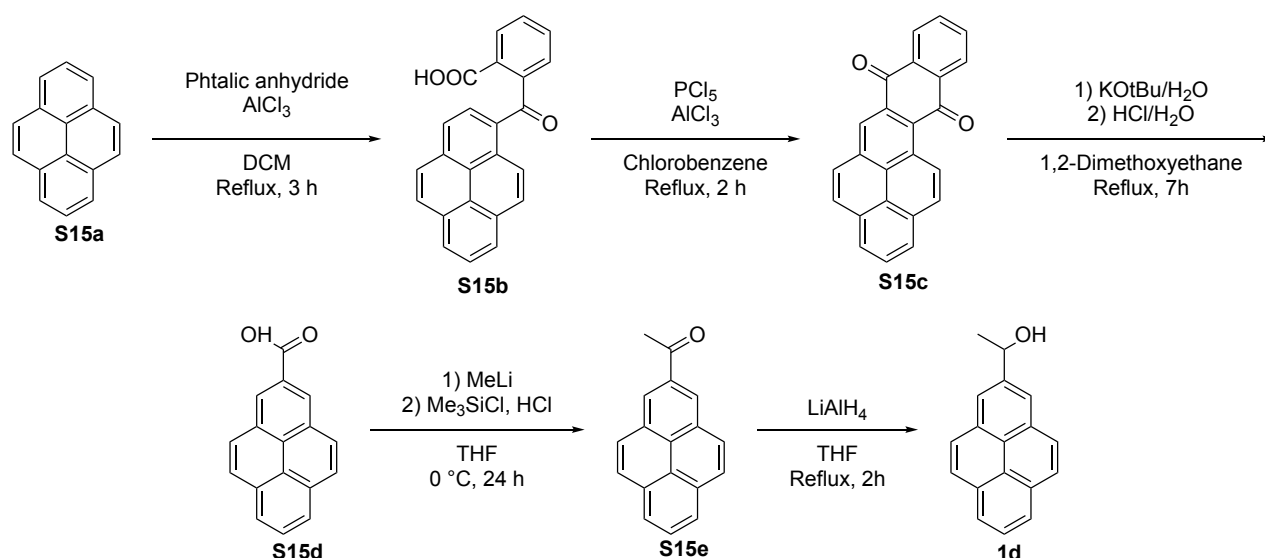
$[\alpha]_{25}^{\text{D}} = -130.1^\circ$  (c 0.54,  $\text{CHCl}_3$ ).  $^1\text{H}$  NMR (400 MHz,  $\text{CDCl}_3$ )  $\delta$  8.83 (s, 1H, Ar-H), 8.23 (d,  $J = 5.9$  Hz, 1H, Ar-H), 7.90 – 7.74 (m, 3H, Ar-H), 7.51 – 7.32 (m, 4H, Ar-H), 6.70 (d,  $J = 5.9$  Hz, 1H, Ar-H), 4.92 (d,  $J = 11.7$  Hz, 1H,  $\text{NCH}_2$ ), 4.15 (d,  $J = 11.7$  Hz, 1H,  $\text{NCH}_2$ ), 3.34 (dd,  $J = 17.0, 9.9$  Hz, 1H,  $\text{CHtBu}$ ), 3.15 (d,  $J = 9.7$  Hz, 1H,  $\text{COCH}_2$ ), 3.03 (s, 6H,  $\text{NEt}_2$ ), 2.51 (d,  $J = 18.2$  Hz, 1H,  $\text{COCH}_2$ ), 0.48 (s, 9H,  $\text{tBuH}$ ) ppm.  $^{13}\text{C}$  NMR (101 MHz,  $\text{CDCl}_3$ )  $\delta$  169.8 (C=O), 152.9 (s), 149.6, 148.7, 133.7 (s), 132.6 (s), 131.9 (s), 129.3, 129.0, 128.5, 126.6, 126.1, 124.8, 124.2, 121.3 (s), 111.5, 66.2, 59.6, 41.2 (2C), 34.5, 31.4, 25.6 (3C) ppm. **ESI-HRMS**  $m/z$  calc. for  $\text{C}_{25}\text{H}_{30}\text{N}_4\text{O}$   $[\text{M}+\text{H}]^+$  403.24924; found 403.24855;  $[\text{M}+\text{Cl}]^-$  437.21137; found 437.2114.

## 3.3. Synthesis of Alcohols

### 1-(2-Phenanthryl)ethanol (1c)

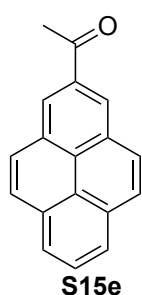


A solution of 2-acetylphenanthren (300 mg, 1.36 mmol, 1.00 eq) in dry THF (10 mL) is dropped into a suspension of  $\text{LiAlH}_4$  (77 mg, 2.03 mmol, 1.50 eq) in 5 mL of dry THF at  $0^\circ\text{C}$ . After heating to reflux for 2 h the reaction mixture is cooled to  $0^\circ\text{C}$  and 5 mL of water is added. The mixture is stirred for 15 min at rt and HCl (2M) is added. The mixture is extracted with DCM (3 x 10 mL), the organic phase washed with brine (10 mL), dried over  $\text{MgSO}_4$  and the solvent is evaporated under reduced pressure. Recrystallization from *i*Hex/EtOAc (9/1) yields 210 mg (0.95 mmol, 70%) **1c** as white needles. Analytical data were found to be in accordance with literature values.<sup>[11]</sup> **mp**  $+126^\circ\text{C}$ .  $^1\text{H}$  NMR (400 MHz,  $\text{CDCl}_3$ )  $\delta$  8.68 (d,  $J = 8.5$  Hz, 2H, Ar-H), 7.96 – 7.85 (m, 2H, Ar-H), 7.75 (d,  $J = 1.5$  Hz, 2H, Ar-H), 7.71 – 7.54 (m, 3H, Ar-H), 5.14 (qd,  $J = 6.4, 2.9$  Hz, 1H,  $\text{CHOH}$ ), 1.95 (d,  $J = 3.1$  Hz, 1H, OH), 1.63 (d,  $J = 6.5$  Hz, 3H,  $\text{CH}_3\text{CHOH}$ ) ppm. **EI-HRMS**  $m/z$  calc. for  $\text{C}_{16}\text{H}_{14}\text{O}$   $[\text{M}]^+$  222.1039; found 222.1039. **HPLC** (Chiralpak IB-N5, 0.5 mL/min, *i*Hex/*i*Prop = 98/2 (13 min)  $\rightarrow$  91/9 (39 min)  $\rightarrow$  70/30,  $T = +10$ ,  $\lambda = 285$  nm)  $t_1$  (S) = 49.7 min,  $t_2$  (R) = 51.9 min.



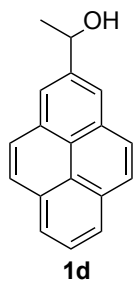
**Scheme S22.** Synthesis of 1-(2-pyrenyl)ethanol (**1d**). The first three steps to **S15d** follow a procedure described in the literature.<sup>[12]</sup> Synthesis of **1d** was adapted from literature.<sup>[13]</sup>

## 2-Acetylpyren (S15e)



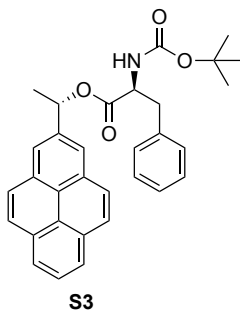
2-Pyrenyl carboxylic acid **S15d** was synthesized following the literature procedure<sup>[12]</sup> shown in **Scheme S22** starting from 5.0 g of pyrene **S15a** (24.7 mmol, 1.0 eq). Crude intermediates NMR data were in accordance with literature values. Crude 2-pyrenyl carboxylic acid **S15d** (4.50 g, 18.2 mmol, 1.0 eq) was solved in 80 mL of dry THF under N<sub>2</sub> atmosphere and cooled to 0 °C. A 1.6 M solution of methyl lithium in diethyl ether (28.5 mL, 45 mmol, 2.5 eq) is dropped slowly into the solution under ice cooling.

The reaction mixture is stirred for 24 h and quenched with trimethyl silyl chloride (12.7 mL, 100 mmol). After addition of 50 mL of HCl (aq) the reaction mixture is extracted with EtOAc (3 x 20 mL), dried over MgSO<sub>4</sub>, filtered and the solvent is evaporated. Column chromatography (silica, *i*Hex/EtOAc = 9/1) gives 1.93 g of **1de** (7.9 mmol, 32% over 4 steps) as brown solid. **mp** +145 °C. **<sup>1</sup>H NMR** (400 MHz, CDCl<sub>3</sub>) δ 8.64 (s, 2H, Ar-*H*), 8.16 (d, *J* = 7.5 Hz, 2H, Ar-*H*), 8.11 – 7.97 (m, 5H, Ar-*H*), 2.87 (s, 3H, COCH<sub>3</sub>) ppm. **<sup>13</sup>C NMR** (101 MHz, CDCl<sub>3</sub>) δ 198.8 (C=O), 134.1 (s), 131.8 (s), 131.0 (s), 128.3, 127.9, 127.2 (s), 127.0 (s), 125.5, 124.5, 124.2 (s), 27.2 ppm. **EI-HRMS** *m/z* calc. for C<sub>18</sub>H<sub>12</sub>O [M]<sup>+</sup> 244.0888; found 244.0890. **IR** *v* = 3039 (w, =C-H), 1674 (vs, C=O), 1292.7 (s), 1205.8 (s), 873.7 (s), 843.8 (s), 838.7 (s), 704.6 (vs) cm<sup>-1</sup>.

**1-(2-Pyrenyl)ethanol (1d)**

A solution of 2-acetylpyren **S15e** (1.9 g, 7.8 mmol, 1.0 eq) in dry THF (50 mL) is dropped to a dispersion of 444 mg of LiAlH<sub>4</sub> (11.7 mmol, 1.5 eq) in 10 ml of dry THF at 0 °C. After heating to reflux for 2 h the reaction mixture is cooled to 0 °C and 10 mL of water is added. The mixture is stirred for 15 min at rt and HCl (2M) is added. The mixture is extracted with DCM (3 x 10 mL), the organic phase washed with brine (10 mL), dried over MgSO<sub>4</sub>, filtered and the solvent is evaporated under reduced pressure. Column chromatography (silica, *i*Hex/EtOAc = 4/1 → 2/1) followed by repeated recrystallization from *i*Hex/EtOAc (9/1) yields 1.8 g (7.32 mmol, 94%) **1d** as brown needles. Synthetic data are in accordance with literature data.<sup>[14]</sup>

**mp** +136°C. **<sup>1</sup>H NMR** (400 MHz, CDCl<sub>3</sub>) δ 8.18 (t, *J* = 3.8, 4H, Ar-*H*), 8.13 – 8.03 (m, 4H, Ar-*H*), 8.00 (t, *J* = 7.6, 7.6 Hz, 1H, Ar-*H*), 5.47 – 5.24 (m, 1H, CHO*H*), 2.12 (d, *J* = 2.4 Hz, 1H, OH), 1.73 (d, *J* = 6.5 Hz, 3H, CH<sub>3</sub>CHO*H*) ppm. **<sup>13</sup>C NMR** (101 MHz, CDCl<sub>3</sub>) δ 143.7 (s), 131.4 (s), 131.1 (s), 127.8, 127.5, 125.9 (s), 125.2, 124.7 (s), 124.3 (s), 122.0, 71.1, 26.1 ppm. **EI-HRMS** *m/z* calc. for C<sub>18</sub>H<sub>14</sub>O [M]<sup>+</sup> 246.1039; found 246.1040. **EA** calc. for C<sub>18</sub>H<sub>14</sub>O C 87.78, H 5.73; found C 87.88, H 5.78. **IR** ν = 3279 (br, O-H), 2961 (w, -C-H), 1474 (m), 1099 (m), 880 (s), 712 (vs) cm<sup>-1</sup>. **Crystal structure** see Chapter 3.5. **HPLC** (Chiralpak IB-N5, 0.5 mL/min, *i*Hex/*i*Prop = 98/2 (19 min) → 87/13 (38 min) → 70/30, *T* = +10, λ = 285 nm) *t*<sub>1</sub> (*S*) = 46.8 min, *t*<sub>2</sub> (*R*) = 51.0 min.

**3.4. Synthesis of Esters****(S)-1-(pyren-2-yl)ethyl (tert-butoxycarbonyl)-L-phenylalaninate (S3)**

In a kinetic resolution experiment alcohol **1d** (98.4 mg, 0.40 mmol, 1.0 eq) and catalyst **3** (16 mg, 0.04 mmol, 0.10 eq) are solved in 8 mL of dry diethyl ether and cooled to -50 °C. Isobutyric anhydride (37.8 mg, 0.24 mmol, 0.60 eq) in 1 mL of diethyl ether is added and stirred for 48 h at -50 °C. The reaction mixture is quenched through addition of methanol and the solvent is removed under reduced pressure. Unreacted alcohol (*S*)-**1d** is isolated from the reaction mixture by column chromatography (silica, *i*Hex/EtOAc = 9/1). 36 mg of enantiopure (*S*)-**1d** (0.15 mmol, 1.0 eq), 34 mg of EDC (1-ethyl-3-(3-dimethylaminopropyl)carbodiimide, 0.22 mmol, 1.5 eq), 3.6 mg DMAP (0.03 mmol, 0.2 eq) and 46 mg (0.18 mmol, 1.2 eq) of *N*-(*tert*-butoxycarbonyl)-L-phenylalanine **S2** are solved under N<sub>2</sub> atmosphere in dry DCM and stirred at rt for 24 hours. The reaction mixture is washed with water and brine, dried over MgSO<sub>4</sub>, filtered and the solvent is removed under reduced pressure. Column chromatography (silica, *i*Hex/EtOAc = 6/1) followed by recrystallization from diethyl ether yields 66 mg (0.13 mmol, 84% over two steps) of **S3** as white crystals.

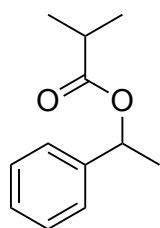
**mp** +148°C. **<sup>1</sup>H NMR** (400 MHz, CDCl<sub>3</sub>) δ 8.24 – 7.98 (m, 9H, Pyr-*H*), 7.07 – 6.77 (m, 5H, Ph-*H*), 6.37 (q, *J* = 6.6 Hz, 1H, PyrCHOR), 4.97 (d, *J* = 8.2 Hz, 1H, NH), 4.68 (q, *J* = 6.0 Hz, 1H, CHNH),

3.12 – 2.94 (m, 2H, PhCH<sub>2</sub>), 1.79 (d, *J* = 6.6 Hz, 3H, CH<sub>3</sub>), 1.41 (s, 9H, *t*Bu-*H*) ppm. <sup>13</sup>C NMR (101 MHz, CDCl<sub>3</sub>) δ 171.5 (s), 155.3 (s), 138.5 (s), 135.7, 131.4 (s), 131.3 (s), 129.4, 128.4, 128.0, 127.5, 126.9 (s), 126.2, 125.3, 124.6 (s, 2C), 123.1, 80.0 (s), 74.2, 54.5, 38.2, 28.5, 22.6 ppm. **EI-HRMS** *m/z* calc. for C<sub>32</sub>H<sub>31</sub>NO<sub>4</sub> [M]<sup>+</sup> 493.2248; found 493.2249. **IR**  $\nu$  = 3377 (m, N-H), 2930 (w, -C-H), 1737 (s, C=O), 1685 (s, C=O), 1515 (s), 1246 (vs), 710 (vs) cm<sup>-1</sup>. **Crystal structure** see Chapter 3.5.

### GP1: Esterification of alcohols

A dry Schlenk flask with 1.0 eq of the corresponding alcohol and 0.1 eq of DMAP is evaporated and purged with N<sub>2</sub>. After addition of 1.1 eq of isobutyric anhydride the mixture is solved in dry THF and stirred at rt under N<sub>2</sub> atmosphere overnight. The reaction is quenched through addition of water, extracted with DCM (3x), dried over MgSO<sub>4</sub>, filtered and the solvent is evaporated. The crude product is purified by column chromatography (*i*Hex/EtOAc = 9/1).

#### 1-Phenylethyl isobutyrate (4a)



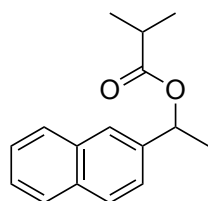
**4a**

**4a** is synthesized following **GP1** with **1c** (1.22 g, 10.0 mmol) and yields 1.40 g (7.29 mmol, 73%) of colorless liquid. <sup>1</sup>H-NMR data were found to be in accordance with literature values.<sup>[15]</sup>

**<sup>1</sup>H NMR** (400 MHz, CDCl<sub>3</sub>) δ 7.39 – 7.27 (m, 5H, Ar-*H*), 5.87 (q, *J* = 6.6 Hz, 1H), 2.57 (hept, *J* = 7.0 Hz, 1H, CH(CH<sub>3</sub>)<sub>2</sub>), 1.53 (d, *J* = 6.6 Hz, 3H, CH<sub>3</sub>CHO), 1.18 (d, *J* = 7.0 Hz, 3H, CH(CH<sub>3</sub>)<sub>2</sub>), 1.16 (d, *J* = 7.0 Hz, 3H, CH(CH<sub>3</sub>)<sub>2</sub>) ppm. **EI-HRMS** *m/z* calc. for

C<sub>12</sub>H<sub>16</sub>O<sub>2</sub> [M]<sup>+</sup> 192.1145; found 192.1141. **HPLC** (Chiralpak IB-N5 250 x 4.6 mm, 0.5 mL/min, *i*Hex/*i*Prop = 100/0 (10 min) → 98/2, *T* = +10,  $\lambda$  = 215 nm) *t*<sub>1</sub> (*R*) = 18.1 min, *t*<sub>2</sub> (*S*) = 20.9 min.

#### 1-(2-Naphthyl)ethyl isobutyrate (4b)

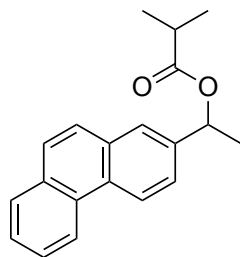


**4b**

**4b** is synthesized following **GP1** with **1b** (320 mg, 1.9 mmol) and yields 310 mg (1.28 mmol, 67%) of colourless liquid. <sup>1</sup>H-NMR data were found to be in accordance with literature values.<sup>[16]</sup>

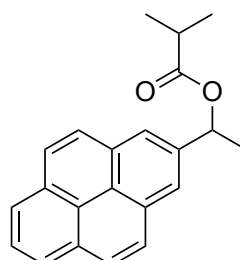
**<sup>1</sup>H NMR** (400 MHz, CDCl<sub>3</sub>) δ 7.90 – 7.73 (m, 4H, Ar-*H*), 7.48 (dd, *J* = 6.7, 2.9 Hz, 3H, Ar-*H*), 6.05 (q, *J* = 6.6 Hz, 1H, CHOCO*i*Pr), 2.60 (hept, *J* = 7.0 Hz, 1H,

CH(CH<sub>3</sub>)<sub>2</sub>), 1.62 (d, *J* = 6.6 Hz, 3H, CH<sub>3</sub>CHO), , 1.20 (d, *J* = 7.0 Hz, 3H, CH(CH<sub>3</sub>)<sub>2</sub>), 1.17 (d, *J* = 7.0 Hz, 3H, CH(CH<sub>3</sub>)<sub>2</sub>) ppm. **EI-HRMS** *m/z* calc. for C<sub>16</sub>H<sub>18</sub>O<sub>2</sub> [M]<sup>+</sup> 242.1301; found 242.1302. **HPLC** (Chiralpak IB-N5, 0.5 mL/min, *i*Hex/*i*Prop = 98/2, *T* = +10,  $\lambda$  = 285 nm) *t*<sub>1</sub> (*R*) = 11.8 min, *t*<sub>2</sub> (*S*) = 13.8 min.

**1-(2-Phenanthryl)ethyl isobutyrate (4c)****4c**

**4c** is synthesized following **GP1** from **1c** (50 mg, 0.23 mmol) and yields 62 mg (0.21 mmol, 94%) as white fluffy solid.

**mp** +73.5°C. **<sup>1</sup>H NMR** (400 MHz, CDCl<sub>3</sub>) δ 8.67 (dd, *J* = 8.3, 2.5 Hz, 2H, Ar-*H*), 7.92 – 7.84 (m, 2H, Ar-*H*), 7.79 – 7.70 (m, 2H, Ar-*H*), 7.66 (t, *J* = 7.1 Hz, 2H, Ar-*H*), 7.60 (t, *J* = 7.3 Hz, 1H, Ar-*H*), 6.10 (q, *J* = 6.6 Hz, 1H, CHOCO*i*Pr), 2.62 (hept, *J* = 6.7 Hz, 1H, CH(CH<sub>3</sub>)<sub>2</sub>), 1.65 (d, *J* = 6.6 Hz, 3H, CH<sub>3</sub>CHO), 1.22 (d, *J* = 7.0 Hz, 3H, CH(CH<sub>3</sub>)<sub>2</sub>), 1.19 (d, *J* = 7.0 Hz, 3H, CH(CH<sub>3</sub>)<sub>2</sub>) ppm. **<sup>13</sup>C NMR** (101 MHz, CDCl<sub>3</sub>) δ 176.5 (C=O), 140.3 (s), 132.2 (s), 132.1 (s), 130.3 (s), 130.0 (s), 128.7, 127.4, 127.0, 126.8, 126.7, 125.9, 124.7, 123.2, 122.8, 72.0, 34.3, 22.5, 19.1 (2C) ppm. **EI-HRMS** *m/z* calc. for C<sub>20</sub>H<sub>20</sub>O<sub>2</sub> [M]<sup>+</sup> 292.1458; found 292.1457. **IR**  $\nu$  = 2974 (w, -C-H), 1726 (vs, C=O), 1196 (s), 1061 (s), 815 (s), 749 (vs), 717 (s) cm<sup>-1</sup>. **HPLC** (Chiralpak IB-N5, 0.5 mL/min, *i*Hex/*i*Prop = 98/2 (13 min) → 91/9, *T* = +10,  $\lambda$  = 285 nm) *t*<sub>1</sub> (*R*) = 19.5 min, *t*<sub>2</sub> (*S*) = 31.5 min (br).

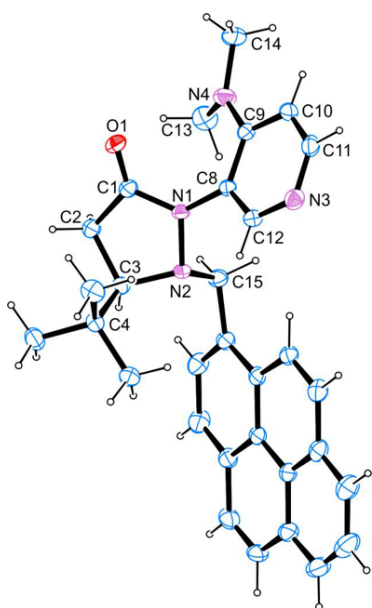
**1-(2-Pyrenyl)ethyl isobutyrate (4d)****4d**

**4d** is synthesized following **GP1** from **1d** (60 mg, 0.24 mmol) and yields 69 mg (0.22 mmol, 91%) of white powder.

**mp** +59.6°C. **<sup>1</sup>H NMR** (400 MHz, CDCl<sub>3</sub>) δ 8.18 (m, 4H, Ar-*H*), 8.08 (m, 4H, Ar-*H*), 8.04 – 7.97 (m, 1H), Ar-*H*, 6.33 (q, *J* = 6.6 Hz, 1H, CHOCO*i*Pr), 2.66 (hept, *J* = 7.0 Hz, 1H, CH(CH<sub>3</sub>)<sub>2</sub>), 1.76 (d, *J* = 6.6 Hz, 3H, CH<sub>3</sub>CHO), 1.24 (d, *J* = 7.0 Hz, 3H, CH(CH<sub>3</sub>)<sub>2</sub>), 1.20 (d, *J* = 7.0 Hz, 3H, CH(CH<sub>3</sub>)<sub>2</sub>) ppm. **<sup>13</sup>C NMR** (101 MHz, CDCl<sub>3</sub>) δ 176.6 (C=O), 139.8 (s), 131.4 (s, 2C), 131.2 (s, 2C), 127.9 (S, 2C), 127.5 (S, 2C), 126.1, 125.2 (2C), 124.6 (s), 124.4 (s), 122.6 (2C), 72.6, 34.4, 23.1, 19.2, 19.1 (2C) ppm. **EI-HRMS** *m/z* calc. for C<sub>22</sub>H<sub>20</sub>O<sub>2</sub> [M]<sup>+</sup> 316.1458; found 316.1460. **IR**  $\nu$  = 2970 (w, -C-H), 1719 (vs, C=O), 1196 (s), 1060 (s), 816 (s), 712 (s) cm<sup>-1</sup>. **HPLC** (Chiralpak IB-N5, 0.5 mL/min, *i*Hex/*i*Prop = 98/2 (19 min) → 87/13, *T* = +10,  $\lambda$  = 285 nm) *t*<sub>1</sub> (*R*) = 18.9 min, *t*<sub>2</sub> (*S*) = 22.4 min.

## 3.5. X-Ray Crystal Structure Data

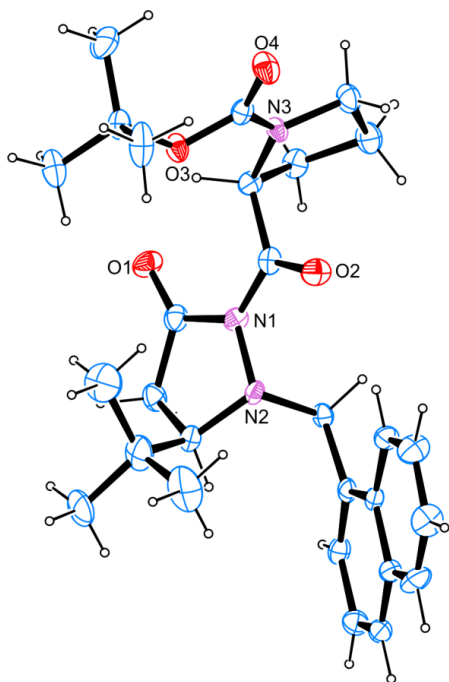
## Catalyst 7



**Figure S25.** X-ray crystal structure of catalyst 7. The crystal structure can be retrieved from the Cambridge Crystallographic Data Centre (CCDC) with deposition number 2008575.

**Table S29.** Crystallographic data for catalyst 7.

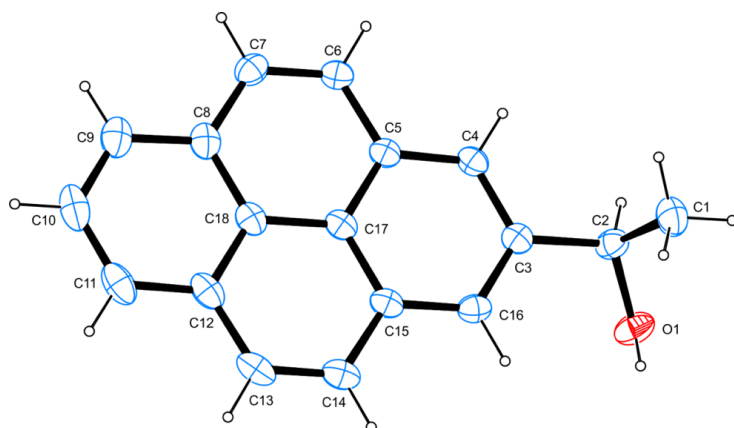
net formula	$C_{31}H_{32}N_4O$	transmission factor range	0.85–1.00
Mr/g mol <sup>-1</sup>	476.60	refls. measured	15007
crystal size/mm	0.100 × 0.070 × 0.050	$R_{int}$	0.0410
T/K	102.(2)	mean $\sigma(I)/I$	0.0498
radiation	MoK $\alpha$	$\theta$ range	3.154–27.478
diffractometer	'Bruker D8 Venture TXS'	observed refls.	5528
crystal system	monoclinic	x, y (weighting scheme)	0.0365, 0.3227
space group	'P 1 21 1'	hydrogen refinement	constr
a/Å	9.5123(4)	Flack parameter	-0.2(7)
b/Å	12.9168(6)	refls in refinement	5913
c/Å	11.0888(5)	parameters	330
$\alpha/^\circ$	90	restraints	1
$\beta/^\circ$	106.633(2)	$R(F_{obs})$	0.0399
$\gamma/^\circ$	90	$R_w(F^2)$	0.1011
V/Å <sup>3</sup>	1305.46(10)	S	1.070
Z	2	shift/error <sub>max</sub>	0.001
calc. density/g cm <sup>-3</sup>	1.212	max electron density/e Å <sup>-3</sup>	0.222
$\mu/mm^{-1}$	0.075	min electron density/e Å <sup>-3</sup>	-0.179
absorption correction	Multi-Scan		

**2-L-Boc-prolin-5-(R)-(tert-butyl)-1-(1-naphthylmethyl)pyrazolidin-3-one (S12)**

**Figure S26.** X-ray crystal structure of precursor **S12** for determination of absolute configuration for catalyst **3**. The crystal structure can be retrieved from Cambridge Crystallographic Data Centre (CCDC) with deposition number 2008577.

**Table S30.** Crystallographic data for precursor **S12**.

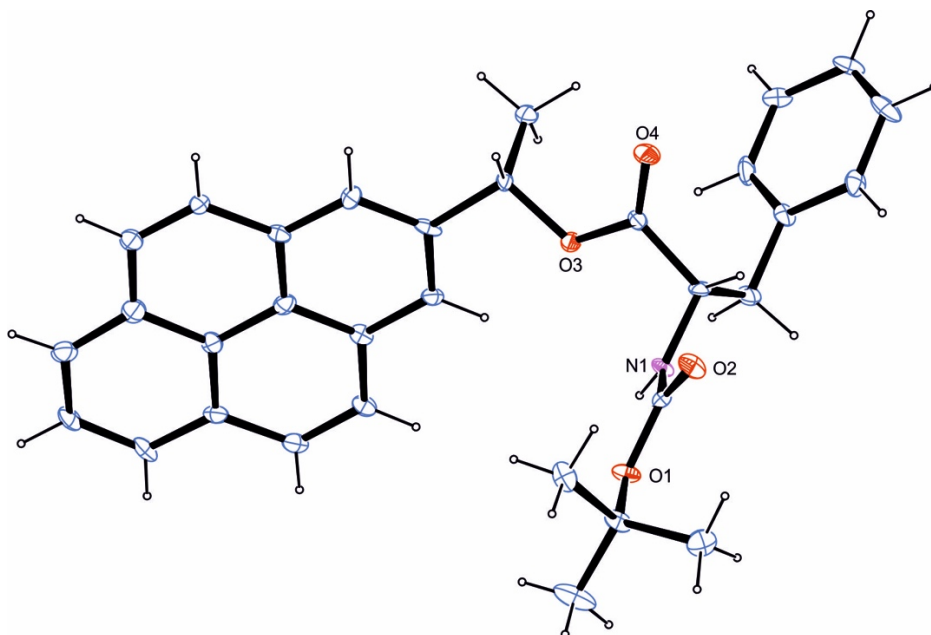
net formula	$C_{28}H_{37}N_3O_4$	transmission factor range	0.82–1.00
Mr/g mol <sup>-1</sup>	479.60	refls. measured	5448
crystal size/mm	0.100 × 0.070 × 0.020	$R_{int}$	0.0815
T/K	102.(2)	mean $\sigma(I)/I$	0.0472
radiation	MoK $\alpha$	$\theta$ range	2.456–26.371
diffractometer	'Bruker D8 Venture TXS'	observed refls.	5050
crystal system	monoclinic	x, y (weighting scheme)	0.0368, 2.0438
space group	'P 1 21 1'	hydrogen refinement	constr
a/Å	8.9974(5)	Flack parameter	0.2(16)
b/Å	11.9330(4)	refls in refinement	5448
c/Å	25.1442(11)	parameters	644
$\alpha$ /°	90	restraints	1
$\beta$ /°	98.388(2)	$R(F_{obs})$	0.0497
$\gamma$ /°	90	$R_w(F^2)$	0.1140
V/Å <sup>3</sup>	2670.8(2)	S	1.098
Z	4	shift/error <sub>max</sub>	0.001
calc. density/g cm <sup>-3</sup>	1.193	max electron density/e Å <sup>-3</sup>	0.212
$\mu$ /mm <sup>-1</sup>	0.080	min electron density/e Å <sup>-3</sup>	-0.227
absorption correction	Multi-Scan		

**1-(2-Pyrenyl)ethanol (1d)**

**Figure S27.** X-ray crystal structure of 1-(2-pyrenyl)ethanol (**1d**). The crystal structure can be retrieved from the Cambridge Crystallographic Data Centre (CCDC) with deposition number 2008574.

**Table S31.** Crystallographic data for 1-(2-pyrenyl)ethanol **1d**.

net formula	$C_{18}H_{14}O$	transmission factor range	0.86–1.00
Mr/g mol <sup>-1</sup>	246.29	refls. measured	12646
crystal size/mm	0.100 × 0.070 × 0.050	$R_{int}$	0.0370
T/K	102.(2)	mean $\sigma(I)/I$	0.0296
radiation	MoK $\alpha$	$\theta$ range	3.210–26.372
diffractometer	'Bruker D8 Venture TXS'	observed refls.	2066
crystal system	monoclinic	x, y (weighting scheme)	0.0614, 0.3144
space group	'P 1 21/c 1'	hydrogen refinement	H(C) constr, H(O) refall
a/Å	20.3785(19)	refls in refinement	2513
b/Å	4.8023(4)	parameters	177
c/Å	13.0679(12)	restraints	0
$\alpha/^\circ$	90	$R(F_{obs})$	0.0416
$\beta/^\circ$	103.761(3)	$R_w(F^2)$	0.1230
$\gamma/^\circ$	90	S	1.090
V/Å <sup>3</sup>	1242.16(19)	shift/error <sub>max</sub>	0.001
Z	4	max electron density/e Å <sup>-3</sup>	0.172
calc. density/g cm <sup>-3</sup>	1.317	min electron density/e Å <sup>-3</sup>	-0.180
$\mu/mm^{-1}$	0.080		
absorption correction	Multi-Scan		

**(S)-1-(2-Pyrenyl)ethyl BOC-L-phenylalaninate (S3)**

**Figure S28.** X-ray crystal structure of (S)-1-(2-pyrenyl)ethyl BOC-L-phenylalaninate (**S3**). The crystal structure can be retrieved from at the Cambridge Crystallographic Data Centre (CCDC) with deposition number 2008576.

**Table S32.** Crystallographic data for (S)-1-(2-pyrenyl)ethyl BOC-L-phenylalaninate (**S3**).

net formula	C <sub>32</sub> H <sub>31</sub> NO <sub>4</sub>	transmission factor range	0.78–1.00
Mr/g mol <sup>-1</sup>	493.58	refls. measured	19775
crystal size/mm	0.100 × 0.030 × 0.020	R <sub>int</sub>	0.0459
T/K	102.(2)	mean σ(I)/I	0.0794
radiation	MoKα	θ range	2.277–25.345
diffractometer	Bruker D8 Venture TXS'	observed refls.	7205
crystal system	monoclinic	x, y (weighting scheme)	0.0408, 0.5045
space group	'P 1 21 1'	hydrogen refinement	constr
a/Å	5.2875(3)	Flack parameter	0.6(7)
b/Å	39.464(2)	refls in refinement	8548
c/Å	12.1953(7)	parameters	676
α/°	90	restraints	1
β/°	90.0081(18)	R(F <sub>obs</sub> )	0.0519
γ/°	90	R <sub>w</sub> (F <sup>2</sup> )	0.1086
V/Å <sup>3</sup>	2544.7(2)	S	1.043
Z	4	shift/error <sub>max</sub>	0.001
calc. density/g cm <sup>-3</sup>	1.288	max electron density/e Å <sup>-3</sup>	0.244
μ/mm <sup>-1</sup>	0.084	min electron density/e Å <sup>-3</sup>	-0.212
absorption correction	Multi-Scan		

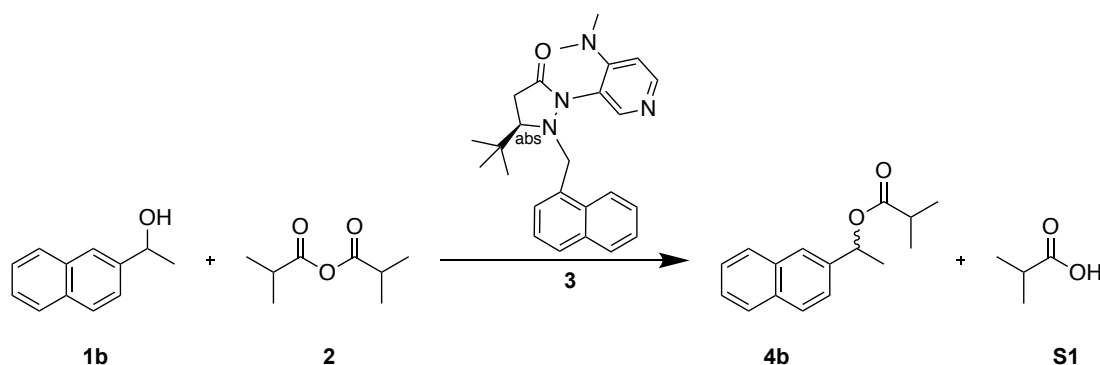
## 4. Computational Study

### 4.1. Computational Methods

All stationary points (substrate, product and transition state structures) were optimized with the B3LYP-D3 hybrid functional<sup>[17]</sup> with the 6-31+G(d) basis set. Solvent effects for diethyl ether have been calculated with the SMD continuum solvation model.<sup>[18]</sup> Frequency and gas phase single point calculations were performed at the same level of theory. As in big systems ubiquitous low-lying frequencies tend to impact entropy and enthalpy in an unpredictable manner a free-rotor approximation for entropy as proposed by Grimme<sup>[19]</sup> and a quasi-harmonic treatment for enthalpy as proposed by Head-Gordon<sup>[20]</sup> was applied together with a correction for a concentration of 0.05 mol/L with GoodVibes<sup>[21]</sup>. All thermochemical properties reported at 298.15 K and 223.15 K were corrected in this manner using (unscaled) frequency calculations at the B3LYP-D3/6-31+G(d) level of theory. Thermochemical corrections as well as solvation energies obtained from the difference of gas and solution phase B3LYP-D3/6-31+G(d) calculations were added to the single point energies calculated at DLPNO-CCSD(T)/def2-TZVPP//SMD(Et<sub>2</sub>O)/B3LYP-D3/6-31+G(d)<sup>[22]</sup> level with auxiliary basis set def2-TZVPP/C<sup>[23]</sup>. This combination was found in previous studies to perform well for this kind of systems.<sup>[8, 24]</sup> All calculations have been performed with Gaussian 09<sup>[25]</sup> and ORCA version 4.0.<sup>[26]</sup> LED calculations were performed with ORCA version 4.2.<sup>[27]</sup> Input structures for reactants and products were generated by a conformational search using Maestro<sup>[28]</sup> with the OPLS3e force field. Input structures for transition states (TS) were adapted and modified from the literature<sup>[29]</sup> (for details see Chapter 4.6). The conformational space of TS structures was explored with frozen reaction center atoms using Maestro<sup>[28]</sup> with the OPLS3e force field. Structures were preoptimized with frozen reaction center atoms at the SMD(Et<sub>2</sub>O)/B3LYP-D3/6-31g(d) level of theory with a convergence criterion of 10<sup>-5</sup> Hartree before full optimization at SMD(Et<sub>2</sub>O)/B3LYP-D3/6-31+G(d) level. Transition state structures were confirmed as correct structures through mode analysis of a single negative frequency. For the best 2-3 conformers of each group (see Chapter 4.6) intrinsic reaction coordinate (IRC) calculations were performed and the final structures optimized to the respective minima at the SMD(Et<sub>2</sub>O)/B3LYP-D3/6-31+G(d) level of theory. AIM analysis was performed with Multiwfn<sup>[30]</sup>. Plots of non-covalent interaction areas were created using NCIPLOT<sup>[31]</sup> and the VMD program.<sup>[32]</sup> NBO version 3.1<sup>[33]</sup> was used for analysis of natural charges. Pictures of structures were created with GaussView 5<sup>[34]</sup> or by CYLview<sup>[35]</sup>. If not stated otherwise, the following atom colour code was applied: hydrogen (white), carbon (grey), nitrogen (blue), oxygen (red).

## 4.2. Energy Profile of the Reaction

The reaction shown in **Scheme S23** was used as a model reaction to determine the origins of stereoselectivity in the computational study.



**Scheme S23.** Model reaction for the computational study.

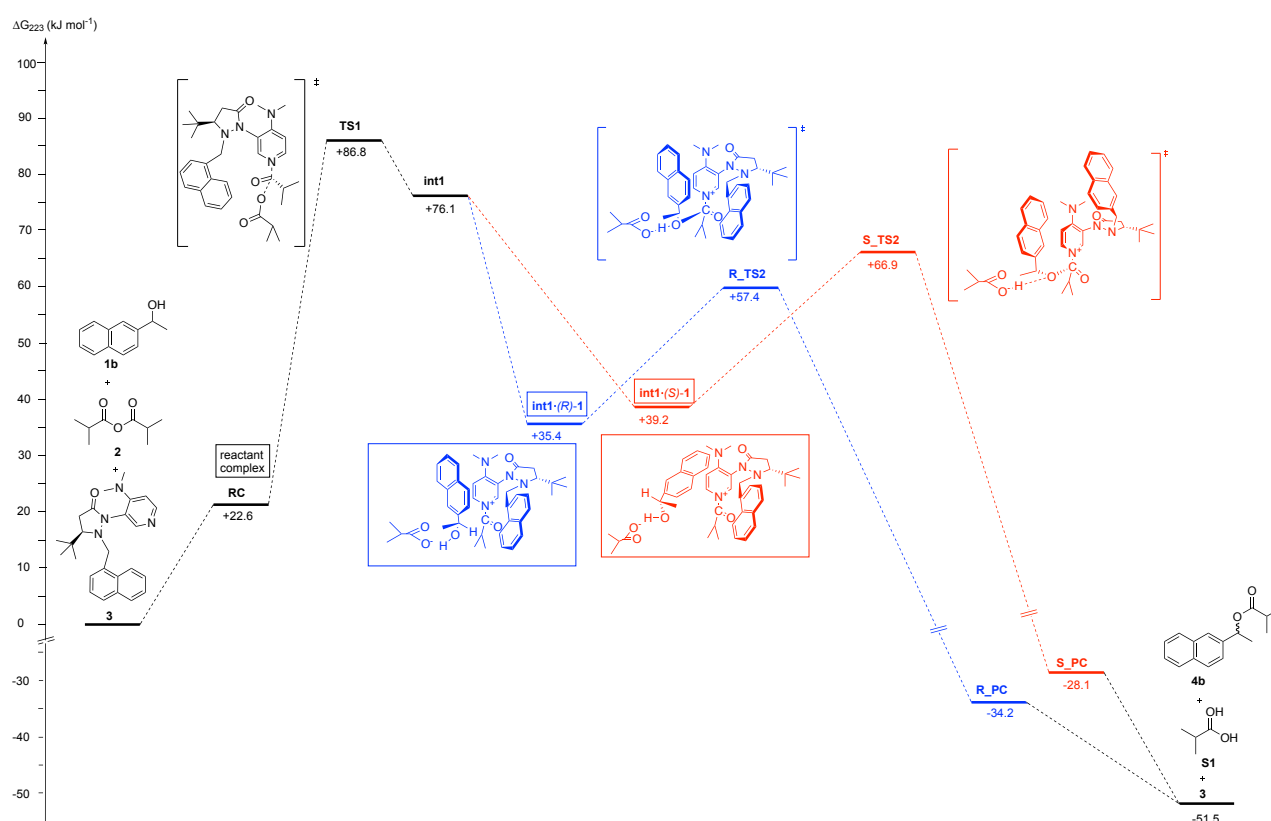
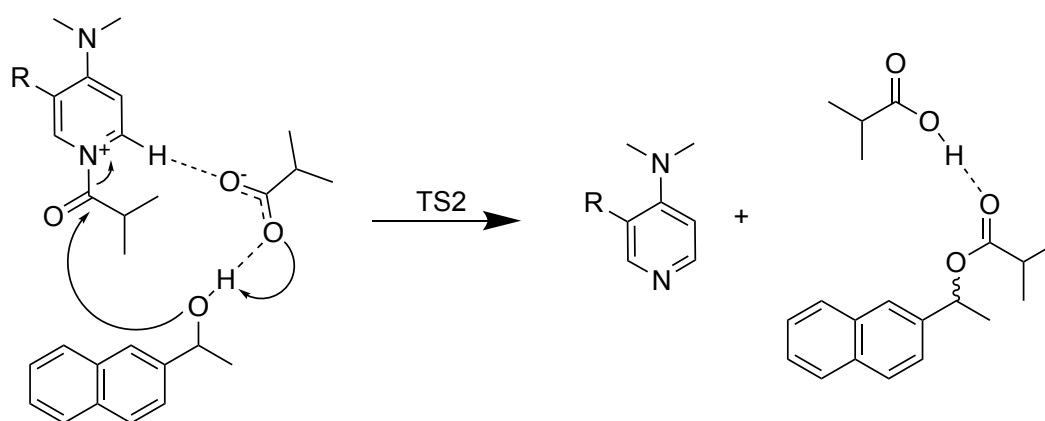


**Figure S29.** Free energy profile for the model reaction as presented in **Scheme S23** calculated at DLPNO-CCSD(T)/def2-TZVPP//SMD(Et<sub>2</sub>O)/B3LYP-D3/6-31+G(d) level of theory. All free energies are Boltzmann averaged and given in kJ mol<sup>-1</sup> relative to the free energy of the reactants. The depicted structures reflect the best conformation.

Several computational studies on the energy profile for the DMAP-(derivative) catalysed acylation of alcohols were already performed.<sup>[29, 36]</sup> All studies found that pathways with DMAP acting as a Lewis base and not as a general base are energetically preferable. Accordingly, in this study only the nucleophilic pathway was investigated. The free energy reaction profile (see **Figure S29**) implies that loading of the catalyst with isobutyric anhydride in **TS1** is the rate-limiting step. This is

in accordance with the findings of Wheeler *et al.*<sup>[29b]</sup> In contrast, for DMAP and Spivey's chiral DMAP catalysts the acyl transfer was found to be rate limiting.<sup>[29a, 36]</sup> In all of the mentioned studies the addition of alcohol substrate to **TS1** to form a ternary complex for the acylation of the catalyst was found to be energetically unfavourable. As all kinetic resolution experiments are competition experiments, relative rates are still dictated by **TS2**. In agreement with the other studies complexing **int1** with the alcohol leads to a major stabilization of the intermediate. This can be mainly attributed to a stabilizing effect on the zwitterionic intermediate through hydrogen bonding and other non-covalent interactions between substrate and loaded catalyst. Interestingly, adduct **int1**•(*R*)-**1b** is more stable by about  $-4 \text{ kJ mol}^{-1}$  as compared to **int1**•(*S*)-**1b**. In all cases, the isobutyrate moiety is hydrogen bonded to the DMAP pyridinium core. Finally, in **TS2** (see **Scheme S24**) the alcohol oxygen atom attacks at the isobutyryl pyridinium cation. In a concerted manner a new C-O-bond is formed and the hydroxyl hydrogen atom is transferred to the isobutyrate moiety. As this step is selectivity determining, the focus of this study lies on **TS2**. Finally, cleavage of the complex leads via product complexes **R\_PC** and **S\_PC** to ester product **4b**, isobutyric acid **S1** and the recovered catalyst **3**.



**Scheme S24.** Reaction occurring via the selectivity-determining step **TS2**.

### 4.3. Correlation of Enantioselectivity and Computational Results

The Eyring equation for a (pseudo-)first order reaction Eq. S47 allows to correlate experimental selectivity values with differences in activation free energy for the selectivity-determining step **TS2** (Eq. S48 with Boltzmann's constant  $k_B$ , Planck's constant  $h$ , temperature  $T$ , gas constant  $R$ ). The computed difference in Gibbs free energy between the relevant transition states for the (*R*)- and the (*S*)- enantiomers can be correlated with experimental selectivity values according to Eq. S49.<sup>[37]</sup>

$$k = \frac{k_B T}{h} \cdot e^{-\frac{\Delta G^\ddagger}{RT}} \quad \text{Eq. S47}$$

$$\ln s = \ln \left( \frac{k_R}{k_S} \right) = \ln \left( \frac{\frac{k_B T}{h} \cdot e^{-\frac{\Delta G_R^\ddagger}{RT}}}{\frac{k_B T}{h} \cdot e^{-\frac{\Delta G_S^\ddagger}{RT}}} \right) = \frac{\Delta G_S^\ddagger - \Delta G_R^\ddagger}{RT} \quad \text{Eq. S48}$$

$$s = e^{\frac{\Delta \Delta G^\ddagger}{RT}} \quad \text{Eq. S49}$$

**Table S33.** Gibbs's free energies for selectivity-determining transition states **TS2** for (*R*)- and (*S*)-**1b** (see **Scheme S23**). Row 2: expected difference in free energy from experimental enantioselectivity value. Row 3 and 4: Results of optimization and thermochemical corrections at B3LYP-D3/6-31+G(d) level of theory. Row 5 and 6: Results for optimized structures without Grimme-D3 dispersion correction. Row 5 and 6 give final values after single point calculations.

method	$G_{223}$ ( <i>S</i> )- <b>TS2</b> [Hartree]	$G_{223}$ ( <i>R</i> )- <b>TS2</b> [Hartree]	$\Delta \Delta G_{223}^\ddagger$ [kJ mol <sup>-1</sup> ]	$G_{298}$ ( <i>S</i> )- <b>TS2</b> [Hartree]	$G_{298}$ ( <i>R</i> )- <b>TS2</b> [Hartree]	$\Delta \Delta G_{298}^\ddagger$ [kJ mol <sup>-1</sup> ]
experimental ( $s = 39$ )			<b>6.8</b>			
SMD(Et2O)/B3LYP-D3/6-31+G(d) Best conformer	-2343.062107 <sup>b</sup>	-2343.067809	15.0	-2343.092182 <sup>b</sup>	-2343.097415	13.7
SMD(Et2O)/B3LYP-D3/6-31+G(d) Boltzmann average	-2343.061329	-2343.067533	16.3	-2343.091056	-2343.097035	15.7
SMD(Et2O)/B3LYP/6-31+G(d) <sup>a</sup> Best conformer	-2342.897980	-2342.898248	0.7	n.d.		
SMD(Et2O)/B3LYP/6-31+G(d) <sup>a</sup> Boltzmann average	-2342.897660	-2342.897892	0.6			
DLPNO-CCSD(T)/def2-TZVPP//SP Best conformer	-2338.801645	-2338.804904	<b>8.6</b>	-2338.831417	-2338.83451	8.1
DLPNO-CCSD(T)/def2-TZVPP//SP Boltzmann average	-2338.800977	-2338.804587	<b>9.5</b>	-2338.830618	-2338.834046	9.0

<sup>a</sup>without D3-Dispersion correction <sup>b</sup>best conformer on DFT level: S\_TS2\_2.

In **Table S33** computational and experimental results are compared. SMD(Et2O)/B3LYP-D3 calculations (row 3 and 4) predict the correct trends for enantioselectivity, but overestimate the differences in free energy. When Grimme-D3 dispersion corrections are not included (row 5 and 6), the SMD(Et2O)/B3LYP/6-31+G(d) free energies are almost identical for the different enantiomers and do not reflect the experimentally found enantioselectivities. These findings point to the significant influence of dispersion interactions in governing the enantioselectivity of this reaction.

Finally, single point calculations (row 7 and 8) predict experimental selectivity properly within the reliability of computational methods. Interestingly, the predictions based on free energies of the best conformer are slightly closer to actual values than Boltzmann averaged free energies at 223.15 K. The deviation of 2-3 kJ mol<sup>-1</sup> from the experimental value is within chemical accuracy (defined as 4 kJ mol<sup>-1</sup>)<sup>[38]</sup>.

#### 4.4. Comparison of Optimization Methods

For an adequate computational description of enantioselective reactions an extensive conformational search is unavoidable. Polarization functions can play a role for the description of dispersion effects, but they also increase computational costs. As a compromise of computational costs and accuracy, optimization was herein performed at the SMD(Et<sub>2</sub>O)/B3LYP-D3/6-31+G(d) level of theory without polarization functions on the hydrogen atoms. The basis set def2-TZVPP for single point calculation includes polarization functions on all atoms. To estimate the error through the smaller basis set during the optimization, the best conformers of TS2 and of the reagents were re-optimized using polarization functions also on hydrogen atoms at the SMD(Et<sub>2</sub>O)/B3LYP-D3/6-31+G(d,p) level of theory.

**Table S34.** Comparison of free energies and reaction free energies for the best conformers of **TS2** for each enantiomer for optimizations with and without polarization functions on hydrogen atoms.

	DLPNO-CCSD(T)/def2-TZVPP// SMD(Et <sub>2</sub> O)/B3LYP-D3/6-31+G(d,p)			DLPNO-CCSD(T)/def2-TZVPP// SMD(Et <sub>2</sub> O)/B3LYP-D3/6-31+G(d)		
	$G_{223.15}$ [Hartree] DFT	$G_{223.15}$ [Hartree] SP	$\Delta\Delta G^\ddagger_{223.15}$ [kJ mol <sup>-1</sup> ] SP	$G_{223.15}$ [Hartree] DFT	$G_{223.15}$ [Hartree] SP	$\Delta\Delta G^\ddagger_{223.15}$ [kJ mol <sup>-1</sup> ] SP
<b>(R)-TS2_1</b>	-2343.153816	-2338.806515	64.3	-2343.067809	-2338.804904	60.5
<b>(R)-TS2_2</b>	-2343.154519	-2338.807312	62.2	-2343.067520	-2338.804699	61.1
<b>(R)-TS2_3</b>	not converged to TS			-2343.067531	-2338.804469	61.7
<b>(S)-TS2_1</b>	-2343.147964	-2338.803553	72.1	-2343.061011	-2338.801645	69.1
<b>(S)-TS2_2</b>	-2343.147964	-2338.802385	75.1	-2343.062107	-2338.801342	69.9
<b>(S)-TS2_3</b>	-2343.148737	-2338.803222	72.9	-2343.061341	-2338.800735	71.5
$\Delta\Delta G^\ddagger_{223.15}$ [kJ mol <sup>-1</sup> ] <sup>a</sup>	15.2		9.9	15.0		8.6

<sup>a</sup>based on the best conformers at the level of theory.

The obtained free energy barriers are slightly higher for the conformers optimized with hydrogen polarization functions. The differences in  $\Delta\Delta G^\ddagger$  based on the best conformer are minor, while computational costs were notably increased. As more than 400 transition state conformers were optimized in this project, it seems to be reasonable to leave out polarization functions on hydrogen atoms.

#### 4.5. Benchmarking of Single Point Calculations

The DLPNO-CCSD(T)/def2-TZVPP//SMD(Et<sub>2</sub>O)/B3LYP-D3/6-31+G(d) combination was already successfully used to describe other Lewis base-catalysed reactions.<sup>[8, 24]</sup> To verify that this level of theory was chosen properly, single point calculations at different levels of theory for the best three conformers of both enantiomers (based on  $G_{223.15}$  after optimization at SMD(Et<sub>2</sub>O)/B3LYP-D3/6-31+G(d) level) were performed. The respective theoretical methods were chosen based on reports for similar systems.<sup>[29]</sup> The experimental enantioselectivity of the model reaction (**Scheme S23**,  $s = 39$  at 223.15 K) was used as a reference.

**Table S35.** Boltzmann-averaged Gibbs's free energy for selectivity-determining transition state **TS2** on different levels of theory. Single point calculations (SP) were performed for the best three conformers after optimization at SMD(Et<sub>2</sub>O)/B3LYP-D3/6-31+G(d) level of theory. Thermochemical corrections were added from frequency calculations at optimization level of theory.

	$G_{223.15}$ (S)- <b>TS2</b> [Hartree]	$G_{223.15}$ (R)- <b>TS2</b> [Hartree]	$\Delta\Delta G_{223.15}^\ddagger$ [kJ mol <sup>-1</sup> ]
experimental			6.8
SMD(Et <sub>2</sub> O)/B3LYP-D3/6-31+G(d) (best 3 conformers)	-2343.937191	-2343.943485	16.5
<b>DLPNO-CCSD(T)/def2-TZVPP//SP</b> (best 3 conformers)	<b>-2338.801413</b>	<b>-2338.804734</b>	<b>8.7</b>
B3LYP-D3/6-311+G(d,p)//SP	-2346.900817	-2346.907257	16.9
M06-2x/6-311+G(d,p)//SP	-2343.532817	-2343.538922	16.0
wB97XD/6-311+G(d,p)//SP	-2342.429061	-2342.434589	14.5

Increasing the basis set for B3LYP-D3 level or use of the M06-2X<sup>[39]</sup> functional has only minor consequences for the calculated free energy differences (see **Table S35**). Results for the long-range corrected method wB97XD<sup>[40]</sup>, that was created to properly describe non-covalent interactions, are much closer to experimental values. However, the use of the coupled cluster method DLPNO-CCSD(T) clearly gives most exact results. CCSD(T)/CBS is known as “golden standard” for calculating noncovalent interactions<sup>[41]</sup> and close to chemical accuracy. However, calculations are too expensive to be performed with big systems. Neese *et al.*<sup>[38]</sup> developed the domain based local pair natural orbital DLPNO-CCSD(T) method that can achieve 99.9% of coupled cluster accuracy. Thus the supremacy of this method as shown above is not surprising.

#### 4.6. Geometrical Analysis of Conformational Space for TS2

In a big and flexible system like the present one, a systematic strategy is required to address the large conformational space of the transition states in an appropriate manner. We therefore define eight conformational subclasses following the criteria defined below.

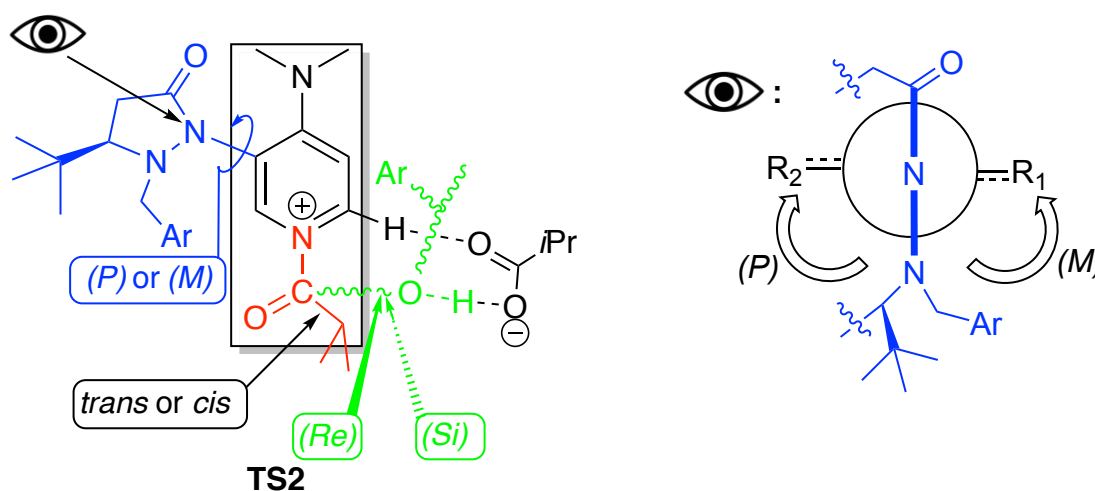


**Figure S30.** Overview of descriptors for the conformation of **TS2** structures based on substituents at the prochiral carbon atom ordered in clockwise decreasing priority. On the right hand the Newman-projection along the atropisomeric C-N-bond is shown. If priority of  $R_1 > R_2$  the isomer is denoted (*M*), if  $R_2 > R_1$  it is called (*P*).

In the loaded catalyst the pyridinium ring and the bonded carbonyl group lie in one plane (see **Figure S30**). If the substituents at the prochiral carbonyl C-atom are arranged in clockwise decreasing Cahn-Ingold-Prelog (CIP) priorities, (*Re*) and (*Si*) nomenclature can be applied. The attack of the oxygen atom on the carbonyl carbon (**Figure S30**, red part) demands an approximately tetrahedral O-C-O angle. Thus, the oxygen atom of the alcohol (**Figure S30**, green part) has to attack the carbon from the “right” side in the so-oriented structure either from (*Re*) or (*Si*). The position of the isobutyrate is predetermined by the hydrogen-bond to a pyridinium H and by the O-H bond, which is to be formed. Rotation of the pyridinium-N-isobutyryl-C-bond leads to *cis* or *trans* conformations of the pyrazolidinone side-chain of the catalyst (**Figure S31**, blue part) relative to the isobutyryl group. Furthermore, atropisomers based on the rotation of the pyrazolidinone ring relative to the pyridinium ring can be distinguished. In the Newman-projection along the pyridinium-C to pyrazolidinone-N-bond CIP (see **Figure S30** right side) priorities are assigned to the *ortho* substituents. Note, that in the DMAP core ghost atoms have to be included. If the shortest connection of the atoms with highest priorities on each side of the atropisomeric bond is clockwise, the conformation is denoted (*P*) (plus); a counter clockwise conformation is called (*M*) (minus).<sup>[42]</sup> All in all, there are eight categories as shown in **Figure S31** that adequately partition the conformational space of **TS2**.

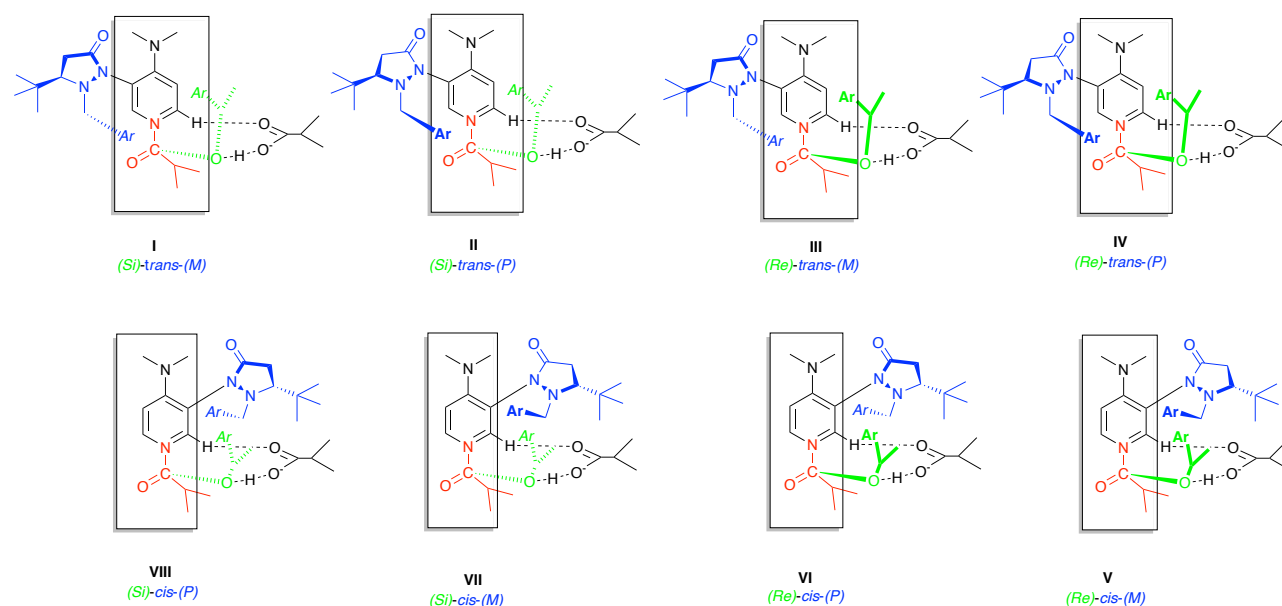


**Figure S31.** Categories defining the conformational space for **TS2**.

Comparable categories were also used before to describe transition states of acylation reactions for other chiral DMAP derivatives.<sup>[29]</sup> However, previous reports only needed four categories: The chiral DMAP catalyst investigated by Zipse *et al.*<sup>[29a]</sup> is less flexible and thus no atropisomers were reported. From each of those four categories of both enantiomers the best three transition state conformations (as far as available) were chosen and adapted through substitution of the catalyst side-chain and the alcohol moiety describing the herein investigated system. For the biaryl systems with catalyst **3** investigated by Wheeler *et al.*<sup>[29b]</sup> no conformers are reported where the alcohol attacks from the more crowded side of the catalyst. This can be rationalized by the much bigger steric demands of a biaryl alcohol compared to the herein investigated secondary alcohols. The reported transition state structures from this study were also adapted to fit the model system. All of these structures were used as starting points for a conformational search with Maestro with frozen reaction centre atoms.

After full optimization of the transition states, the resulting geometries were categorized according to **Figure S31**. If for a category no adequate transition state structure existed, new input structures were generated manually either from relevant structures of the other enantiomer or from related categories of the same enantiomer. Also, the best conformers of both enantiomers were cross changed to create new input structures. Overall almost 200 different structures per enantiomer were submitted to transition state optimization after pre-optimization with frozen reaction centres. **Figure S32** represents the total energies for all transition state optimizations. All green lines converged to the actual transition states while the negative frequency of red dotted conformers does not fit the investigated reaction (and usually represent e.g. a methyl rotation). Grey marks did not converge to any stationary point. **Figure S32** visualizes that a transition state search was performed unbiased and the conformational space is covered in an appropriate manner.

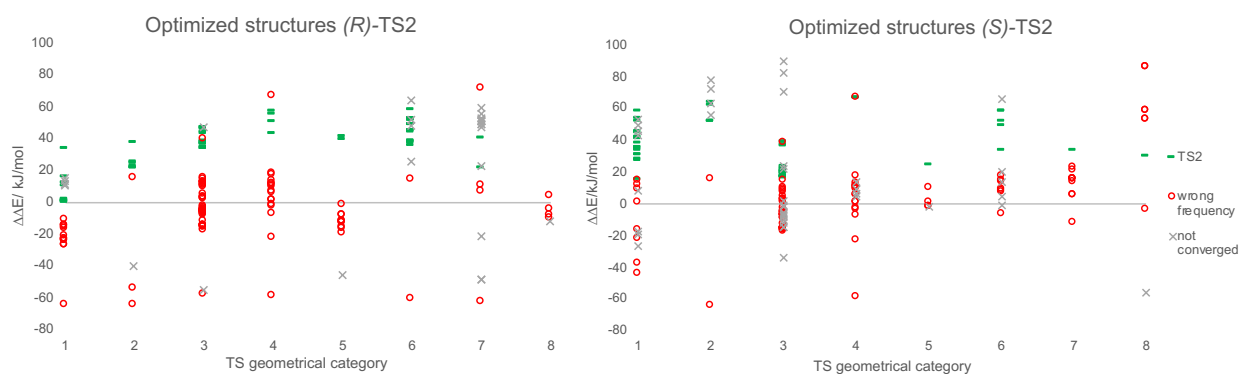


**Figure S32.** Relative energies (in  $\text{kJ mol}^{-1}$  relative to **R\_TS2\_1**) at SMD( $\text{Et}_2\text{O}$ )/B3LYP-D3/6-31+G(d) level of theory of all conformers optimized for **TS2** sorted by geometry categories. Green lines represent optimizations that led to the correct transition state, for structures with red signs the negative frequency does not represent the searched transition state. Grey crossed structures did not converge to a stationary point.

As an overview of actual transition state structures **Figure S33** show Gibb's free energies at optimization level of theory for all structures that converged into the search transition state relative to best conformer **R\_TS2\_1**. The structure for the best conformer of each category with relative single point free energy is finally displayed in **Figure S34** and **Figure S35**.

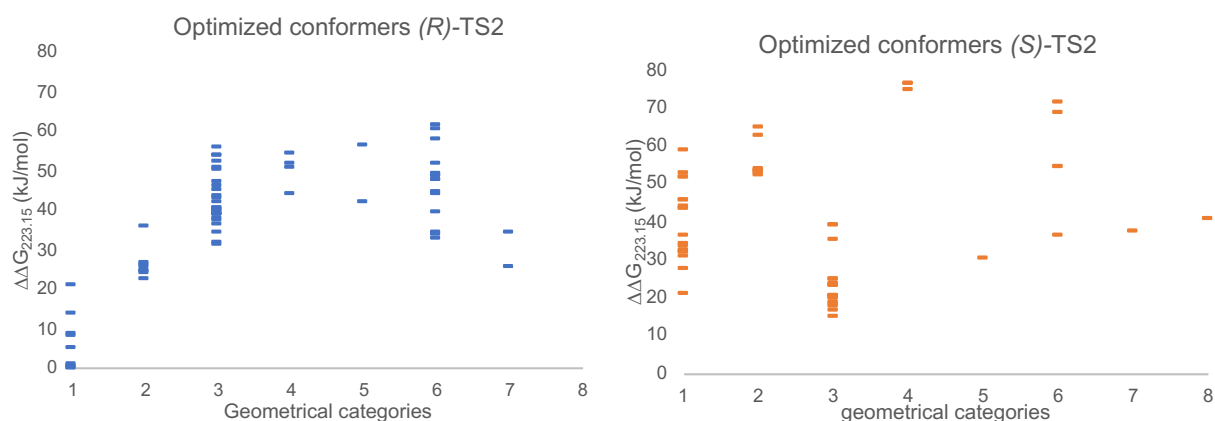


**Figure S33.** Gibb's free energy for optimized conformers for **TS2** (in  $\text{kJ mol}^{-1}$  relative to **R\_TS2\_1**) at SMD( $\text{Et}_2\text{O}$ )/B3LYP-D3/6-31+G(d) level of theory sorted by geometrical categories. Transition states were confirmed by mode analysis of the negative frequency and by intrinsic reaction coordinates (IRC) analysis for the best conformers.

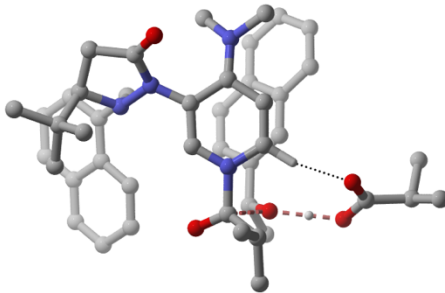
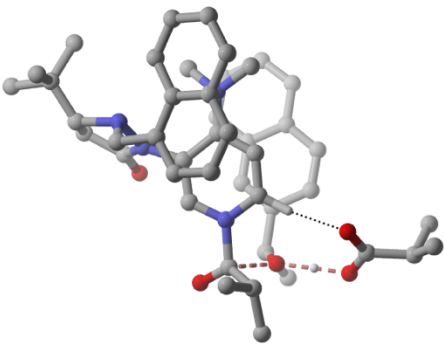
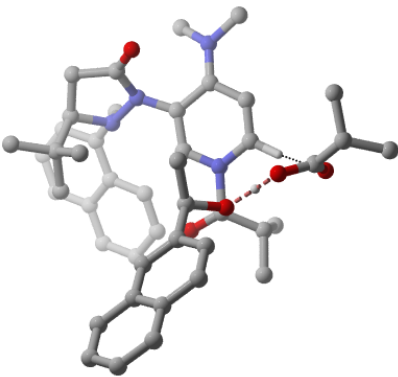
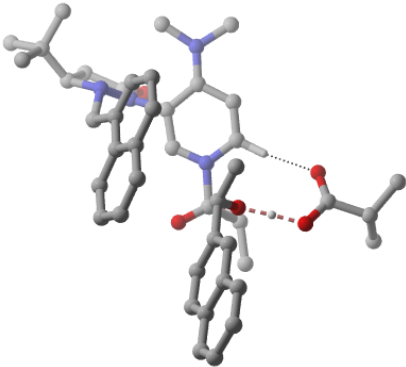
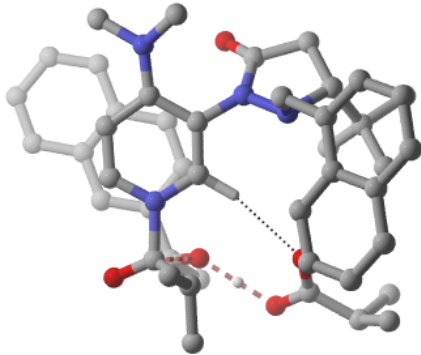
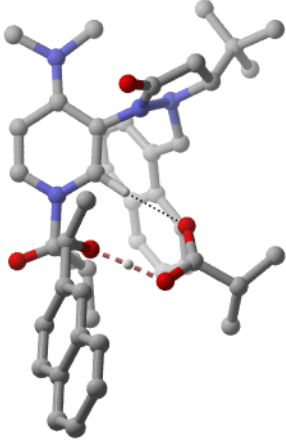
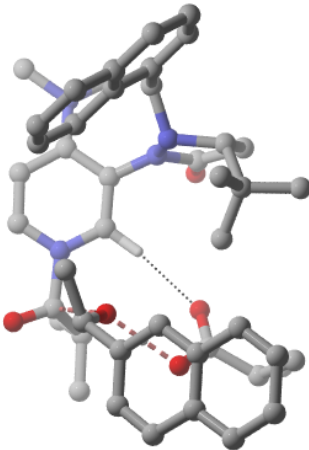
Those categories allow a discussion of factors influencing the stability of the transition states. One general trend within the categories is that (*Si*) attack is preferable for the (*R*)-alcohol, while reaction for (*S*)-**1b** proceeds best via a (*Re*)-attack. This can be rationalized by the position of the alcohol methyl group. Moreover, conformations with *trans*-orientation of catalyst side-chain and alcohol are in general more favourable.

Alcohol attack from the more crowded side (category I, IV, V, VIII): For this classes the energetically most preferable conformation may best be described as "cage" structure. (*Si*)-attack of (*R*)-**1b** on *trans*-(*M*)-oriented catalyst (e.g. **R\_TS2\_1**) is energetically most favourable. In this class the aromatic side chains of alcohol and catalyst are on the same side of the DMAP core and can interact with each other. In contrast, for the (*S*)-alcohol this perfect geometry interferes with the position of

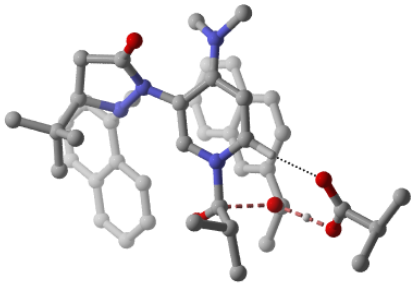
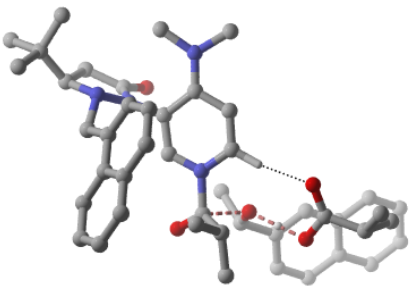
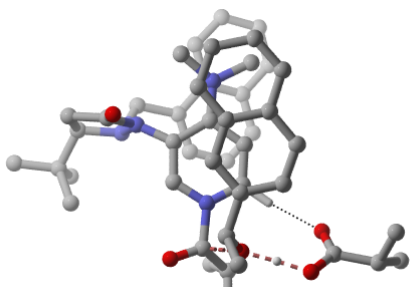
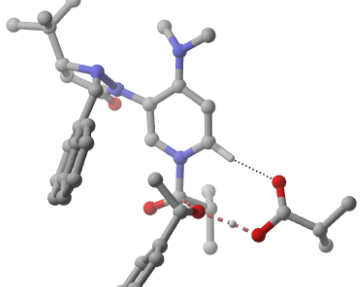
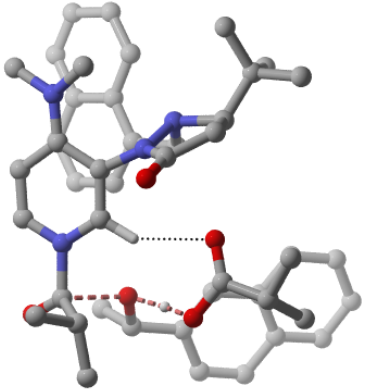
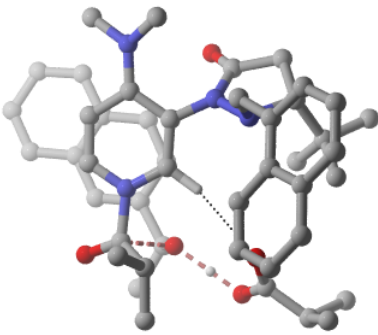
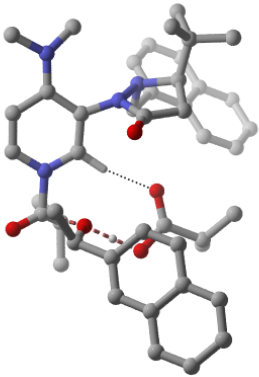
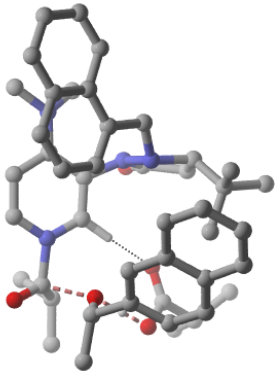
the methyl group of the alcohol. Thus, it should be expected that a (*Re*)-attack of the (*S*)-alcohol could give a similarly good geometry if the catalyst sidechain is also positioned (*Re*) (cat. IV, V). However, for those positions repulsive interactions of the aromatic rings with the chiral *tert*-butyl group avoids formation of cage structures and significantly higher energies were found. Indeed, the categories with alcohol, catalyst sidechain and *tert*-butyl group together either (*Re*) (cat. IV) or (*Si*) (cat VIII) are most destabilized. Especially for category VIII creation of input structures without overlapping atoms proved to be difficult; for the (*R*)-enantiomer no conformer converged into the correct transition state.

Alcohol attack from the less crowded side (category II, III, VI, VII): In those structures “triple sandwich structures” of catalyst sidechain, pyridinium DMAP core and aromatic alcohol are energetically most favourable. Due to the different orientations of the methyl group in the alcohol enantiomers, those structures are found for (*S*)-**1b** by a (*Re*)-attack (cat. III) and for (*R*)-**1b** by a (*Si*)-attack (cat II). In analogous *cis*-structure (VI and VII) the orientation of chiral *tert*-butyl group of the catalyst disturbs the formation of a triple sandwich to some extent.

As analysis of free energies and calculation of Boltzmann population showed that for (*R*)-**TS2** only category I conformers and for (*S*)-**TS2** only category III conformers are populated by more than 1% those categories are discussed below in detail.

category	I	II	III	IV
geometry				
name	R_TS2_1	R_TS2_10	R_TS2_16	R_TS2_33
$\Delta\Delta G^\ddagger$	+0.0	+15.3	+31.9	+40.3
category	VIII	VII	VI	V
geometry	No conformer found			
name		R_TS2_15	R_TS2_18	R_TS2_39
$\Delta\Delta G^\ddagger$		+23.3	+32.4	+43.3

**Figure S34.** Structures for the best conformers for each geometrical group for (*R*)-1-(2-naphthyl)ethanol (**1b**). Hydrogens not involved in the reaction are hidden for visual clarity. Differences of free reaction energy of **TS2** relative to best conformer **R\_TS2\_1** are given in  $\text{kJ mol}^{-1}$  as calculated on DLPNO-CCSD(T)/def2-TZVPP//SMD(Et<sub>2</sub>O)/B3LYP-D3/6-31+G(d) level of theory.

category	I	II	III	IV
geometry				
name	S_TS2_13	S_TS2_29	S_TS2_1	S_TS2_34
$\Delta\Delta G^\ddagger$	+15.7	+48.4	+8.6	+75.3
category	VIII	VII	VI	V
geometry				
name	S_TS2_27	S_TS2_25	S_TS2_24	S_TS2_18
$\Delta\Delta G^\ddagger$	+39.6	+34.71	+34.18	+27.75

**Figure S35.** Structures of the best conformers for each geometrical group for (*S*)-1-(2-naphthyl)ethanol (**1b**). Hydrogens not involved in the reaction are hidden for visual clarity. Differences of free reaction energy of **TS2** relative to best conformer **R\_TS2\_1** are given in  $\text{kJ mol}^{-1}$  as calculated on DLPNO-CCSD(T)/def2-TZVPP//SMD(Et<sub>2</sub>O)/B3LYP-D3/6-31+G(d) level of theory.

#### 4.7. Energetical Analysis of Selectivity-Determining Transition State Structures

The final free energy is composed of gas-phase single-point energies at DLPNO-CCSD(T)/def2-TZVPP level of theory, thermal corrections for free energy and solvation corrections calculated by SMD (Et<sub>2</sub>O). In order to analyse which of those contributions is mainly responsible for the selectivity-determining differences in Gibbs free energy, individual differences for each of those terms relative to those of the best conformer **R\_TS2\_1** are presented in **Figure S36**.

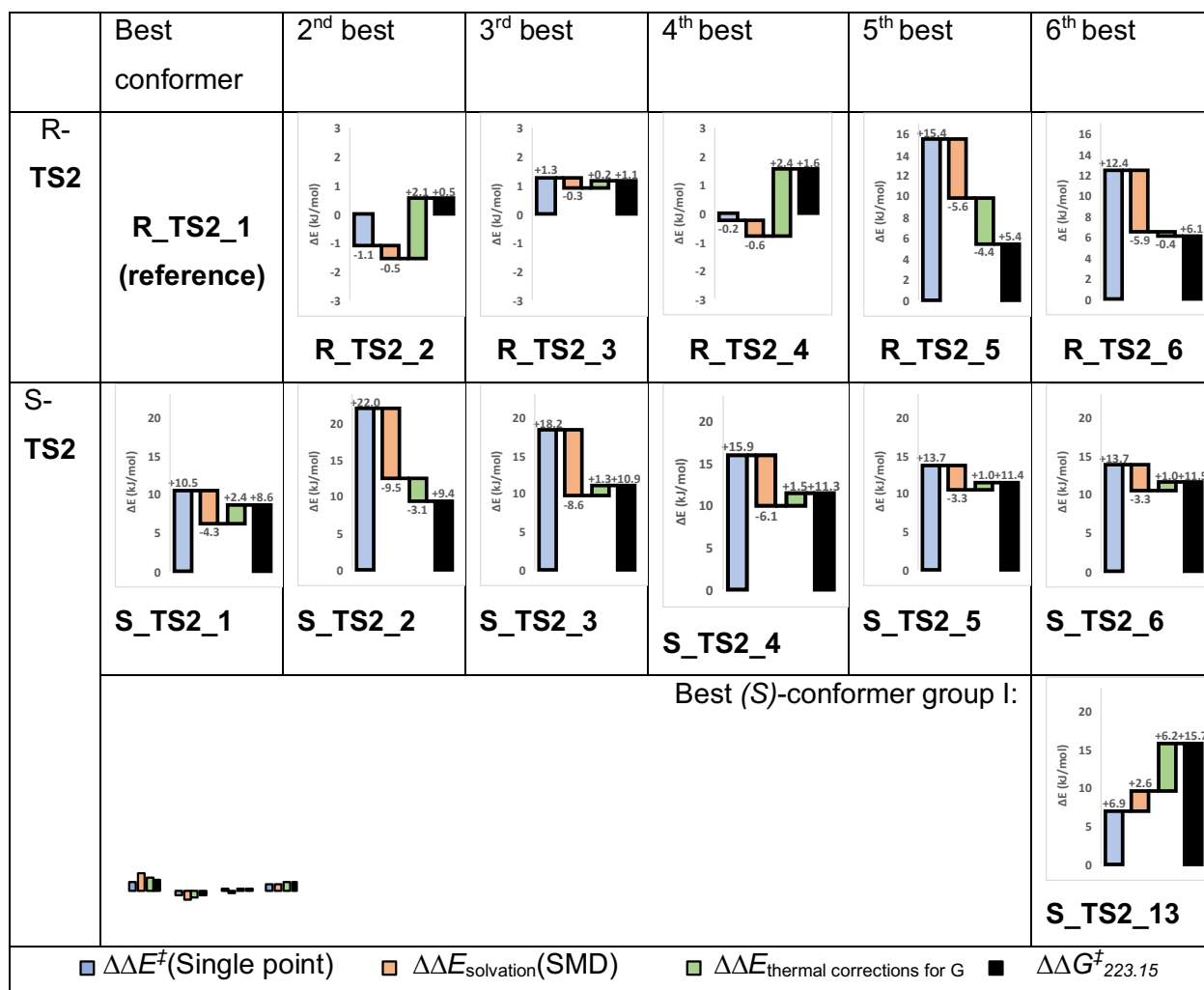


**Figure S36.** Analysis of contributions to Gibbs free energy of the best six conformers for **TS2** of both enantiomers. All energies are given relative to the best conformer for **R-TS2** in kJ mol<sup>-1</sup>. Blue bars give single point energies at DLPNO-CCSD(T)/def2-TZVPP level of theory, red bars solvation energy from SMD (Et<sub>2</sub>O) at B3LYP-D3/6-31+G(d) level, green bars thermal correction calculated for the quasi-harmonic rotator Gibbs free energy at 223.15 K and a concentration of 0.05 mol/L, black bars sum of the three former differences resulting in total difference in free energy of conformers.

### Best Conformers of (R)-TS2

Within the four best conformers of R-TS2 only negligible differences are found. Despite the fact that R\_TS2\_5 and R\_TS2\_6 are also in geometrical class I their single point energy is much higher compared to the other conformers, while solvation and thermal correction have both more negative contribution and are thus more stabilizing. Interestingly, such different patterns in energies reflect a specific difference in geometries in all cases: in R\_TS2\_1 to R\_TS2\_4 the naphthyl moiety of the catalyst sidechain is oriented towards the hydrophobic pocket formed by pyridine and naphthyl of the alcohol (see **Figure S37** left side). In contrast, for R\_TS2\_5 and R\_TS2\_6 the bigger part of the naphthyl moiety of the sidechain is oriented away from this pocket (see **Figure S37** right side). Thus, for those two conformer subgroups the attractive interaction of catalyst side chain with the other aromatic groups in the systems can be estimated. Single point energies (blue bars in **Figure S36**) are favoured by around 11 – 16 kJ mol<sup>-1</sup> through the additional dispersive interactions at DLPNO-CCSD(T) level of theory, which is also reflected by the Grimme D3-dispersion correction for B3LYP-D3/6-31+G(d) calculations, which is in R\_TS2\_5 +12.8 kJ mol<sup>-1</sup> (resp. +8.7 kJ mol<sup>-1</sup> for R\_TS2\_6) less stabilizing than for R\_TS2\_1. However, those conformations gain stabilizing solvation energy (red bars in **Figure S36**). These energetic differences agree with experimental results of Sibi *et al.*<sup>[3]</sup> that found for catalyst **3** at 0 °C a enantioselectivity of *s* = 23 while the analogues catalyst bearing a phenyl instead of a naphthyl moiety (in which only interactions as found in R\_TS2\_5 are possible) only gave *s* = 15.

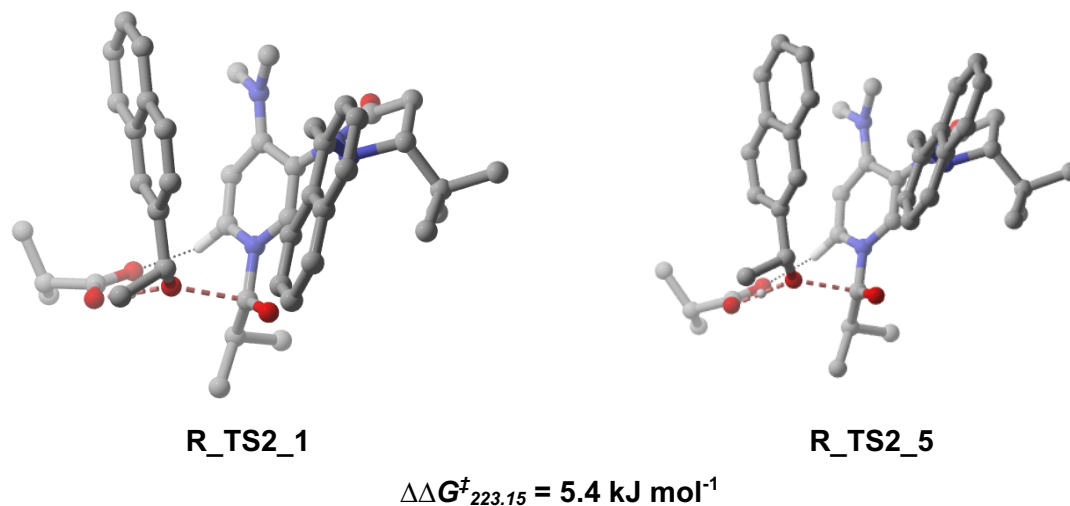


**Figure S37.** Conformation of optimized structures R\_TS2\_1 and R\_TS2\_5. The main difference between those two structures is orientation of naphthyl moiety at the catalyst that is either oriented towards or away from hydrophobic pocket.

**Best Conformers of (S)-TS2**

Regarding the differences in between the best six conformers for (S)-**TS2** there are also two distinguished subgroups. **S\_TS2\_2** and **S\_TS2\_3** have a much higher single point energy compared to other conformers but they are better stabilized by solvation energy. Basically, **S\_TS2\_2** and **S\_TS2\_3** show an edge-to-face aromatic stacking of catalyst naphthyl chain and pyridine moiety, while the other conformers have a triple sandwich structure with face-to-face aromatic stacking (**Figure S38**). This is also reflected in Grimme D3-dispersion correction for B3LYP-D3/6-31+G(d) calculations, that is around 15 kJ mol<sup>-1</sup> less stabilizing for **S\_TS2\_2** and **S\_TS2\_3** compared to triple sandwich structure **S\_TS2\_1**. Parts of this energy difference is equalized by a better stabilization through solvation for **S\_TS2\_2** and **S\_TS2\_3**. This result is in agreement with studies indicating that face-to-face and edge-to-face aromatic stacking are energetically comparable.<sup>[43]</sup>

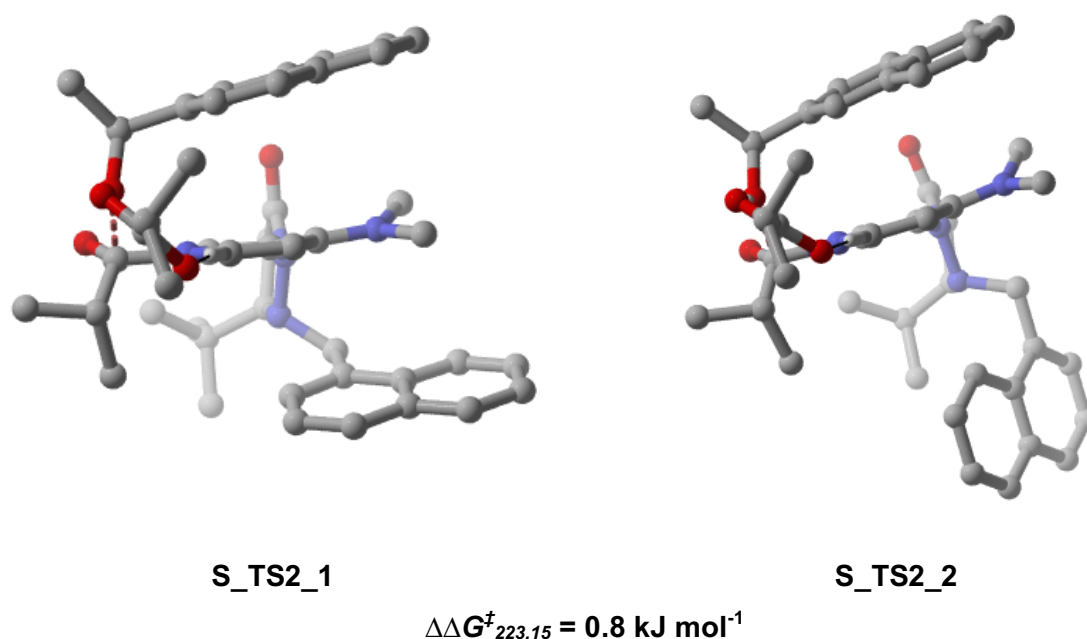


**Figure S38.** Conformation of optimized structures **S\_TS2\_1** and **S\_TS2\_2**. The main difference between those two structures is orientation of naphthyl moiety at the catalyst that is either parallel or vertical to the pyridine ring.

## Influence of Thermal Correction and Solvation Energy

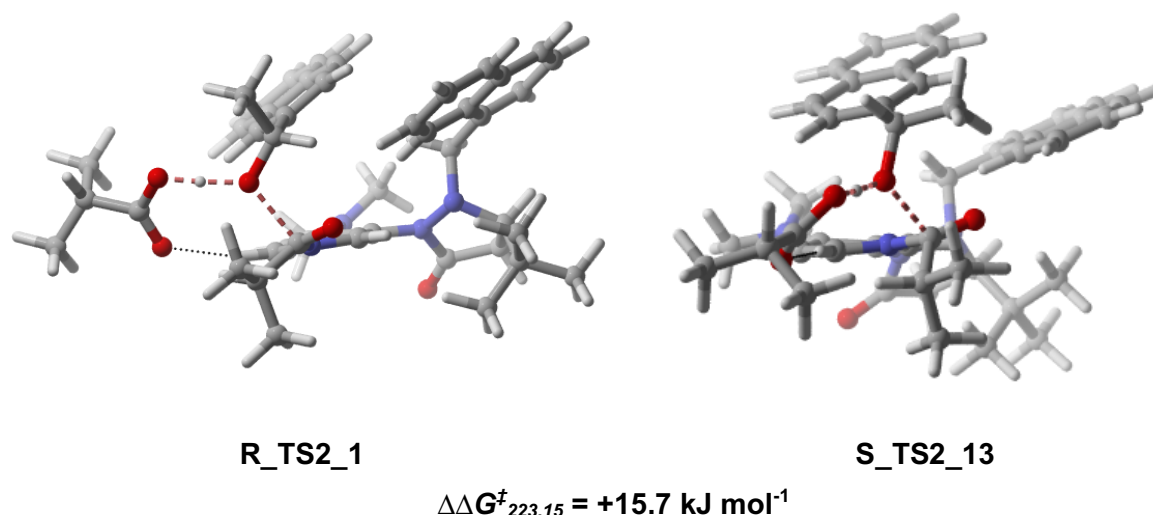


**Figure S39.** Conformation of optimized structures for the best structures in category I for (*R*)- and (*S*)-enantiomer **R\_TS2\_1** and **S\_TS2\_13**.

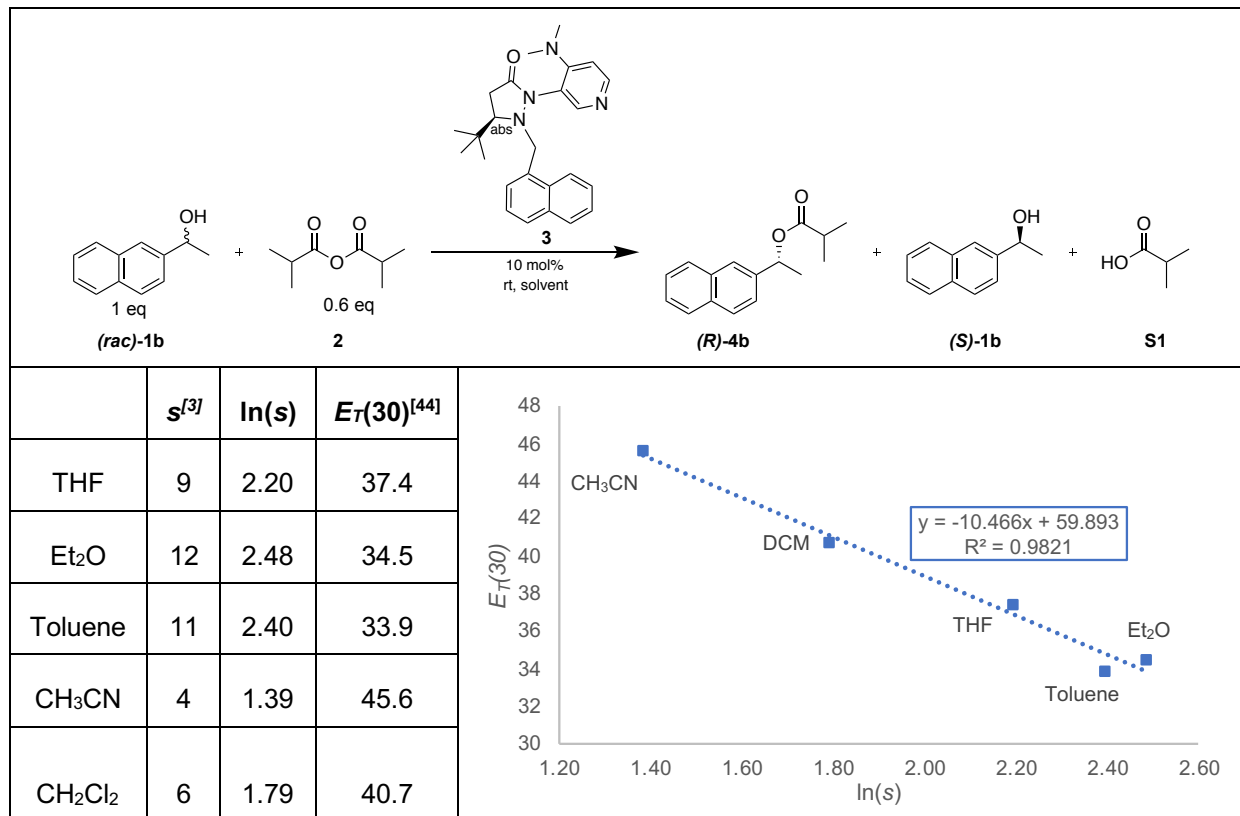
The best (*S*)-conformer in category I **S\_TS2\_13** has a very similar structure to **R\_TS2\_1** (see **Figure S39**). Interestingly, the single point gas phase energy for **S\_TS2\_13** is the lowest of all (*S*)-enantiomers, but still disfavoured by +6.9 kJ mol<sup>-1</sup> relative to **R\_TS2\_1**. Additionally, the solvation energy of **S\_TS2\_13** is the least stabilizing of all **TS2** conformers and thermal corrections are energetically unfavourable by +6.2 kJ mol<sup>-1</sup> relative to **R\_TS2\_1** (see **Figure S36**). The main reason for this difference is the vibrational energy that has a clearly higher impact on thermal corrections for **S\_TS2\_13** than in **R\_TS2\_1**. Accordingly, the calculated IR spectrum for **S\_TS2\_13** shows a very intense scissoring vibration of the alcohol methyl group at 1517 cm<sup>-1</sup> that does not appear prominently for **R\_TS2\_1**. The changed position of the methyl group for the (*S*)-enantiomer is thus also thermochemically unfavourable.

However, one should keep in mind that all of the more than 1% populated (*R*)-**TS2** conformers are in category I, while all relevant (*S*)-**TS2**-conformers are in category III. For discussing selectivity determining differences in Gibbs free energy between those (*R*)- and (*S*)-conformers thermal corrections play in general a minor role and do not follow a clear trend.

Solvation energies (red bars in **Figure S36**) are more stabilizing for all (*S*)-conformers compared to the best (*R*)-conformers. Strikingly, solvation energy for best conformer **R\_TS2\_1** is among the least stabilizing of all found **TS2** conformers. Solvation is therefore a counterplayer of the desired enantioselectivity. This is also reflected by a strong solvent-dependence of enantioselectivity values as observed in the original study by Sibi *et al.*<sup>[3]</sup>. The more detailed analysis of those experimentally reported selectivity values in **Table S36** reveals a surprisingly good inverse correlation of ln(*S*) with solvent polarity as described by Reichardt's solvent parameter  $E_T(30)$ <sup>[44]</sup>. In more polar solvents stronger solvent-solute interactions appear and energetical contribution of solvation energy grows. Thus, better solved transition state structures are further stabilized by more polar solvents, while this effect is much smaller for complexes with low solvation energy like **R\_TS2\_1**. This growth in

solvation energy diminishes  $\Delta\Delta G^\ddagger$  yielding a lower enantioselectivity. From another point of view enantioselectivity is also driven by solvophobic effects that are most prominent in less polar solvents. As the system is already at solvation limit in diethyl ether, it is not possible to increase that effect experimentally by using even less polar solvents.

**Table S36.** Solvent effects on the kinetic resolution of **1b** with **3** at room temperature. Experimental data are reported following Sibi *et al.*<sup>[3]</sup>. A very good correlation with Reichardt's solvent parameter  $E_T(30)$ <sup>[44]</sup> was found.



Nonetheless, selectivity-determining differences in Gibbs free energy between the best (*R*)- and (*S*)- conformations are mainly governed by the differences in gas phase single point energies (blue bars in **Figure S36**). The following chapter investigates the question in how far those energy differences can be attributed to non-covalent interactions.

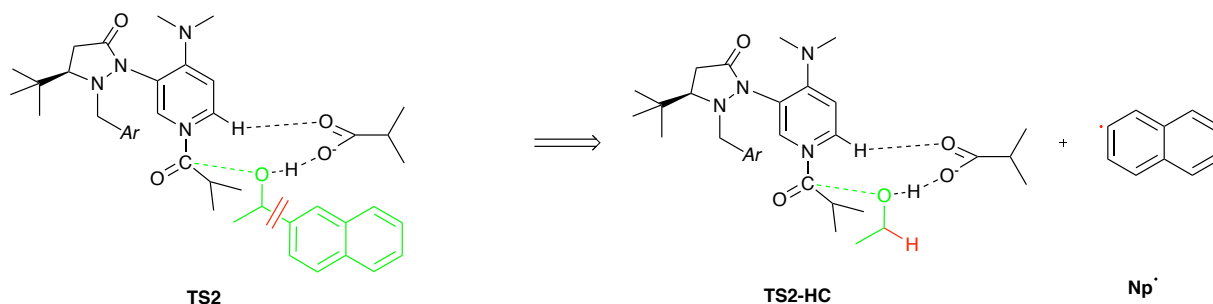
#### 4.8. Quantification of Intramolecular Non-Covalent Interactions

One way to quantify the strength of non-covalent interactions is to compare Grimme D3-dispersion corrections terms for different systems.<sup>[19, 45]</sup> As shown in Chapter 4.3 ignoring D3-dispersion corrections yields similar free energies for (*R*)- and (*S*)-**TS2**. However, this approach is only partially meaningful. First of all, free energies at B3LYP-D3 level of theory do not reproduce experimental results quantitatively. Deviations for dispersion-corrected DFT methods from high accuracy coupled-cluster methods like DLPNO-CCSD(T) are still in the range of 5%-10%<sup>[46]</sup>. For coupled-cluster methods no dispersion correction is needed. Secondly, the D3 correction is not designed to quantify the total of non-covalent interactions in a system, but to correct the shortage of DFT methods in describing medium- to long-range dispersion interactions.<sup>[47]</sup> Thus, especially short-

distance dispersion energies are not reflected by this term. Finally, the D3-dispersion reflects dispersion distributions of inter- and intramolecular non-covalent interactions. While also notable intramolecular dispersion interactions are present in the catalyst, only intermolecular interactions influence the relative rates of the enantiomers in the enantioselectivity determining step **TS2**. Thus, an appropriate method should quantify solely intermolecular dispersion interactions between the alcohol and the loaded catalyst in **TS2** on the coupled-cluster level.

#### 4.8.1.H-Capping Strategy

One possible strategy is to separate the transition state structure into two or more parts and to calculate single point energies for each of the structures.<sup>[45, 48]</sup> Energy differences between the separated parts in relation to the full structure reflect then the non-covalent interactions between those two parts. Separation should not be performed at atoms directly involved in the reaction centre as there are presumably very strong intermolecular interactions. Thus, the bond of alcohol and aromatic moiety in **TS2** was cleaved homolytically. The open shell was capped by a H-atom<sup>[45, 49]</sup> leading to hypothetical structure **TS2-HC** and a naphthyl radical (**Scheme S25**). This computational approach is in line with the experimental approach of constantly increasing aromatic surfaces.



**Scheme S25.** Hypothetical cleavage of **TS2** into H-capped **TS2-HC** and a naphthyl radical.

The energy of any conformer of **TS2** can then be separated into the energy of the H-capped residue **TS2\_HC**, the energy of the naphthyl radical, the energy differences of a C-C-bond relative to the new C-H bond and finally the non-covalent interaction energy between the naphthyl moiety and the rest of the catalyst (Eq. S50). As for all conformers an identical naphthyl radical results from the cleavage, a similar C-C-bond is cleaved and the same C-H bond is formed additionally, those terms disappear in Eq. S51 for the energy difference to a reference system (herein best conformer **R\_TS2\_1** is used as reference). The basis set superposition error (BSSE) is supposed to be negligible as a big basis set is used. Moreover, a hypothetical BSSE would be cancelled as only differences of energy differences of similar systems are investigated. Relative interaction energies between the naphthyl moiety and the rest of the structure in **TS2** can then be calculated by Eq. S52.

$$E^\ddagger(\mathbf{TS2}) = E^\ddagger(\mathbf{TS2\_HC}) + E(\mathbf{Np\cdot}) + E(\text{C-C}) - E(\text{C-H}) + E_{\text{NCI}} \quad \text{Eq. S50}$$

$$\Delta\Delta E^\ddagger(\text{TS2}) = \Delta\Delta E^\ddagger(\text{TS2\_HC}) + \Delta E_{\text{NCI}}$$

Eq. S51

$$\Delta E_{\text{NCI}} = \Delta\Delta E^\ddagger(\text{TS2}) - \Delta\Delta E^\ddagger(\text{TS2\_HC})$$

Eq. S52

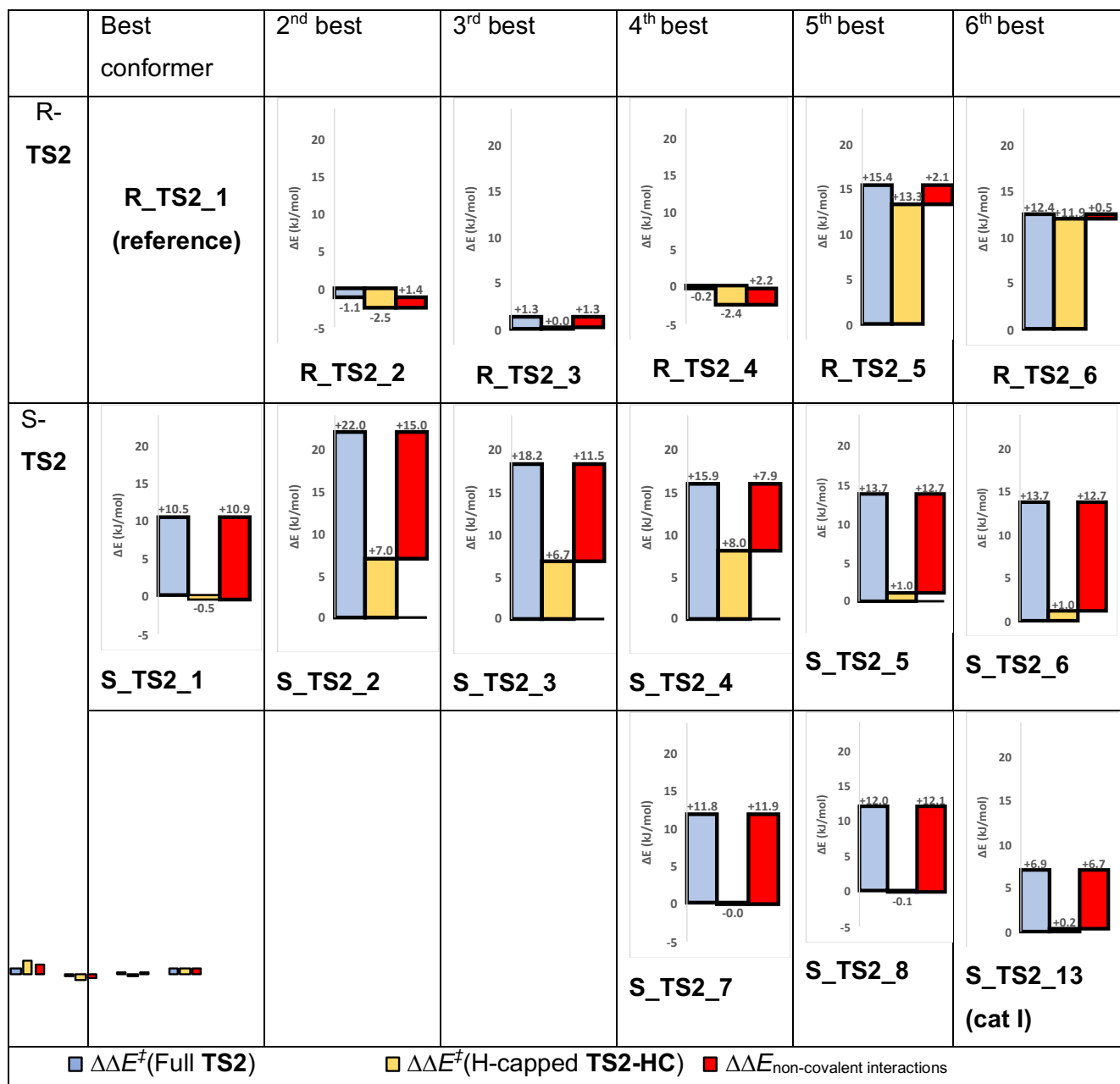


**Figure S40.** Relative single point energies for **TS2** structures (blue bars) compared to relative energy of H-capped structures **TS2-HC** (yellow bars) as shown in **Scheme S25** for all conformers populated to more than 5% and the best category-I-(S)-conformer. The difference of those terms gives the difference non-covalent interaction energy (red bars) between naphthyl moiety of the alcohol and the rest of transition state structure. All energies are given relative to the best conformer for R-**TS2** in kJ mol<sup>-1</sup> and energies were obtained at DLPNO-CCSD(T)/def2-TZVPP level of theory.

Interestingly, single point energies for the H-capped structure of **TS2** without aromatic moiety are almost identical for the best (*R*)- and (*S*)-**TS2** conformers (yellow bars in **Figure S40**). Moreover, this is also true for most of the other conformers that are populated by more than 5% according to the Boltzmann distribution. Exceptions are the above discussed subgroups **S\_TS2\_2** – **S\_TS2\_4** with T-stacking of the naphthyl system and pyridinium ring and **S\_TS2\_5** and **S\_TS2\_6**. However,

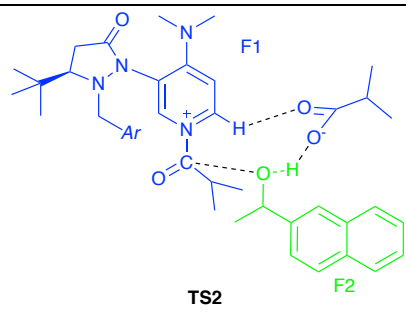
those differences are readily compensated by the increase in solvation energies as shown in **Figure S36**, leaving non-covalent interactions as the free-energy determining factors.

As only the naphthyl group was cleaved, relative H-capped energies (yellow bars in **Figure S40**) comprise energy differences due to the structure of the loaded catalyst, interactions of the alcohol-methyl group with the rest of the system and the reacting atoms themselves. Interestingly, none of those factors determines the energy differences between the most important (*R*)- and (*S*)-conformers. Indeed, energy differences mainly result from interactions between the naphthyl ring with the rest of the system. Quantification of these interactions by Eq. S52 results in relative non-covalent interaction energies symbolized by the red bars in **Figure S40**. The non-covalent interaction energy is around +7.9 kJ mol<sup>-1</sup> to +15.0 kJ mol<sup>-1</sup> less stabilizing for all of the more than 5% populated (*S*)-conformers compared to the best (*R*)-enantiomer. Also for the best category-I (*S*)-conformer **S\_TS2\_13** almost all of the energy difference to **R\_TS2\_1** can be attributed to non-covalent interactions.

#### 4.8.2. Local Energy Decomposition (LED) analysis

Another possibility for the investigation of intermolecular forces is provided by the local energy decomposition (LED) analysis, that is implemented in the Orca program suite.<sup>[27]</sup> Therein Hartree-Fock and correlation energies are decomposed into intra- and inter-molecular forces based on the definition of molecular subsets. We defined the loaded catalyst with the isobutyrate as fragment 1 (F1) and the attacking alcohol with the proton as fragment 2 (F2). After performing the LED analysis for the best two conformations **R\_TS2\_1** and **S\_TS2\_1** the resulting energies were compared. As two separate molecules are needed for this analysis, it is not avoidable to split the reaction center. Thus, it should not come as a surprise that electrostatic contributions are prominent for the interaction energy of the two fragments. However, it was also found that the intermolecular dispersion forces are -6.7 kJ mol<sup>-1</sup> more stabilizing for the (*R*)-enantiomer. This energy difference is exactly the expected energy difference for a selectivity of *s* = 39.

**Table S37.** LED analysis of DLPNO-CCSD(T) results for the best conformers of (*R*)-**TS2** and (*S*)-**TS2**. All energies are reported in kJ mol<sup>-1</sup>.

	<b>R_TS2_1</b>	<b>S_TS2_1</b>	$\Delta E = E(\mathbf{R\_TS2\_1}) - E(\mathbf{S\_TS2\_1})$	
$E_{int}(\mathbf{F1} - \mathbf{F2})$	-357.7	-322.5	-35.2	
$\Delta E_{int}^{C(T)}$	-6.9	-8.7	1.9	triples correction contribution
$\Delta E_{el-prep}(\mathbf{F1})$	1055.0	1116.3	-61.4	electronic preparation energy

$\Delta E_{el\text{-}prep}$ (F2)	1121.0	1280.1	-159.1	
$E_{elstat}^{ref}$	-2142.8	-2295.5	152.7	electrostatic interaction energy
$E_{exch}^{ref}$	-266.0	-300.9	34.9	inter-fragment exchange interaction
$\Delta E^{C\text{-}CCSD}_{nondisp}$	32.6	30.0	2.6	contributions to the binding energy approximately included in the reference energy
$\Delta E^{C\text{-}CCSD}_{disp}$	-148.0	-141.3	-6.7	London dispersion contribution
<b>Error</b>	-2.6	-2.6	0.0	Energy gap e.g. through basis set incompleteness error (BSIE)

## 4.9. Qualitative Investigation of Non-Covalent Interactions

### 4.9.1. AIM Analysis

Different methods for qualifying non-covalent interactions are found in the literature. The straightforward analysis of pairwise distances can be readily applied for distinct and relatively strong non-covalent interactions like hydrogen bonding.<sup>[50]</sup> However, if a multitude of rather weak and diffuse interactions between several atoms is present in a big system, this approach does not allow a complete analysis of non-covalent interactions. Bader<sup>[51]</sup> approached this question with the hypothesis that all atom-atom interactions – covalent as well as non-covalent – root on molecular level in an accumulation of electron density between the nuclei. Thus the atoms in molecules (AIM)<sup>[52]</sup> theory proposes to analyse critical points of electron density  $\rho$  (with  $\nabla\rho(r) = 0$ ) on the bond paths between two atoms. If analysis of the curvature indicates the critical point to be a maximum it is classified as a (3, -1) bond critical point (bcp). The line following the maximal increase in  $\rho$  in both directions connects two nuclei and is called bond path.<sup>[51]</sup> The value of electron density at the bond critical point  $\rho_{bcp}$  allows to distinguish different types of bonding: hydrogen bonds are characterized by an approximately 10 times smaller value of  $\rho_{bcp}$  compared to covalent bonds, while  $\rho_{bcp}$  for van-der-Waals interactions is around 100 times smaller.<sup>[53]</sup> For several cases like hydrogen bonding a correlation between density parameters and the strengths of the interactions were found.<sup>[54]</sup> However, no clear correlation of the strength of van-der-Waals interactions with density interaction parameter is known.<sup>[53]</sup> Thus, AIM analysis is a very common tool in the qualitative analysis of non-covalent interactions.<sup>[29b, 48, 55]</sup>

AIM analysis was performed for the best conformers of both enantiomers using Multiwfn<sup>[30]</sup> restricted to (3,-1) bcp in a density region of 0.0 – 0.1 *au* for interactions between alcohol substrate and the rest of the transition state structure. Results are presented in **Figure S41** and **Figure S42**. Reported descriptors of those interactions in **Table S38** and **Table S39** comprise distance of the two nuclei

$d$ , electron density at the bcp  $\rho_{bcp}$ , Laplacian of electron density  $\nabla^2\rho$ , potential electron density  $V(R)$  and Hamilton kinetic energy  $K(R)$ . Additionally, the type of non-covalent interaction is described. Note, that the term  $\pi - \pi$  may be misleading as it implicates an interaction of the two delocalized  $\pi$ -electron systems, while most of aromatic-aromatic interactions are caused by the polarizability of the aromatic system.<sup>[43a, 43b]</sup> In that sense  $\pi$  refers here always to the total of the aromatic system. AIM analysis shows that aromatic face-to-face stacking of alcohol and DMAP core is comparable for **R\_TS2\_1** and **S\_TS2\_1** (*bcp 1* in **Figure S41** and **Figure S42**). In **R\_TS2\_1** one CH- $\pi$  interaction (*bcp 2* in **Figure S41**) between the aromatic system of the alcohol and the methyl groups of the DMAP-core is found while two of them are present in **S\_TS2\_1** (*bcp 2a,b* in **Figure S42**). The most important differences regarding non-covalent interactions is the additional tilted aromatic stacking (*bcp 3a* in **Figure S41**) and a CH- $\pi$  interaction (*bcp 3b* in **Figure S41**) between the aromatic system of the alcohol and the sidechain of the catalyst. Those interactions are not possible in triple-sandwich-structures like **S\_TS2\_1**. In **S\_TS2\_1** an additional interaction between the carbonyl unit of the catalyst with the aromatic system of the alcohol can be seen (*bcp 3* in **Figure S42**). Further interactions comprise CH- $\pi$  interaction (*bcp 4*) of the aromatic system with the isobutyrate and interactions of the CH-group of the alcohol with C=O group of the loaded catalyst (*bcp 4*) and catalyst sidechain in **R\_TS2\_1** (*bcp 6* in **Figure S41**) resp. with the carbonyl group of the free isobutyrate for **S\_TS2\_1** (*bcp 3* in **Figure S42**).

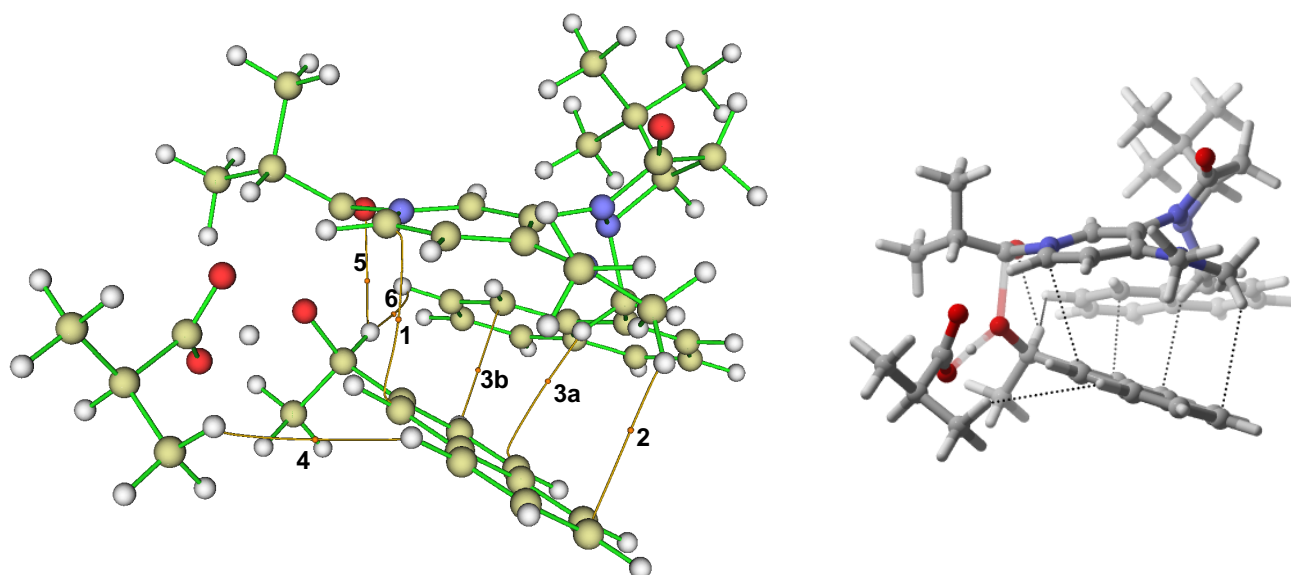


**Figure S41.** AIM analysis of **R\_TS2\_1**. Yellow dots symbolize bond critical points, yellow lines bond paths. Analysis and left picture was performed using Multiwfn<sup>[30]</sup> (yellow: carbon), the picture on the right hand is plotted for better visualization with CYLview<sup>[35]</sup>.

**Table S38.** Parameters of AIM analysis describing non-covalent interactions between alcohol and the rest of the transition state structure for **R\_TS2\_1**.

bcp	type	description	Distance nuclei [pm]	electron density $\rho_{\text{bcp}}$ [ $10^{-2}$ au]	Laplacian of electron density $\nabla^2 \rho$ [ $10^{-2}$ au]	potential electron density $V(R)$ [ $10^{-2}$ au]	Hamilton kinetic energy $K(R)$ [ $10^{-2}$ au]
1	$\pi-\pi^+$ face-to-face stacking	$\pi$ (alcohol) to $\pi$ (DMAP)	333	0.6567	1.9862	-0.2856	-0.1055
2	CH- $\pi$	$\pi$ (alcohol) to $\text{CH}_3$ (DMAP)	312	0.3791	1.1124	-0.1551	-0.0615
3a	Tilted aromatic stacking	$\pi$ (alcohol) to $\pi$ (catalyst sidechain)	288	0.5813	1.7011	-0.2419	-0.0917
3b	CH- $\pi$	$\pi$ (alcohol) to CH(catalyst sidechain)	283	0.6163	1.9716	-0.2699	-0.1115
4	CH- $\pi$	$\pi$ (alcohol) to CH(isobutyrate)	325	0.0906	0.2801	-0.0323	-0.0188
5	CH-O	CH(alcohol) to C=O(loaded isobutyrate)	236	1.3332	4.7732	-0.9642	-0.1145
6	CH- $\pi$	CH(alcohol) to $\pi$ (catalyst sidechain)	236	0.5407	1.9962	-0.2385	-0.1303

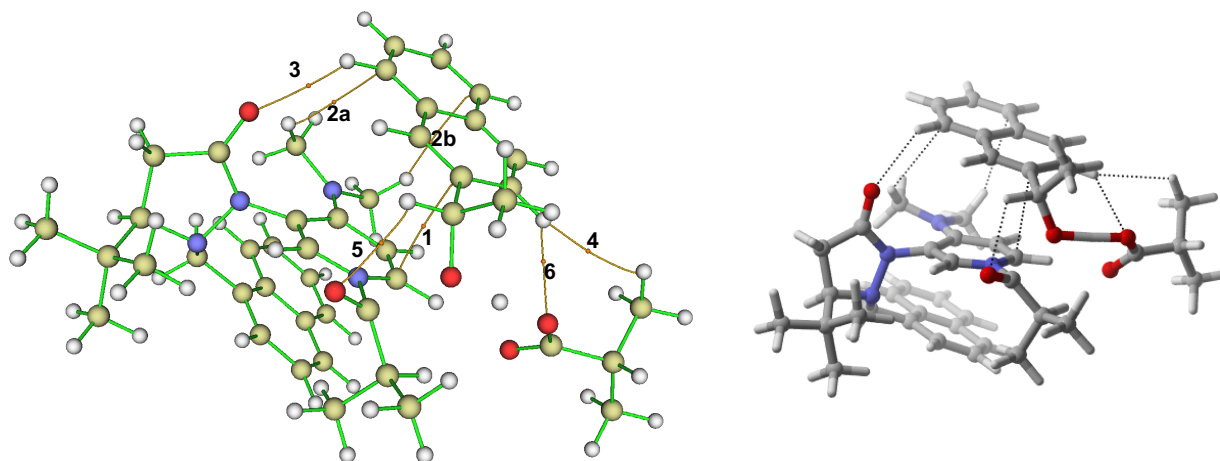


**Figure S42.** AIM analysis of **S\_TS2\_1**. Yellow dots symbolize bond critical points, yellow lines bond paths. Analysis and left picture was performed using Multiwfn<sup>[30]</sup> (yellow: carbon), the picture on the right hand is plotted for better visualization with CYLview<sup>[35]</sup>.

**Table S39.** Parameters of AIM analysis describing non-covalent interactions between alcohol and the rest of the transition state structure for **S\_TS2\_1**.

bcp	type	description	Distance nuclei [pm]	electron density $\rho_{\text{bcp}}$ [ $10^{-2}$ au]	Laplacian of electron density $\nabla^2 \rho$ [ $10^{-2}$ au]	potential electron density $V(R)$ [ $10^{-2}$ au]	Hamilton kinetic energy $K(R)$ [ $10^{-2}$ au]
1	$\pi$ - $\pi^+$ face-to-face stacking	$\pi$ (alcohol) to $\pi$ (DMAP)	321	0.6963	2.2440	-0.3466	-0.1072
2a	CH- $\pi$	$\pi$ (alcohol) to CH <sub>3</sub> (DMAP)	296	0.4970	0.3067	-0.2205	-0.0862
2b	CH- $\pi$	$\pi$ (alcohol) to CH <sub>3</sub> (DMAP)	313	0.3568	1.0386	-0.1414	-0.0591
3	O- $\pi$	$\pi$ (alcohol) to C=O(catalyst sidechain)	261	0.6760	2.5653	-0.4333	-0.1040
4	CH- $\pi$	$\pi$ (alcohol) to CH(isobutyrate)	264	0.2944	1.0606	-0.1186	-0.0733
5	CH-O	CH(alcohol) to C=O(loaded isobutyrate)	248	1.0967	4.5172	-0.8160	-0.1567
6	CH-O	CH(alcohol) to C=O(isobutyrate)	256	0.9332	3.2569	-0.6392	-0.0875

#### 4.9.2.NCI Plots

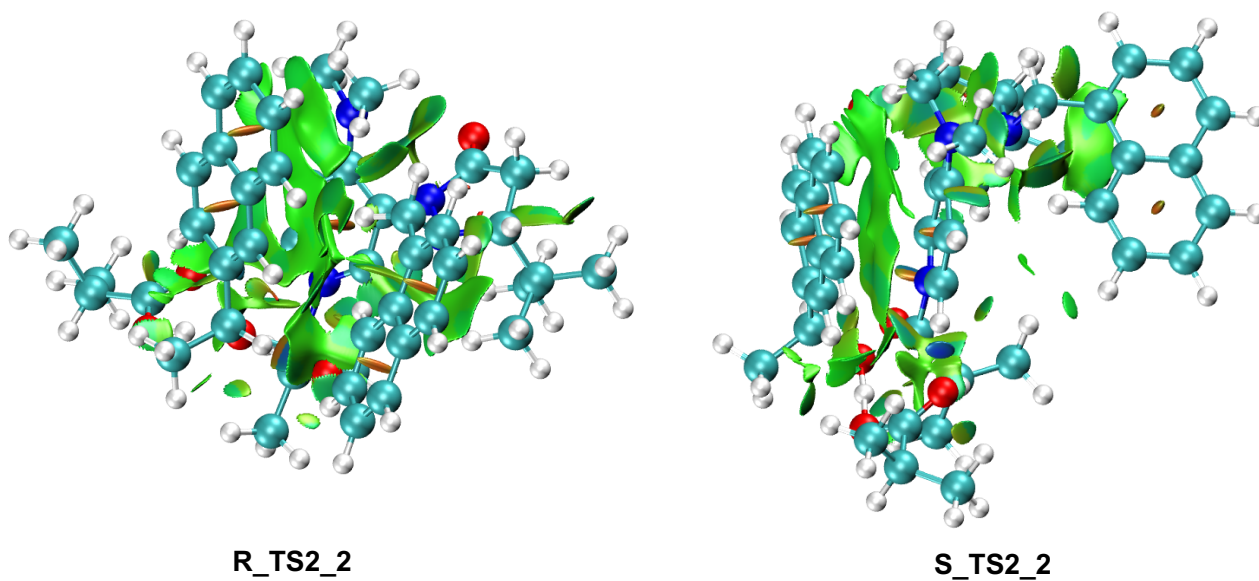
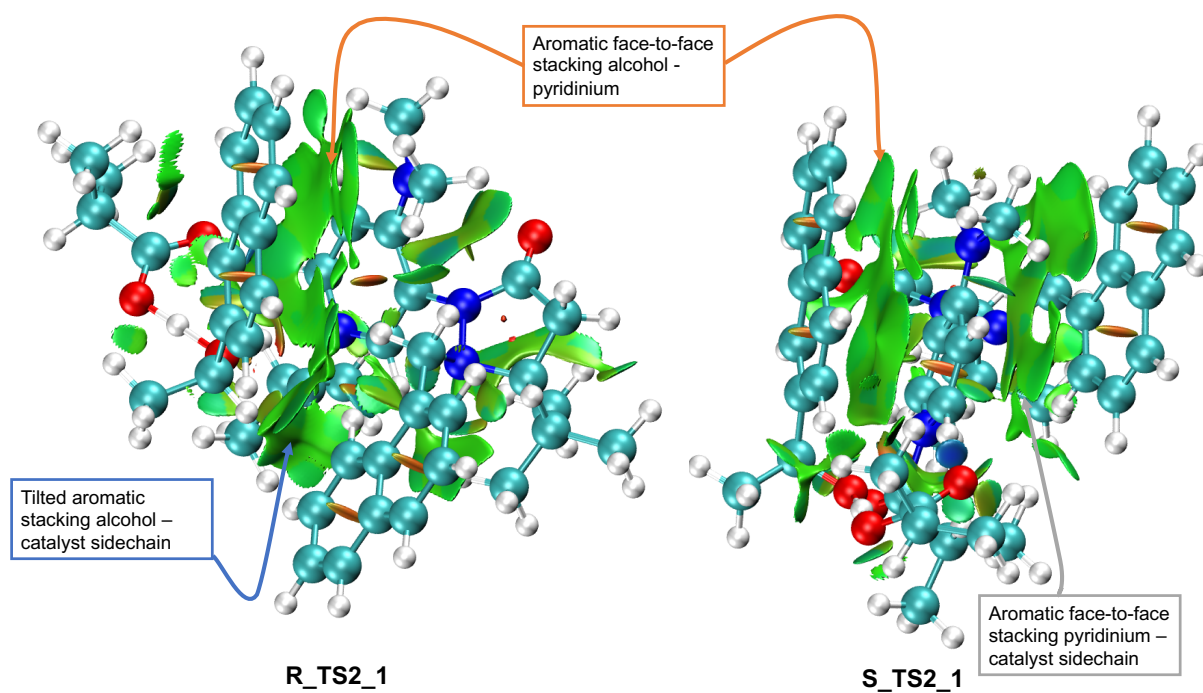
Another approach is the analysis of the reduced density gradient (RDG). While covalent bonds are characterized by saddle points of the electron density, non-covalent bonds lead to steep troughs of the RDG in the low density region.<sup>[56]</sup> Those patterns in the RDG are comparable for repulsive and attractive interactions. However, analysis of the second eigenvalue of the electron-density Hessian  $\text{sign}(\lambda_2)$  allows to analyse the variation of electron density  $\rho$  along internuclear connections.<sup>[31]</sup> Van-der-Waals interactions are characterized by a second eigenvalue of the Hessian close to zero in an area of small energy density  $\rho$ . Thus, it is possible to only plot van-der-Waals interactions if an appropriately small cut-off value (here 0.03 au) for the density is chosen.

Both NCIplots for the best conformers **R\_TS2\_1** and **S\_TS2\_1** show big areas of non-covalent interactions between the alcohol and the pyridinium ring (**Figure S43**, first line). In agreement with the AIM analysis performed above for **R\_TS2\_1** an additional area of non-covalent interactions is found between the aromatic moiety of the alcohol and the aromatic sidechain of the catalyst which corresponds to a tilted aromatic stacking interaction. In contrast, in **S\_TS2\_1** a big area of aromatic stacking between this aromatic moiety and the pyridinium is found. However, this interaction does not involve the alcohol and does thus not impact enantioselectivity.

Second best conformers (**Figure S43**, second line) show similar trends. In **S\_TS2\_2** the smaller interaction between pyridinium and vertical oriented catalyst sidechain interaction explains the lower single point energy of **S\_TS2\_2** compared to **S\_TS2\_1**. As seen above, parts of this energy are compensated by an increased solvation energy.

The third line in **Figure S43** shows some special cases for category I structures. **R\_TS2\_5** has a lower non-covalent interaction surface compared to **R\_TS2\_1** due to the different orientation of the naphthyl group as discussed in **Figure S37**.

The structure of the best (S)-conformer in category I (**S\_TS\_13**) is quite similar to **R\_TS2\_1**. However, the alcohol-methyl group forces the alcohol to orient differently yielding a smaller aromatic interaction surface between the alcohol, pyridinium and catalyst sidechain. Consequently, in **S\_TS\_13** non-covalent interaction energy is lowered compared to **R\_TS2\_1**.



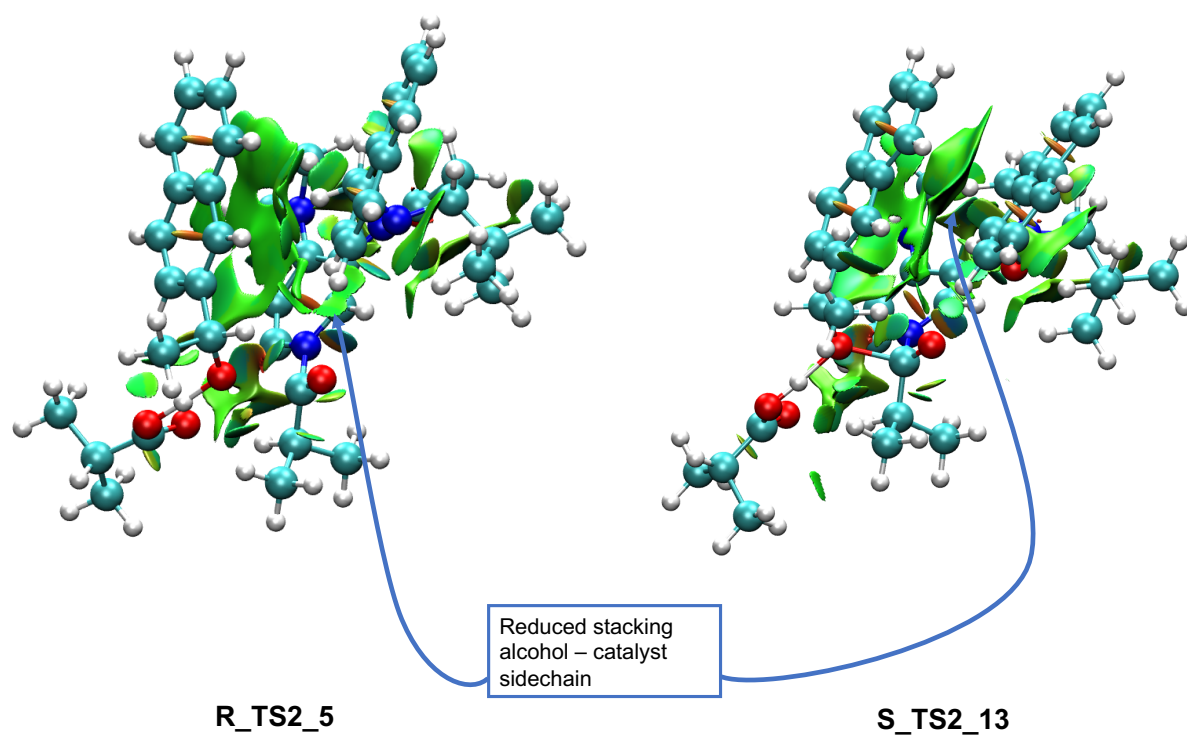


**Figure S43.** NCI plots for TS2 structures generated from wavefunction at B3LYP-D3/6-31+G(d) level of theory with NCIPLOT<sup>[31]</sup> and plotted with VMD<sup>[57]</sup> with density cutoff at 0.03 au. Colours reflect  $\text{sign}(\lambda_2)\rho$  on a scale of -0.03 au (blue) over 0 (green) to +0.03 (red). Accordingly, green surfaces represent van der Waals interaction areas. Colour code: hydrogen (white), carbon (turquoise), nitrogen (blue), oxygen (red).

#### 4.10. Analysis of Thermodynamics and Substrate Properties

The design of the experiments in this study rely on the hypothesis that the reactivity of substrate alcohols mainly depends on their strength as dispersion-energy donors (DED). To examine whether other factors impact the reactivity of the different alcohols, several other properties were investigated. Most importantly, the competition experiments with non-aromatic catalyst *n*Bu<sub>3</sub>P (**6**) show that acylation of all alcohols occurs at similar reaction rates (see chapter 2.7). In addition, the thermodynamics of the acylation of the different alcohols was analysed in order to exclude a thermodynamic control of selectivity. Therefore, reaction free energies for the acylation were calculated. **Table S40** reports reaction free energies calculated from Boltzmann averaged free energies of substrates and products. Reaction free energies are almost identical for all of the investigated reactions. Thus, a thermodynamic control of selectivity can be excluded.

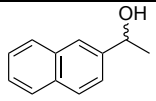
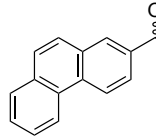
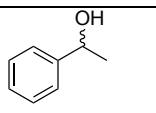
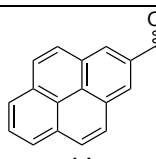
**Table S40.** Reaction free energy for the acylations of the alcohols used in this project.

Reaction	$\Delta G_{223.15}$ CCSD(T)/def2-TZVPP//SMD(Et <sub>2</sub> O)/B3LYP-D3/6-31+G(d) [kJ mol <sup>-1</sup> ]
<p>1a + 2 <math>\xrightarrow{\Delta G}</math> 4a + S1</p>	-51.1
<p>1b + 2 <math>\xrightarrow{\Delta G}</math> 4a + S1</p>	-51.5
<p>1c + 2 <math>\xrightarrow{\Delta G}</math> 4c + S1</p>	-49.4
<p>1d + 2 <math>\xrightarrow{\Delta G}</math> 4d + S1</p>	-50.6

As in selectivity determining **TS2** (see **Scheme S24**) the partial charge of the oxygen atom as well as the acidity of the hydroxyl proton could influence the reactivity of the alcohol, those two factors were also analysed with DFT methods. The natural charge of the oxygen atom was determined by natural bond orbital (NBO) calculations on the optimized alcohols at SMD(Et<sub>2</sub>O)/B3LYP-D3/6-31+G(d) level. From the natural population analysis, the natural charge of the oxygen was obtained

and Boltzmann-averaged over the conformers. **Table S41** shows that natural charges on the oxygen atoms are almost identical for all four alcohols used in the experiment.

**Table S41.** Results of natural bond order analysis of alcohol substrates.

Alcohol	Conformer	Natural Charge Oxygen	Natural population				Boltzmann factor (see Chapter 8)	Boltzmann averaged natural charge
			Core	Valence	Rydberg	Total		
 <b>1b</b>	SNp_2	-0.7885	1.9998	6.7702	0.0184	8.7885	1.00	<b>-0.7880</b>
	SNp_1	-0.7867	1.9998	6.7687	0.0182	8.7867	0.44	
	SNp_4	-0.7893	1.9998	6.7709	0.0187	8.7893	0.11	
	SNp_3	-0.7885	1.9998	6.7695	0.0193	8.7885	0.08	
	SNp_7	-0.7831	1.9998	6.7654	0.0178	8.7831	0.03	
 <b>1c</b>	SPhant_1	-0.7883	1.9998	6.7700	0.0184	8.7883	1.00	<b>-0.7881</b>
	SPhant_3	-0.7890	1.9998	6.7705	0.0187	8.7890	0.04	
	SPhant_7	-0.7809	1.9998	6.7630	0.0180	8.7809	0.03	
 <b>1a</b>	SPhe_1	-0.7887	1.9998	6.7704	0.0184	8.7887	1.00	<b>-0.7884</b>
	SPhe_3	-0.7892	1.9998	6.7705	0.0190	8.7892	0.16	
	SPhe_7	-0.7807	1.9998	6.7634	0.0175	8.7807	0.05	
 <b>1d</b>	SPyr_1	-0.7880	1.9998	6.7697	0.0184	8.7880	1.00	<b>-0.7880</b>
	SPyr_4	-0.7888	1.9998	6.7700	0.0190	8.7888	0.15	
	SPyr_7	-0.7832	1.9998	6.7653	0.0181	8.7832	0.01	

Another factor describing reactivity of the alcohols is the acidity of the hydroxyl group. As reactions are conducted in anhydrous diethyl ether, the investigation of aqueous  $pK_a$  values is not appropriate. The calculation of  $pK_a$  values is very dependent on the solvent and should ideally be performed with an explicit solvation model.<sup>[58]</sup> As the accurate determination of absolute  $pK_a$  values is not needed in this context, the reaction free energies for isodesmic proton transfer reactions with reference alcohol **1b** are reported in **Table S42**. The acidity increases in the order phenyl < phenanthryl < naphthyl < pyrenyl. The calculated energy differences are quite small and lie within the limits of confidence of the chosen theoretical approach. Furthermore, the order of relative acidities does not fit the experimentally observed relative rates.

**Table S42.** Reaction free energies for isodesmic proton transfer reactions to estimate acidity of the hydrogen protons.

Isodesmic reaction	$\Delta G_{223.15}$ [kJ mol <sup>-1</sup> ] (DLPNO-CCSD(T)/ SMD(Et <sub>2</sub> O)/B3LYP- D3/ 6-31+G(d))
<p>Reaction 1: 1b<sup>-</sup> + 1a → 1b + 1a<sup>-</sup></p>	<b>+3.5</b>
<p>Reaction 2: 1b<sup>-</sup> + 1c → 1b + 1c<sup>-</sup></p>	<b>+0.5</b>
<p>Reaction 3: 1b<sup>-</sup> + 1d → 1b + 1d<sup>-</sup></p>	<b>-1.4</b>

Analysis of the substrates confirms that the main difference between investigated alcohols is the size of DED groups.

## 5. Supplementary References

- [1] H. B. Kagan, J. C. Fiaud, *Top. Stereochem.* **1988**, *18*, 249-300.
- [2] C. E. Müller, P. R. Schreiner, *Angew. Chem. Int. Ed.* **2011**, *50*, 6012-6042.
- [3] G. Ma, J. Deng, M. P. Sibi, *Angew. Chem. Int. Ed.* **2014**, *53*, 11818-11821.
- [4] a) H. F. Klare, M. Oestreich, *Angew. Chem. Int. Ed.* **2007**, *46*, 9335-9338; b) M. D. Greenhalgh, J. E. Taylor, A. D. Smith, *Tetrahedron* **2018**, *74*, 5554-5560.
- [5] S. Hoops, S. Sahle, R. Gauges, C. Lee, J. Pahle, N. Simus, M. Singhal, L. Xu, P. Mendes, U. Kummer, *Bioinformatics* **2006**, *22*, 3067-3074.
- [6] I. Vasilief, QtiPlot 0.9.8.9, **2011**.
- [7] S. F. Musolino, O. S. Ojo, N. J. Westwood, J. E. Taylor, A. D. Smith, *Chem. Eur. J.* **2016**, *22*, 18916-18922.
- [8] M. Marin-Luna, B. Pölloth, F. Zott, H. Zipse, *Chem. Sci.* **2018**, *9*, 6509-6515.
- [9] a) K. Naemura, M. Murata, R. Tanaka, M. Yano, K. Hirose, Y. Tobe, *Tetrahedron: Asymmetry* **1996**, *7*, 3285-3294; b) W. H. Pirkle, S. D. Beare, *J. Am. Chem. Soc.* **1967**, *89*, 5485-5487.
- [10] M. P. Sibi, K. Kawashima, L. M. Stanley, *Org. Lett.* **2009**, *11*, 3894-3897.
- [11] F. Fernandez, C. Gonzalez, G. Gomez, C. Lopez, L. Medina, J. M. Calleja, E. Cano, *Arch. Pharm.* **1990**, *323*, 239-242.
- [12] A. Davis, J. Casas-Solvas, T. Mooibroek, S. Sandramurthy, J. Howgego, *Synlett* **2014**, *25*, 2591-2594.
- [13] J. Malmquist, P. Ström, *J. Labelled Compd. Radiopharm.* **2012**, *55*, 387-392.
- [14] R. G. Harvey, M. Konieczny, J. Pataki, *J. Org. Chem.* **1983**, *48*, 2930-2932.
- [15] P. Toy, S. Ma, *Synlett* **2016**, *27*, 1207-1210.
- [16] K. Fujii, K. Mitsudo, H. Mandai, S. Suga, *Bull. Chem. Soc. Jpn.* **2016**, *89*, 1081-1092.
- [17] a) A. D. Becke, *J. Chem. Phys.* **1993**, *98*, 1372-1377; b) C. Lee, W. Yang, R. G. Parr, *Phys. Rev. B* **1988**, *37*, 785-789; c) S. Grimme, *J. Chem. Phys.* **2006**, *124*, 034108.
- [18] A. V. Marenich, C. J. Cramer, D. G. Truhlar, *J. Phys. Chem. B* **2009**, *113*, 6378-6396.
- [19] S. Grimme, *Chem. Eur. J.* **2012**, *18*, 9955-9964.
- [20] Y.-P. Li, J. Gomes, S. Mallikarjun Sharada, A. T. Bell, M. Head-Gordon, *J. Phys. Chem. C* **2015**, *119*, 1840-1850.
- [21] G. Luchini, J. V. Alegre-Requena, Y. Guan, I. Funes-Ardoiz, R. S. Paton, GoodVibes 3.0.0, **2019**.
- [22] a) C. Riplinger, B. Sandhoefer, A. Hansen, F. Neese, *J. Chem. Phys.* **2013**, *139*, 134101; b) C. Riplinger, F. Neese, *J. Chem. Phys.* **2013**, *138*, 034106; c) F. Weigend, R. Ahlrichs, *Phys. Chem. Chem. Phys.* **2005**, *7*, 3297-3305.
- [23] A. Hellweg, C. Hättig, S. Höfener, W. Klopper, *Theor. Chem. Acc.* **2007**, *117*, 587-597.
- [24] M. Marin-Luna, P. Patschinski, H. Zipse, *Chem. Eur. J.* **2018**, *24*, 15052-15058.
- [25] G. W. T. M. J. Frisch, H. B. Schlegel, G. E. Scuseria, M. A. Robb, J. R. Cheeseman, G. Scalmani, V. Barone, B. Mennucci, G. A. Petersson, H. Nakatsuji, M. Caricato, X. Li, H. P. Hratchian, A. F. Izmaylov, J. Bloino, G. Zheng, J. L. Sonnenberg, M. Hada, M. Ehara, K. Toyota, R. Fukuda, J. Hasegawa, M. Ishida, T. Nakajima, Y. Honda, O. Kitao, H. Nakai, T. Vreven, J. A. Montgomery, Jr., J. E. Peralta, F. Ogliaro, M. Bearpark, J. J. Heyd, E. Brothers, K. N. Kudin, V. N. Staroverov, T. Keith, R. Kobayashi, J. Normand, K. Raghavachari, A. Rendell, J. C. Burant, S. S. Iyengar, J. Tomasi, M. Cossi, N. Rega, J. M. Millam, M. Klene, J. E. Knox, J. B. Cross, V. Bakken, C. Adamo, J. Jaramillo, R. Gomperts, R. E. Stratmann, O. Yazyev, A. J. Austin, R. Cammi, C. Pomelli, J. W. Ochterski, R. L. Martin, K. Morokuma, V. G. Zakrzewski, G. A. Voth, P. Salvador, J. J. Dannenberg, S. Dapprich, A. D. Daniels, O. Farkas, J. B. Foresman, J. V. Ortiz, J. Cioslowski, and D. J. Fox, Gaussian 09, Revision D.01, Wallingford CT, **2010**.
- [26] F. Neese, *Comput. Mol. Sci.* **2012**, *2*, 73-78.
- [27] W. B. Schneider, G. Bistoni, M. Sparta, M. Saitow, C. Riplinger, A. A. Auer, F. Neese, *J. Chem. Theory Comput.* **2016**, *12*, 4778-4792.
- [28] Maestro 12.2.012, New York, **2019**.
- [29] a) E. Larionov, M. Mahesh, A. C. Spivey, Y. Wei, H. Zipse, *J. Am. Chem. Soc.* **2012**, *134*, 9390-9399; b) R. Maji, H. Ugale, S. E. Wheeler, *Chem. Eur. J.* **2019**, *25*, 4452-4459.
- [30] T. Lu, F. Chen, *J. Comput. Chem.* **2012**, *33*, 580-592.
- [31] J. Contreras-Garcia, E. R. Johnson, S. Keinan, R. Chaudret, J. P. Piquemal, D. N. Beratan, W. Yang, *J. Chem. Theory Comput.* **2011**, *7*, 625-632.
- [32] W. Humphrey, A. Dalke, K. Schulten, *J. Molec. Graphics* **1996**, *14*, 33-38.
- [33] E. D. Glendening, A. E. Reed, J. E. Carpenter, F. Weinhold, NBO Version 3.1
- [34] R. Dennington, A. K. Todd, J. M. Millam, GaussView 5, **2009**.
- [35] C. Y. Legault, CYLview 1.0b, Université de Sherbrooke, **2009**.
- [36] S. Xu, I. Held, B. Kempf, H. Mayr, W. Steglich, H. Zipse, *Chem. Eur. J.* **2005**, *11*, 4751-4757.
- [37] J. M. Keith, J. F. Larrow, E. N. Jacobsen, *Adv. Synth. Catal.* **2001**, *343*, 5-26.
- [38] C. Riplinger, P. Pinski, U. Becker, E. F. Valeev, F. Neese, *J. Chem. Phys.* **2016**, *144*, 024109.
- [39] Y. Zhao, D. G. Truhlar, *Theor. Chem. Acc.* **2007**, *120*, 215-241.
- [40] J. D. Chai, M. Head-Gordon, *Phys. Chem. Chem. Phys.* **2008**, *10*, 6615-6620.
- [41] a) K. E. Riley, M. Pitonak, P. Jurecka, P. Hobza, *Chem. Rev.* **2010**, *110*, 5023-5063; b) T. M. Parker, L. A. Burns, R. M. Parrish, A. G. Ryno, C. D. Sherrill, *J. Chem. Phys.* **2014**, *140*, 094106.
- [42] G. Bringmann, A. J. Price Mortimer, P. A. Keller, M. J. Gresser, J. Garner, M. Breuning, *Angew. Chem. Int. Ed.* **2005**, *44*, 5384-5427.
- [43] a) J. W. Hwang, P. Li, K. D. Shimizu, *Org. Biomol. Chem.* **2017**, *15*, 1554-1564; b) C. R. Martinez, B. L. Iverson, *Chem. Sci.* **2012**, *3*, 2191; c) A. J. Neel, M. J. Hilton, M. S. Sigman, F. D. Toste, *Nature* **2017**, *543*, 637-646.
- [44] C. Reichardt, "ET(30) Werte", Philipps-Universität Marburg, <https://www.uni-marburg.de/de/fb15/arbeitsgruppen/ag-reichardt/et30-werte-prof-reichardt>, accessed at 14.04.2020.
- [45] T. J. Seguin, T. Lu, S. E. Wheeler, *Org. Lett.* **2015**, *17*, 3066-3069.
- [46] S. Grimme, J. Antony, S. Ehrlich, H. Krieg, *J. Chem. Phys.* **2010**, *132*, 154104.
- [47] S. Grimme, R. Huenerbein, S. Ehrlich, *ChemPhysChem* **2011**, *12*, 1258-1261.
- [48] S. Malakar, S. V. Shree Sowndarya, R. B. Sunoj, *Org. Biomol. Chem.* **2018**, *16*, 5643-5652.
- [49] T. Lu, R. Zhu, Y. An, S. E. Wheeler, *J. Am. Chem. Soc.* **2012**, *134*, 3095-3102.
- [50] R. A. Klein, *Chem. Phys. Lett.* **2006**, *425*, 128-133.
- [51] R. F. Bader, *J. Phys. Chem. A* **2010**, *114*, 7431-7444.
- [52] R. F. W. Bader, *Acc. Chem. Res.* **1985**, *18*, 9-15.
- [53] R. G. A. Bone, R. F. W. Bader, *J. Phys. Chem.* **1996**, *100*, 10892-10911.
- [54] S. J. Grabowski, *J. Phys. Chem. A* **2001**, *105*, 10739-10746.
- [55] T. Maity, H. Mandal, A. Bauzá, B. C. Samanta, A. Frontera, S. K. Seth, *New J. Chem.* **2018**, *42*, 10202-10213.
- [56] E. R. Johnson, S. Keinan, P. Mori-Sanchez, J. Contreras-Garcia, A. J. Cohen, W. Yang, *J. Am. Chem. Soc.* **2010**, *132*, 6498-6506.
- [57] W. Humphrey, A. Dalke, K. Schulten, *J. Mol. Graphics* **1996**, *14*, 33-38.
- [58] a) B. Thapa, H. B. Schlegel, *J. Phys. Chem. A* **2015**, *119*, 5134-5144; b) P. G. Seybold, G. C. Shields, *Wiley Interdiscip. Rev. Comput. Mol. Sci.* **2015**, *5*, 290-297.

## 6. NMR spectra

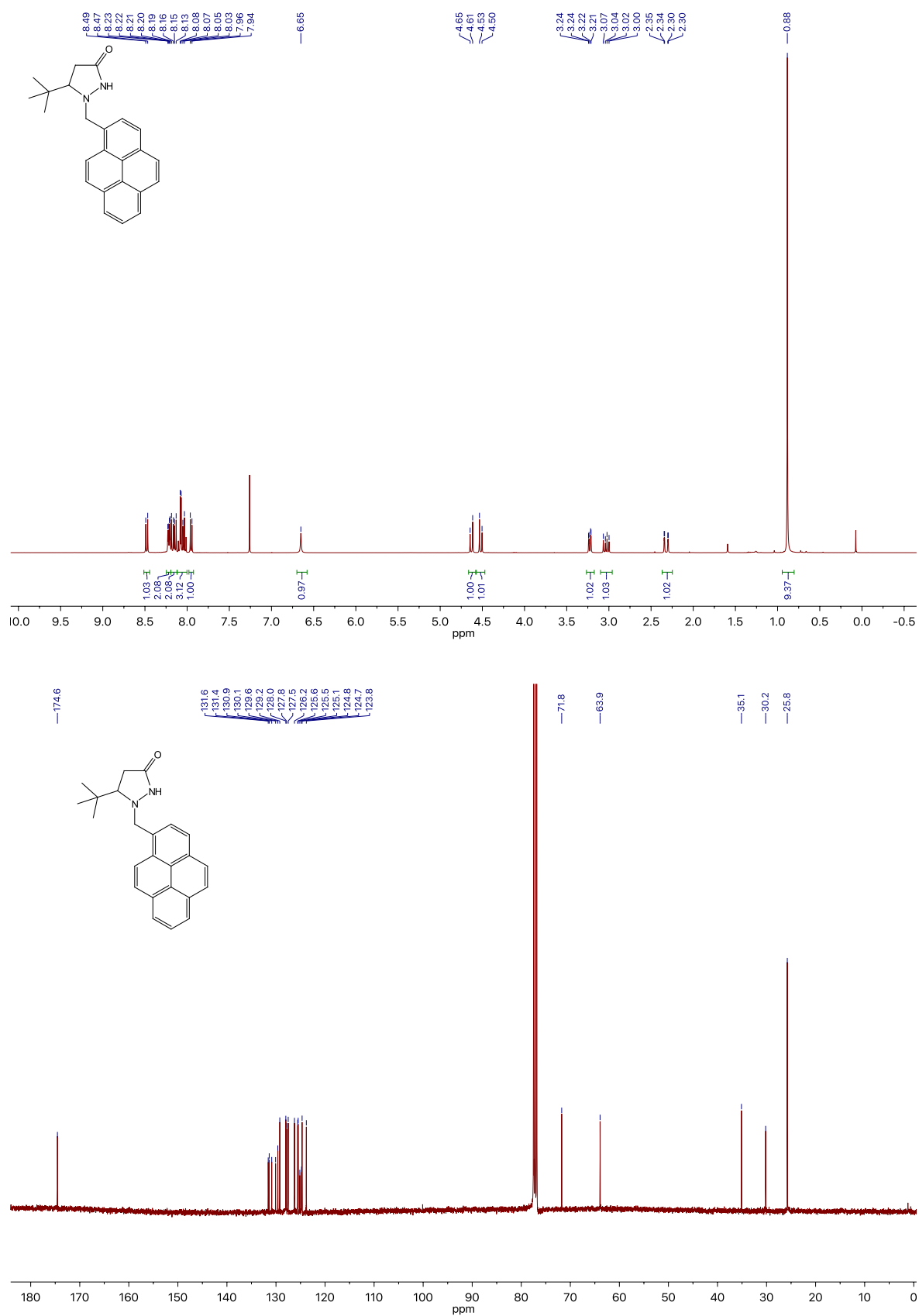
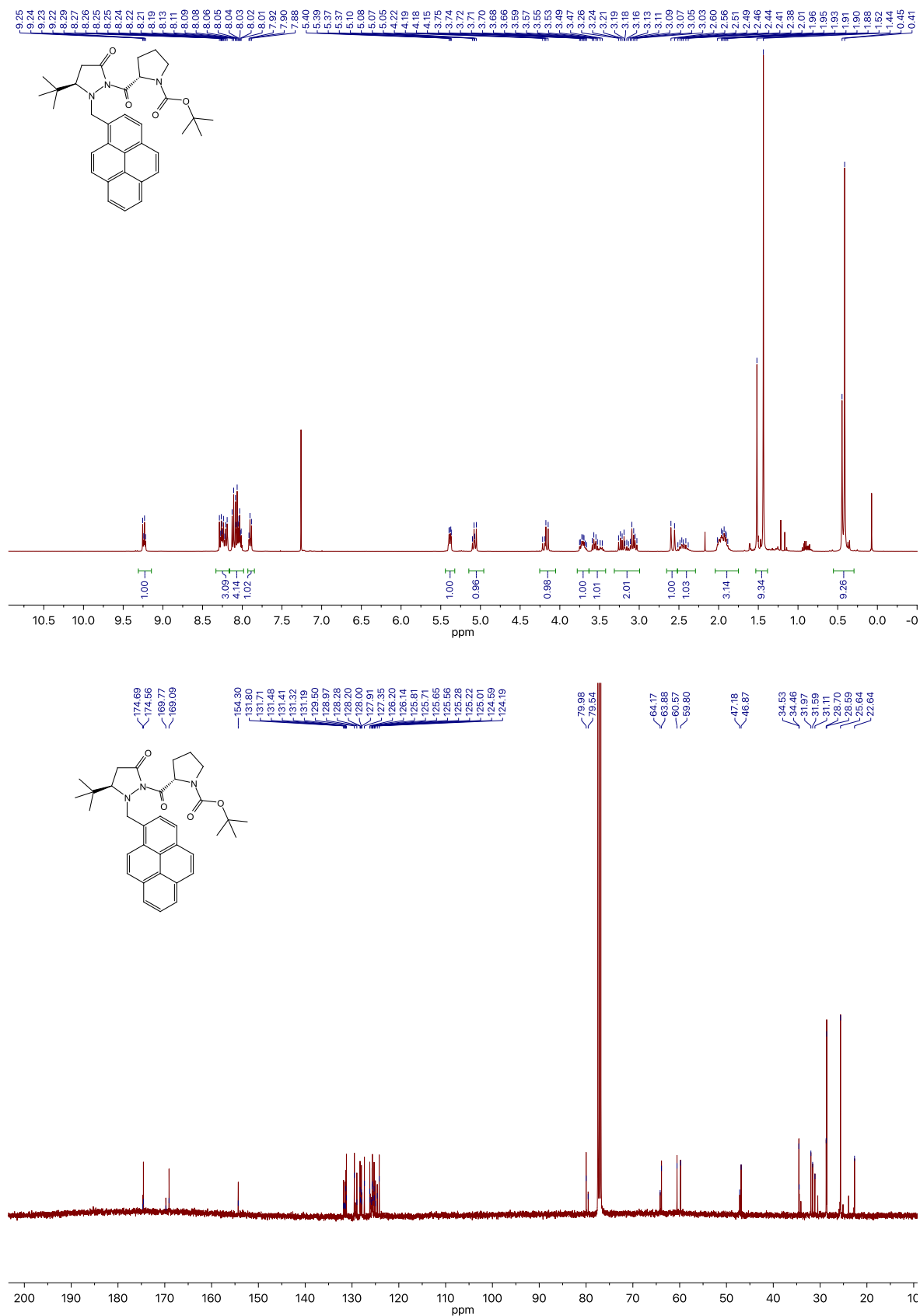


Figure S44.  $^1\text{H-NMR}$  (top) and  $^{13}\text{C-NMR}$  (bottom) NMR for catalyst synthesis intermediate **S7**.



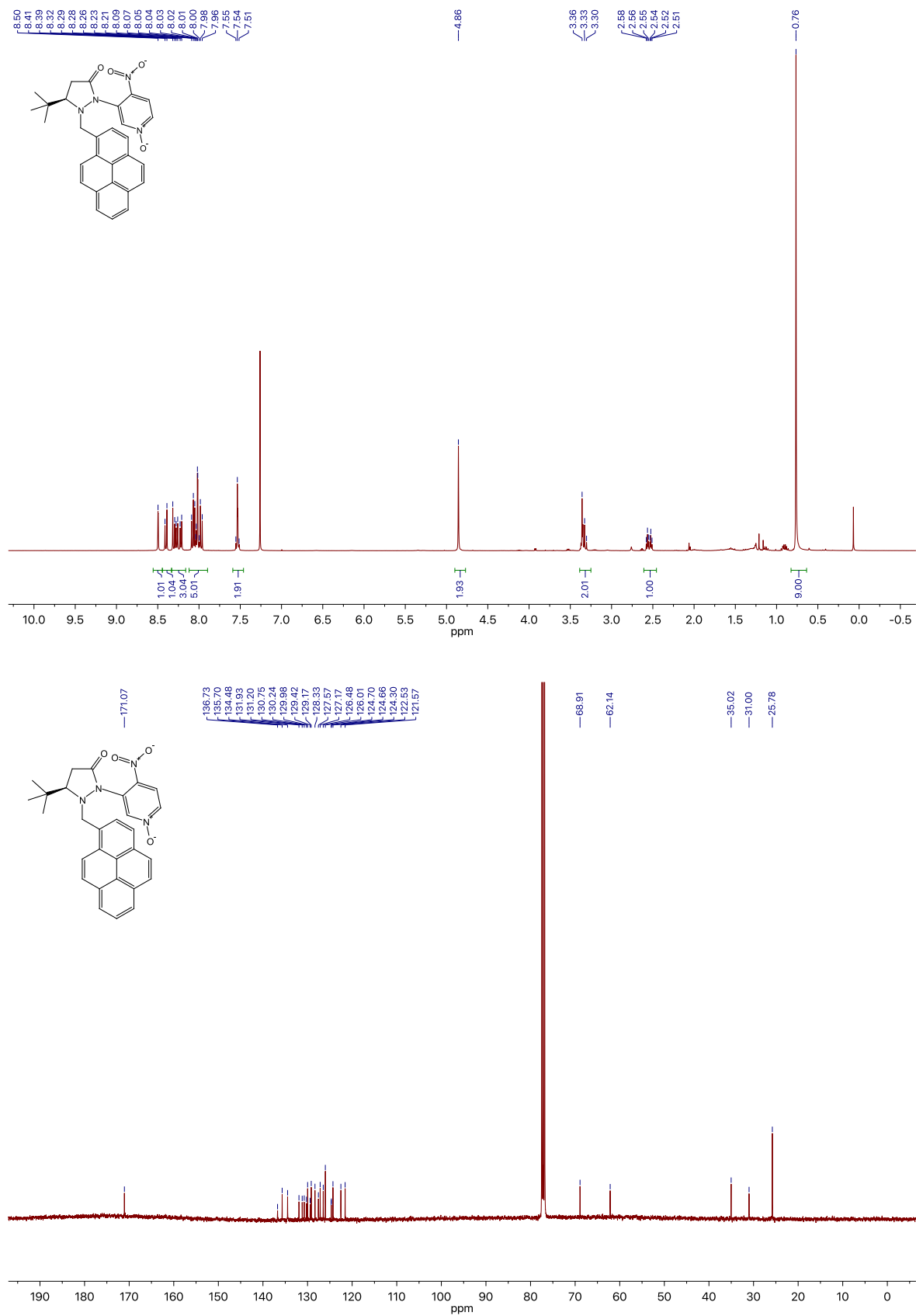


Figure S46. <sup>1</sup>H-NMR (top) and <sup>13</sup>C-NMR (bottom) NMR for catalyst synthesis intermediate **S9**.

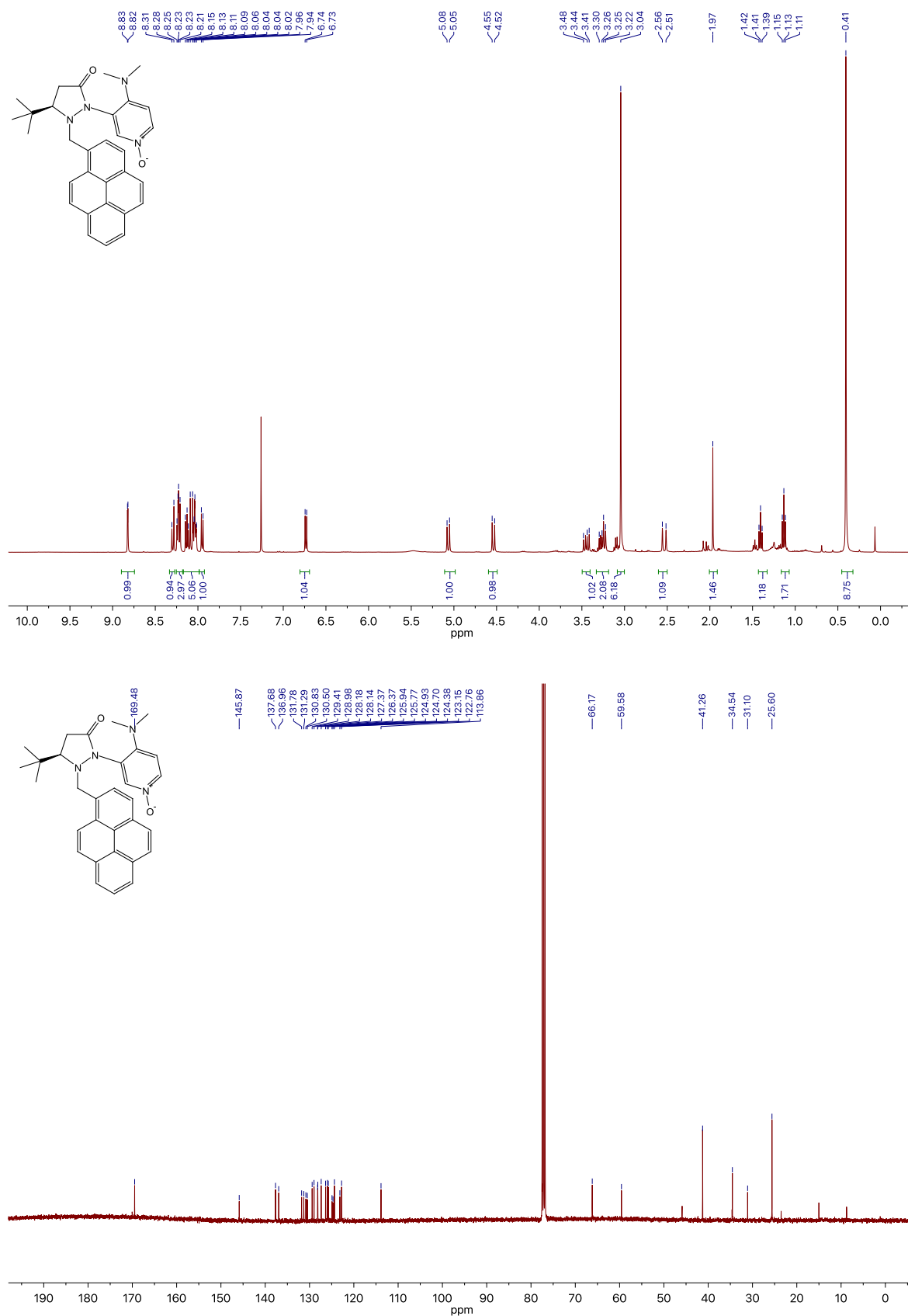


Figure S47. <sup>1</sup>H-NMR (top) and <sup>13</sup>C-NMR (bottom) NMR for catalyst synthesis intermediate **S10**.

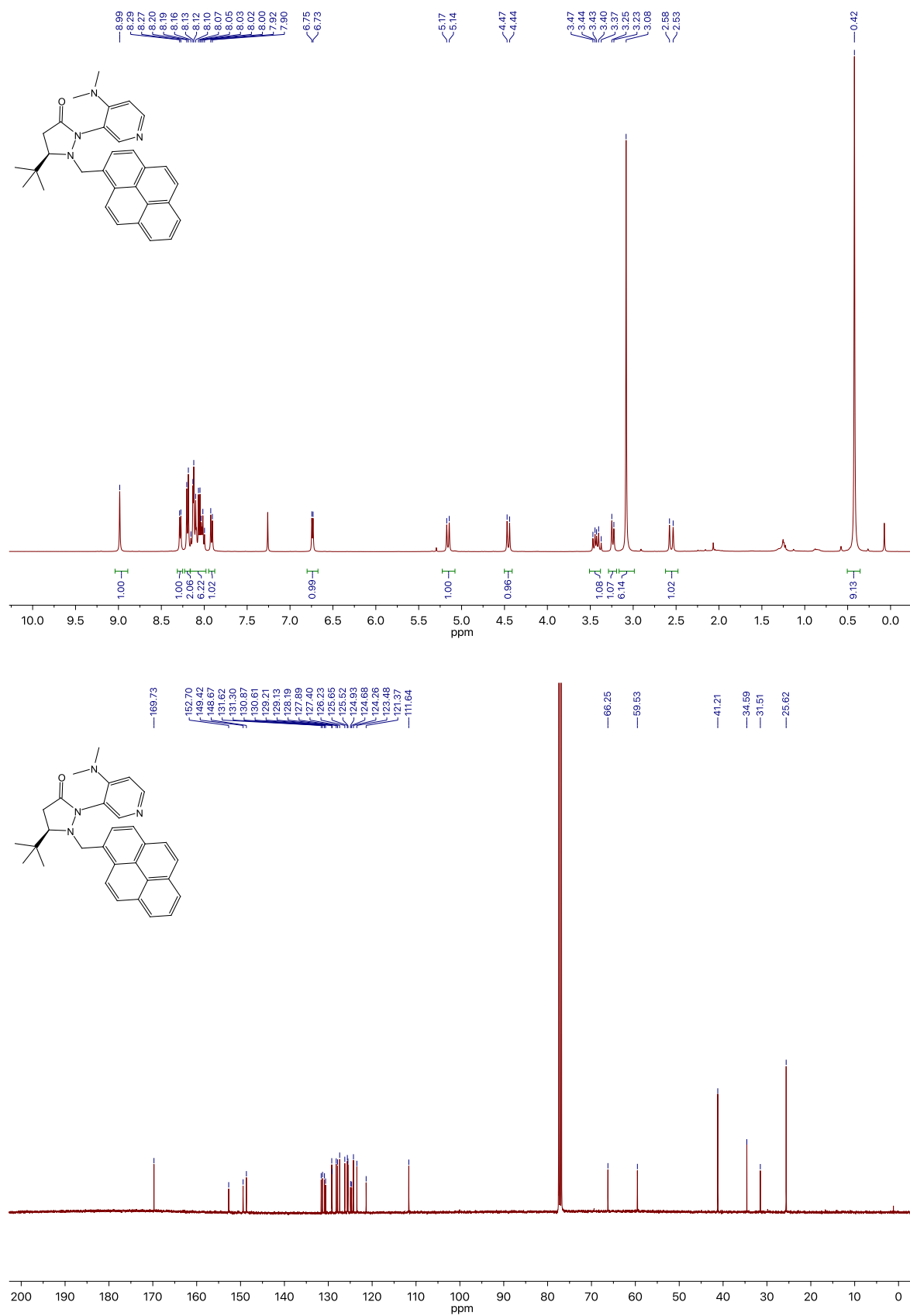


Figure S48. <sup>1</sup>H-NMR (top) and <sup>13</sup>C-NMR (bottom) NMR for catalyst 7.

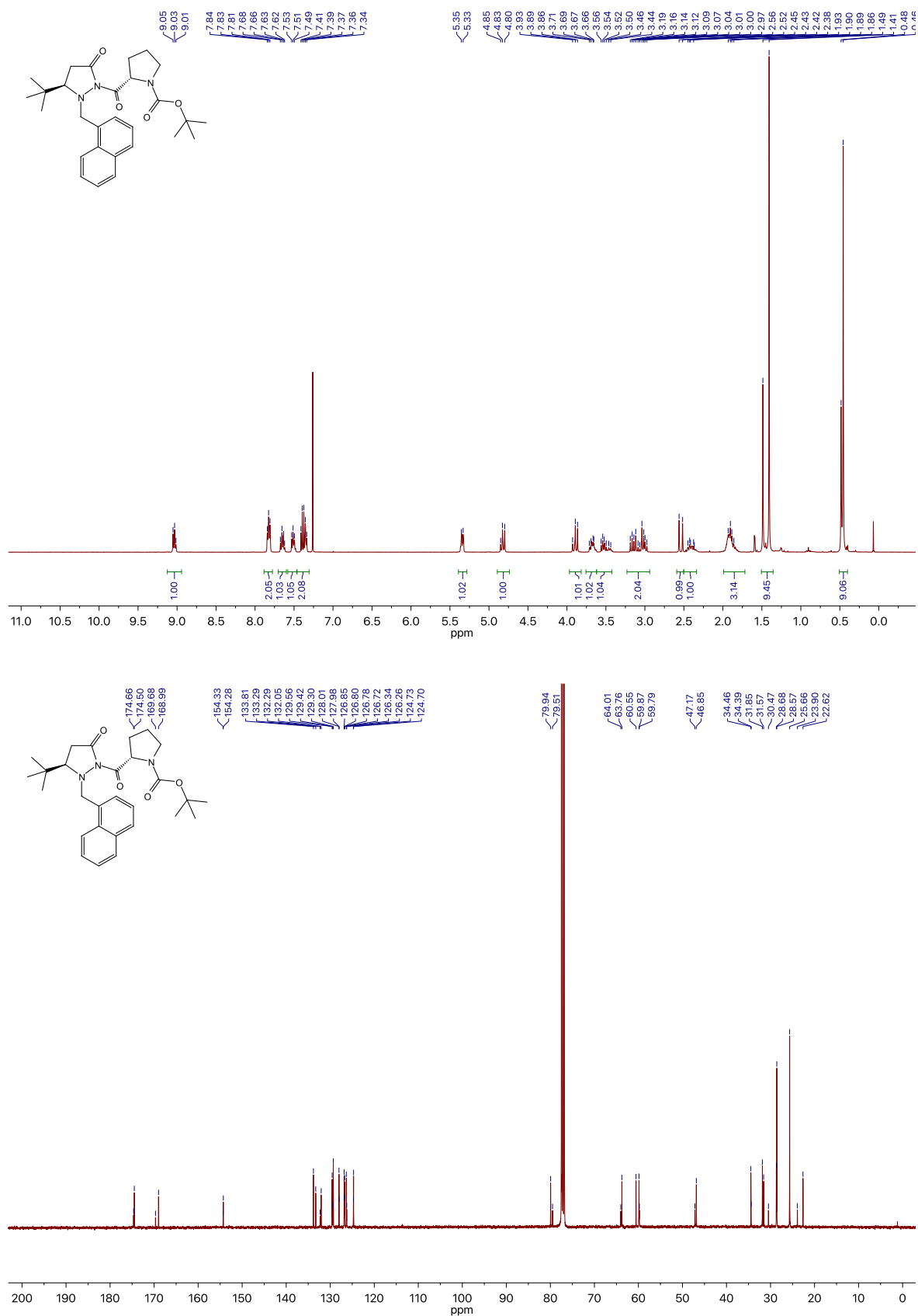


Figure S49. <sup>1</sup>H-NMR (top) and <sup>13</sup>C-NMR (bottom) NMR for catalyst synthesis intermediate **S12**.

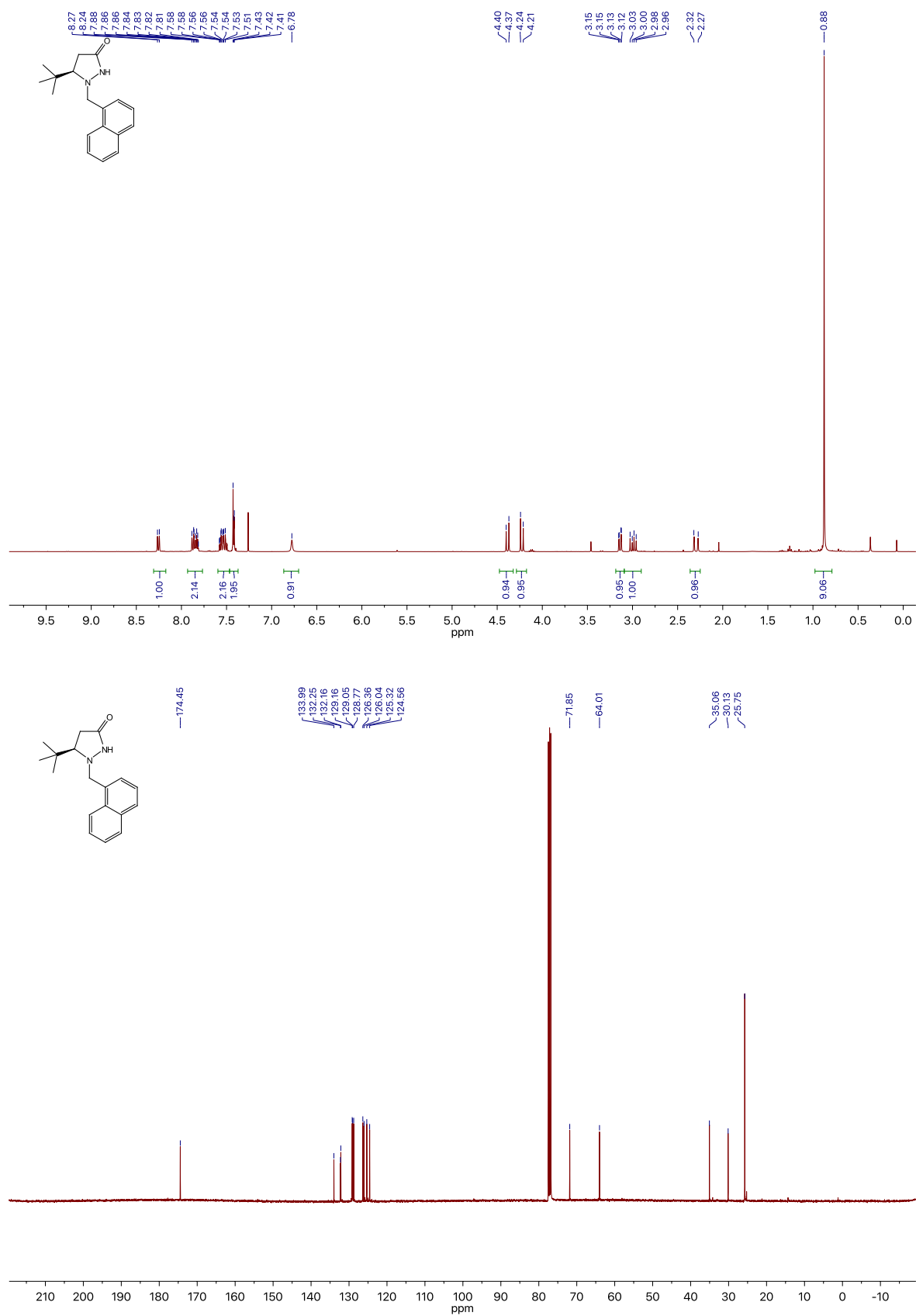


Figure S50. <sup>1</sup>H-NMR (top) and <sup>13</sup>C-NMR (bottom) NMR for catalyst synthesis intermediate **S11**.

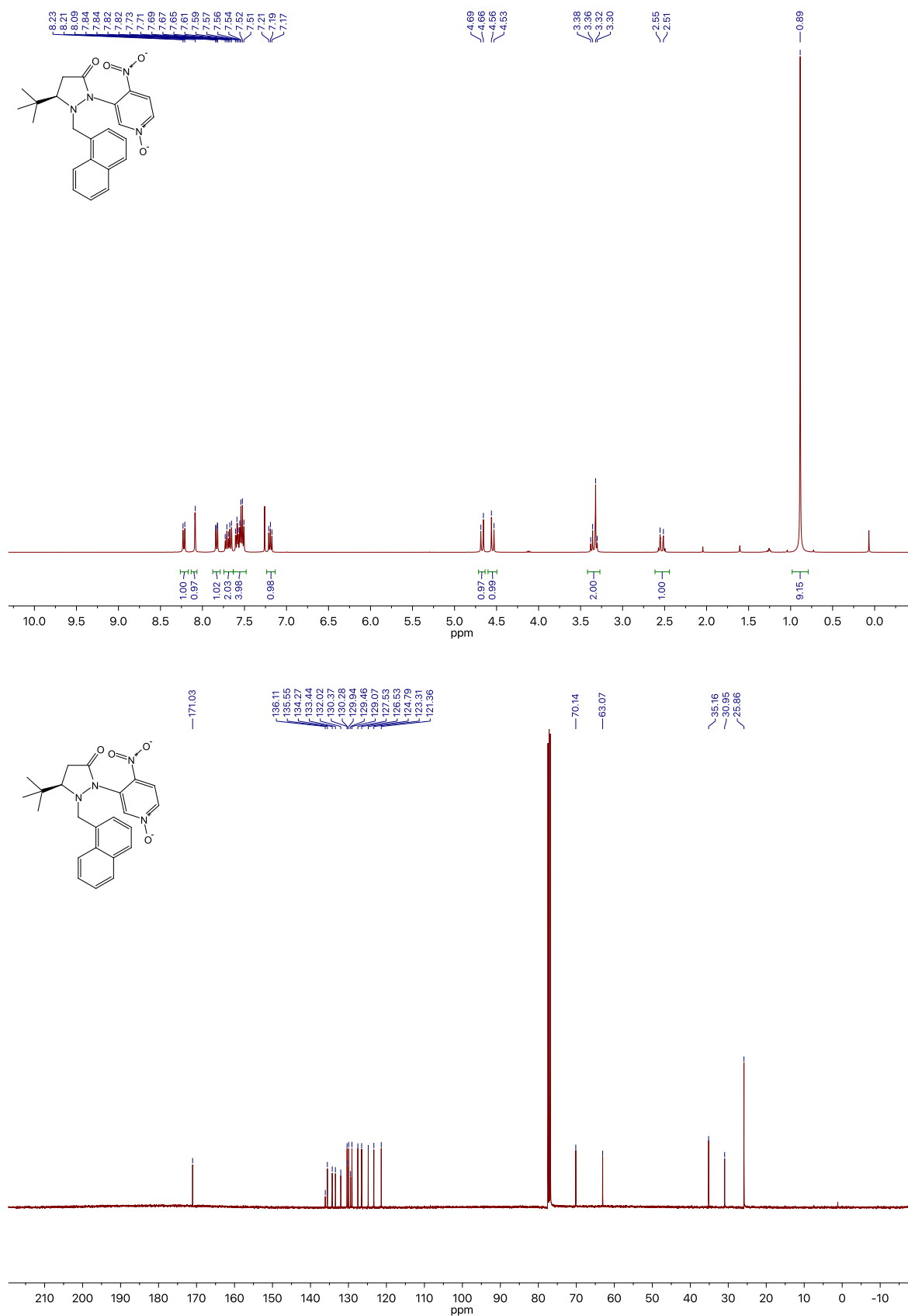


Figure S51. <sup>1</sup>H-NMR (top) and <sup>13</sup>C-NMR (bottom) NMR for catalyst synthesis intermediate **S13**.

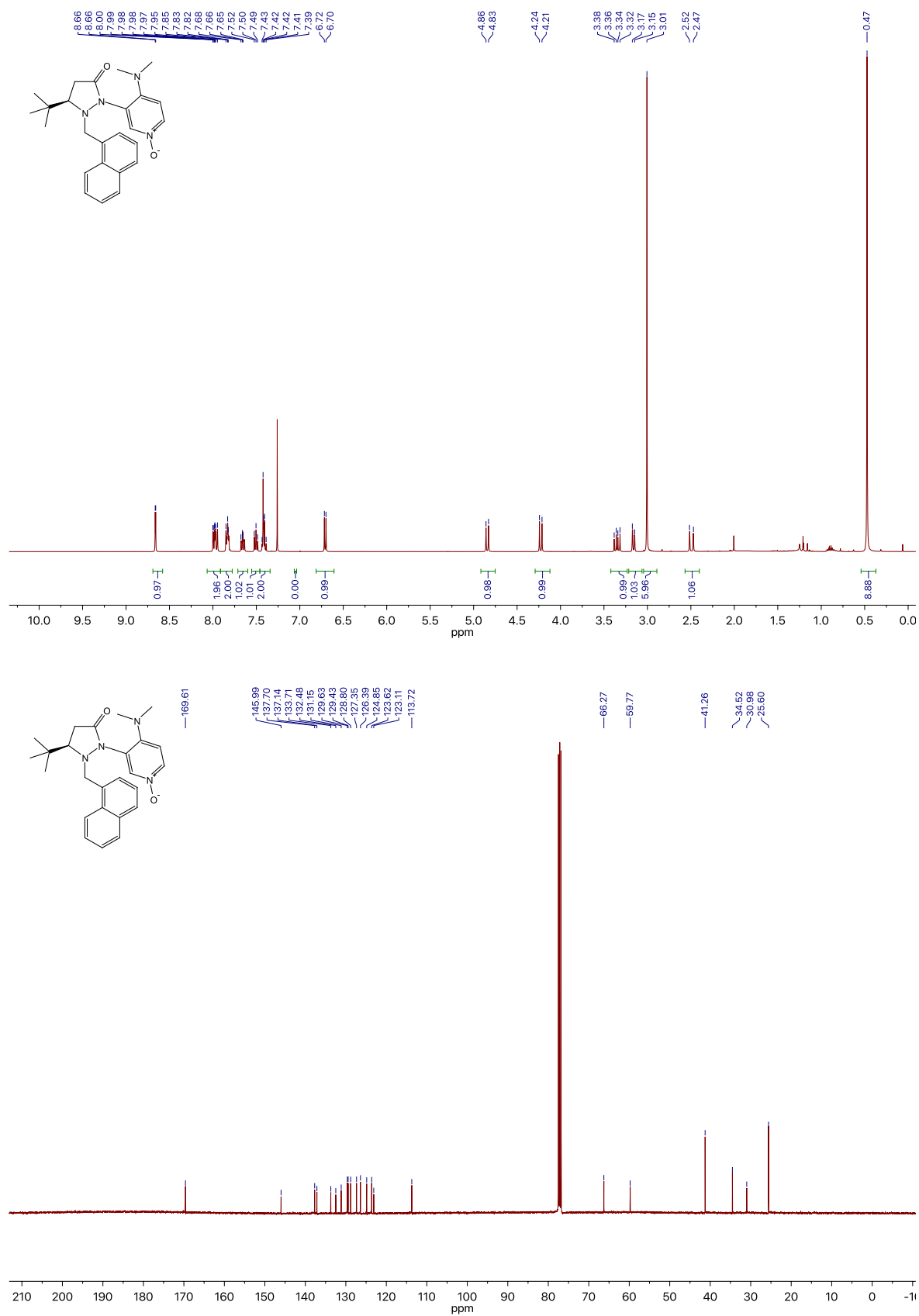


Figure S52. <sup>1</sup>H-NMR (top) and <sup>13</sup>C-NMR (bottom) NMR for catalyst synthesis intermediate **S14**.

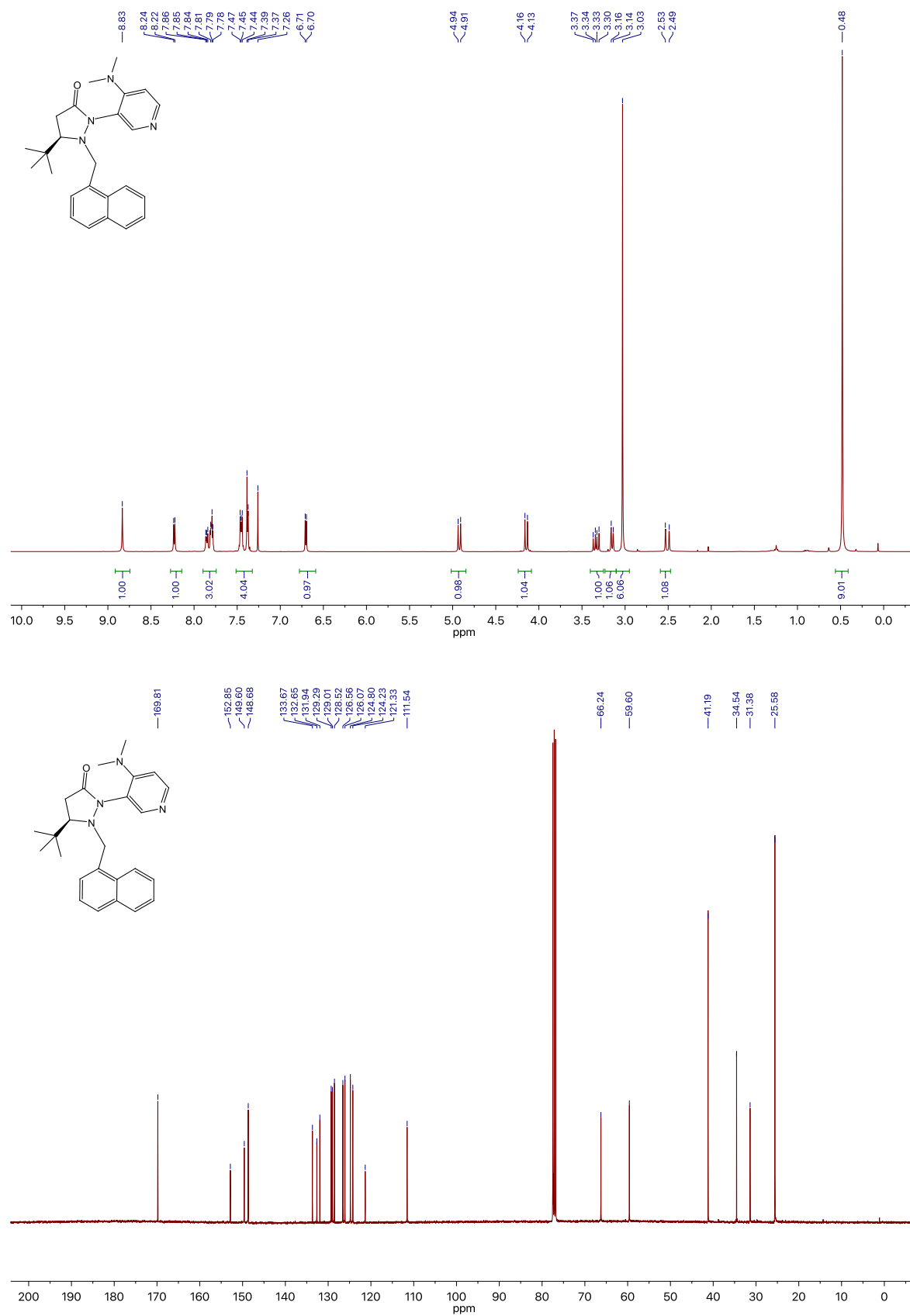


Figure S53. <sup>1</sup>H-NMR (top) and <sup>13</sup>C-NMR (bottom) NMR for catalyst 3.

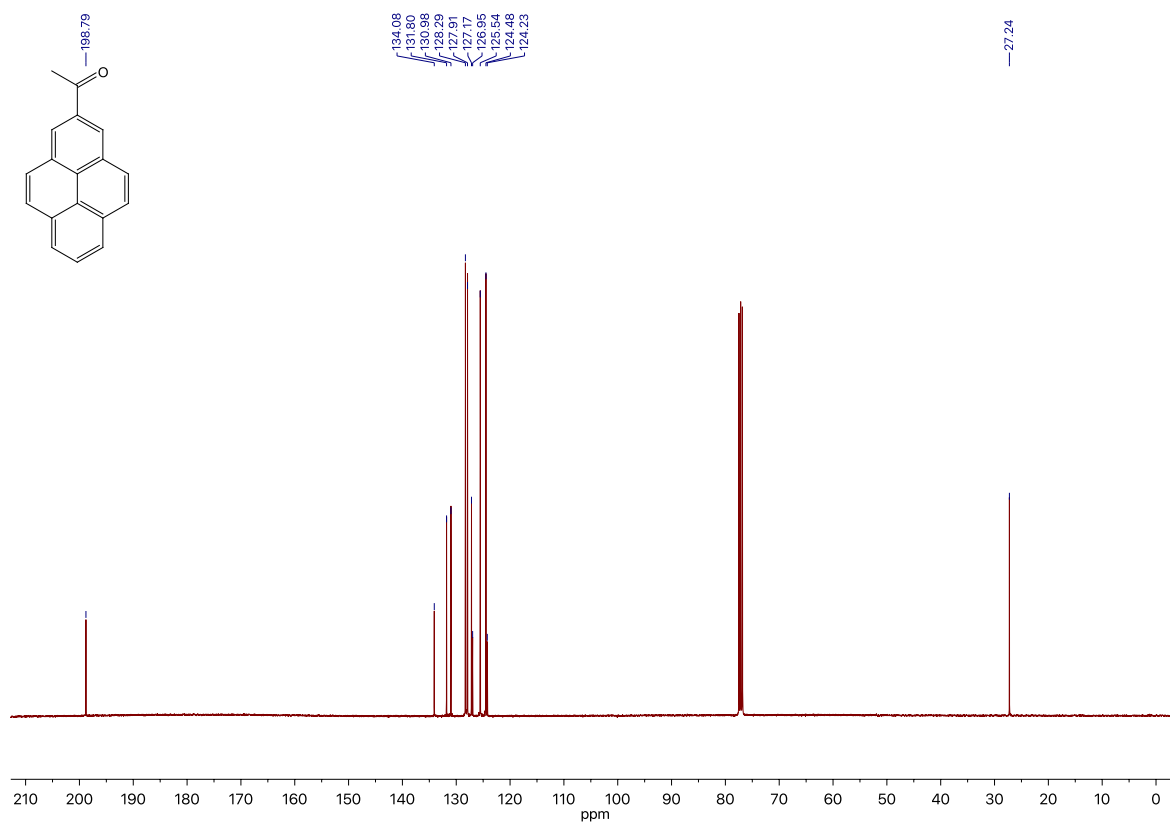
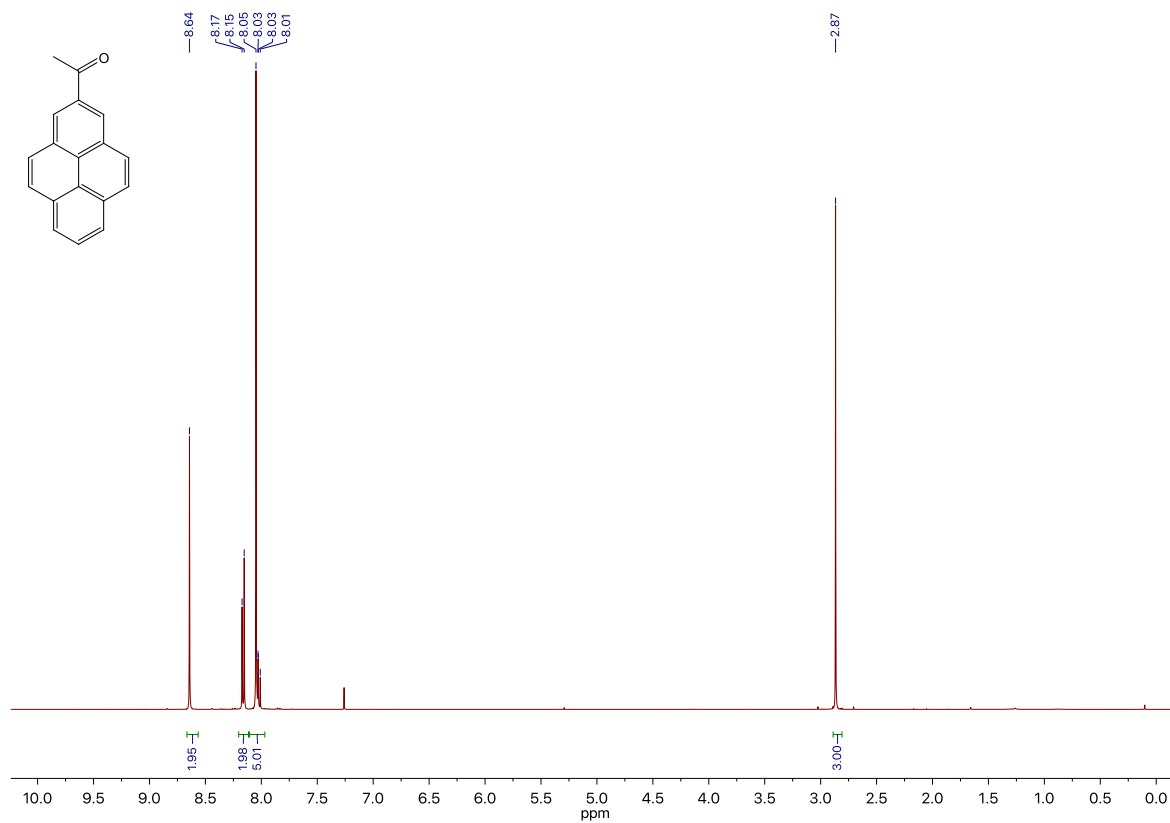


Figure S54. <sup>1</sup>H-NMR (top) and <sup>13</sup>C-NMR (bottom) NMR for 2-Acetylpyrene 1de.

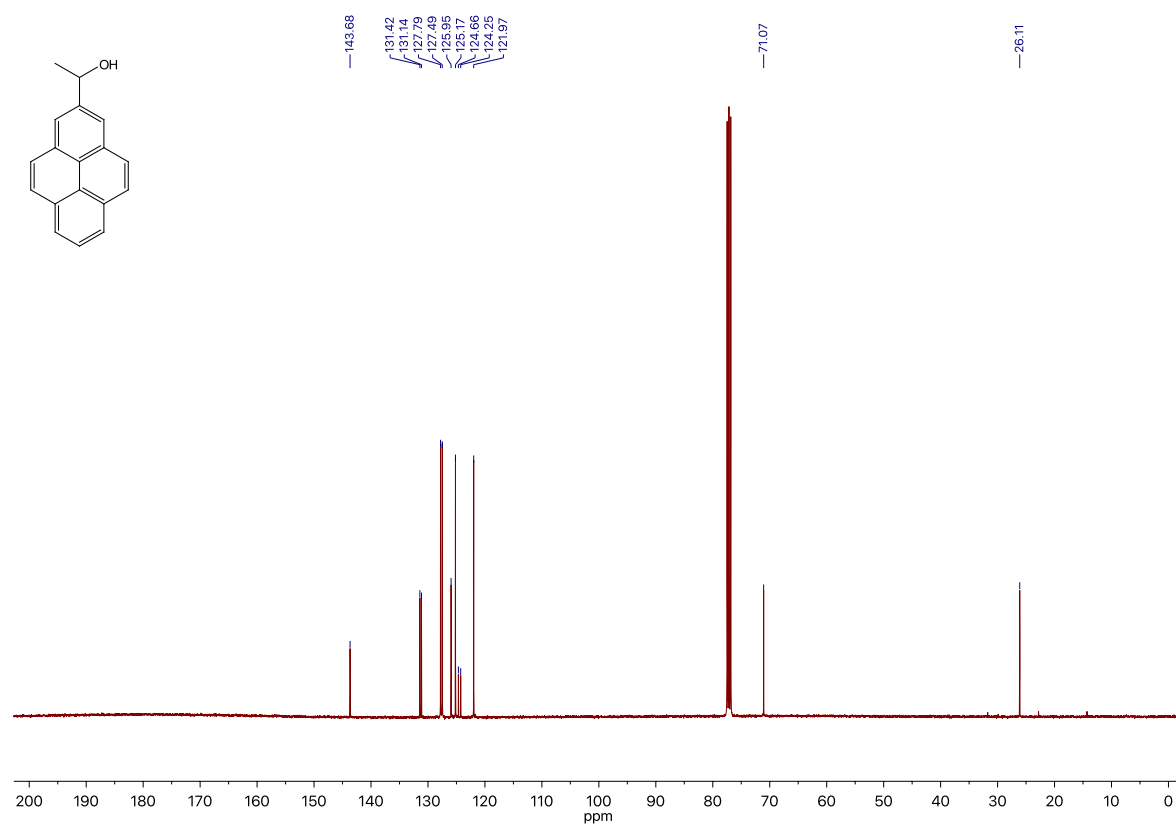
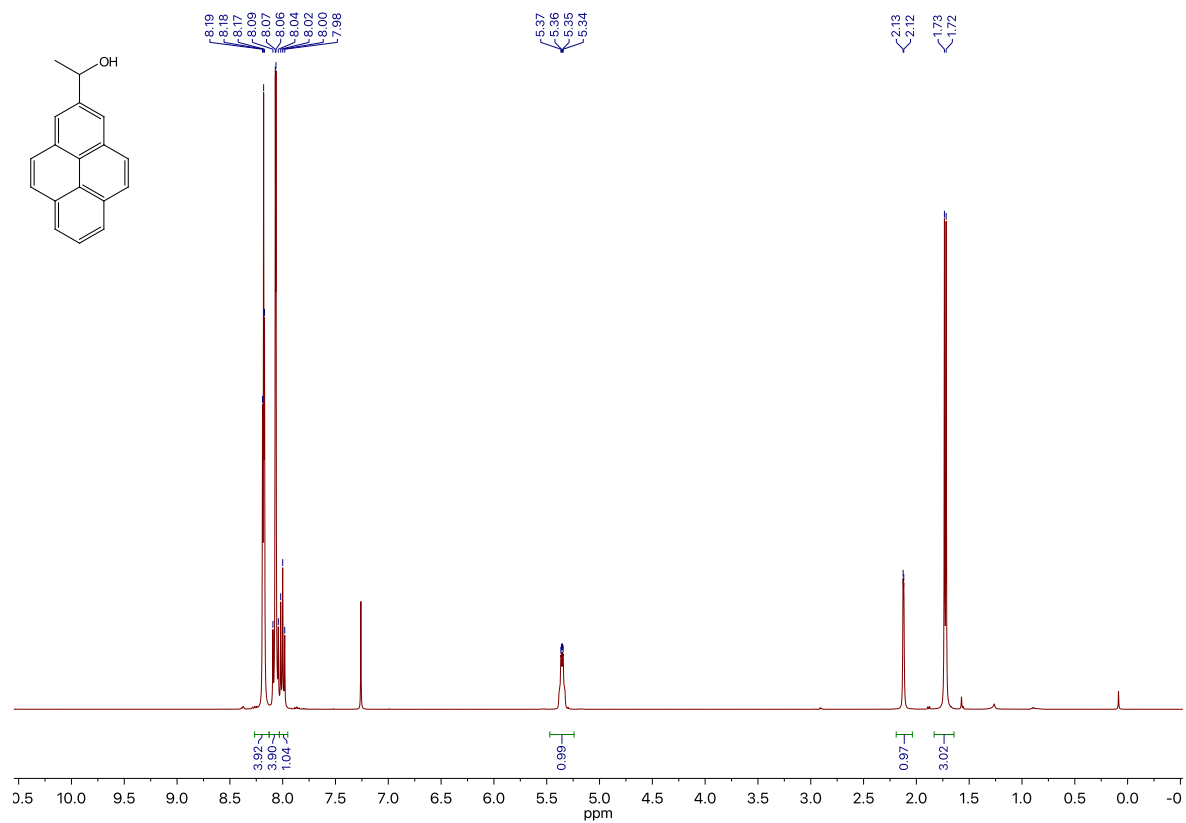


Figure S55. <sup>1</sup>H-NMR (top) and <sup>13</sup>C-NMR (bottom) NMR for 1-(2-pyrenyl)ethanol **1d**.

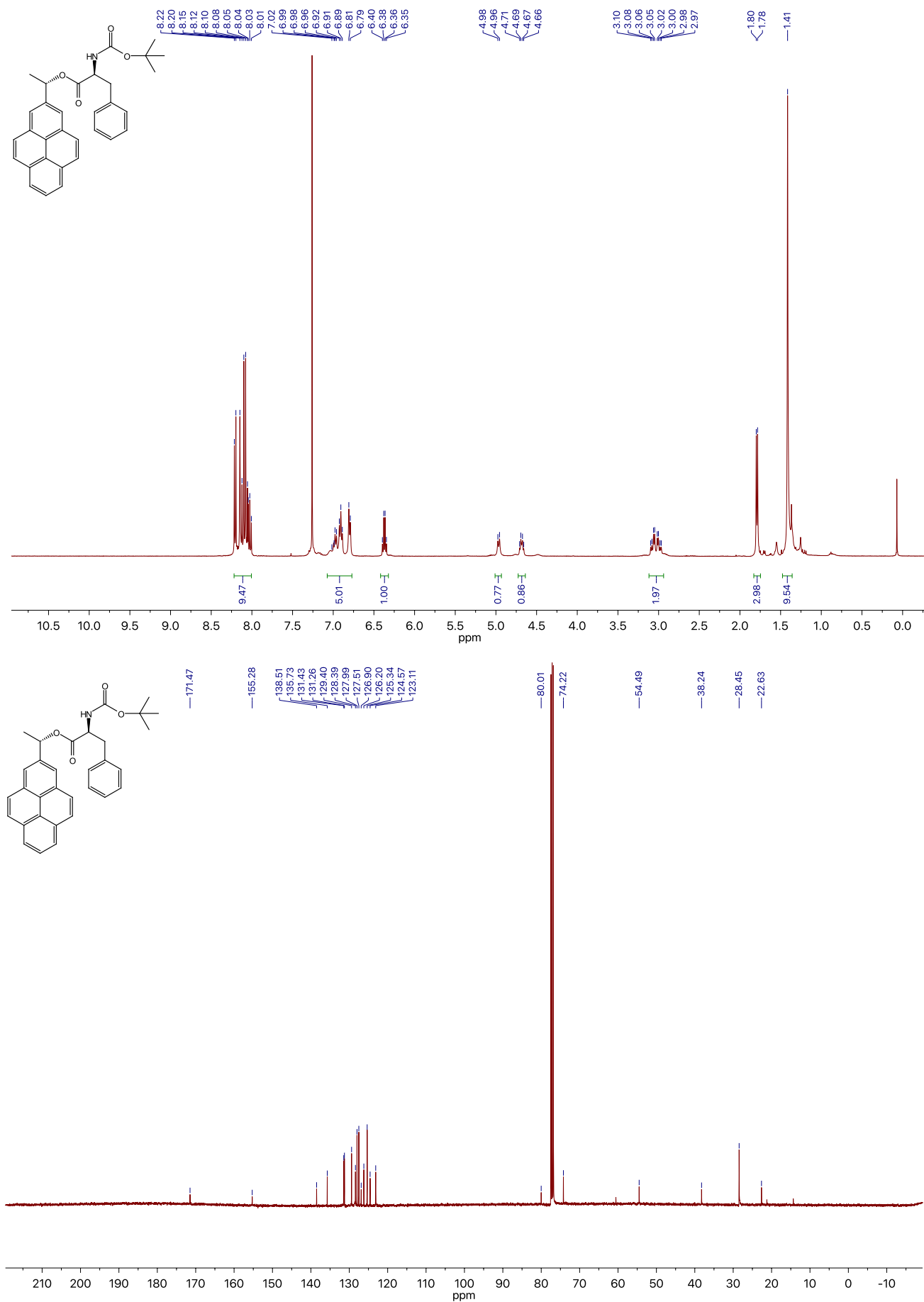


Figure S56. <sup>1</sup>H-NMR (top) and <sup>13</sup>C-NMR (bottom) NMR for (S)-1-(pyren-2-yl)ethyl (tert-butoxycarbonyl)-L-phenylalaninate **S3**.

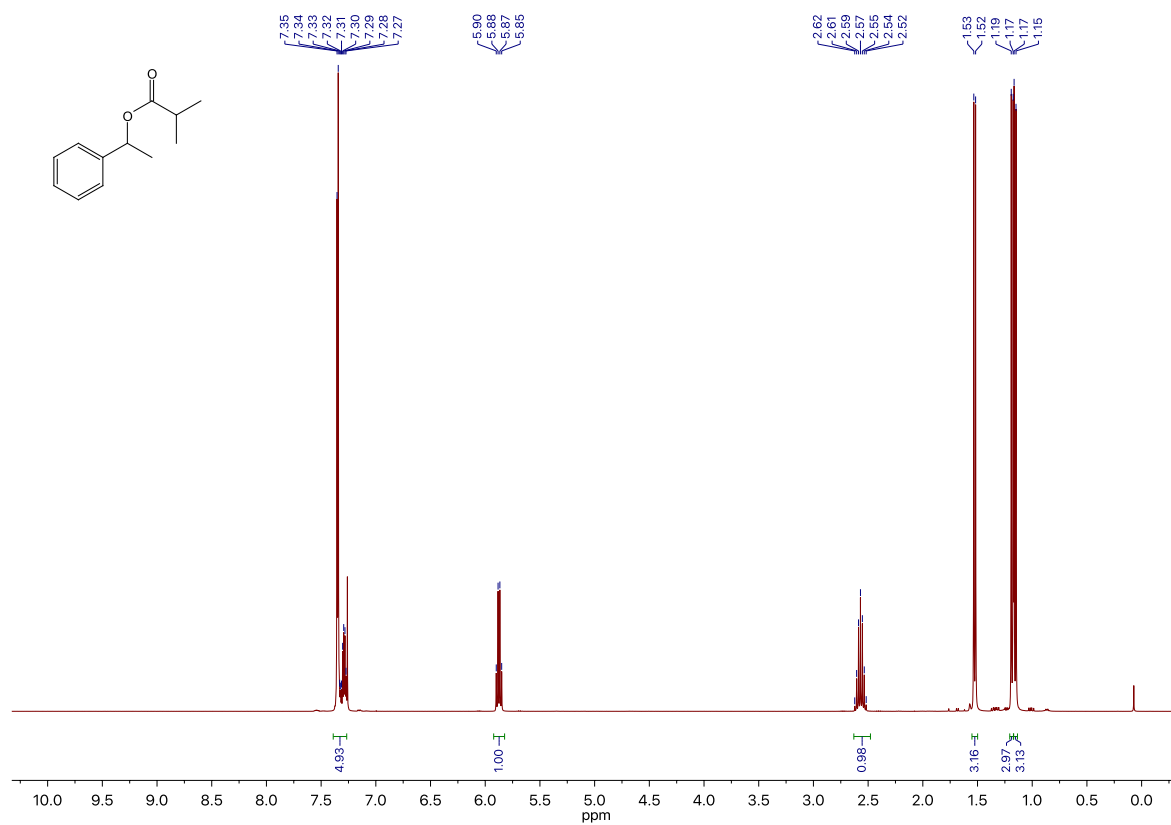


Figure S57. <sup>1</sup>H-NMR for 1-phenylethyl isobutyrate 4a.

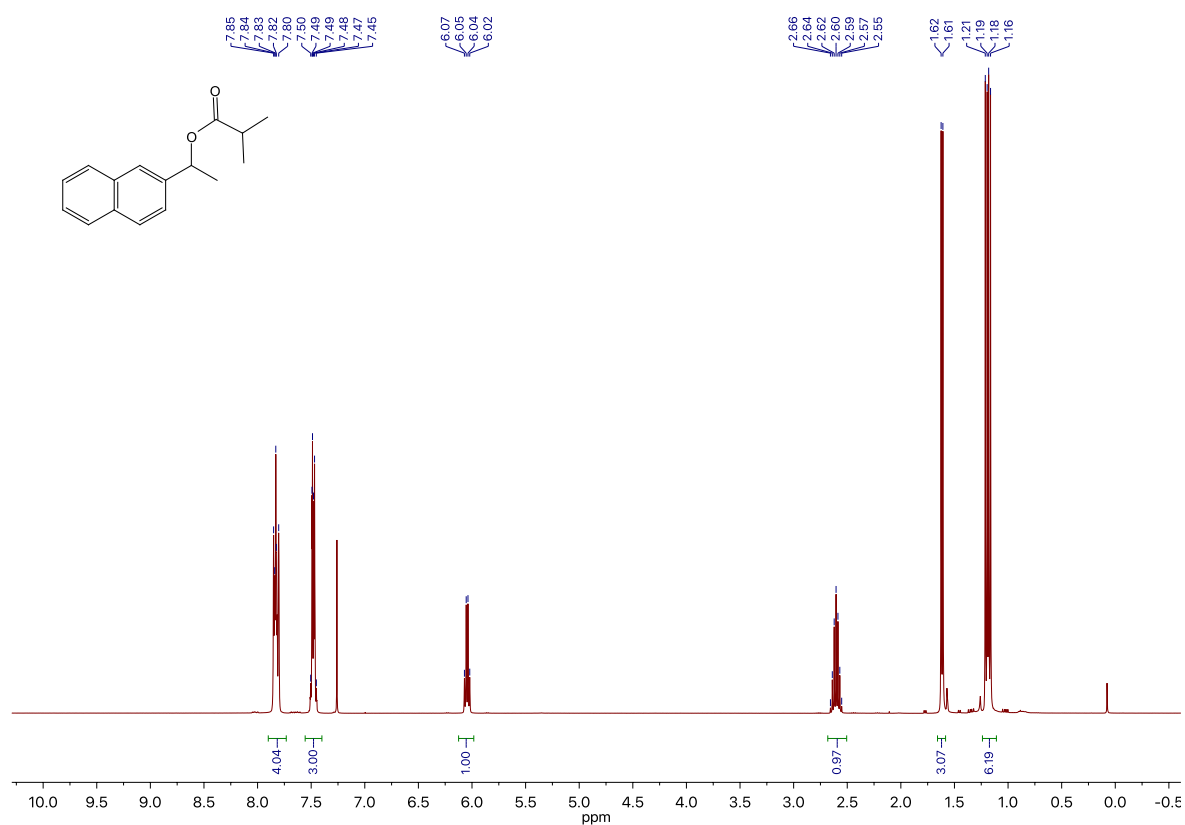


Figure S58. <sup>1</sup>H-NMR for 1-(2-naphthyl)ethyl isobutyrate 4b.

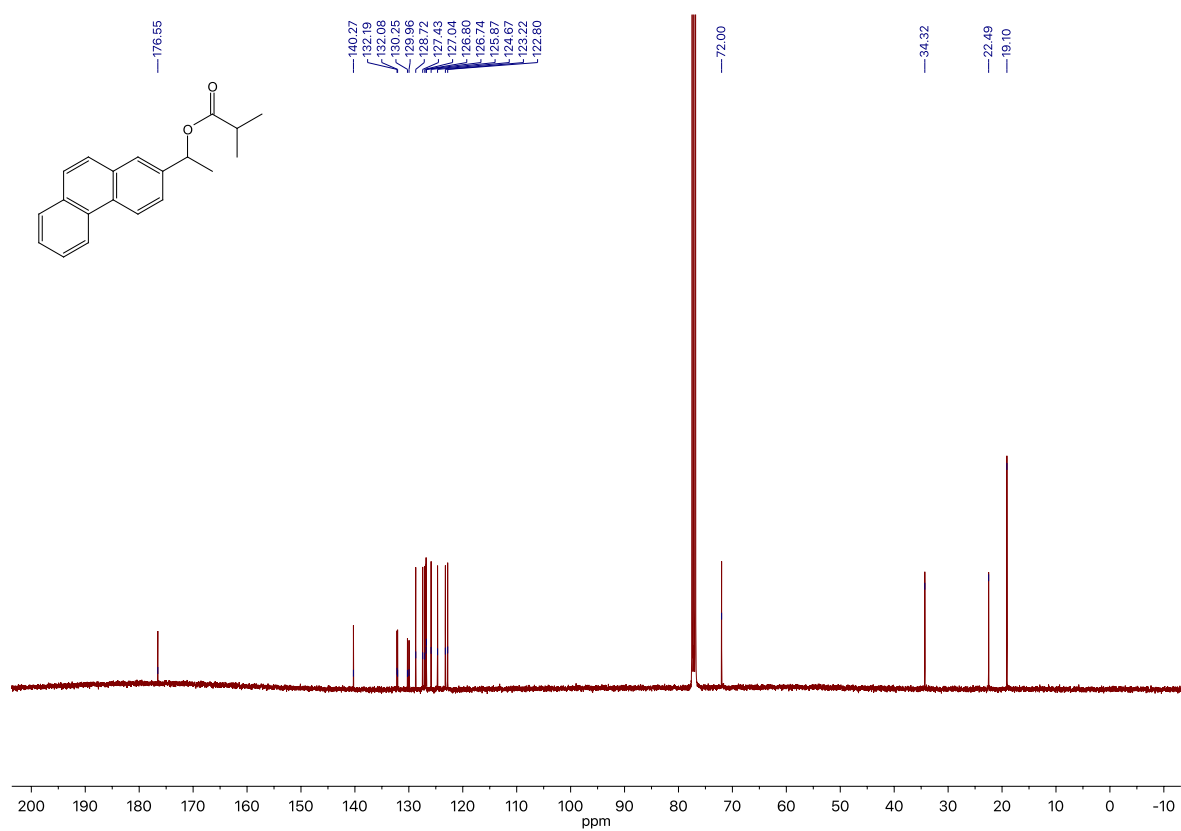
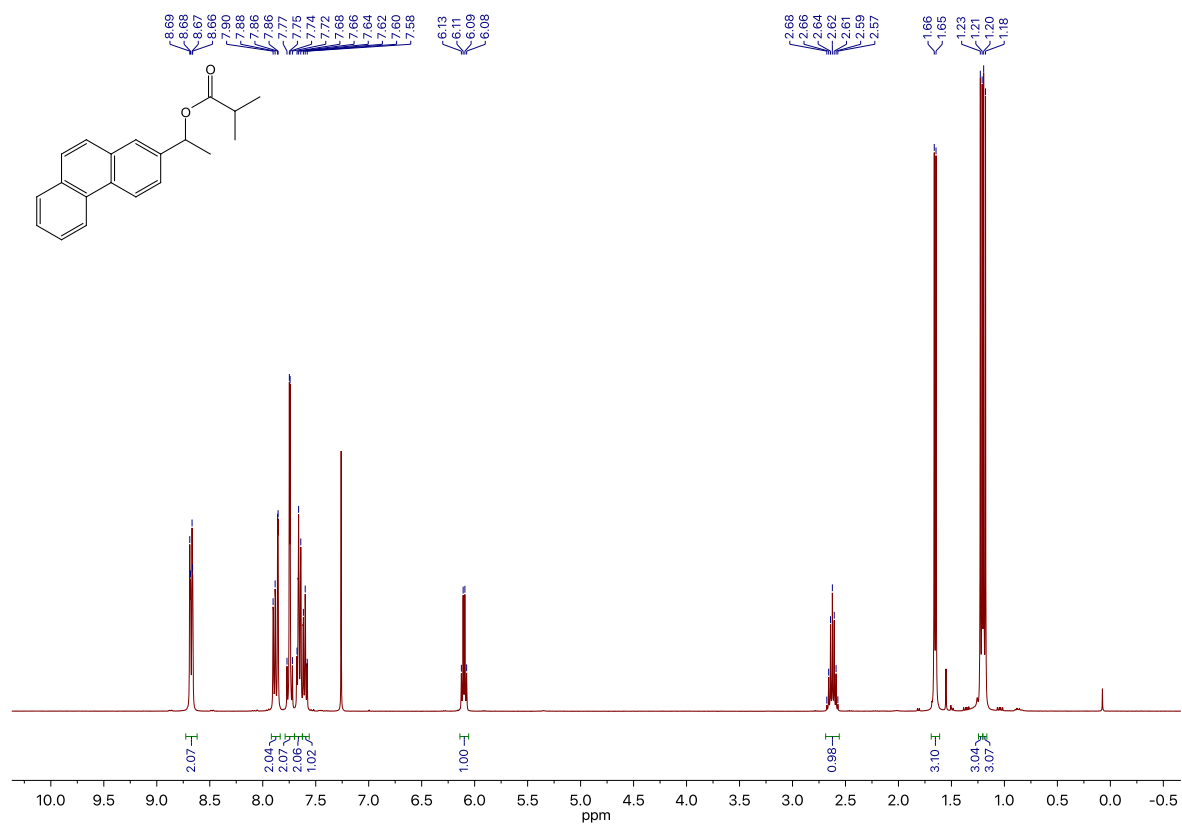


Figure S59. <sup>1</sup>H-NMR (top) and <sup>13</sup>C-NMR (bottom) NMR for 1-(2-phenanthryl)ethyl isobutyrate **4c**.

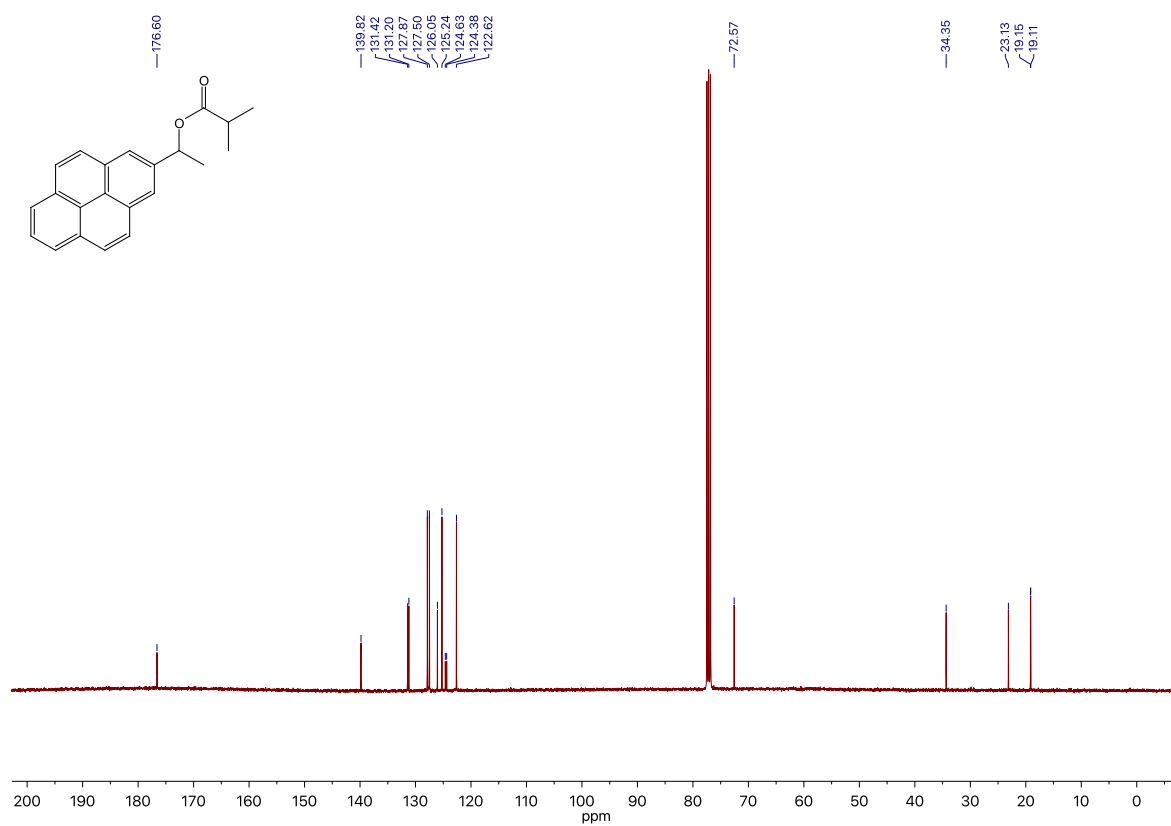
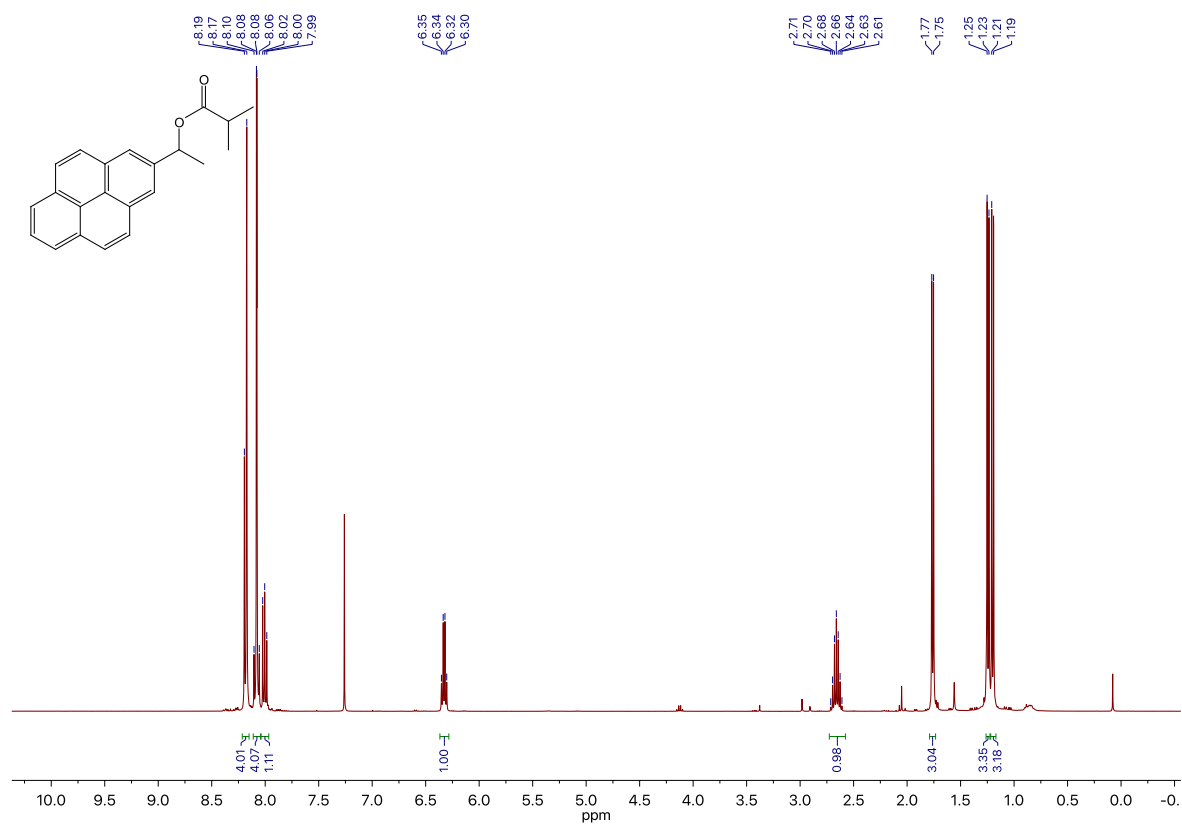
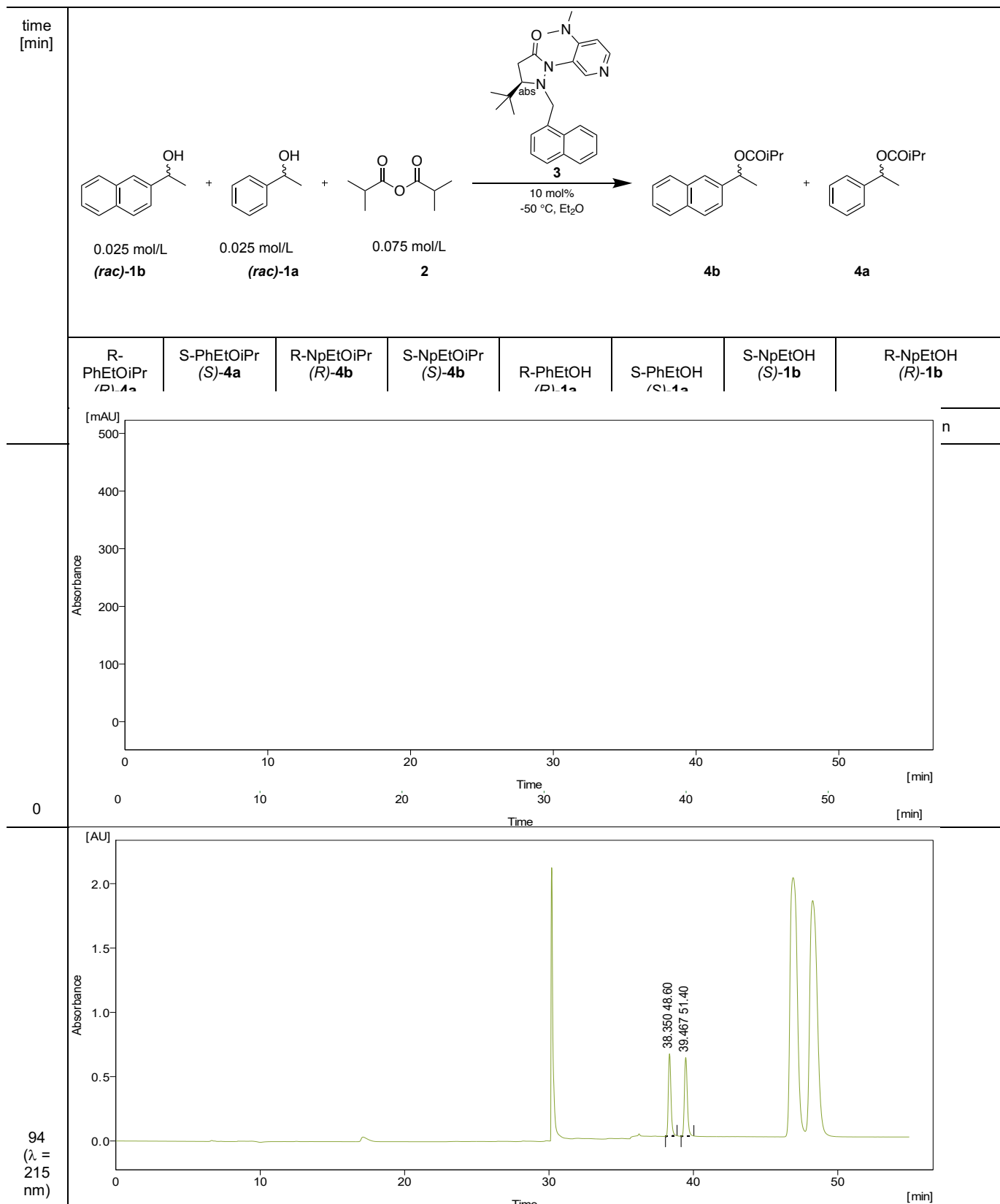
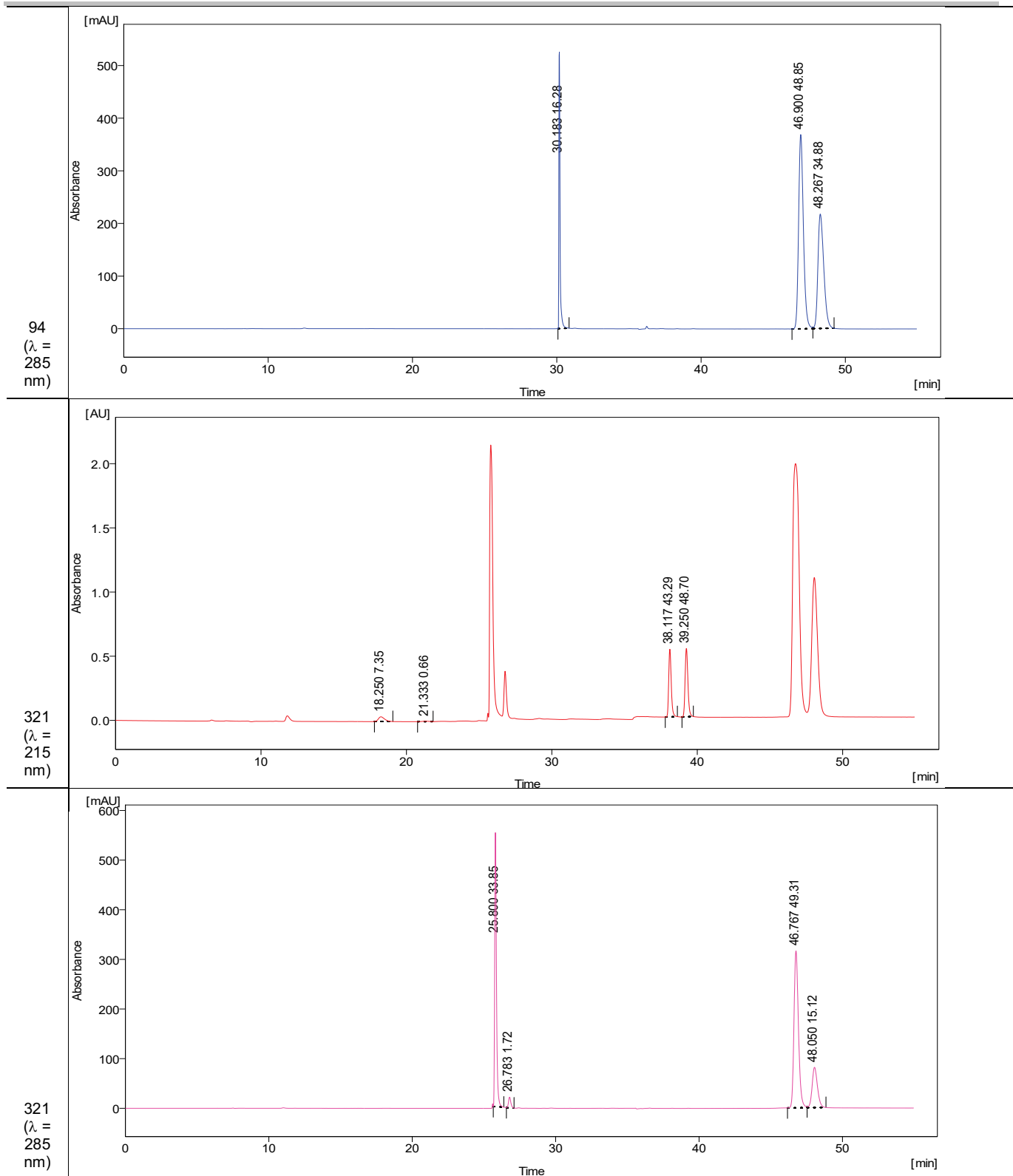


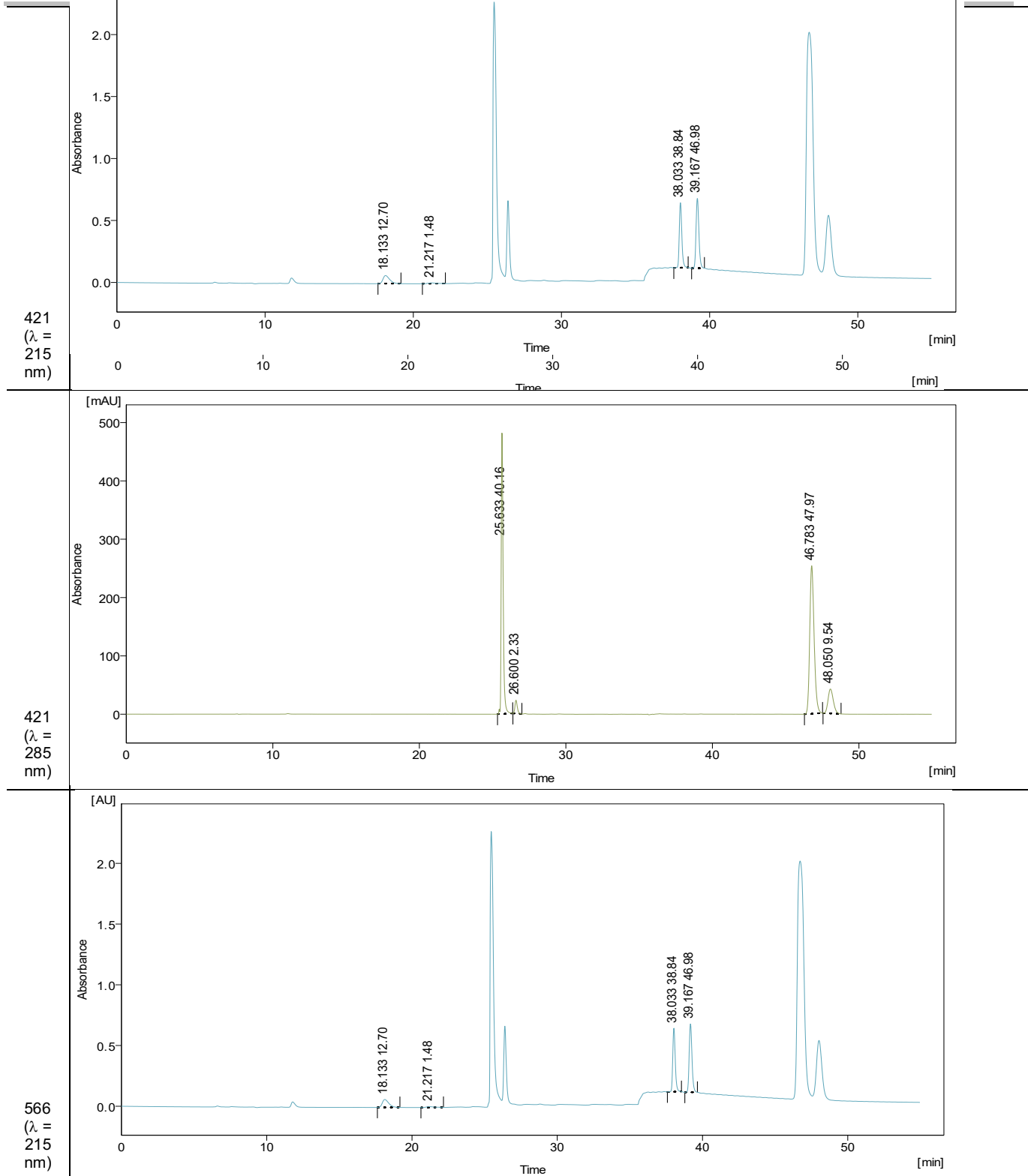
Figure S60. <sup>1</sup>H-NMR (top) and <sup>13</sup>C-NMR (bottom) NMR for 1-(2-pyrenyl)ethyl isobutyrate 4d.

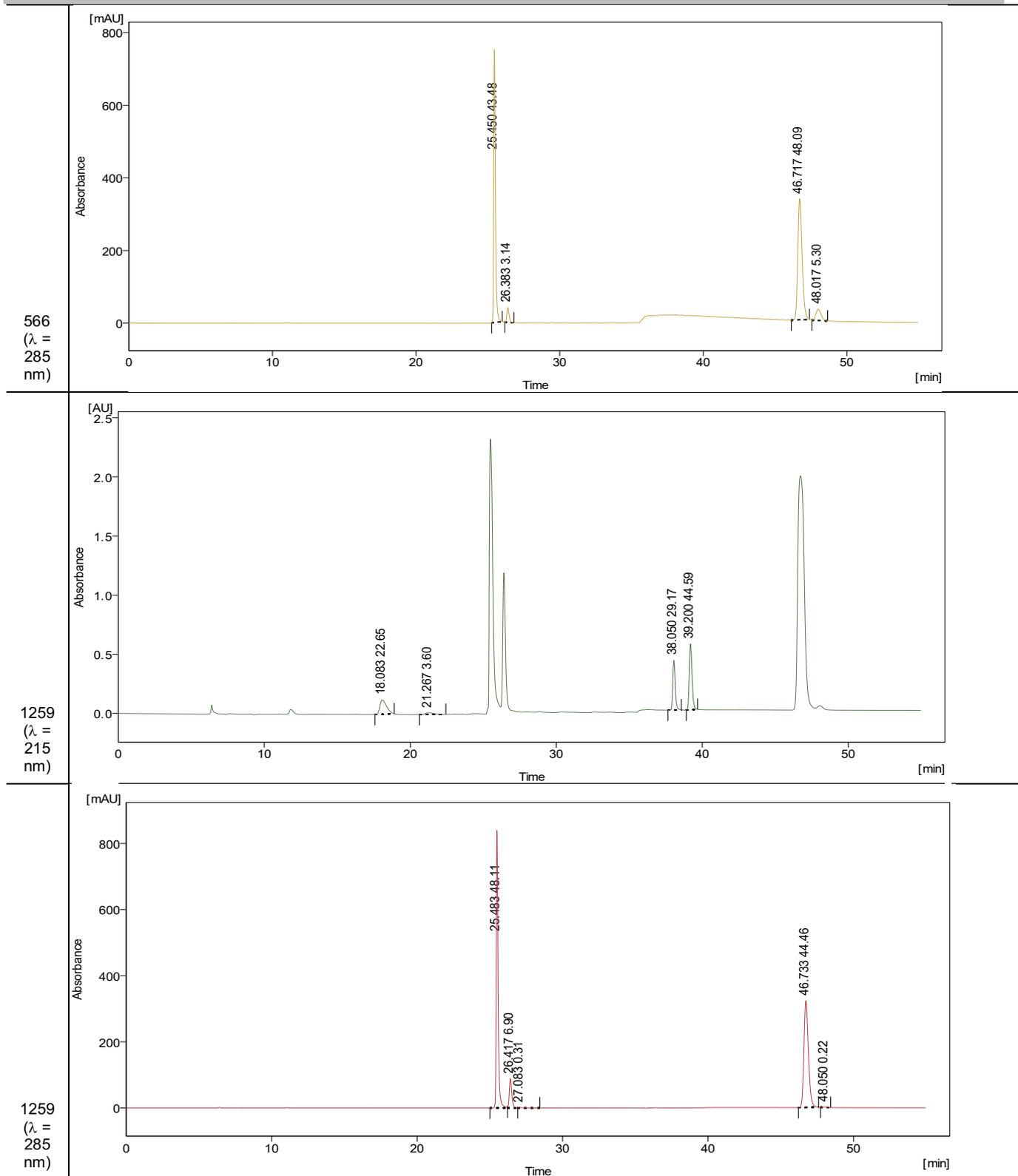
## 7. HPLC traces

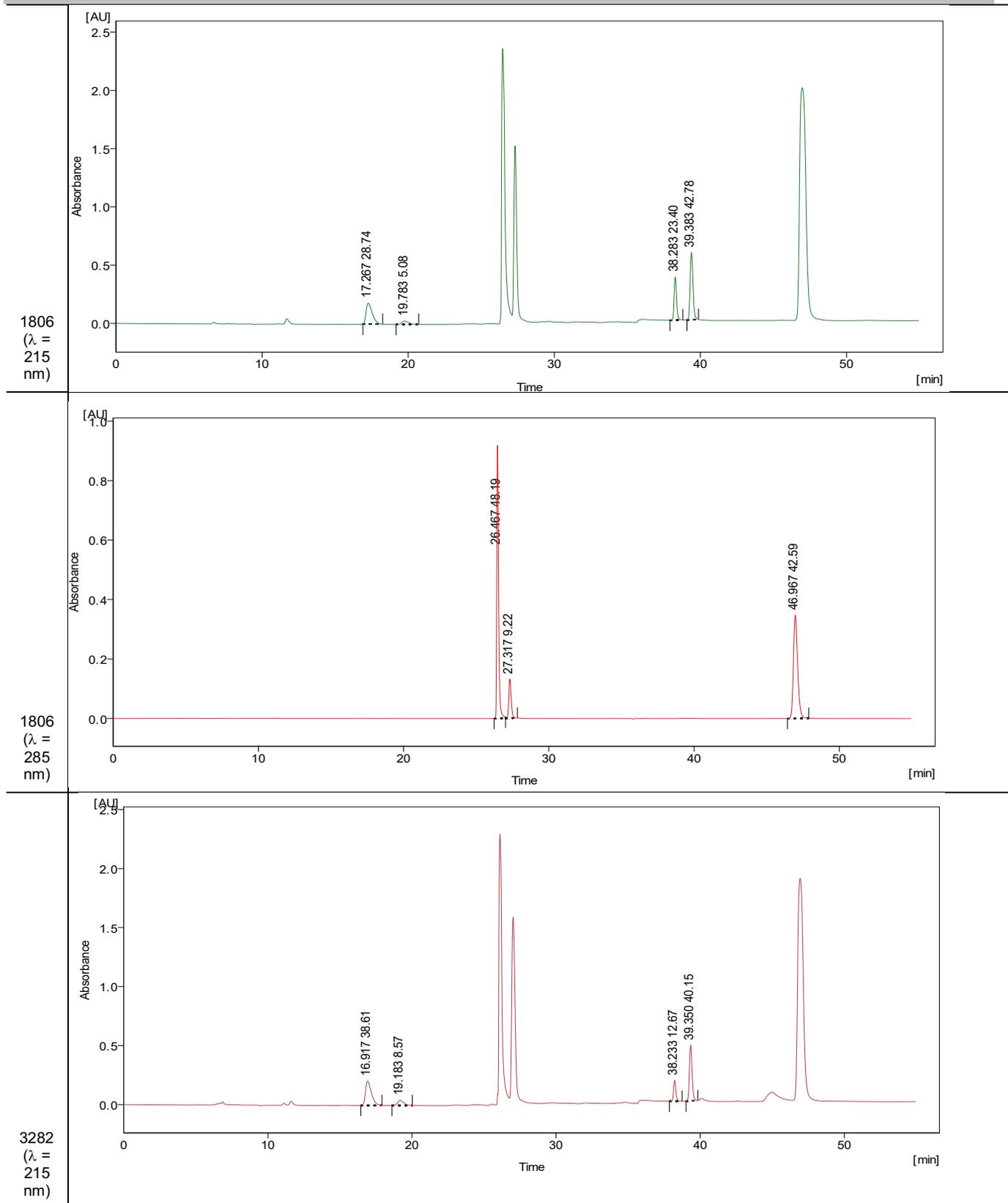
**Table S43.** HPLC traces (Chiralpak IB-N5, 0.5 mL/min, *i*Hex/*i*Prop = 100/0 (10 min) → 98/2 (28 min) → 88/12, *T* = +10,  $\lambda$  = 215 nm) for competitive linear regression shown in **Scheme S6** (run 1). Second row shows assignment of peaks as described in Chapter 2.2. Integrals for naphthyl-bearing substrates were integrated at 285 nm. Minor deviations of retention times are due to use of gradient methods.











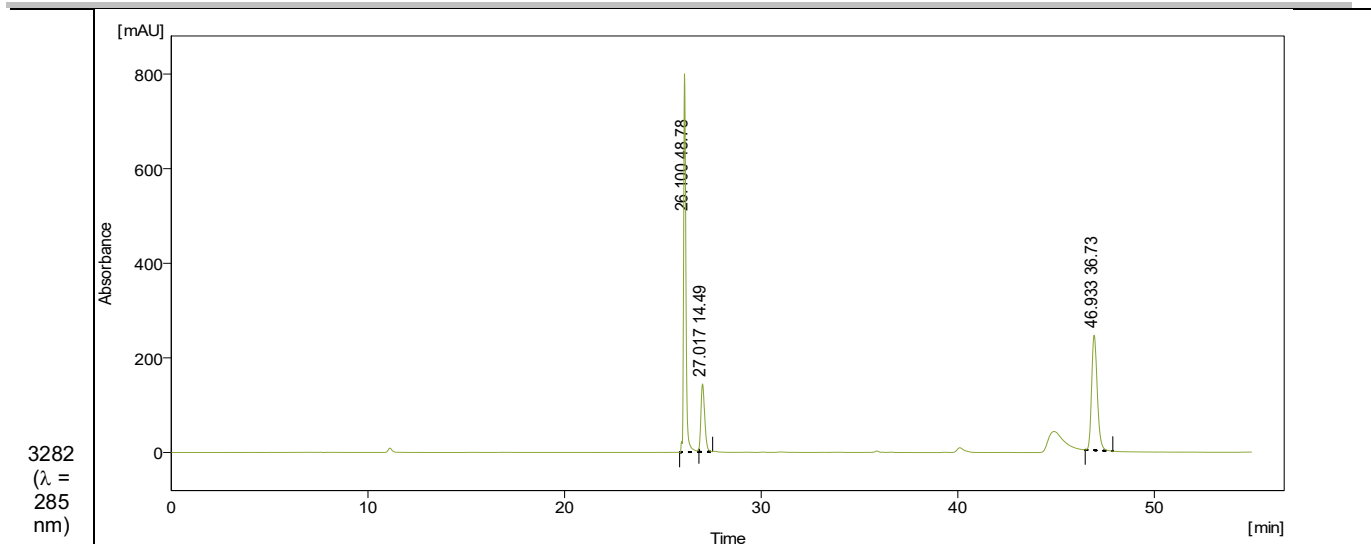
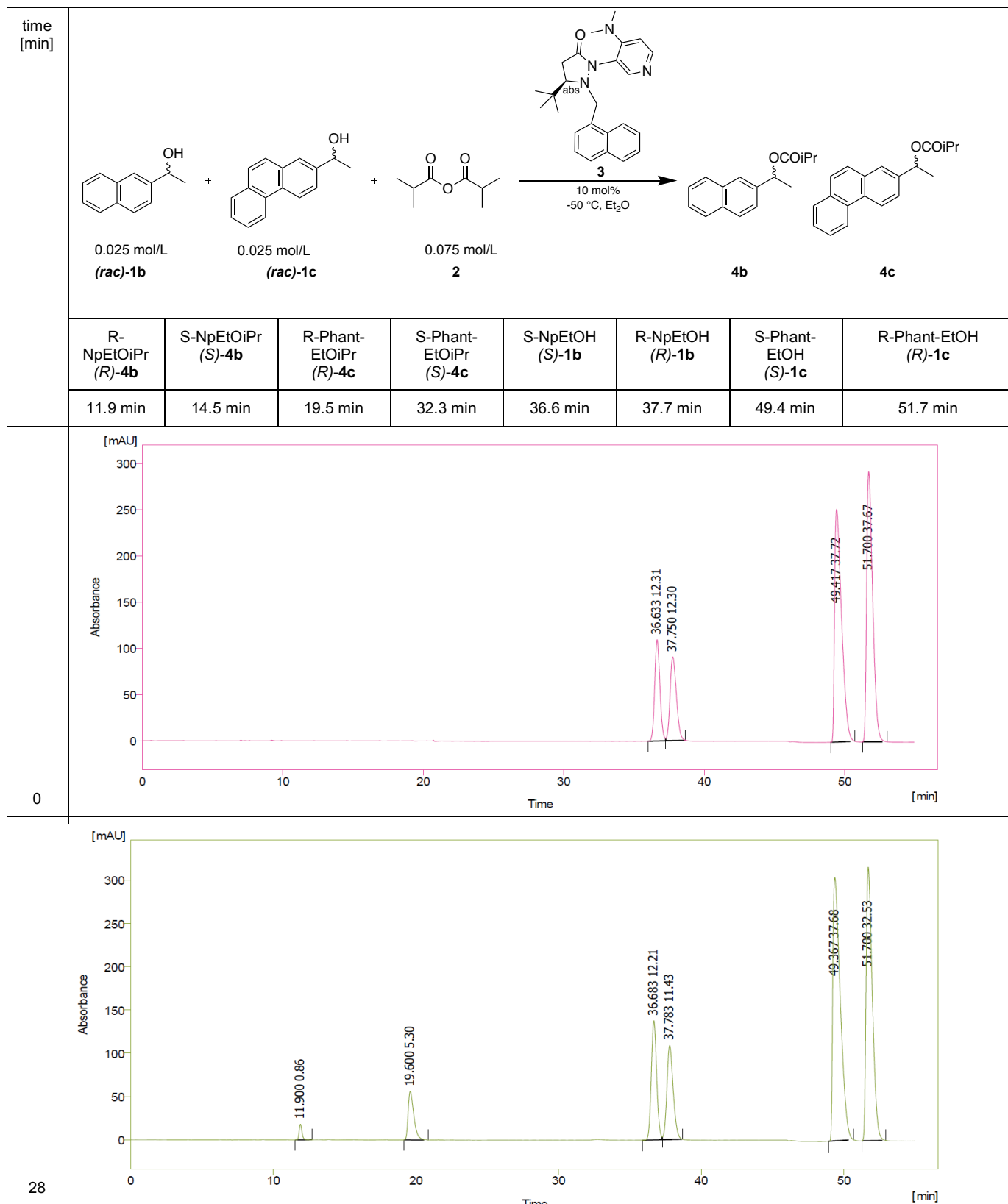
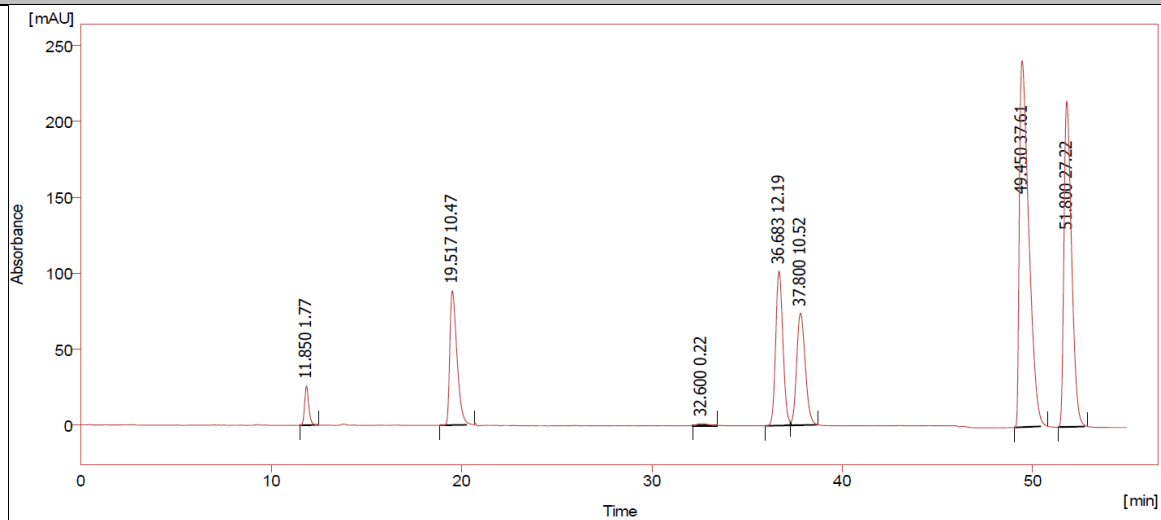


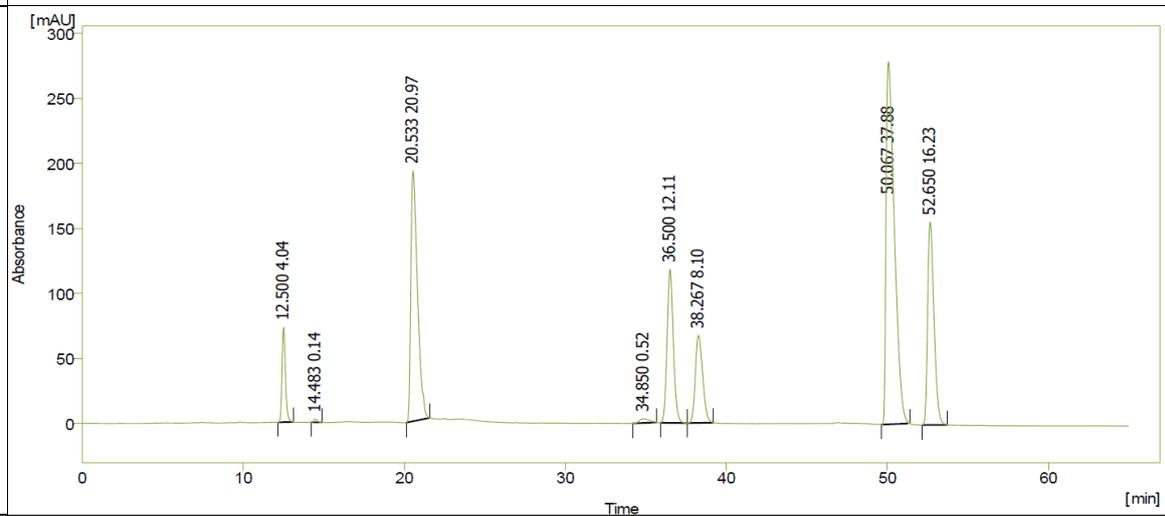
**Table S44.** HPLC traces (Chiralpak IB-N5, 0.5 mL/min, *i*-Hex/*i*Prop = 98/2 (13 min) → 91/9 (39 min) → 70/30, *T* = +10,  $\lambda$  = 285 nm) for competitive linear regression shown in **Scheme S7** (run 1). Second row shows assignment of peaks as described in Chapter 2.2. Minor deviations of retention times are due to use of gradient methods.



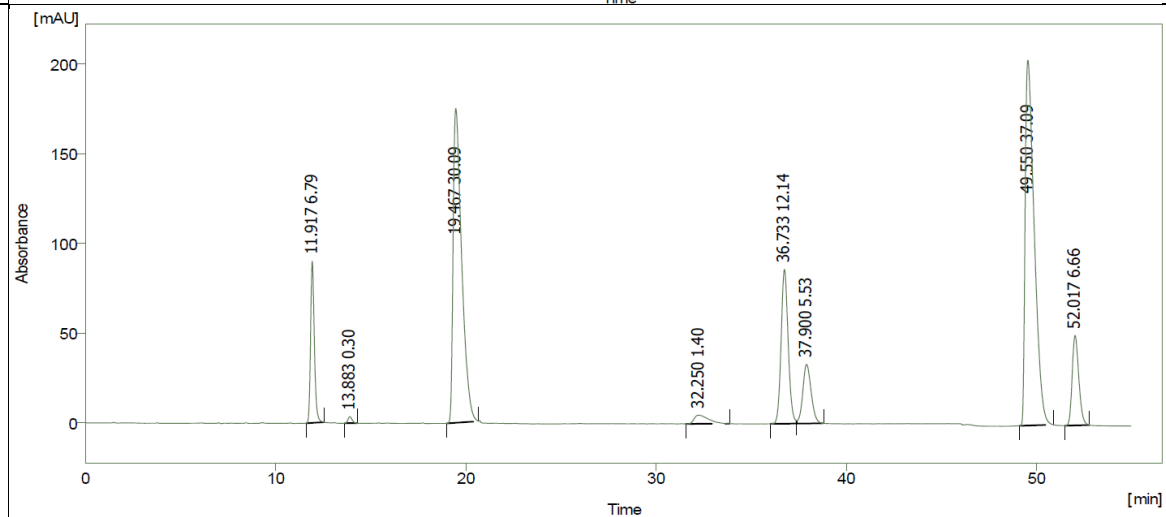
66

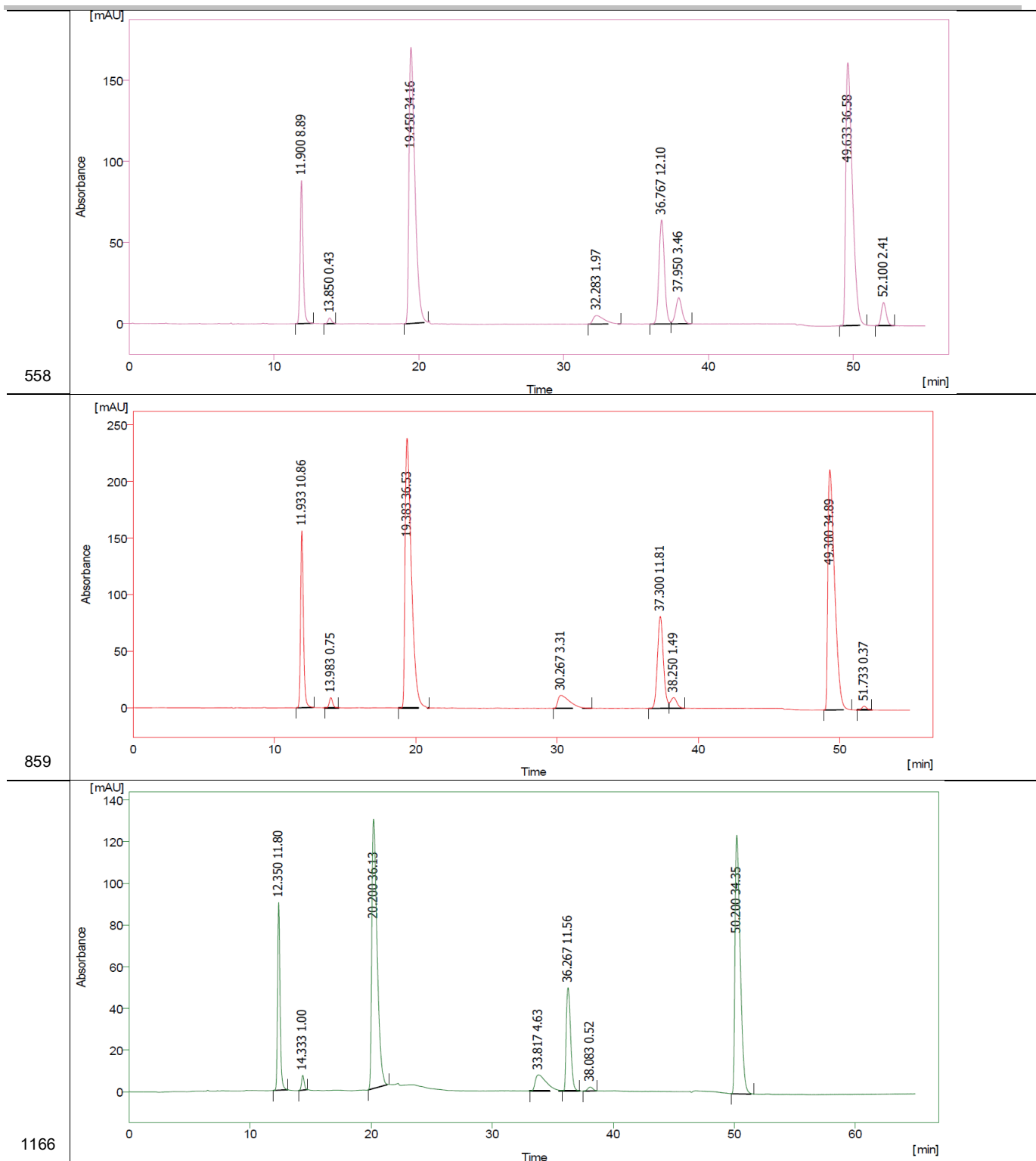


182



362





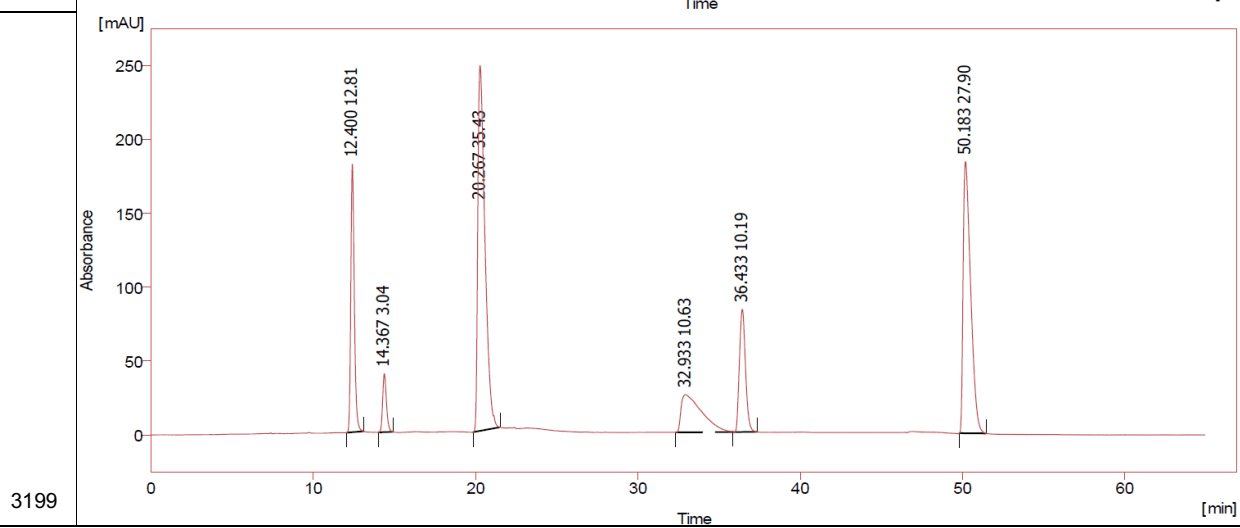
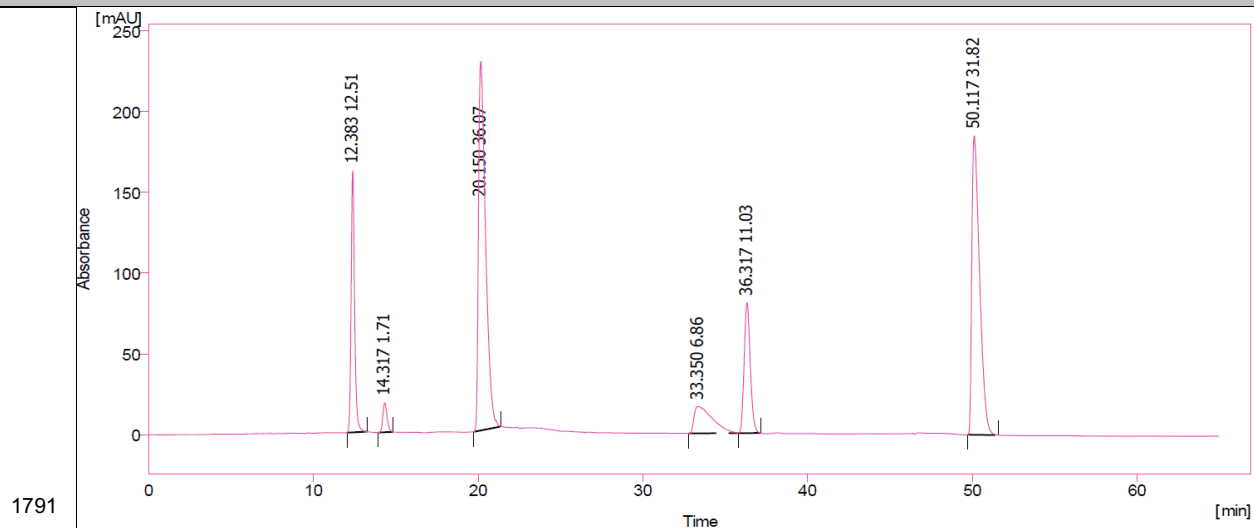
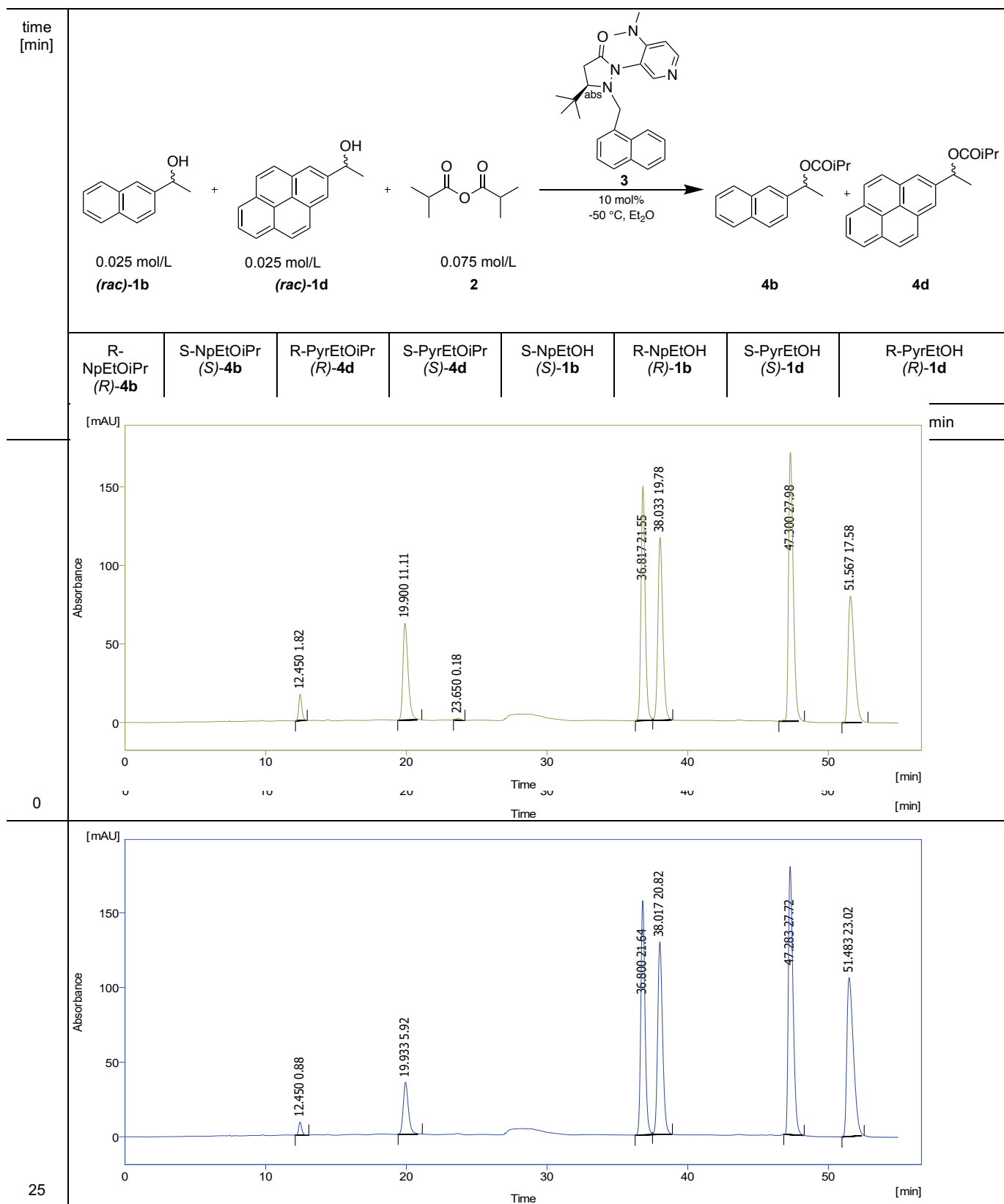
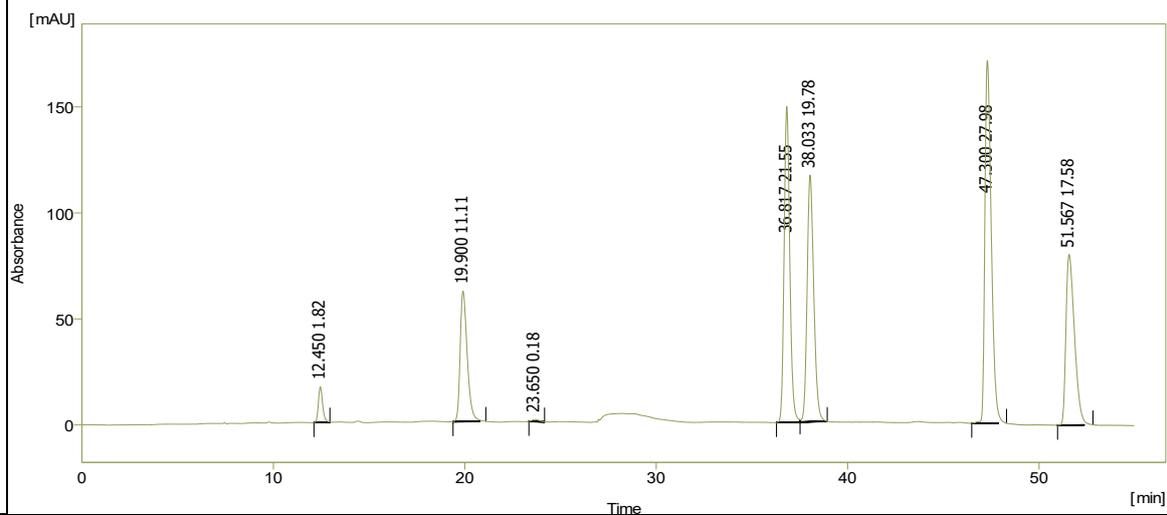


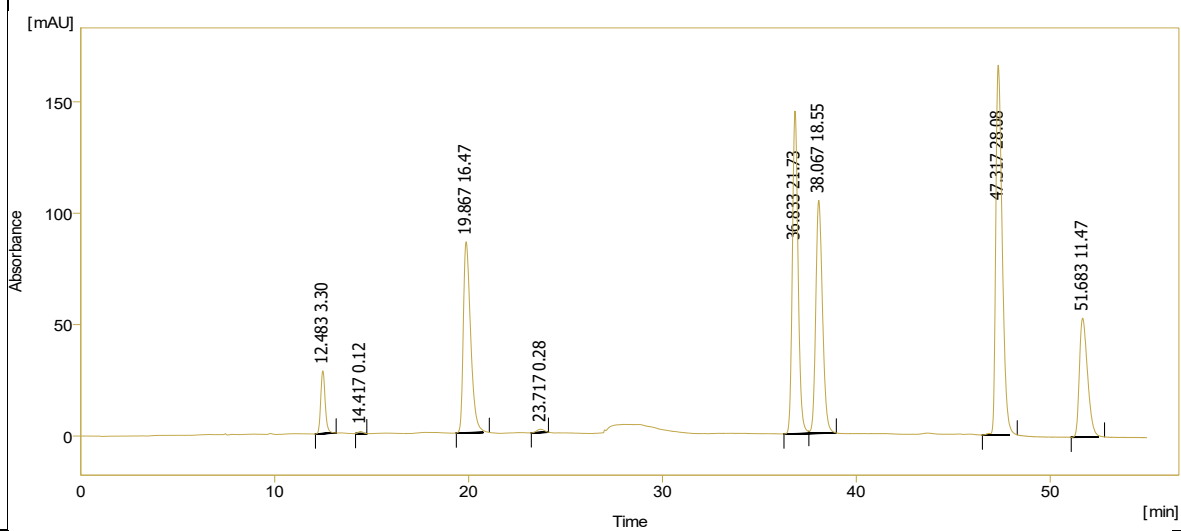
**Table S45.** HPLC traces (Chiralpak IB-N5, 0.5 mL/min, *i*-Hex/*i*Prop = 98/2 (13 min) → 91/9 (39 min) → 70/30, *T* = +10,  $\lambda$  = 285 nm) for competitive linear regression shown in **Scheme S8** (run 1). Second row shows assignment of peaks as described in Chapter 2.2. Minor deviations of retention times are due to use of gradient methods.



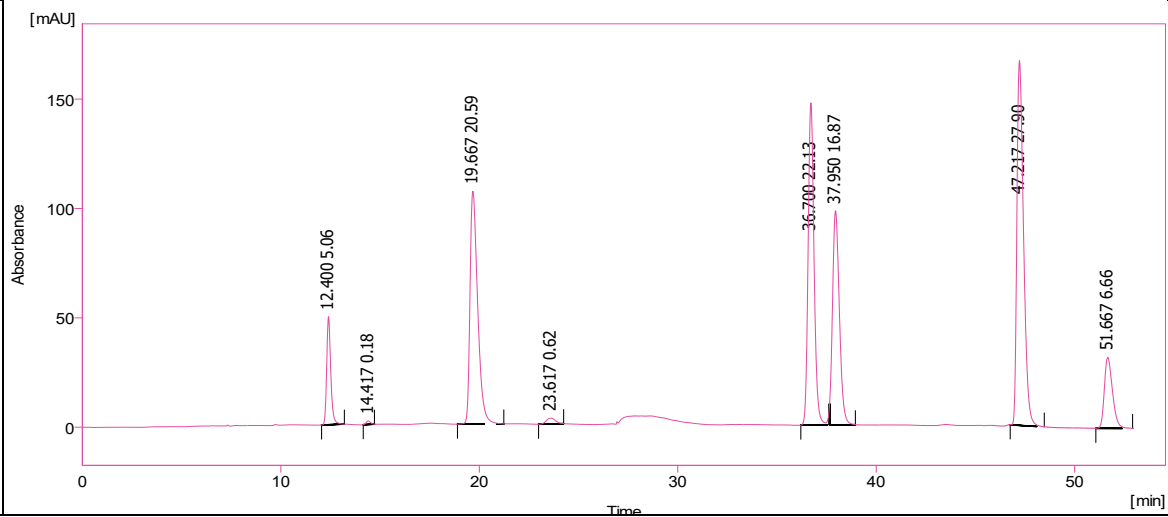
62

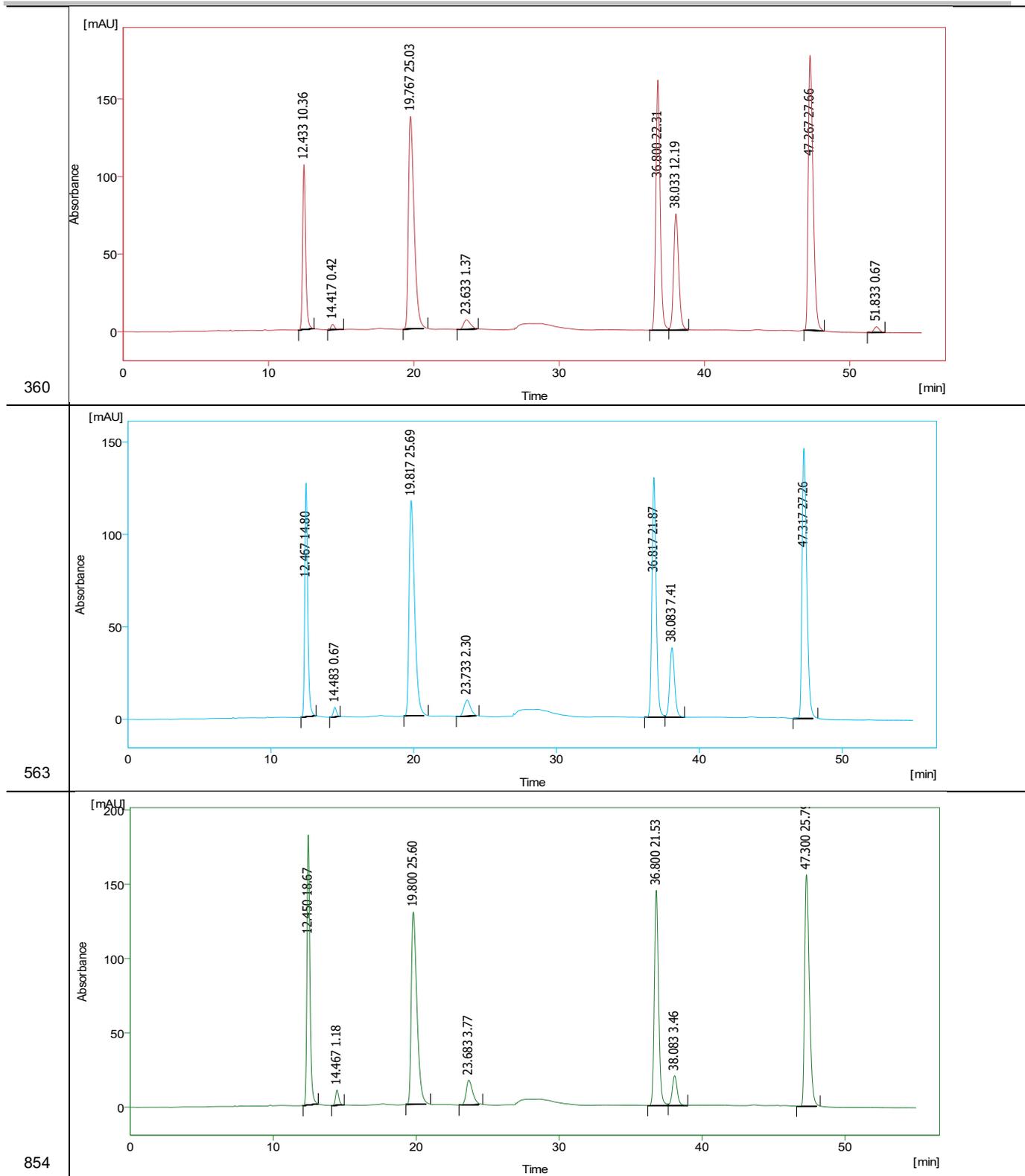


117

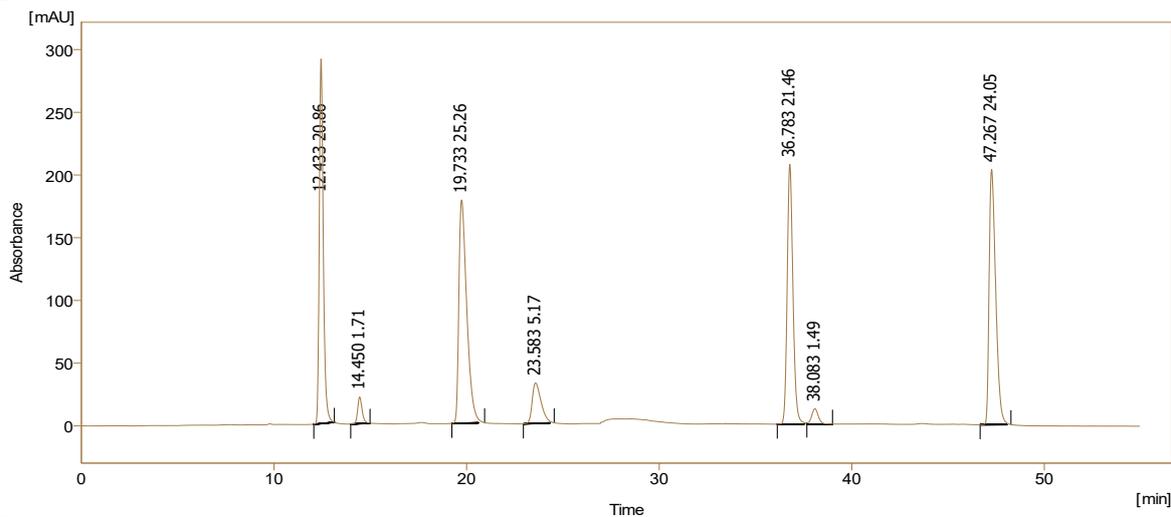


176

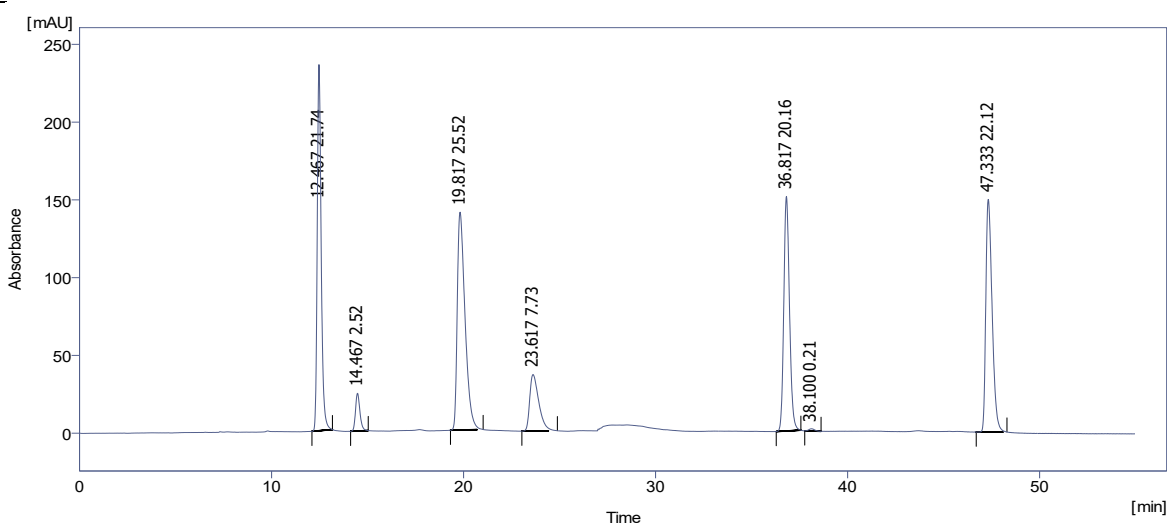




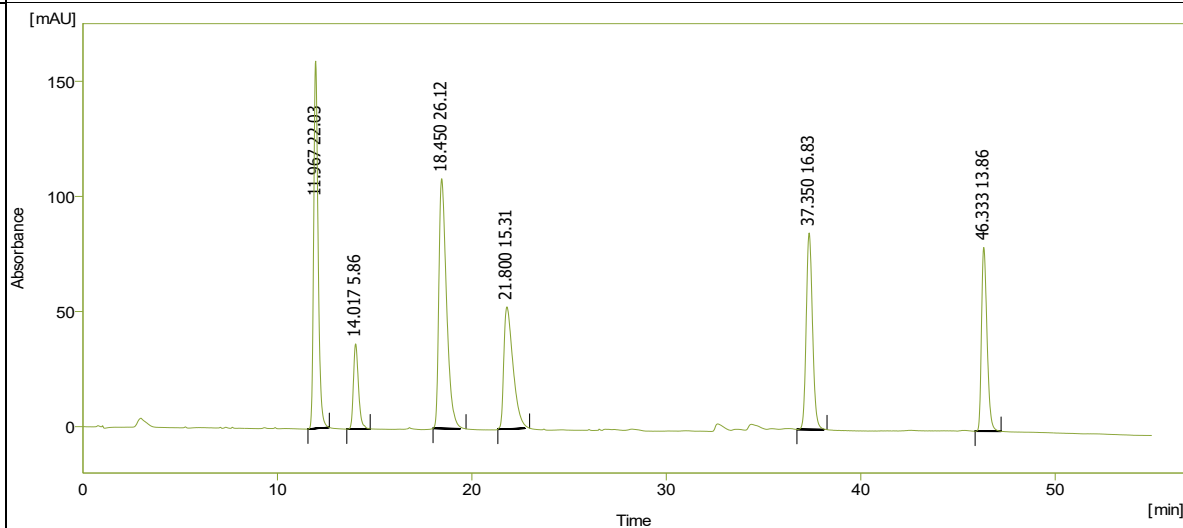
1174



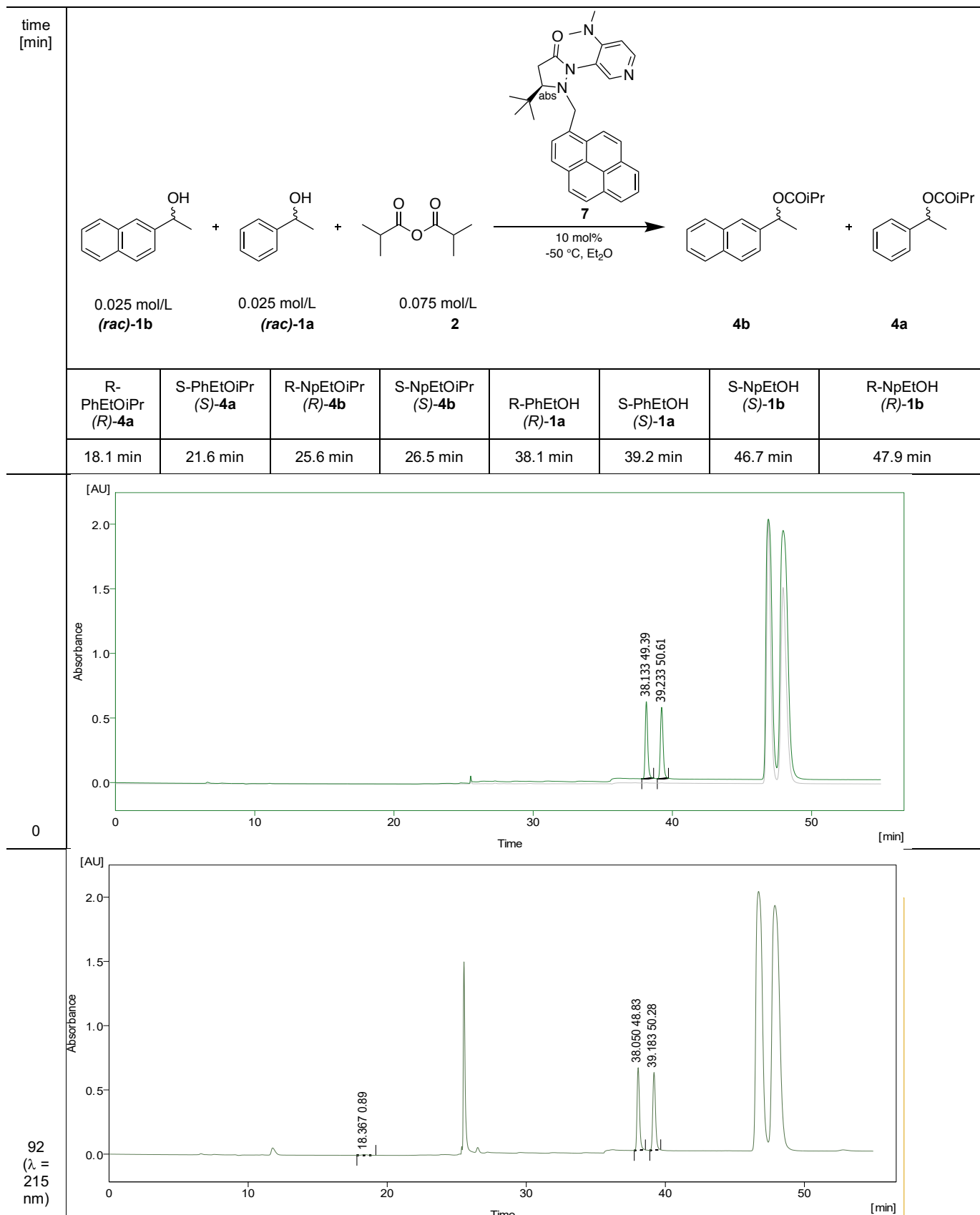
1789

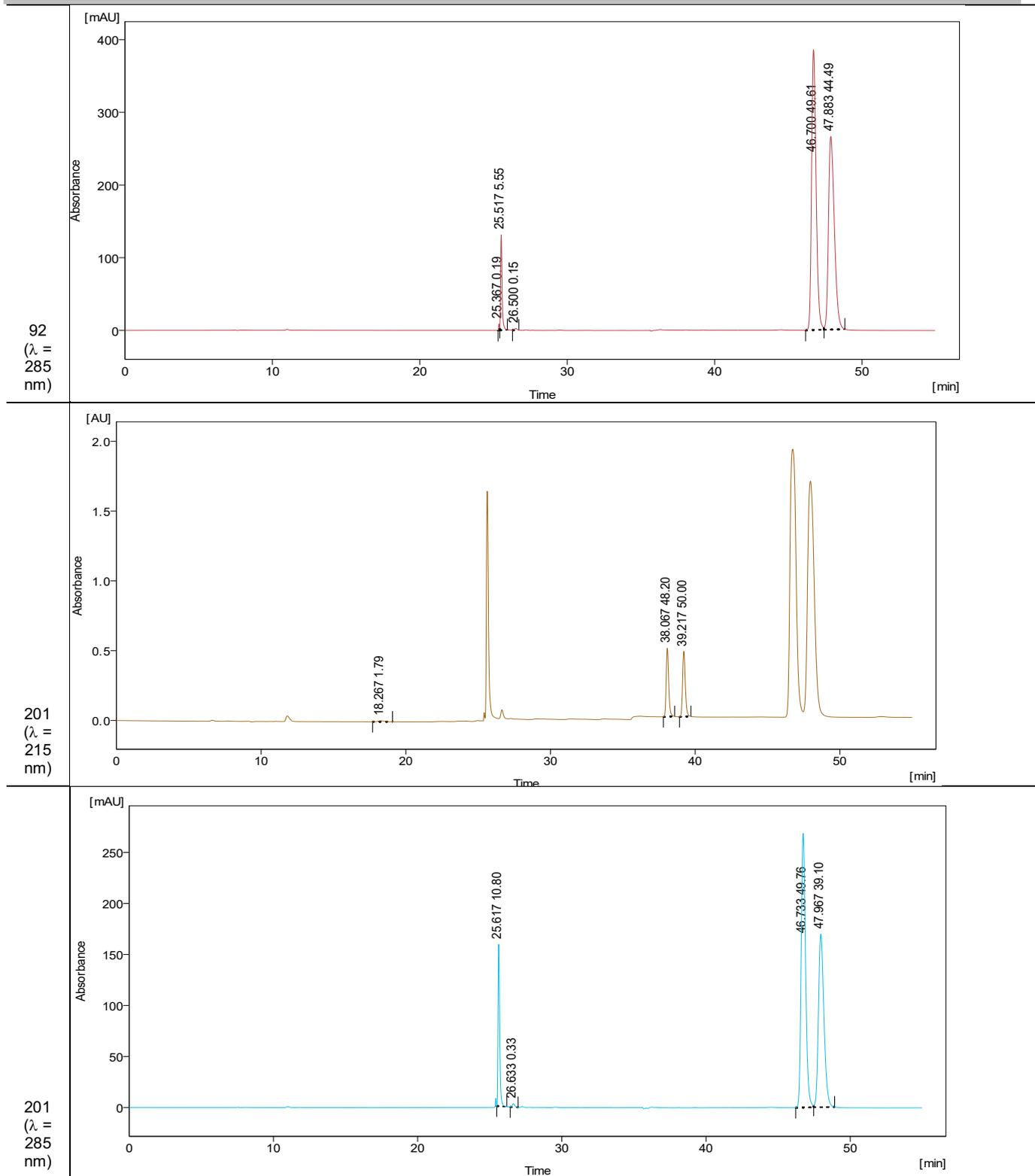


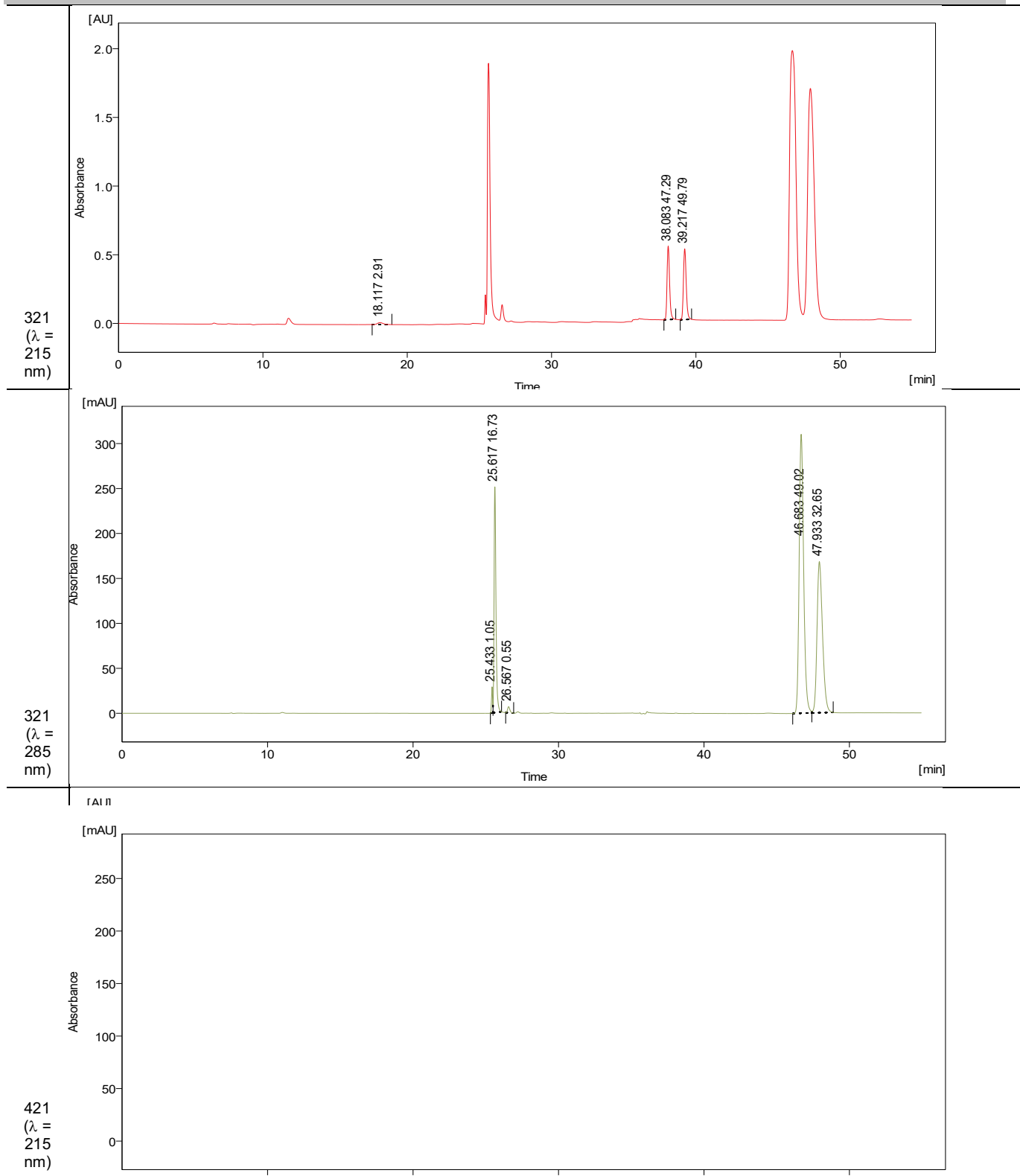
4688

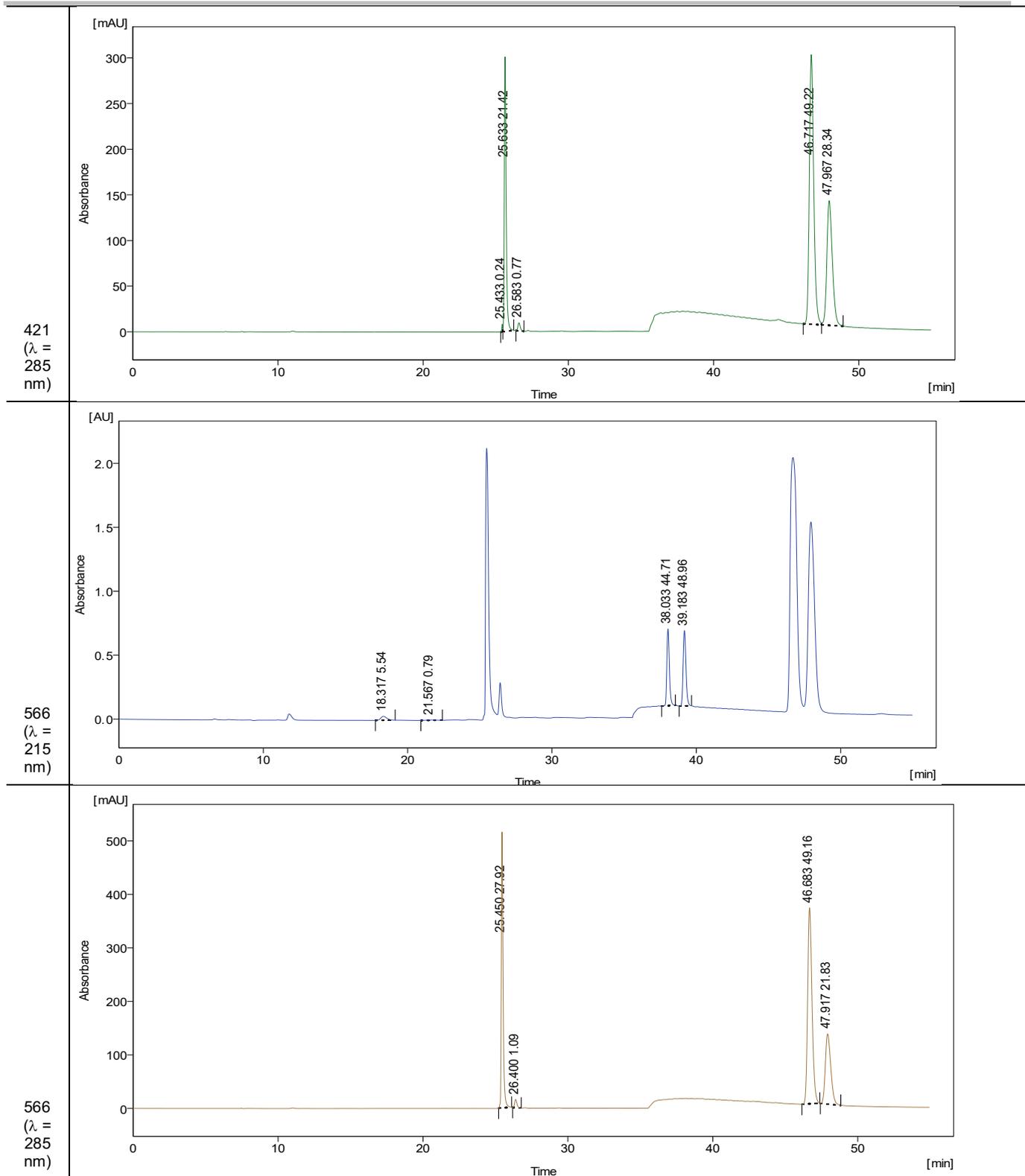


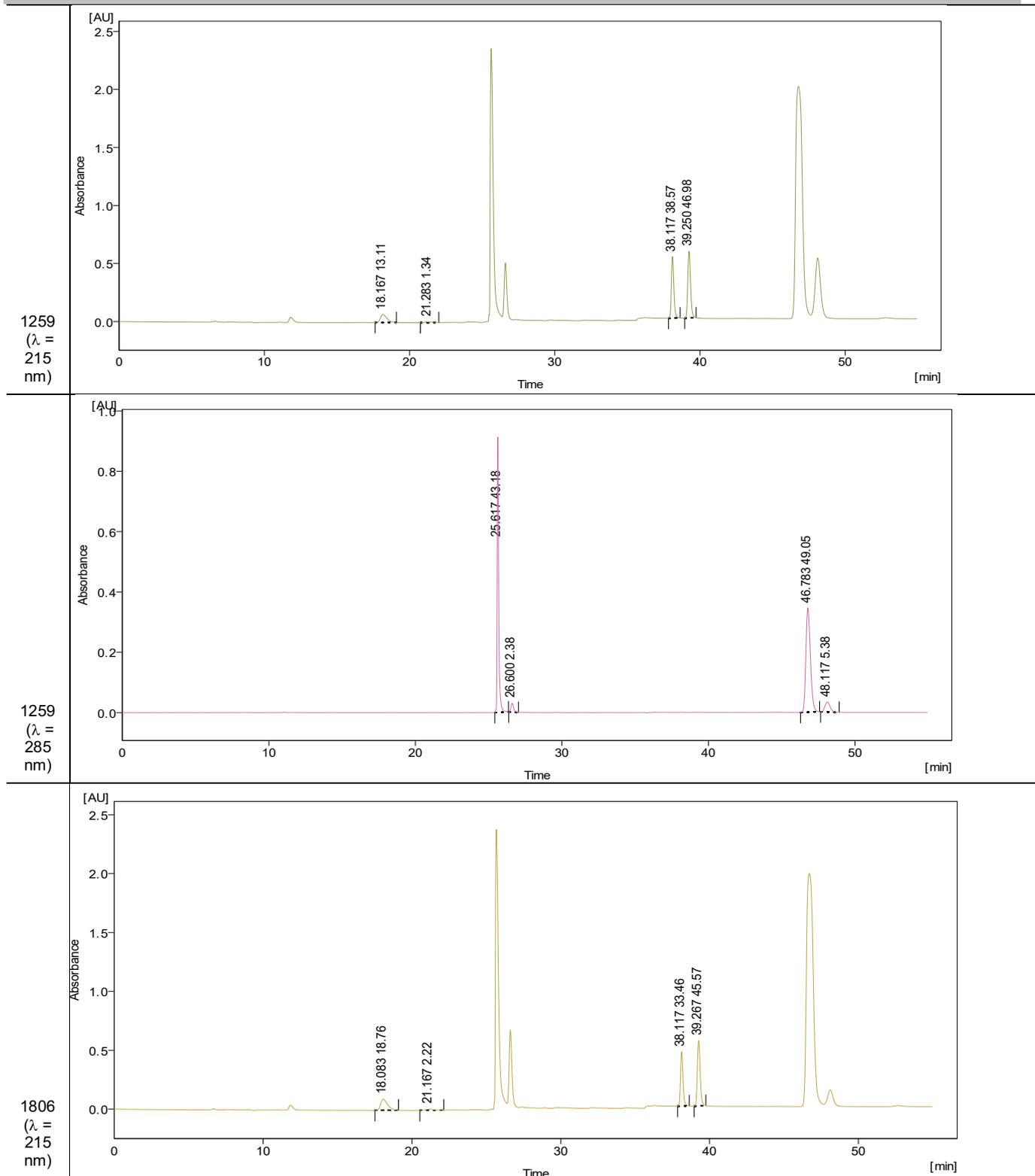
**Table S46.** HPLC traces (Chiralpak IB-N5, 0.5 mL/min, *i*Hex/*i*Prop = 100/0 (10 min) → 98/2 (28 min) → 88/12, *T* = +10,  $\lambda$  = 215 nm) for competitive linear regression shown in **Scheme S9** (run 1). Second row shows assignment of peaks as described in Chapter 2.2. Integrals for naphthyl-bearing substrates were integrated at 285 nm. Minor deviations of retention times are due to use of gradient methods.

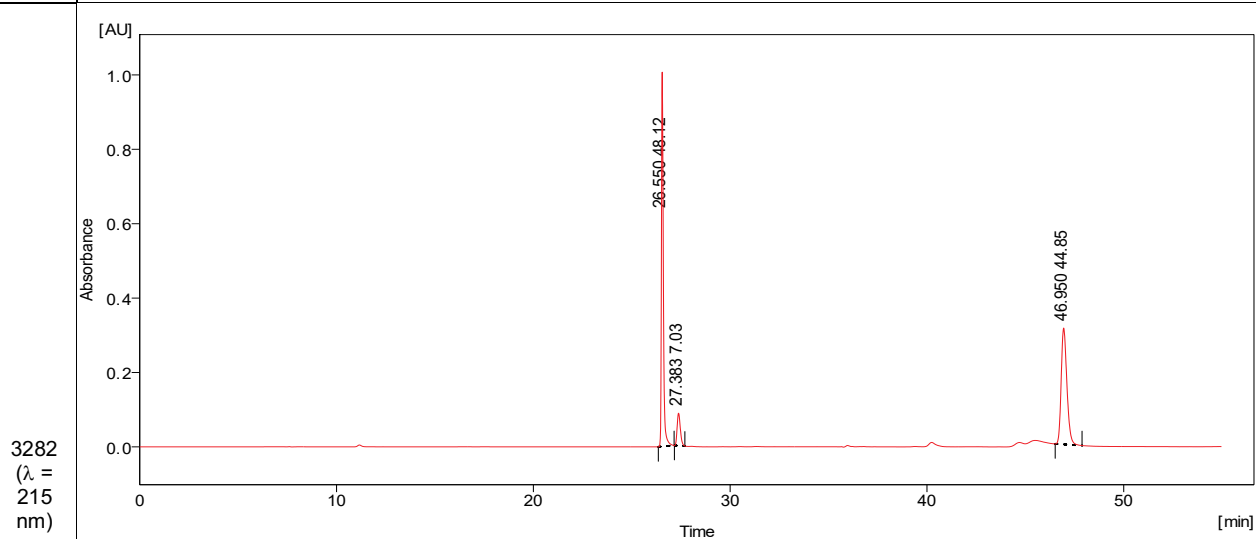
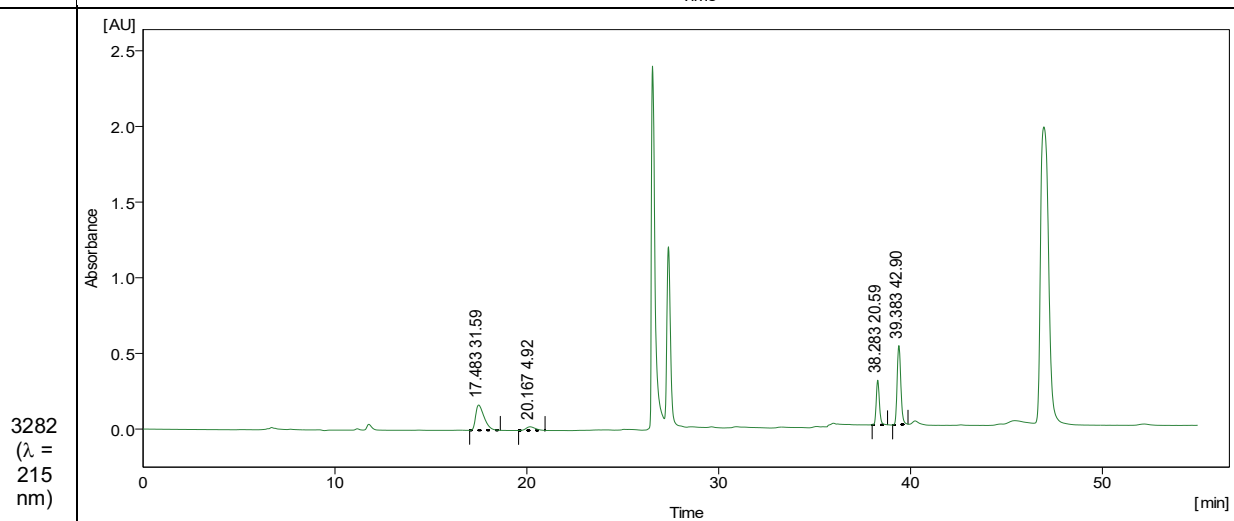
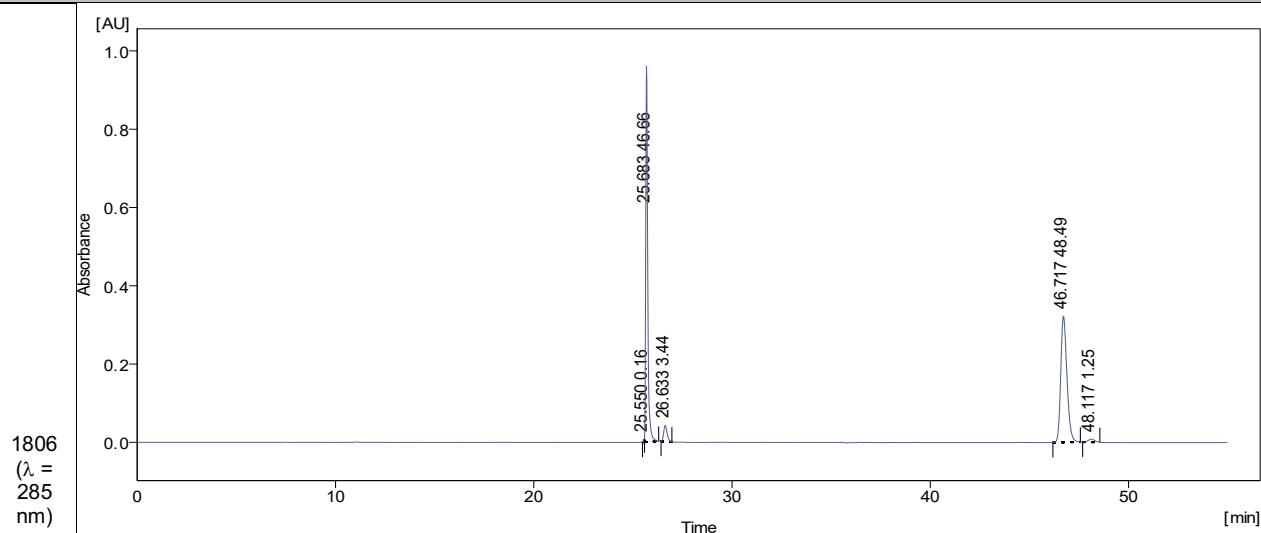






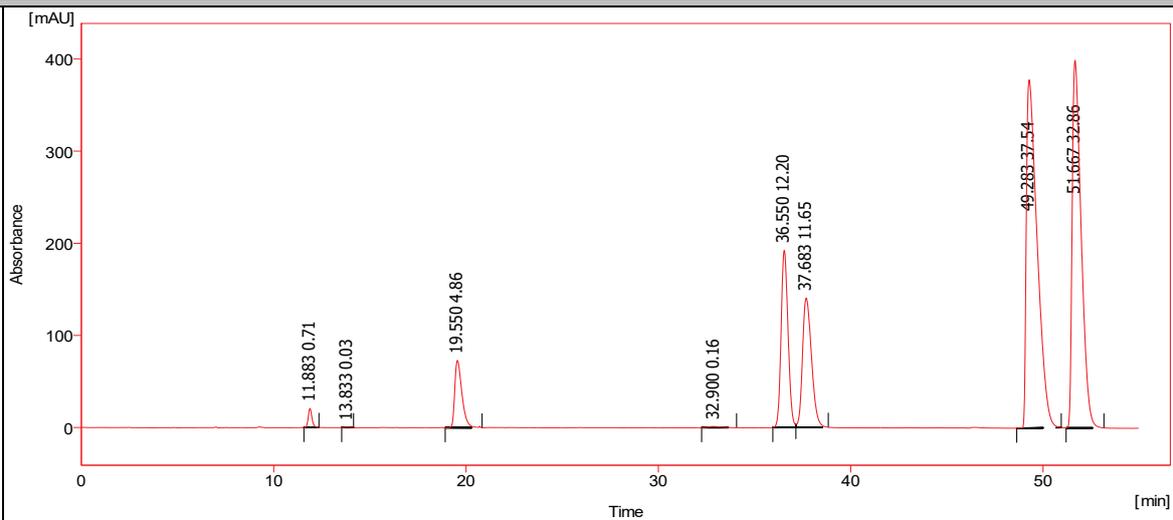




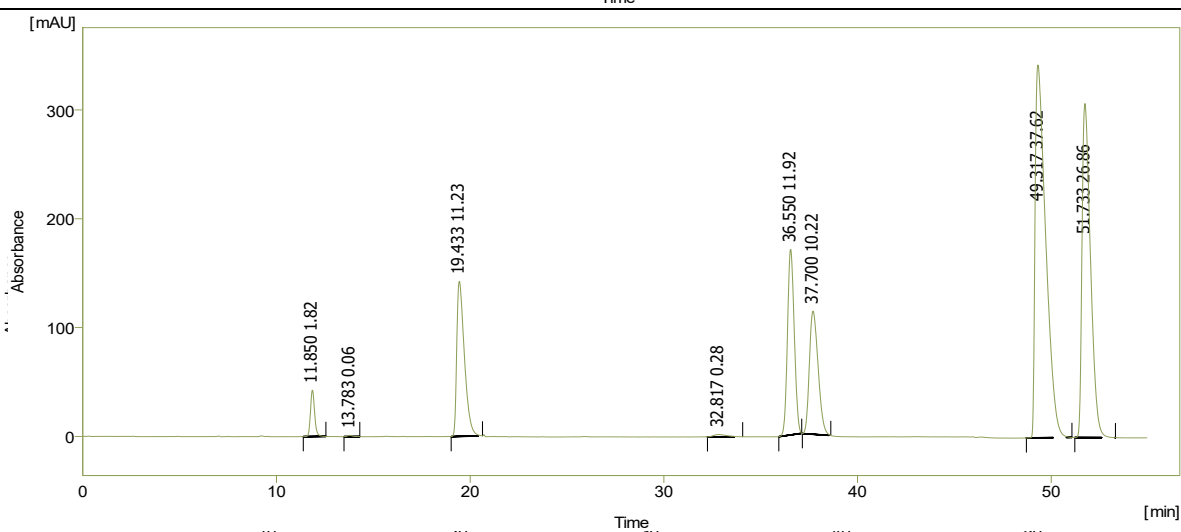




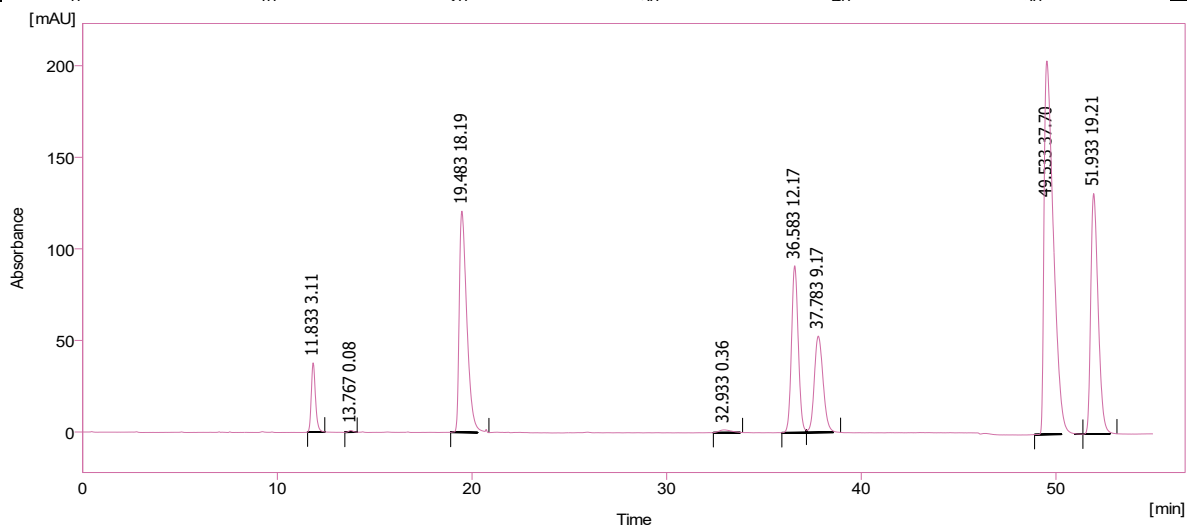
66

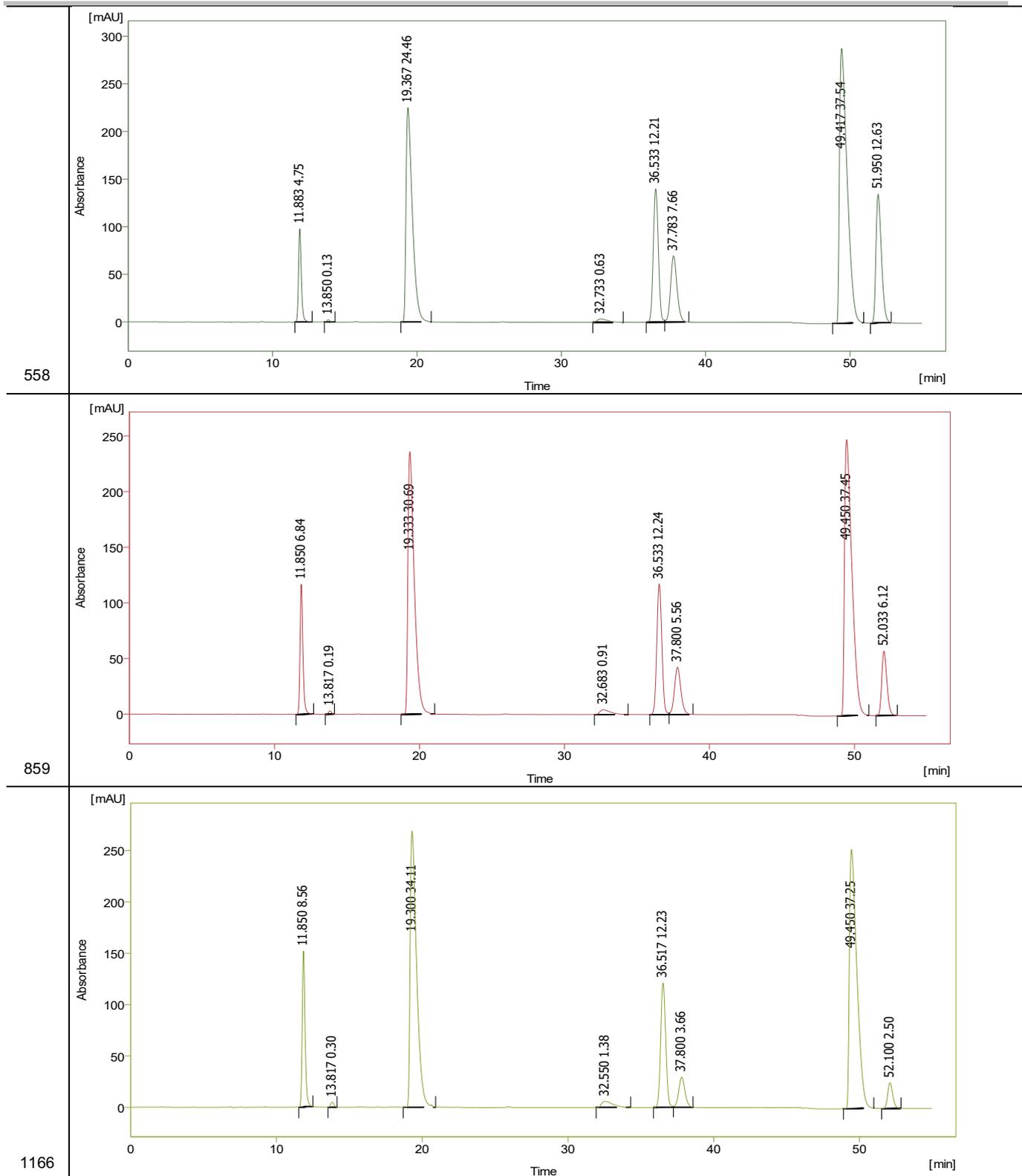


182

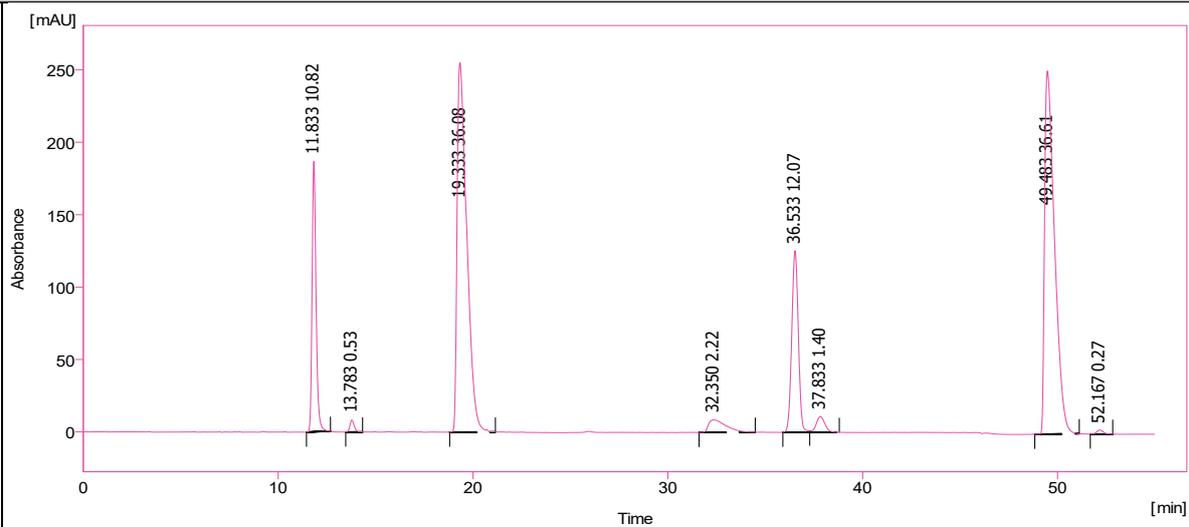


362





1791



3199

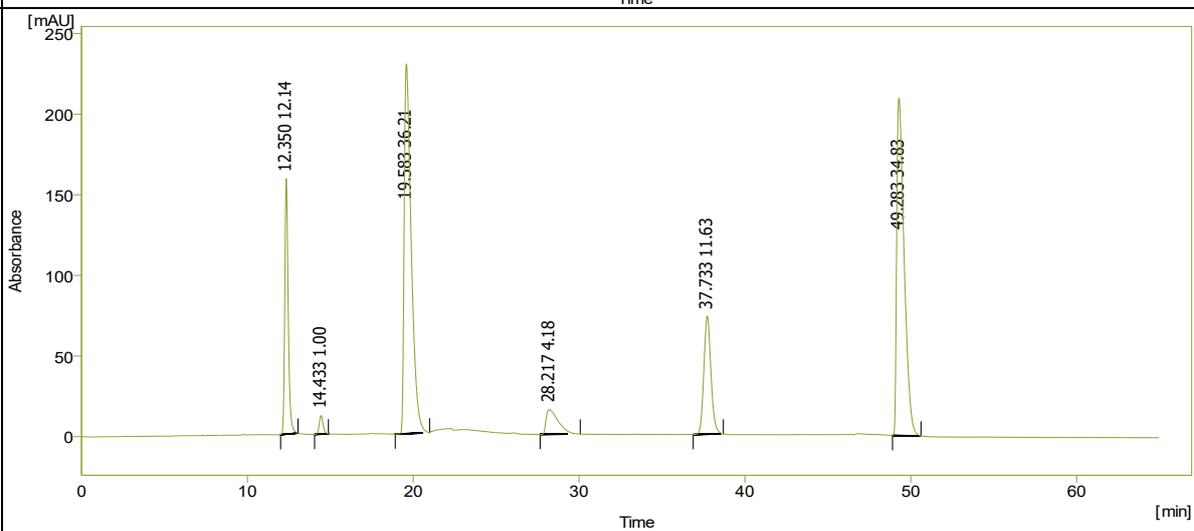
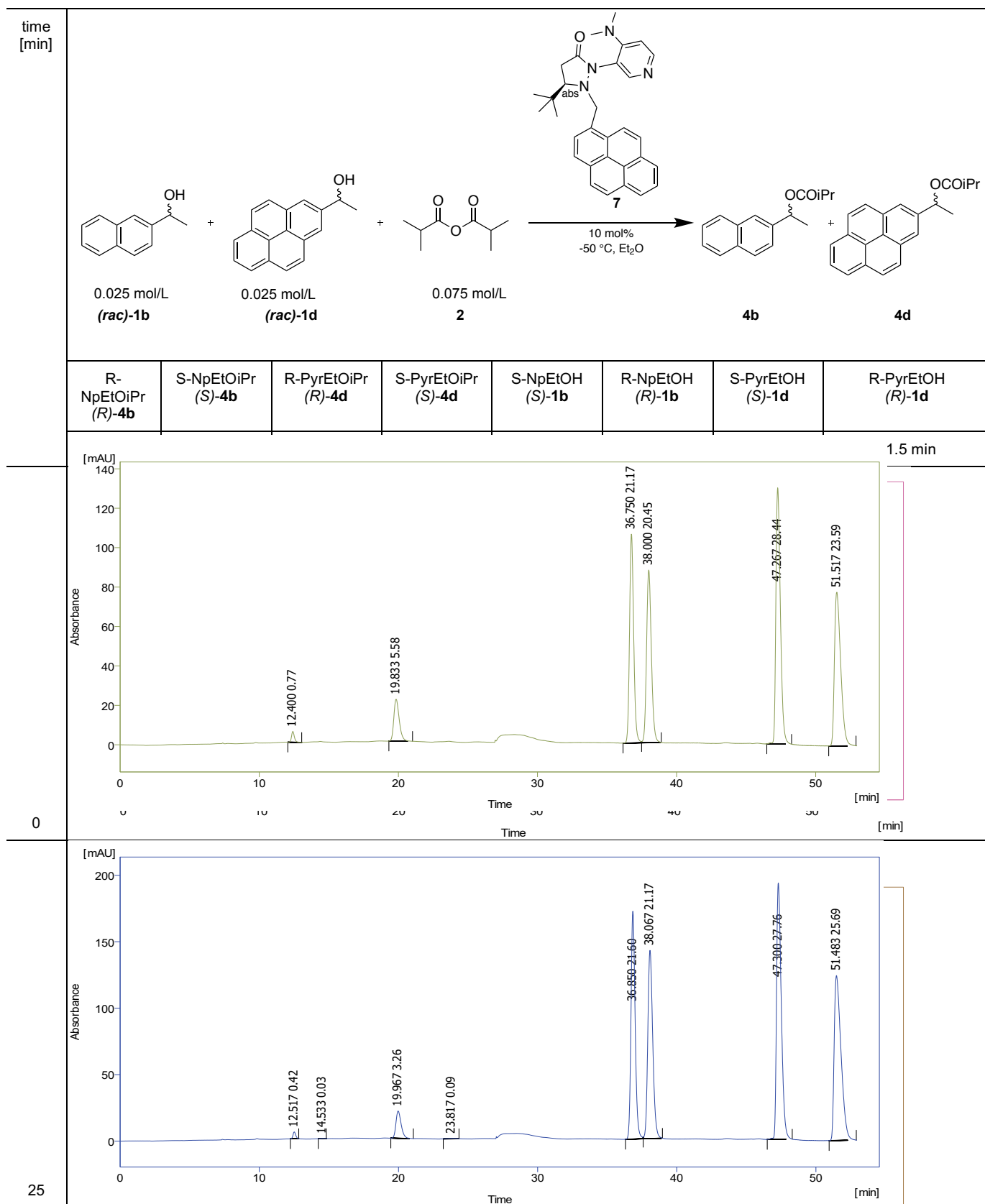
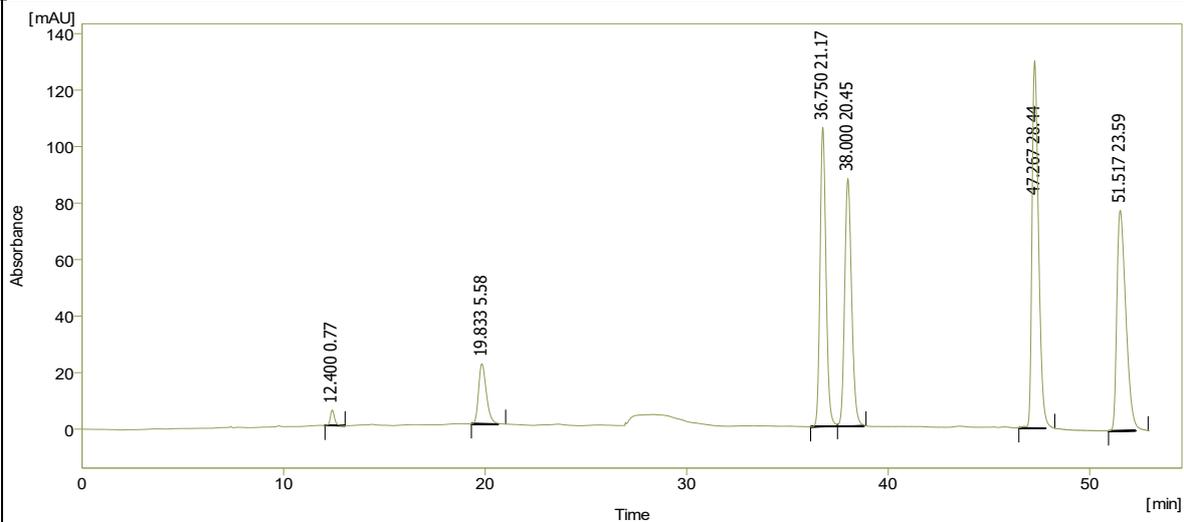


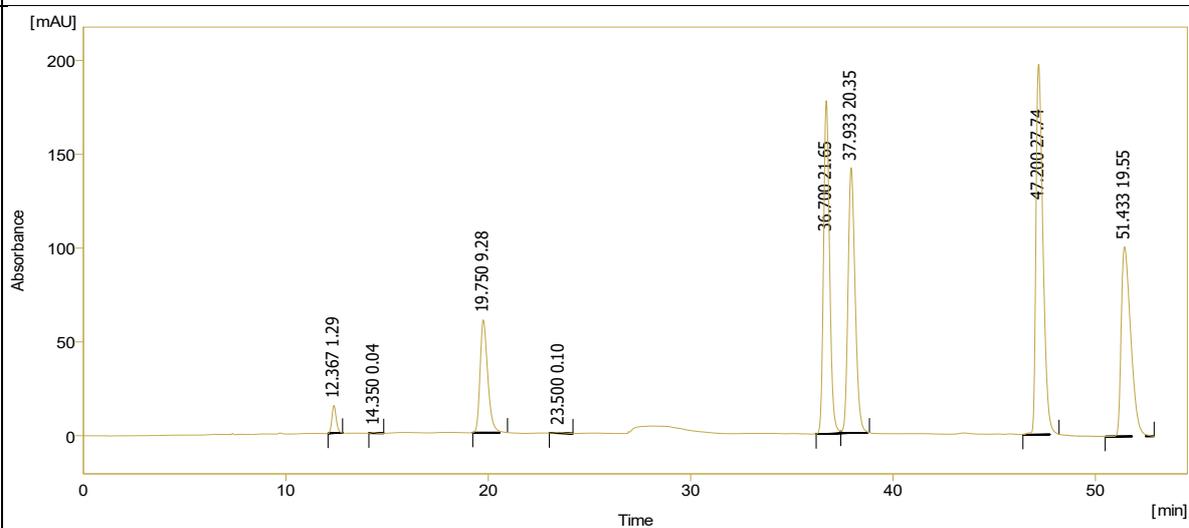
**Table S48.** HPLC traces (Chiralpak IB-N5, 0.5 mL/min, *i*-Hex/*i*Prop = 98/2 (13 min) → 91/9 (39 min) → 70/30, *T* = +10,  $\lambda$  = 285 nm) for competitive linear regression shown in **Scheme S11** (run 1). Second row shows assignment of peaks as described in Chapter 2.2. Minor deviations of retention times are due to use of gradient methods.



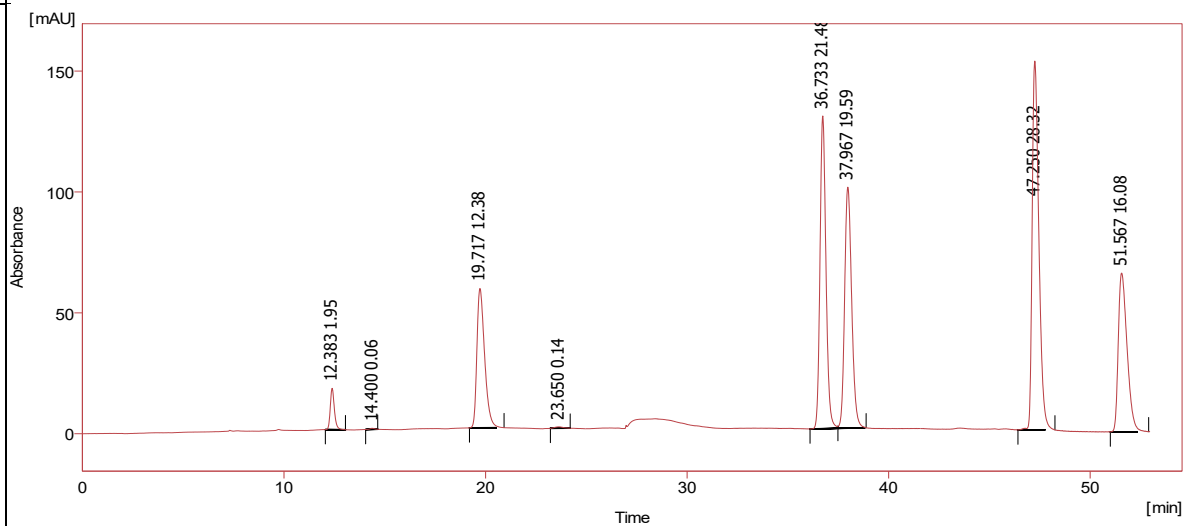
64

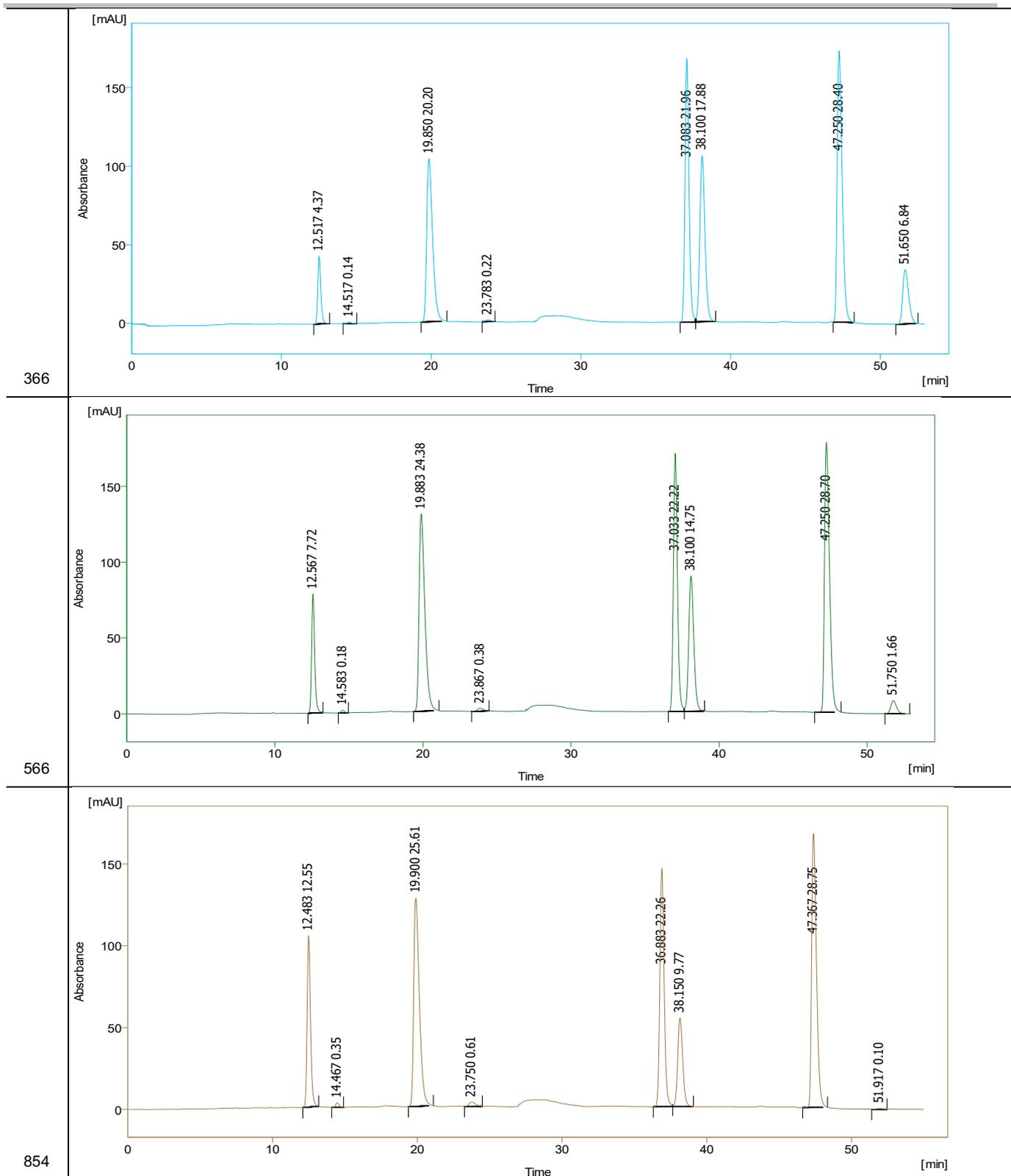


119

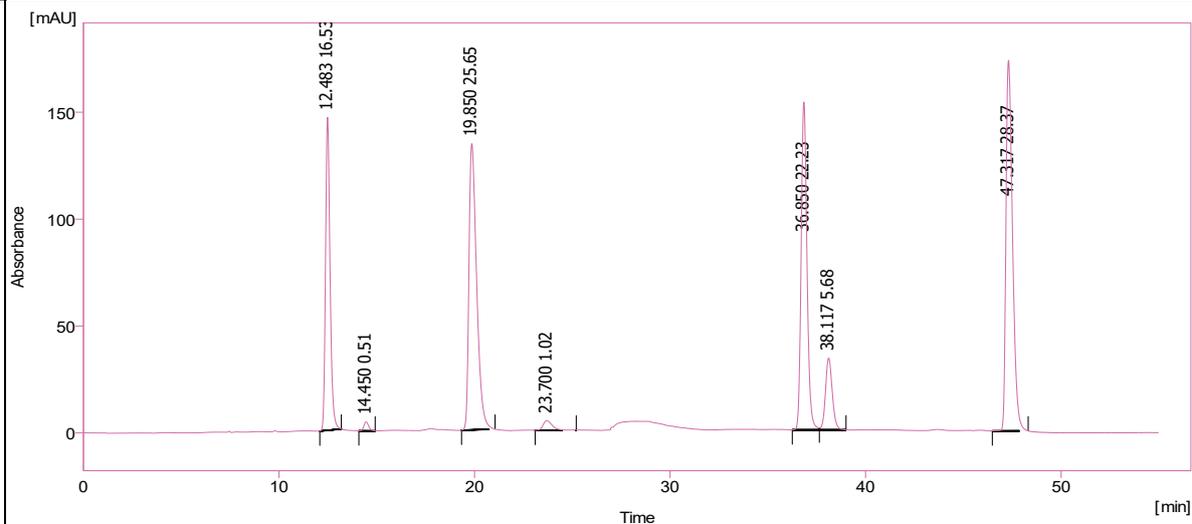


178

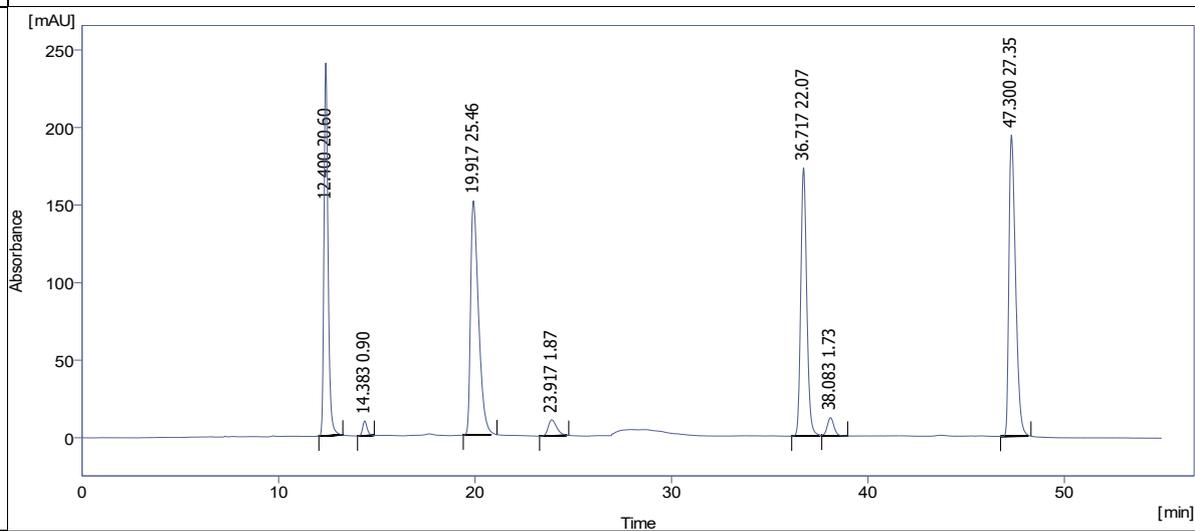




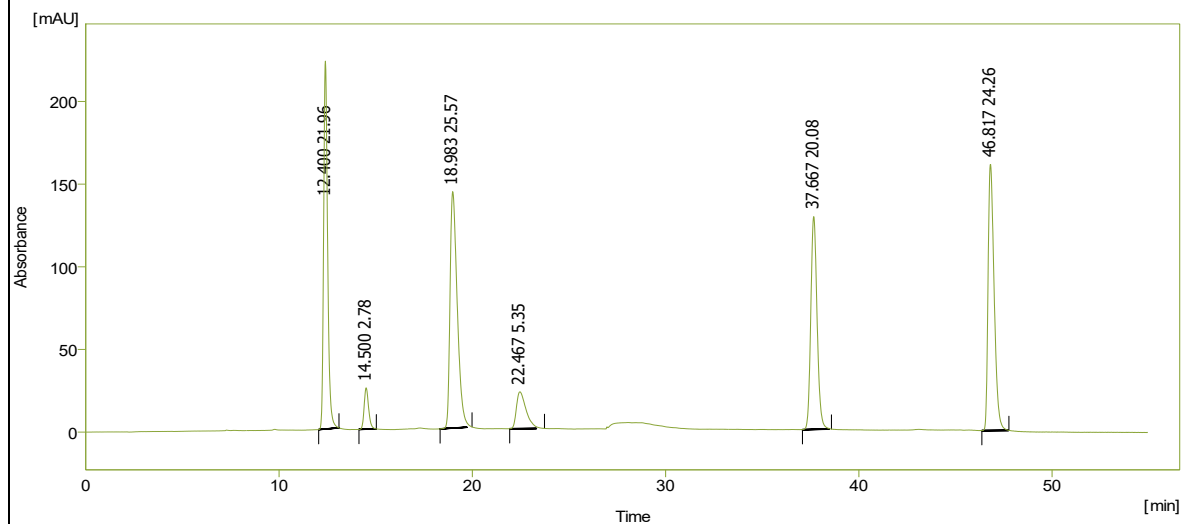
1174



1789



4688



## 8. Tables of Energies, Free Energies and Enthalpies

## 8.1. Conformers of TS2

**Table S49.** Overview of energies of all conformers of **TS2**. Column 1 gives name as used in the manuscript, column 2 refers to categories as defined in Chapter 4.6., the single negative frequency (in  $\text{cm}^{-1}$ ) is reported in column 3. Total energy, enthalpy and free energy calculated at SMD( $\text{Et}_2\text{O}$ )/B3LYP-D3/6-31+G(d) and at DLPNO-CCSD(T)/def2-TZVPP are reported for all conformers of **TS2**. All enthalpies are corrected for a quasi-harmonic rotor, free energies with a free-rotor approximation (for details see Chapter 4.1). Solvation energy was calculated from the difference of single point calculations in gas phase and total energy with SMD model on B3LYP-D3/6-31+G(d) level of theory and added to enthalpy and free energy at coupled cluster calculations. Differences in free energy are reported relative to the best conformer R\_TS2\_1 in  $\text{kJ mol}^{-1}$  for both methods. The geometries of all listed conformers are provided as SDF file.

Name	Category	SMD( $\text{Et}_2\text{O}$ )/B3LYP-D3/6-31+G(d)							DLPNO-CCSD(T)/def2-TZVPP			
		neg. freq. [ $\text{cm}^{-1}$ ]	$E_{\text{tot}}$ [Hartree]	$H_{223.15}$ [Hartree]	$G_{223.15}$ [Hartree]	$\Delta\Delta G_{223.15}^{\ddagger}$ [ $\text{kJ mol}^{-1}$ ]	Grimme-D3 correction [ $\text{kJ mol}^{-1}$ ]	solvation energy [ $\text{kJ mol}^{-1}$ ]	$E_{\text{tot}}$ [Hartree]	$H_{223.15, \text{sol}}$ [Hartree]	$G_{223.15, \text{sol}}$ [Hartree]	$\Delta\Delta G_{223.15}^{\ddagger}$ [ $\text{kJ mol}^{-1}$ ]
R_TS2_1	1	-605.2	-2343.943762	-2342.987297	-2343.067809	0.00	-456.20	-129.64	-2339.6314779	-2338.7243919	-2338.8049039	0.00
R_TS2_2	1	-790.7	-2343.944273	-2342.987557	-2343.067520	0.76	-456.50	-130.10	-2339.6318998	-2338.7247358	-2338.8046988	0.54
R_TS2_3	1	-603.2	-2343.943565	-2342.986935	-2343.067531	0.73	-455.29	-129.98	-2339.6309954	-2338.7238734	-2338.8044694	1.14
R_TS2_4	1	-761.2	-2343.944191	-2342.986515	-2343.067337	1.24	-456.20	-130.21	-2339.6315717	-2338.7234907	-2338.8043127	1.55
R_TS2_5	1	-763.1	-2343.940108	-2342.983262	-2343.065842	5.16	-443.44	-135.22	-2339.6256115	-2338.7202695	-2338.8028495	5.39
R_TS2_6	1	-816.2	-2343.940278	-2342.984201	-2343.064481	8.74	-447.47	-135.58	-2339.6267504	-2338.7223114	-2338.8025914	6.07
R_TS2_7	1	-826.8	-2343.939581	-2342.983538	-2343.064615	8.39	-443.60	-136.07	-2339.6250004	-2338.7207834	-2338.8018604	7.99
R_TS2_8	1	-362.3	-2343.940306	-2342.982902	-2343.062445	14.08	-451.00	-137.33	-2339.6256638	-2338.7205658	-2338.8001088	12.59
R_TS2_9	1	-844.6	-2343.938085	-2342.980911	-2343.059826	20.96	-469.62	-135.99	-2339.6260457	-2338.7206687	-2338.7995837	13.97
R_TS2_10	2	-849.6	-2343.935906	-2342.977990	-2343.058398	24.71	-467.68	-134.37	-2339.6254076	-2338.7186686	-2338.7990766	15.30
R_TS2_11	2	-695.8	-2343.935063	-2342.978683	-2343.058668	24.00	-458.73	-138.03	-2339.6225253	-2338.7187183	-2338.7987033	16.28
R_TS2_12	2	-658.6	-2343.935036	-2342.978666	-2343.059091	22.89	-450.52	-142.85	-2339.6198897	-2338.7179267	-2338.7983517	17.20
R_TS2_13	2	-866.8	-2343.936139	-2342.979839	-2343.058358	24.81	-455.35	-139.00	-2339.6230849	-2338.7197289	-2338.7982479	17.48
R_TS2_14	2	-846.0	-2343.936093	-2342.979480	-2343.057798	26.28	-454.59	-139.24	-2339.6227413	-2338.7191633	-2338.7974813	19.49

Name	Category	SMD(Et <sub>2</sub> O)/B3LYP-D3/6-31+G(d)							DLPNO-CCSD(T)/def2-TZVPP			
		neg. freq. [cm <sup>-1</sup> ]	$E_{tot}$ [Hartree]	$H_{223.15}$ [Hartree]	$G_{223.15}$ [Hartree]	$\Delta\Delta G_{223.15}^\ddagger$ [kJ mol <sup>-1</sup> ]	Grimme-D3 correction [kJ mol <sup>-1</sup> ]	solvation energy [kJ mol <sup>-1</sup> ]	$E_{tot}$ [Hartree]	$H_{223.15, sol}$ [Hartree]	$G_{223.15, sol}$ [Hartree]	$\Delta\Delta G_{223.15}^\ddagger$ [kJ mol <sup>-1</sup> ]
R_TS2_15	7	-913.0	-2343.936213	-2342.978440	-2343.058041	25.65	-473.27	-125.26	-2339.6264948	-2338.7164308	-2338.7960318	23.29
R_TS2_16	3	-689.4	-2343.930187	-2342.973273	-2343.055630	31.98	-414.44	-149.28	-2339.6104712	-2338.7104152	-2338.7927722	31.85
R_TS2_17	3	-636.3	-2343.930378	-2342.974133	-2343.055908	31.25	-414.63	-150.42	-2339.6099266	-2338.7109736	-2338.7927486	31.91
R_TS2_18	6	-912.4	-2343.930151	-2342.972814	-2343.055273	32.91	-436.78	-142.51	-2339.6131484	-2338.7100914	-2338.7925504	32.43
R_TS2_19	6	-844.0	-2343.930052	-2342.972917	-2343.054817	34.11	-435.67	-143.97	-2339.6128509	-2338.7105509	-2338.7924509	32.70
R_TS2_20	6	-868.1	-2343.929690	-2342.972649	-2343.054717	34.37	-432.23	-142.17	-2339.6131707	-2338.7102807	-2338.7923487	32.96
R_TS2_21	3	-226.9	-2343.931421	-2342.973511	-2343.052976	38.94	-427.62	-149.05	-2339.6135723	-2338.7124333	-2338.7918983	34.15
R_TS2_22	3	-188.3	-2343.931886	-2342.972865	-2343.053530	37.49	-432.07	-149.96	-2339.6130567	-2338.7111527	-2338.7918177	34.36
R_TS2_23	3	-881.3	-2343.926932	-2342.970970	-2343.052417	40.41	-416.73	-151.69	-2339.6084744	-2338.7102874	-2338.7917344	34.58
R_TS2_24	3	-188.1	-2343.931513	-2342.973479	-2343.053384	37.87	-430.73	-148.19	-2339.6133695	-2338.7117765	-2338.7916815	34.72
R_TS2_25	3	-848.0	-2343.926742	-2342.969634	-2343.052554	40.05	-413.64	-150.49	-2339.6085378	-2338.7087498	-2338.7916698	34.75
R_TS2_26	3	-185.3	-2343.931489	-2342.972329	-2343.052939	39.04	-432.26	-148.60	-2339.6134463	-2338.7108863	-2338.7914963	35.20
R_TS2_27	3	-185.3	-2343.931488	-2342.972330	-2343.052941	39.04	-432.26	-148.61	-2339.6134160	-2338.7108590	-2338.7914700	35.27
R_TS2_28	3	-625.7	-2343.930451	-2342.973793	-2343.054602	34.67	-416.09	-152.09	-2339.6093086	-2338.7105776	-2338.7913866	35.49
R_TS2_29	6	-930.4	-2343.930757	-2342.973549	-2343.052736	39.57	-448.58	-141.47	-2339.6148231	-2338.7114991	-2338.7906861	37.33
R_TS2_30	3	-864.8	-2343.927182	-2342.969592	-2343.051336	43.25	-421.10	-146.05	-2339.6102724	-2338.7083104	-2338.7900544	38.99
R_TS2_31	3	-383.4	-2343.927917	-2342.970513	-2343.052733	39.58	-425.23	-152.12	-2339.6072361	-2338.7077721	-2338.7899921	39.15
R_TS2_32	3	-655.0	-2343.926665	-2342.970197	-2343.052888	39.18	-406.21	-154.75	-2339.6045072	-2338.7069822	-2338.7896732	39.99
R_TS2_33	4	-928.3	-2343.927797	-2342.970164	-2343.050946	44.27	-428.50	-154.20	-2339.6076619	-2338.7087599	-2338.7895419	40.33
R_TS2_34	3	-796.1	-2343.926665	-2342.969986	-2343.052374	40.52	-406.02	-151.44	-2339.6061041	-2338.7071061	-2338.7894941	40.46
R_TS2_35	3	-144.4	-2343.930186	-2342.969226	-2343.048491	50.72	-471.66	-132.77	-2339.6205668	-2338.7101748	-2338.7894398	40.60
R_TS2_36	3	-688.8	-2343.926778	-2342.969982	-2343.052503	40.19	-405.00	-153.46	-2339.6050368	-2338.7066898	-2338.7892108	41.20

Name	Category	SMD(Et <sub>2</sub> O)/B3LYP-D3/6-31+G(d)							DLPNO-CCSD(T)/def2-TZVPP			
		neg. freq. [cm <sup>-1</sup> ]	$E_{tot}$ [Hartree]	$H_{223.15}$ [Hartree]	$G_{223.15}$ [Hartree]	$\Delta\Delta G_{223.15}^\ddagger$ [kJ mol <sup>-1</sup> ]	Grimme-D3 correction [kJ mol <sup>-1</sup> ]	solvation energy [kJ mol <sup>-1</sup> ]	$E_{tot}$ [Hartree]	$H_{223.15, sol}$ [Hartree]	$G_{223.15, sol}$ [Hartree]	$\Delta\Delta G_{223.15}^\ddagger$ [kJ mol <sup>-1</sup> ]
R_TS2_37	3	-378.5	-2343.927332	-2342.969945	-2343.050174	46.30	-422.31	-151.34	-2339.6084954	-2338.7087504	-2338.7889794	41.81
R_TS2_38	6	-923.4	-2343.927307	-2342.970546	-2343.050811	44.63	-442.02	-136.61	-2339.6131851	-2338.7084571	-2338.7887221	42.49
R_TS2_39	5	-1036.8	-2343.928608	-2342.971273	-2343.051708	42.27	-450.33	-150.97	-2339.6078224	-2338.7079904	-2338.7884254	43.26
R_TS2_40	5	-564.9	-2343.929464	-2342.971027	-2343.050927	44.32	-456.42	-135.06	-2339.6154760	-2338.7084810	-2338.7883810	43.38
R_TS2_41	3	-539.2	-2343.926583	-2342.969424	-2343.049776	47.35	-425.90	-153.04	-2339.6068067	-2338.7079357	-2338.7882877	43.63
R_TS2_42	3	-300.8	-2343.927442	-2342.970122	-2343.050496	45.46	-426.65	-149.73	-2339.6076505	-2338.7073595	-2338.7877335	45.08
R_TS2_43	6	-937.7	-2343.927205	-2342.969542	-2343.049167	48.94	-433.82	-137.27	-2339.6131482	-2338.7077702	-2338.7873952	45.97
R_TS2_44	6	-914.9	-2343.925677	-2342.967816	-2343.049661	47.65	-436.01	-133.96	-2339.6120309	-2338.7051919	-2338.7870369	46.91
R_TS2_45	6	-940.8	-2343.925689	-2342.968843	-2343.048945	49.53	-424.06	-140.24	-2339.6102744	-2338.7068414	-2338.7869434	47.16
R_TS2_46	6	-964.0	-2343.927421	-2342.970089	-2343.049635	47.72	-447.02	-135.18	-2339.6127628	-2338.7069198	-2338.7864658	48.41
R_TS2_47	3	-279.5	-2343.925799	-2342.967946	-2343.047209	54.09	-430.27	-151.03	-2339.6069468	-2338.7066188	-2338.7858818	49.94
R_TS2_48	3	-278.7	-2343.925800	-2342.967939	-2343.047191	54.13	-430.28	-151.03	-2339.6069384	-2338.7066034	-2338.7858554	50.01
R_TS2_49	6	-887.1	-2343.924704	-2342.967334	-2343.049110	49.09	-426.63	-137.31	-2339.6090915	-2338.7040215	-2338.7857975	50.16
R_TS2_50	3	-735.3	-2343.919181	-2342.962870	-2343.046410	56.18	-412.03	-159.72	-2339.5974794	-2338.7020024	-2338.7855424	50.83
R_TS2_51	6	-907.0	-2343.924621	-2342.967909	-2343.048081	51.80	-426.18	-135.47	-2339.6100547	-2338.7049397	-2338.7851117	51.96
R_TS2_52	3	-934.2	-2343.922308	-2342.966079	-2343.047795	52.55	-395.60	-158.61	-2339.5990887	-2338.7032727	-2338.7849887	52.29
R_TS2_53	4	-866.8	-2343.922716	-2342.965688	-2343.047986	52.05	-418.16	-154.91	-2339.6004123	-2338.7023873	-2338.7846853	53.08
R_TS2_54	4	-911.5	-2343.925098	-2342.967687	-2343.047070	54.45	-435.42	-150.22	-2339.6053392	-2338.7051422	-2338.7845252	53.50
R_TS2_55	6	-643.5	-2343.924598	-2342.966849	-2343.045636	58.22	-463.34	-126.84	-2339.6143608	-2338.7049208	-2338.7837078	55.65
R_TS2_56	4	-904.9	-2343.923283	-2342.966108	-2343.046288	56.50	-422.33	-151.92	-2339.6022247	-2338.7029137	-2338.7830937	57.26
R_TS2_57	6	-951.8	-2343.922279	-2342.965043	-2343.044703	60.66	-437.24	-131.97	-2339.6100984	-2338.7031264	-2338.7827864	58.07
R_TS2_58	6	-820.2	-2343.924247	-2342.965924	-2343.044228	61.91	-454.12	-129.39	-2339.6130265	-2338.7039845	-2338.7822885	59.38

Name	Category	SMD(Et <sub>2</sub> O)/B3LYP-D3/6-31+G(d)						DLPNO-CCSD(T)/def2-TZVPP				
		neg. freq. [cm <sup>-1</sup> ]	$E_{tot}$ [Hartree]	$H_{223.15}$ [Hartree]	$G_{223.15}$ [Hartree]	$\Delta\Delta G_{223.15}^\ddagger$ [kJ mol <sup>-1</sup> ]	Grimme-D3 correction [kJ mol <sup>-1</sup> ]	solvation energy [kJ mol <sup>-1</sup> ]	$E_{tot}$ [Hartree]	$H_{223.15, sol}$ [Hartree]	$G_{223.15, sol}$ [Hartree]	$\Delta\Delta G_{223.15}^\ddagger$ [kJ mol <sup>-1</sup> ]
R_TS2_59	2	-739.1	-2343.934803	-2342.978023	-2343.057999	25.76	-460.36	n.d.				
R_TS2_60	2	-822.3	-2343.935824	-2342.978160	-2343.057576	26.87	-465.14					
R_TS2_61	6	-877.2	-2343.929735	-2342.972683	-2343.054763	34.25	-431.66					
R_TS2_62	1	-898.8	-2343.929854	-2342.975254	-2343.054069	36.07	-437.25					
R_TS2_63	2	-831.6	-2343.930279	-2342.972648	-2343.053834	36.69	-448.50					
R_TS2_64	3	-161.4	-2343.930808	-2342.971306	-2343.051711	42.27	-464.08					
R_TS2_65	7	-897.8	-2343.929147	-2342.971633	-2343.051203	43.60	-443.35					
R_TS2_66	3	-157.7	-2343.931282	-2342.971428	-2343.051138	43.77	-465.71					
R_TS2_67	3	-150.6	-2343.929832	-2342.969173	-2343.048615	50.39	-471.04					
R_TS2_68	3	-144.6	-2343.930186	-2342.969226	-2343.048495	50.71	-471.67					
S_TS2_1	3	-893.4	-2343.937881	-2342.980430	-2343.061011	17.85	-461.76	-133.96	-2339.6274930	-2338.7210640	-2338.8016450	8.56
S_TS2_2	3	-879.8	-2343.936887	-2342.980251	-2343.062107	14.97	-445.60	-139.18	-2339.6231105	-2338.7194865	-2338.8013425	9.35
S_TS2_3	3	-915.5	-2343.937789	-2342.980847	-2343.061341	16.98	-443.59	-138.25	-2339.6245273	-2338.7202413	-2338.8007353	10.94
S_TS2_4	3	-808.2	-2343.936702	-2342.979004	-2343.060192	20.00	-463.60	-135.70	-2339.6254136	-2338.7194026	-2338.8005906	11.32
S_TS2_5	3	-858.6	-2343.936397	-2342.979993	-2343.060065	20.33	-462.29	-132.90	-2339.6262607	-2338.7204767	-2338.8005487	11.43
S_TS2_6	3	-858.8	-2343.936397	-2342.979995	-2343.060052	20.37	-462.31	-132.91	-2339.6262560	-2338.7204750	-2338.8005320	11.48
S_TS2_7	3	-895.5	-2343.937587	-2342.980326	-2343.060001	20.50	-461.17	-134.13	-2339.6269707	-2338.7207977	-2338.8004727	11.63
S_TS2_8	3	-895.4	-2343.937587	-2342.980325	-2343.059972	20.58	-461.18	-134.13	-2339.6269222	-2338.7207472	-2338.8003942	11.84
S_TS2_9	3	-908.5	-2343.937746	-2342.980919	-2343.060739	18.56	-442.53	-138.61	-2339.6240499	-2338.7200179	-2338.7998379	13.30
S_TS2_10	3	-907.8	-2343.937773	-2342.981010	-2343.060612	18.90	-442.75	-138.65	-2339.6240868	-2338.7201338	-2338.7997358	13.57
S_TS2_11	3	-812.3	-2343.936728	-2342.979588	-2343.058937	23.29	-463.56	-135.50	-2339.6253869	-2338.7198559	-2338.7992049	14.96
S_TS2_12	3	-767.4	-2343.937063	-2342.979310	-2343.058960	23.23	-457.70	-137.59	-2339.6246193	-2338.7192733	-2338.7989233	15.70

Name	Category	SMD(Et <sub>2</sub> O)/B3LYP-D3/6-31+G(d)							DLPNO-CCSD(T)/def2-TZVPP			
		neg. freq. [cm <sup>-1</sup> ]	$E_{tot}$ [Hartree]	$H_{223.15}$ [Hartree]	$G_{223.15}$ [Hartree]	$\Delta\Delta G_{223.15}^\ddagger$ [kJ mol <sup>-1</sup> ]	Grimme-D3 correction [kJ mol <sup>-1</sup> ]	solvation energy [kJ mol <sup>-1</sup> ]	$E_{tot}$ [Hartree]	$H_{223.15, sol}$ [Hartree]	$G_{223.15, sol}$ [Hartree]	$\Delta\Delta G_{223.15}^\ddagger$ [kJ mol <sup>-1</sup> ]
S_TS2_13	1	-162.2	-2343.938155	-2342.979319	-2343.059840	20.92	-467.34	-127.06	-2339.6288338	-2338.7183938	-2338.7989148	15.72
S_TS2_14	3	-755.1	-2343.936436	-2342.979121	-2343.058611	24.15	-462.51	-135.16	-2339.6249573	-2338.7191203	-2338.7986103	16.52
S_TS2_15	3	-698.9	-2343.935194	-2342.977798	-2343.058844	23.54	-463.12	-134.73	-2339.6234622	-2338.7173822	-2338.7984282	17.00
S_TS2_16	1	-184.4	-2343.933857	-2342.976068	-2343.057229	27.78	-434.45	-141.81	-2339.6175647	-2338.7137887	-2338.7949497	26.13
S_TS2_17	1	-913.3	-2343.932489	-2342.974761	-2343.055433	32.49	-436.78	-146.85	-2339.6160100	-2338.7142150	-2338.7948870	26.30
S_TS2_18	5	-924.5	-2343.934645	-2342.977384	-2343.056193	30.50	-469.84	-128.46	-2339.6238565	-2338.7155245	-2338.7943335	27.75
S_TS2_19	1	-157.8	-2343.933451	-2342.976355	-2343.055971	31.08	-437.53	-140.73	-2339.6181927	-2338.7146977	-2338.7943137	27.80
S_TS2_20	1	-907.7	-2343.932389	-2342.975167	-2343.054834	34.07	-436.91	-146.57	-2339.6158194	-2338.7144224	-2338.7940894	28.39
S_TS2_21	1	-929.6	-2343.930721	-2342.973667	-2343.055669	31.87	-420.18	-146.84	-2339.6116657	-2338.7105407	-2338.7925427	32.45
S_TS2_22	1	-929.7	-2343.930721	-2342.973669	-2343.055677	31.85	-420.17	-146.84	-2339.6116489	-2338.7105269	-2338.7925349	32.47
S_TS2_23	1	-838.8	-2343.931485	-2342.974381	-2343.053814	36.74	-432.68	-144.46	-2339.6148052	-2338.7127222	-2338.7921552	33.47
S_TS2_24	6	-875.3	-2343.931464	-2342.974150	-2343.053836	36.69	-452.82	-123.49	-2339.6224788	-2338.7121998	-2338.7918858	34.18
S_TS2_25	7	-439.0	-2343.931372	-2342.973476	-2343.053580	37.36	-474.87	-124.81	-2339.6219383	-2338.7115813	-2338.7916853	34.71
S_TS2_26	1	-895.8	-2343.931183	-2342.974606	-2343.055007	33.61	-415.32	-147.94	-2339.6114980	-2338.7112680	-2338.7916690	34.75
S_TS2_27	8	-116.9	-2343.932658	-2342.972549	-2343.052287	40.75	-474.73	-126.10	-2339.6221757	-2338.7100957	-2338.7898337	39.57
S_TS2_28	1	-566.5	-2343.927998	-2342.971531	-2343.050262	46.07	-429.63	-144.79	-2339.6117403	-2338.7104223	-2338.7891533	41.35
S_TS2_29	1	-566.8	-2343.927999	-2342.971526	-2343.050255	46.09	-429.63	-144.80	-2339.6117267	-2338.7104047	-2338.7891337	41.40
S_TS2_30	1	-821.4	-2343.928670	-2342.971145	-2343.050928	44.32	-424.71	-150.33	-2339.6089766	-2338.7087086	-2338.7884916	43.09
S_TS2_31	1	-765.6	-2343.926850	-2342.969568	-2343.051290	43.37	-402.52	-152.65	-2339.6055133	-2338.7063743	-2338.7880963	44.13
S_TS2_32	1	-134.1	-2343.929728	-2342.968688	-2343.048070	51.82	-457.51	-134.06	-2339.6183341	-2338.7083531	-2338.7877351	45.08
S_TS2_33	2	-884.0	-2343.924225	-2342.966518	-2343.047759	52.64	-418.73	-158.18	-2339.6026715	-2338.7052105	-2338.7864515	48.45
S_TS2_34	4	-129.7	-2343.918823	-2342.958822	-2343.039314	74.81	-429.49	-150.85	-2339.5982761	-2338.6957301	-2338.7762221	75.30

Name	Category	SMD(Et <sub>2</sub> O)/B3LYP-D3/6-31+G(d)						DLPNO-CCSD(T)/def2-TZVPP			
		neg. freq. [cm <sup>-1</sup> ]	$E_{tot}$ [Hartree]	$H_{223.15}$ [Hartree]	$G_{223.15}$ [Hartree]	$\Delta\Delta G_{223.15}^\ddagger$ [kJ mol <sup>-1</sup> ]	Grimme-D3 correction [kJ mol <sup>-1</sup> ]	solvation energy [kJ mol <sup>-1</sup> ]	$E_{tot}$ [Hartree]	$H_{223.15, sol}$ [Hartree]	$G_{223.15, sol}$ [Hartree]
S_TS2_35	3	-720.3	-2343.935699	-2342.978741	-2343.058283	25.01	-464.61				
S_TS2_36	3	-837.8	-2343.935912	-2342.980603	-2343.058222	25.17	-461.85				
S_TS2_37	3	-805.6	-2343.930166	-2342.973722	-2343.054282	35.52	-453.22				
S_TS2_38	3	-453.9	-2343.929162	-2342.971672	-2343.052951	39.01	-459.65				
S_TS2_39	3	-729.5	-2343.930317	-2342.973197	-2343.052817	39.36	-455.06				
S_TS2_40	1	-872.9	-2343.927194	-2342.970344	-2343.051198	43.61	-417.72				
S_TS2_41	1	-879.5	-2343.924513	-2342.967490	-2343.048088	51.78	-410.35				
S_TS2_42	1	-921.5	-2343.923793	-2342.966912	-2343.047700	52.80	-420.56				
S_TS2_43	2	-152.3	-2343.928696	-2342.969087	-2343.047696	52.81	-470.98				
S_TS2_44	2	-716.6	-2343.924438	-2342.967078	-2343.047417	53.54	-435.77				
S_TS2_45	2	-715.0	-2343.924437	-2342.967077	-2343.047412	53.55	-435.78			n.d.	
S_TS2_46	2	-885.5	-2343.924652	-2342.967145	-2343.047230	54.03	-416.00				
S_TS2_47	6	-582.7	-2343.924316	-2342.966907	-2343.046947	54.77	-439.86				
S_TS2_48	6	-768.1	-2343.925267	-2342.968286	-2343.046942	54.79	-445.90				
S_TS2_49	1	-930.9	-2343.921990	-2342.964440	-2343.045423	58.77	-425.58				
S_TS2_50	2	-889.8	-2343.919702	-2342.962770	-2343.043912	62.74	-416.97				
S_TS2_51	2	-793.1	-2343.920340	-2342.963087	-2343.042980	65.19	-433.73				
S_TS2_52	6	-793.3	-2343.921838	-2342.962836	-2343.041680	68.60	-463.75				
S_TS2_53	6	-424.1	-2343.921987	-2342.963176	-2343.040601	71.43	-454.96				
S_TS2_54	4	-127.9	-2343.919015	-2342.959466	-2343.038740	76.32	-431.49				
S_TS2_55	4	-128.0	-2343.919015	-2342.959461	-2343.038734	76.34	-431.48				

**Table S50.** Single point energies for best three **TS2** conformers (based on B3LYP-D3/6-31+G(d) energies) on different levels of theory.

	Single point energies [Hartree]				
Single point method	B3LYP/6-31+G(d)	DLPNO/CCSD(T)	B3LYP/6-311+G(d,p)	M06-2x/6-311+G(d,p)	wB97XD/6-311+G(d,p)
S_TS2_1	-2343.937363	-2339.627500	-2344.409500	-2343.306200	-2343.532100
S_TS2_2	-2343.936338	-2339.623100	-2344.407900	-2343.303700	-2343.529200
S_TS2_3	-2343.937223	-2339.624500	-2344.408700	-2343.304800	-2343.529800
R_TS2_1	-2343.943332	-2339.631500	-2344.415100	-2343.310500	-2343.535400
R_TS2_2	-2343.943738	-2339.631900	-2344.415300	-2343.310000	-2343.536000
R_TS2_3	-2343.943020	-2339.631000	-2344.414800	-2343.310200	-2343.535100

**Table S51.** Single point energies for **TS2** structures (column 1) compared to energies of H-capped structures **TS2-HC** (column 2) as shown in **Scheme S25** for all conformers populated to more than 5% and the best category-I-(S)-conformer at DLPNO-CCSD(T)/def2-TZVPP level of theory. Difference of relative energies compared to R\_TS2\_1 gives the difference of non-covalent interaction energy (column 6) between naphthyl moiety of the alcohol and the rest of transition state structure.

name	$E_{tot}$ (full <b>TS2</b> ) [Hartree]	$E_{tot}$ (H-capped <b>TS2_HC</b> ) [Hartree]	$\Delta\Delta E_{tot}$ (full <b>TS2</b> ) relative to R_TS2_1 [kJ mol <sup>-1</sup> ]	$\Delta\Delta E_{tot}$ (H-capped <b>TS2_HC</b> ) relative to R_TS2_1 [kJ mol <sup>-1</sup> ]	$\Delta E_{\text{non-covalent interactions}}$ relative to R_TS2_1 [kJ mol <sup>-1</sup> ]
R_TS2_1	-2339.6314779	-1955.6298980	0.00	0.00	0.00
R_TS2_2	-2339.6318998	-1955.6308586	-1.11	-2.52	1.41
R_TS2_3	-2339.6309954	-1955.6298939	1.27	0.01	1.26
R_TS2_4	-2339.6315717	-1955.6308136	-0.25	-2.40	2.16
R_TS2_5	-2339.6256115	-1955.6248157	15.40	13.34	2.06
R_TS2_6	-2339.6267504	-1955.6253533	12.41	11.93	0.48
S_TS2_1	-2339.6274930	-1955.6300808	10.46	-0.48	10.94
S_TS2_2	-2339.6231105	-1955.6272284	21.97	7.01	14.96
S_TS2_3	-2339.6245273	-1955.6273449	18.25	6.70	11.55
S_TS2_4	-2339.6254136	-1955.6268408	15.92	8.03	7.90
S_TS2_5	-2339.6262607	-1955.6294994	13.70	1.05	12.65
S_TS2_6	-2339.6262560	-1955.6295027	13.71	1.04	12.67
S_TS2_7	-2339.6269707	-1955.6299134	11.83	-0.04	11.87
S_TS2_8	-2339.6269220	-1955.6299526	11.96	-0.14	12.10
S_TS2_13	-2339.6288338	-1955.6298110	6.94	0.23	6.71

## 8.2. Reactants, products, intermediates, TS1 of energy profile

**Table S52.** Overview of energies of all species used for the calculation of **Figure S29**. Column 1 gives the name as used in the manuscript. Total energy, enthalpy and free energy calculated at SMD(Et<sub>2</sub>O)/B3LYP-D3/6-31+G(d) and at DLPNO-CCSD(T)/def2-TZVPP are reported. All enthalpies are corrected for a quasi-harmonic rotor, free energies with a free-rotor approximation (for details see Chapter 4.1). Solvation energy was calculated from the difference of single point calculations in gas phase and total energy with SMD model on B3LYP-D3/6-31+G(d) level of theory and added to enthalpy and free energy at coupled cluster calculations. Differences in free energy are reported relative to the best conformer of each species. **Figure S29** gives Boltzman-averaged values for the reported species. The geometries of all listed conformers are provided as SDF file.

	SMD(Et <sub>2</sub> O)/B3LYP-D3/6-31+G(d)				DLPNO-CCSD(T)/def2-TZVPP			$\Delta\Delta G_{223,15}^{\ddagger}$ [kJ mol <sup>-1</sup> ]
	neg. freq. [cm <sup>-1</sup> ]	$E_{tot}$ [Hartree]	$H_{223,15}$ [Hartree]	$G_{223,15}$ [Hartree]	$E_{tot}$ [Hartree]	$H_{223,15, sol}$ [Hartree]	$G_{223,15, sol}$ [Hartree]	
<b>1-(2-Naphthyl)ethanol 1b</b>								
Np_2		-539.792410	-539.577163	-539.609665	-538.7728677	-538.5737047	-538.6062067	0.00
Np_1		-539.791981	-539.576699	-539.609081	-538.7725927	-538.5734537	-538.6058357	0.97
Np_4		-539.790532	-539.575469	-539.608124	-538.7708248	-538.5727048	-538.6053598	2.22
Np_3		-539.790500	-539.575357	-539.607892	-538.7709622	-538.5725092	-538.6050442	3.05
Np_6		-539.790599	-539.575184	-539.607147	-538.7705978	-538.5722728	-538.6042358	5.17
Np_5		-539.790526	-539.575033	-539.607378	-538.7698245	-538.5718155	-538.6041605	5.37
Np_7		-539.790541	-539.575093	-539.607175	-538.7707620	-538.5718830	-538.6039650	5.89
<b>Isobutyric anhydride 2</b>								
BuAnh_5		-539.041217	-538.819860	-538.857278	-538.1227585	-537.9165355	-537.9539535	0.00
BuAnh_9		-539.040379	-538.818801	-538.856018	-538.1223955	-537.9158285	-537.9530455	2.38
BuAnh_13		-539.040086	-538.818309	-538.855310	-538.1223625	-537.9153995	-537.9524005	4.08
BuAnh_17		-539.039895	-538.819309	-538.855856	-538.1213231	-537.9157881	-537.9523351	4.25
BuAnh_8		-539.040070	-538.819199	-538.855445	-538.1217371	-537.9158821	-537.9521281	4.79
BuAnh_24		-539.040343	-538.818726	-538.855916	-538.1206501	-537.9148161	-537.9520061	5.11
BuAnh_11		-539.040676	-538.819962	-538.855205	-538.1221099	-537.9165669	-537.9518099	5.63
BuAnh_1		-539.040111	-538.818504	-538.854446	-538.1217500	-537.9146200	-537.9505620	8.90
BuAnh_19		-539.040186	-538.819415	-538.854166	-538.1210363	-537.9157523	-537.9505033	9.06

	SMD(Et <sub>2</sub> O)/B3LYP-D3/6-31+G(d)				DLPNO-CCSD(T)/def2-TZVPP			$\Delta\Delta G_{223,15}^\ddagger$ [kJ mol <sup>-1</sup> ]
	neg. freq. [cm <sup>-1</sup> ]	$E_{tot}$ [Hartree]	$H_{223,15}$ [Hartree]	$G_{223,15}$ [Hartree]	$E_{tot}$ [Hartree]	$H_{223,15, sol}$ [Hartree]	$G_{223,15, sol}$ [Hartree]	
BuAnh_3		-539.039887	-538.818123	-538.853978	-538.1215155	-537.9143255	-537.9501805	9.91
BuAnh_36		-539.037689	-538.816112	-538.853061	-538.1198159	-537.9127909	-537.9497399	11.06
<b>Catalyst 3</b>								
Np1cat_2		-1265.084160	-1264.555993	-1264.610351	-1262.7091374	-1262.2134454	-1262.2678034	0.00
Np1cat_8		-1265.084137	-1264.555968	-1264.610158	-1262.7091179	-1262.2133669	-1262.2675569	0.65
Np1cat_1		-1265.084308	-1264.556116	-1264.609641	-1262.7088450	-1262.2129840	-1262.2665090	3.40
Np1cat_9		-1265.082111	-1264.554261	-1264.608164	-1262.7085405	-1262.2125905	-1262.2664935	3.44
Np1cat_15		-1265.080951	-1264.552957	-1264.605804	-1262.7081570	-1262.2128750	-1262.2657220	5.46
Np1cat_4		-1265.082441	-1264.554186	-1264.607223	-1262.7086104	-1262.2125964	-1262.2656334	5.70
Np1cat_10		-1265.079887	-1264.551856	-1264.606398	-1262.7050302	-1262.2108552	-1262.2653972	6.32
Np1cat_7		-1265.081501	-1264.553177	-1264.605999	-1262.7074145	-1262.2120565	-1262.2648785	7.68
Np1cat_12		-1265.080970	-1264.552825	-1264.607439	-1262.7045538	-1262.2095268	-1262.2641408	9.62
Np1cat_16		-1265.078409	-1264.550184	-1264.603510	-1262.7030736	-1262.2078236	-1262.2611496	17.47
Np1cat_13		-1265.075620	-1264.548928	-1264.600180	-1262.7057730	-1262.2090880	-1262.2603400	19.60
Np1cat_11		-1265.077245	-1264.548887	-1264.601938	-1262.7022462	-1262.2069922	-1262.2600432	20.37
Np1cat_14		-1265.073393	-1264.545026	-1264.598403	-1262.6983454	-1262.2042604	-1262.2576374	26.69
<b>rc (reactant complex)</b>								
TS1_int1_7		-1804.136592	-1803.391751	-1803.461219	-1800.8478986	-1800.1426916	-1800.2121596	0.00
TS1_int1_2		-1804.132816	-1803.388199	-1803.456308	-1800.8456756	-1800.1411076	-1800.2092166	7.73
<b>TS1</b>								
TS1_7	-108.3	-1804.120081	-1803.374404	-1803.441224	-1800.8222098	-1800.1212708	-1800.1880908	0.00
TS1_29	-90.5	-1804.117960	-1803.371568	-1803.437141	-1800.8217588	-1800.1209588	-1800.1865318	4.09
TS1_2	-103.3	-1804.116977	-1803.371197	-1803.437486	-1800.8193990	-1800.1200180	-1800.1863070	4.68

	SMD(Et <sub>2</sub> O)/B3LYP-D3/6-31+G(d)				DLPNO-CCSD(T)/def2-TZVPP			$\Delta\Delta G_{223.15}^{\ddagger}$ [kJ mol <sup>-1</sup> ]
	neg. freq. [cm <sup>-1</sup> ]	$E_{tot}$ [Hartree]	$H_{223.15}$ [Hartree]	$G_{223.15}$ [Hartree]	$E_{tot}$ [Hartree]	$H_{223.15, sol}$ [Hartree]	$G_{223.15, sol}$ [Hartree]	
TS1_5	-73.1	-1804.116886	-1803.371104	-1803.437977	-1800.8200986	-1800.1193066	-1800.1861796	5.02
TS1_30	-87.2	-1804.117912	-1803.372080	-1803.436669	-1800.8220158	-1800.1215858	-1800.1861748	5.03
<b>int1</b>								
TS1_int2_2		-1804.128126	-1803.381081	-1803.448480	-1800.8243260	-1800.1247270	-1800.1921260	0.00
TS1_int2_1		-1804.126601	-1803.380166	-1803.447055	-1800.8209411	-1800.1239831	-1800.1908721	3.29
TS1_int2_4		-1804.123038	-1803.376947	-1803.444131	-1800.8141043	-1800.1236373	-1800.1908213	3.43
TS1_int2_5		-1804.120496	-1803.374240	-1803.443338	-1800.8108111	-1800.1205441	-1800.1896421	6.52
TS1_int2_7		-1804.123245	-1803.377103	-1803.445157	-1800.8169188	-1800.1202538	-1800.1883078	10.02
TS1_int2_8		-1804.120625	-1803.374621	-1803.441784	-1800.8123244	-1800.1201414	-1800.1873044	12.66
TS1_int2_6		-1804.119890	-1803.373927	-1803.441719	-1800.8064232	-1800.1185942	-1800.1863862	15.07
<b>int1-(R)-1b</b>								
R_TS2_2_int1		-2343.956718	-2342.993737	-2343.075732	-2339.6395214	-2338.7310974	-2338.8130924	0.00
R_TS2_1_int1		-2343.955291	-2342.992558	-2343.074046	-2339.6377416	-2338.7295366	-2338.8110246	5.43
R_TS2_10_int1		-2343.947723	-2342.985765	-2343.066304	-2339.6332081	-2338.7266931	-2338.8072321	15.39
R_TS2_29_int1		-2343.947605	-2342.983939	-2343.065333	-2339.6302057	-2338.7220637	-2338.8034577	25.30
R_TS2_18_int1		-2343.940014	-2342.977574	-2343.060428	-2339.6184913	-2338.7138393	-2338.7966933	43.06
R_TS2_33_int1		-2343.937157	-2342.974958	-2343.056376	-2339.6106117	-2338.7133847	-2338.7948027	48.02
R_TS2_39_int1		-2343.936733	-2342.975406	-2343.056613	-2339.6096403	-2338.7118473	-2338.7930543	52.61
<b>int1-(S)-1b</b>								
S_TS2_13_int1		-2343.953411	-2342.991685	-2343.072235	-2339.6356956	-2338.7312156	-2338.8117656	0.00
S_TS2_4_int1		-2343.950929	-2342.988107	-2343.070083	-2339.6353026	-2338.7282276	-2338.8102036	4.10
S_TS2_2_int1		-2343.948371	-2342.986316	-2343.068935	-2339.6298045	-2338.7254555	-2338.8080745	9.69
S_TS2_1_int1		-2343.949060	-2342.986139	-2343.068152	-2339.6339291	-2338.7270211	-2338.8090341	7.17

	SMD(Et <sub>2</sub> O)/B3LYP-D3/6-31+G(d)				DLPNO-CCSD(T)/def2-TZVPP			$\Delta\Delta G_{223,15}^\ddagger$ [kJ mol <sup>-1</sup> ]
	neg. freq. [cm <sup>-1</sup> ]	$E_{tot}$ [Hartree]	$H_{223,15}$ [Hartree]	$G_{223,15}$ [Hartree]	$E_{tot}$ [Hartree]	$H_{223,15, sol}$ [Hartree]	$G_{223,15, sol}$ [Hartree]	
S_TS2_29_int1		-2343.946897	-2342.984120	-2343.066568	-2339.6297438	-2338.7243568	-2338.8068048	13.02
S_TS2_19_int1		-2343.940691	-2342.978717	-2343.059653	-2339.6165278	-2338.7174448	-2338.7983808	35.14
<b>R_TS2</b>								
See <b>Table S49</b>								
<b>S_TS2</b>								
See <b>Table S49</b>								
<b>R_pc</b>								
R_TS2_1_int2		-2343.974700	-2343.012104	-2343.094978	-2339.6732150	-2338.7568760	-2338.8397500	0.00
R_TS2_2_int2		-2343.974442	-2343.011945	-2343.094312	-2339.6719276	-2338.7567226	-2338.8390896	1.73
R_TS2_29_int2		-2343.971849	-2343.010294	-2343.093945	-2339.6721305	-2338.7541405	-2338.8377915	5.14
R_TS2_10_int2		-2343.967484	-2343.005615	-2343.087545	-2339.6677751	-2338.7520611	-2338.8339911	15.12
R_TS2_17_int2		-2343.970220	-2343.009474	-2343.090229	-2339.6633827	-2338.7521297	-2338.8328847	18.02
R_TS2_29_int2		-2343.969169	-2343.007718	-2343.089382	-2339.6601197	-2338.7507977	-2338.8324617	19.14
R_TS2_33_int2		-2343.964178	-2343.002805	-2343.084458	-2339.6589181	-2338.7475431	-2338.8291961	27.71
<b>S_pc</b>								
S_TS2_2_int2		-2343.970247	-2343.008684	-2343.092002	-2339.6696016	-2338.7540366	-2338.8373546	0.00
S_TS2_1_int2		-2343.968537	-2343.006608	-2343.089413	-2339.6686379	-2338.7529299	-2338.8357349	4.25
S_TS2_4_int2		-2343.968799	-2343.006270	-2343.088895	-2339.6678364	-2338.7518124	-2338.8344374	7.66
S_TS2_13_int2		-2343.970588	-2343.008901	-2343.089003	-2339.6676108	-2338.7528468	-2338.8329488	11.57
S_TS2_29_int2		-2343.963205	-2343.001708	-2343.084024	-2339.6589355	-2338.7479865	-2338.8303025	18.52
S_TS2_19_int2		-2343.963093	-2343.001218	-2343.083299	-2339.6583631	-2338.7455261	-2338.8276071	25.59
<b>1-(2-Naphthyl)ethyl isobutyrate 4b</b>								
BuNp_14		-771.110150	-770.796010	-770.839042	-769.6780170	-769.3845640	-769.4275960	0.00

	SMD(Et <sub>2</sub> O)/B3LYP-D3/6-31+G(d)				DLPNO-CCSD(T)/def2-TZVPP			$\Delta\Delta G_{223,15}^\ddagger$ [kJ mol <sup>-1</sup> ]
	neg. freq. [cm <sup>-1</sup> ]	$E_{tot}$ [Hartree]	$H_{223,15}$ [Hartree]	$G_{223,15}$ [Hartree]	$E_{tot}$ [Hartree]	$H_{223,15, sol}$ [Hartree]	$G_{223,15, sol}$ [Hartree]	
BuNp_2		-771.110858	-770.797639	-770.837966	-769.6794698	-769.3863198	-769.4266468	2.49
BuNp_1		-771.110424	-770.797145	-770.837627	-769.6789633	-769.3858923	-769.4263743	3.21
BuNp_3		-771.110059	-770.795888	-770.837536	-769.6784682	-769.3844592	-769.4261072	3.91
BuNp_12		-771.109814	-770.795745	-770.837623	-769.6776864	-769.3839374	-769.4258154	4.67
BuNp_16		-771.108858	-770.794544	-770.837378	-769.6765941	-769.3829261	-769.4257601	4.82
BuNp_5		-771.109277	-770.795994	-770.837167	-769.6780016	-769.3845626	-769.4257356	4.88
BuNp_4		-771.110007	-770.796619	-770.836558	-769.6784931	-769.3852561	-769.4251951	6.30
BuNp_6		-771.109393	-770.796156	-770.835922	-769.6778903	-769.3847053	-769.4244713	8.20
BuNp_13		-771.109092	-770.795860	-770.836234	-769.6771990	-769.3840740	-769.4244480	8.26
BuNp_7		-771.110084	-770.797481	-770.835483	-769.6782621	-769.3863051	-769.4243071	8.63
BuNp_11		-771.110435	-770.797676	-770.835688	-769.6784988	-769.3861368	-769.4241488	9.05
<b>Isobutyric acid S1</b>								
BuAc_2		-307.744967	-307.621513	-307.648003	-307.2388891	-307.1255001	-307.1519901	0.00
BuAc_4		-307.744470	-307.620544	-307.647407	-307.2378954	-307.1242164	-307.1510794	2.39

## 8.3. Analysis of reactants and products

**Table S53.** Overview of energies of all species used for the calculation of thermodynamics in Chapter 4.10. Column 1 gives name as used in the manuscript. Total energy, enthalpy and free energy calculated at SMD(Et<sub>2</sub>O)/B3LYP-D3/6-31+G(d) and at DLPNO-CCSD(T)/def2-TZVPP are reported. All enthalpies are corrected for a quasi-harmonic rotor, free energies with a free-rotor approximation (for details see Chapter 4.1). Solvation energy was calculated from the difference of single point calculations in gas phase and total energy with SMD model on B3LYP-D3/6-31+G(d) level of theory and added to enthalpy and free energy at coupled cluster calculations. Differences in free energy are reported relative to the best conformer of each species. In Chapter 4.10 Boltzman-averaged values are reported. The geometries of all listed conformers are provided as SDF file.

	SMD(Et <sub>2</sub> O)/B3LYP-D3/6-31+G(d)					DLPNO-CCSD(T)/def2-TZVPP			
	$E_{tot}$ [Hartree]	$H_{223.15}$ [Hartree]	$G_{223.15}$ [Hartree]	Cavity volume [10 <sup>-30</sup> m <sup>3</sup> ]	Exact polarizability [a.u. <sup>3</sup> ]	$E_{tot}$ [Hartree]	$H_{223.15, sol}$ [Hartree]	$G_{223.15, sol}$ [Hartree]	$\Delta\Delta G_{223.15}^\ddagger$ [kJ mol <sup>-1</sup> ]
<b>1-(2-Naphthyl)ethanol 1b</b>									
Np_2	See Table S52			205.2	248.0	See Table S52			
Np_1				205.4	253.1				
Np_4				205.5	256.7				
<b>1-Phenylethanol 1a</b>									
Phe_1	-386.133758	-385.966887	-385.995840	156.8	134.3	-385.4197194	-385.2649814	-385.2939344	0.00
Phe_3	-386.132004	-385.965270	-385.994554	156.2	137.7	-385.4178981	-385.2639991	-385.2932831	1.71
Phe_7	-386.131881	-385.964735	-385.993667	157.8	134.4	-385.4164389	-385.2627149	-385.2916469	6.01
<b>1-(2-Phenanthryl)ethanol 1c</b>									
Phant_1	-693.452764	-693.189073	-693.225403	254.8	368.3	-692.1290715	-691.8853695	-691.9216995	0.00
Phant_3	-693.450935	-693.187321	-693.223165	254.5	372.5	-692.1271056	-691.8842896	-691.9201336	4.11
Phant_7	-693.450890	-693.186997	-693.222991	255.0	368.5	-692.1258997	-691.8833687	-691.9193627	6.14
<b>1-(2-Pyrenyl)ethanol 1d</b>									
Pyr_1	-769.692444	-769.415726	-769.451915	273.1	440.8	-768.2180779	-767.9627269	-767.9989159	0.00
Pyr_4	-769.690634	-769.414178	-769.450575	272.8	445.5	-768.2162984	-767.9618824	-767.9982794	1.67
Pyr_7	-769.690088	-769.414020	-769.448598	272.5	440.9	-768.2152306	-767.9610546	-767.9956326	8.62
<b>1-(2-Naphthyl)ethyl isobutyrate 4b</b>									
See Table S52									

	SMD(Et <sub>2</sub> O)/B3LYP-D3/6-31+G(d)					DLPNO-CCSD(T)/def2-TZVPP			
	$E_{tot}$ [Hartree]	$H_{223.15}$ [Hartree]	$G_{223.15}$ [Hartree]	Cavity volume [10 <sup>-30</sup> m <sup>3</sup> ]	Exact polarizability [a.u. <sup>3</sup> ]	$E_{tot}$ [Hartree]	$H_{223.15, sol}$ [Hartree]	$G_{223.15, sol}$ [Hartree]	$\Delta\Delta G_{223.15}^\ddagger$ [kJ mol <sup>-1</sup> ]
<b>1-Phenylethyl isobutyrate 4a</b>									
BuPhe1	-617.452392	-617.186437	-617.224894	n.d.		-616.3261749	-616.0765269	-616.1149839	0.00
BuPhe12	-617.451160	-617.185253	-617.224543			-616.3245000	-616.0749470	-616.1142370	1.96
BuPhe3	-617.451410	-617.185356	-617.223276			-616.3250736	-616.0752836	-616.1132036	4.67
<b>1-(2-Phenanthryl)ethyl isobutyrate 4c</b>									
BuPhant2	-924.771182	-924.408763	-924.453948	n.d.		-923.0353478	-922.6971158	-922.7423008	0.00
BuPhant01	-924.770870	-924.408976	-924.453024			-923.0349477	-922.6972287	-922.7412767	2.69
BuPhant3	-924.770211	-924.408629	-924.453005			-923.0344924	-922.6968014	-922.7411774	2.95
BuPhant14	-924.770757	-924.408947	-924.452942			-923.0346513	-922.6971273	-922.7411223	3.09
BuPhant12	-924.770130	-924.408233	-924.452131			-923.0338320	-922.6961000	-922.7399980	6.05
<b>1-(2-Pyrenyl)ethyl isobutyrate 4d</b>									
BuPyr_4	-1001.009716	-1000.634346	-1000.680978	n.d.		-999.1234426	-998.7732866	-998.8199186	0.00
BuPyr_7	-1001.010997	-1000.635323	-1000.680270			-999.1247086	-998.7744416	-998.8193886	1.39
BuPyr01	-1001.010643	-1000.635667	-1000.679896			-999.1244784	-998.7749534	-998.8191824	1.93
BuPyr_3	-1001.009657	-1000.634323	-1000.680169			-999.1233822	-998.7732492	-998.8190952	2.16
BuPyr_12	-1001.009746	-1000.634892	-1000.678510			-999.1228592	-998.7735672	-998.8171852	7.18

**Table S54.** Overview of energies of all species used for the calculation of alcoholates for isodesmic proton transfer reactions in Chapter 4.10. Column 1 gives name as used in the manuscript. Total energy, enthalpy and free energy calculated at SMD(Et<sub>2</sub>O)/B3LYP-D3/6-31+G(d) are reported. All enthalpies are corrected for a quasi-harmonic rotor, free energies with a free-rotor approximation (for details see Chapter 4.1). Differences in free energy are reported relative to the best conformer of each species. In Chapter 4.10 Boltzman-averaged values are reported.

	SMD(Et <sub>2</sub> O)/B3LYP-D3/6-31+G(d)		
	$E_{tot}$ [Hartree]	$G_{223,15, sol}$ [Hartree]	$\Delta\Delta G_{223,15}^\ddagger$ [kJ mol <sup>-1</sup> ]
<b>1-(2-Naphtyl)ethanolat 1b-</b>			
Np_1_anion	-539.259586	-539.091001	0.00
Np_4_anion	-539.258750	-539.090213	2.07
Np_7_anion	-539.256635	-539.087902	8.14
<b>1-Phenylethanolat 1a-</b>			
Phe_1_anion	-385.599818	-385.476182	0.00
Phe_7_anion	-385.551226	-385.429096	123.62
<b>1-(2-Phenanthryl)ethanolat 1c-</b>			
Phant_anion	-692.919475	-692.707197	0.00
Phant_anion	-692.919511	-692.706576	1.63
Phant_anion	-692.871727	-692.659734	124.61
<b>1-(2-Pyrenyl)ethanolat 1d-</b>			
Pyr_3_anion	-769.160263	-768.934461	0.00
Pyr_7_anion	-769.111143	-768.886677	125.46